NOTICE

The quality of this microform is heavily dependent upon the quality of the original thesis submitted for microfilming. Every effort has been made to ensure the highest quality of reproduction possible.

If pages are missing, contact the university which granted the degree.

Some pages may have indistinct print especially if the original pages were typed with a poor typewriter ribbon or if the university sent us an inferior photocopy.

Reproduction in full or in part of this microform is governed by the Canadian Copyright Act, R.S.C. 1970, c. C-30, and subsequent amendments.

AVIS

La qualité de cette microforme dépend grandement de la qualité de la thèse soumise au microfilmage. Nous avons tout fait pour assurer une qualité supérieure de reproduction.

S'il manque des pages, veuillez communiquer avec l'université qui a conféré le grade.

La qualité d'impression de certaines pages peut laisser à désirer, surtout si les pages originales ont été dactylographiées à l'aide d'un ruban usé ou si l'université nous a fait parvenir une photocopie de qualité inférieure.

La reproduction, même partielle, de cette microforme est soumise à la Loi canadienne sur le droit d'auteur, SRC 1970, c. C-30, et ses amendements subséquents.

A STUDY ON FRICTION-DAMPED-FRAMES

Meng Heng Tan

A Thesis

in

The Centre

for

Building Studies

Presented in Partial Fulfilments of the Requirements
for the Degree of Master of Engineering at
Concordia University
Montreal, Quebec, Canada
January 1992

ISBN 0-315-73678-X

ABSTRACT

A STUDY ON FRICTION-DAMPED-FRAMES

M.H. TAN

A detailed investigation for a single-degree-of-freedom friction-damped-braced-frame was carried out. A refined derivation for the so called optimum slip load was obtained based on quasi-static loadings. A simple computer routine was written for the time-history analysis of the SDOF FDF. From the new, refined equation and the time-history analyses it was concluded that the relative stiffness α between the brace and the columns did not have to exceed 10 for optimum energy dissipation. A detailed study was also carried out for multi-storey single bay steel frames. From the time-history analyses it appeared that there was no direct evidence to relate the optimum slip load with the building weight. From the deformations obtained from these frames, a response spectrum was generated for the FDF for modal analysis. The response spectrum was tested by using several examples and it was concluded that the results obtained by using the response spectrum were reasonable. Finally, a new force reduction factor was introduced for the FDF systems. It was concluded that the force reduction factor for the FDF systems was higher than that for the MRF systems.

Acknowledgements

The constant encouragements, and the kind and helpful assistance provided by Prof. K. H. Ha are gratefully acknowledged. The financial assistance provided by the NSERC for the study is also acknowledged and also special thanks to SIRICON for allowing the use of the VAX 11/785 for all the computational works.

TABLE OF CONTENTS

List of Figures

List of Tables

List of Symbols

A	Cross-sectional area
C	viscous damping coefficient
[C]	system's viscous damping matrix
D	Deflection
E	Modulus of elasticity
F	Foundation factor
F_d	Frictional force
F_f	horizontal component of frictional force
I	Moment of inertia; foundation importance factor
K	Member stiffness; structural response factor
¦K	Total stiffness
[K]	Stiffness matrix
L	Length of member
[M]	Mass matrix
P	Total force or load
P_s	Slip load
R	Force modification factor
S	seismic response factor
T	Fundamental period of vibration
V	Total base shear; shear force
v	zonal velocity ratio
W	Weight of member or building; total work done
X	Lateral displacement of building/system
$\dot{X}$	system's response velocity

$\ddot{X}$	system's response acceleration
X_g	Ground displacement
$\ddot{X}_g$	Ground acceleraion
α	Ratio of lateral stiffness of brace member to the lateral stiffness of columns
β	Angle of brace member to the horizontal
Δ	Member deformation
ξ	Critical damping ratio
ω	Angular velocity or undamped natural circular frequency

1.0 INTRODUCTION

During severe earthquakes, even well-engineered buildings have been known to collapse or to sustain extensive damages caused by the immense amount of kinetic energy fed into them. The literature abounds with well-documented cases of many destructive earthquakes. The recent one that occurred in Mexico on September 1986 was reputed to have destroyed over two hundred buildings and 30000 lives in Mexico City (1), and in the more recent Armenia earthquake of December 1988, in which thousands of lives and hundreds of buildings were destroyed (2). Researchers and engineers are still trying to find ways to predict the occurrence of earthquakes, and ways to prevent the destruction of built structures. In seismic zones, almost all building codes stipulate that buildings and engineered structures must be designed to resist lateral loads induced by earthquakes to prevent collapse, permitting a certain degree of plastic yielding or minor structural damage, but it is also now increasingly being recognized that not only the main structural frame and its load carrying components must be protected from damage, but also the secondary non-structural elements such as sensitive electronic and mechanical equipments, curtain walls and windows should be protected from the amplified acceleration induced at the higher floor levels (3).

1.1 Recent Developments in Aseismic Design of Building Structures

The basic philosophy in aseismic design in most building codes is to design buildings to withstand minor and even moderate earthquakes without any structural damage. In the event of a major earthquake, the building must stand, albeit with some damages, to allow occupants to escape safely. Engineers and scientists have strived to develop systems and devices to prevent the destruction of built engineering facilities. The Applied Technology Council conference in 1985, ACT-17 (4) presented the state of the art technology in energy dissipation methods and devices in aseismic design for buildings and civil engineering structures. One of the first recorded patents on earthquake resistant design was awarded to a certain British doctor in 1909 by the name Calantarients. His design consists of a base isolation system in which a building is separated from its foundation by a layer of sand or talc. The first person who applied the principle of base isolation was the famed American architect Frank Lyold Wright who designed the Tokyo Imperial Hotel in 1923. He put the foundation piles of the building on a layer of soft mud which was located close to the surface. The building performed well during the devastated 1923 Tokyo earthquake and received hardly any damage whereas buildings nearby were totally destroyed (5).

Unfortunately not every building is located above a suitable layer of soft mud, therefore the search for a better system continued. The so called first-soft story concept was put forward by Green in 1943. In this system, the first floor of the building was deliberately made flexible so that most of the yielding would occur at the first floor level, and thereby the upper levels are protected from seismic excitations. This system, however, was proved by Chopra, Clough and Clough (6) to be unstable since large deformations would occur at the first floor level columns.

Many other systems followed but few were developed and put into use. Among the better known ones are the French base isolation systems used in several facilities in France and in South Africa. Rubber pads have been used as energy absorbers in bridge structures by engineers for vibration control. The first use of rubber pads in buildings seems to have been initiated by a Hungarian engineer but this was thought to have the effect of bouncing the building at the corners during an earthquake. The invention of multi-layered steel-plated rubber plate and subsequently the invention of lead filled multi-layered pad by Robinson (7) in 1982 proved to be an effective method for reducing the effects of earthquakes on buildings. Kelly (8) has tested many reinforced rubber pad isolation systems and shown that

they are effective and economically feasible especially for the renovation of existing buildings to meet the current building code requirements. Mayes, Buckle (9) summarized the use of rubber pad isolators in a recent article and gave details of buildings and structures currently built in the United States and other parts of the world. Stiemer and Barwig (10) showed the results of experimental investigations of various schemes of first-storey designs for steel buildings with base isolation. Three basic elements are required for any particular base isolation system, and these are:

i. a flexible mounting so that the period of vibration of the total system is sufficiently lengthened to reduce the system response;

ii. a damper or energy dissipation device so that the relative deflections between the building and ground can be controlled to a practical design level;

iii. a means of providing rigidity under low (service) load levels such as wind and minor earthquakes.

Popov in 1979 (11) advanced the eccentric-braced frames where he intentionally offset the diagonal bracing element to cause yielding of the beams in the event of severe ground shaking. But this system has the handicap of having to replace the damaged beams, a costly reparation job. Hanson, Bergman and Ashour (12) studied the effects of using viscoelastic dampers on moment resisting frames as supplemental damping devices. They showed that the

response of the structures was greatly reduced with these devices. For the response spectrum analysis, typical response spectra used are generated for critical damping ratios up to 20%. With supplemental damping the fraction of critical damping is no longer restrained to these low values. Nine earthquake records were used and damping values of up to 150 % critical were considered. A relationship between displacement response and the fraction of critical damping was established, and this was deemed useful in estimating the maximum modal displacements for structures with increased levels of damping. A critical damping ratio of from one to five percent is normally assumed when performing dynamic analysis of structural systems, but now it seems that damping of more than five percent of critical damping ratio is feasible with the use of supplemental dampers.

The newest system to enter the scene is known as the Friction Pendulum system (F.P.S.), developed by an engineering firm in California (13). It consists of two steel plates in which one has a concave surface and sliding is allowed on the contact surface. The F.P.S. appears to look like a modified system for a base isolation technique but using dry friction between two surfaces instead of reinforced rubber pads. It was experimentally tested and found to be effective in reducing system response to some degree.

1.2 Friction-Damped-Frames

In 1982 Pall and Marsh (14) put forward the idea of removing the excess energy fed into building frames during earthquake loadings by using friction damper devices. These simple devices have been tested and shown to have a reliable hysteretic loop over many cycles. These devices dissipate energy by slipping at a pre-set force level. These dampers can be installed in several ways in the building structures. The new Friction Damped Frames (F.D.F.) system has gained great attention in the earthquake engineering community in recent years.

1.2.1 Description of the System

The friction devices are made of simple steel elements with heavy duty brake lining pads attached to the slipping surfaces. Clamping force is provided by a bolt tightened against the braking pads to obtain the required force to produce the design slip load of the device. The slip load of the friction damper device is the force level in the brace clamping element. Figure 1.1 shows a schematic picture of a typical tension friction device, which forms part of the diagonals braces of a building. Figure 1.2 shows a typical hysteretic loop of the tension damper under cyclic load testing. Test results carried out showed the stable

hysteretic loop of the device over repetitive loading. The performance is stable and non-degrading.

If a brace element is effective in both tension and compression, the damper can dissipate the kinetic energy in both tension and compression by installing a damper in each element. Since the brace element is normally designed to work only in tension, the damper would slip in tension but not in the compression cycle (reverse cycle during cyclic loading). To compensate for this, the four corner links acts as a special mechanism to force slipping in the brace for both half cycles of movements. Figure 1.3 shows the actual hysteretic loop of a damper as installed in an diagonal brace of a building frame, when both the tension and compression braces take part in slipping.

1.2.2 Behaviour of Friction-Damped-Frames

Among the common systems for resisting lateral loads in multistorey buildings are the moment resisting frames, frames with shear walls, and braced frames. The friction-damped-frame is a modification of the braced moment resisting frame in that the cross-bracing members are furnished with friction dampers. The locations of the dampers can be arranged to suit any architectural requirements. Some of the possible arrangements are shown in Figure 1.4 as proposed by the

inventors. These dampers are also applicable for retrofitting existing structures to satisfy present day seismic criteria.

Baktash (15) has shown, by computer simulation, the superior performance of the friction damped frames when compared with eccentric braced frames (EBF). Filiatrault and Cherry (16) have carried out testing of a 1/3 scale steel frame with the devices installed at the cross-bracings of the frame. They have described the superior performance of friction damped frame during a severe earthquake where other traditional structural systems behaved unsatisfactorily. Pall (17) has recently compared the F.D.F. to that of a shear wall structure and concluded that the F.D.F. system was far superior to that of the shear wall system. Kelly and Aiken (18) have recently tested a nine storey steel frame incorporating friction dampers and they reached similar conclusions. Filiatrault and Cherry (19) have also recently compared the performance of a FDF system and that of a base isolation system, and they concluded that the FDF system performed better than the base isolation system for earthquakes of different characteristics.

1.3 NBCC Procedure For Aseismic Design

The 1985 NBCC and its Supplements (20) present a

basic equation for the design of buildings for earthquake loads. It specifies the minimum design base shear given by the equation:

$$V = v\ S\ I\ K\ F\ W$$

where

V = the total base shear induced in the structure during an earthquake

v = zonal velocity ratio for a particular site

K = a ratio which takes into account the type of structures and its energy dissipation capability

S = seismic response factor which takes into account the dynamic response of the building depending on the fundamental period of the building

I = importance factor for the structure

F = soil or foundation factor

W = total reactive weight of the building assumed to be vibrating with the building

Two approaches are provided by the NBCC for the distribution of the total base shear. In the quasi-static method, the total lateral load is distributed according to an approximate linear first modal shape, plus an additional load at the roof level to account for any higher mode contribution. The resulting total V so obtained is then distributed over the height of the building by the following

equation:

$$F_x = V \left[\frac{W_x h_x}{\sum W_i h_i} \right]$$

where

F_x = computed lateral shear assumed acting at that floor level

W_x = total floor weight acting at that floor level

h_x = height to that floor level

$W_i h_i$ = total moment product of all the floor from the ground

The NBCC code also stipulates that an additional lateral shear force must be applied at the roof level to account for the contribution of higher modes for slender structures. In the dynamic method, the code allows the use of more exact method of determining the period of the frame and distribute the total lateral load V according to the results of a response spectrum analysis.

The present K factors in the NBCC codes do not acknowledge the energy dissipation capabilities of the FDF system as it is still a new concept. For the moment resisting frame a K factor of 0.7 is assigned because of the ability of the rigid beam-column connection to undergo inelastic rotation. A K factor of 0.8 to 1.0 is assigned to the braced frames because it is deemed that the braced frames are less ductile than the MRF due to the degrading stiffness of the bracing elements during cyclic loadings. A K factor of less

than 0.7 is to be expected for the FDF systems as its energy dissipation capabilities is higher than that of the MRF and braced frames, but this is still to be resolved by further studies.

The NBCC has decided to make major changes to the seismic design requirements of structures for the next edition of the NBCC. The concept of the force reduction factor, or the force modification factor, R, will be introduced in the next edition of the NBCC. The new R factor will replace the K factor assigned to the various structural systems. This will be studied in more details in later chapter.

1.4 An "Interim" Procedure for the Design of Friction-Damped Frames

Even though the present NBCC provisions do not deal specifically with the FDF system, it is anticipated that with further developments and demonstration, the system will be recognized as an effective earthquake resistant structural system in future building code amendments. It appears that it will be sometime before simplified design criteria are developed and incorporated into NBCC revisions. For the present moment, designers of FDF systems must carry out complicated computer time-history analyses to determine the realistic forces in the members and the optimum slip loads in

the dampers. Nevertheless, the 1990 proposed revision for the NBCC and its supplement (to be released) have introduced a clause allowing the use of new earthquake resistant systems such as the rubber pad isolators, eccentrically-braced-frame, and the friction-damped-frames. The California legislature have also introduced amendments to its clauses such that all new buildings must be built using the new technology for aseismic design.

1.4.1 General Methodology

Pall (17) in 1985 proposed a conservative design procedure for the FDF that conforms to the current NBCC guide line. He proposed that the building first be sized as a moment resisting frame with K=0.70 to obtain the required base shear. Then the shear is distributed as per the NBCC guide lines. A linear analysis is then carried out to determine the member forces. After obtaining the preliminary member sizes, the same frame is then equipped with the friction dampers to become the FDF. The rational for choosing the K factor of 0.70 is that during a major earthquake, all the friction dampers will probably be slipping, and hence the frame itself will behave essentially like a moment resisting frame. This approach satisfies the code requirements, and is conservative since it ignores the energy dissipated (in the dampers) which would reduce the member forces to a level

lower than that required by the factor K = 0.70.

Because of the non-linearity of the FDF system, an inelastic nonlinear step by step integration over the time domain is required for its analysis. Two popular computer packages suitable for this analysis may be mentioned: the program DRAIN-2D(21) and DRAIN-TABS (22) developed at the University of California, Berkeley. The programs are for two and three-dimensional systems respectively. Since DRAIN-2D is extensively used in the present study, a brief description of its basic working scheme is given below.

1.4.2 Non-Linear Time History Analysis

Most commercially available structural analysis programs employ the direct stiffness method of analysis. This is done by summing the appropriate stiffness of the members and solving for the unknowns displacements given any set of external forces. For dynamic analysis, the external forces will include the damping and inertia effects. If the system behaviour is nonlinear, it is usual that the stiffness matrix is updated to account for the yielding of individual members or components.

The general equation of motion for a SDOF system subjected to an external forcing function at any time t is

with reference to Fig. 1.5 :

$$M \ddot{X}(t) + C \dot{X}(t) + R(t) = P(t)$$

where

M = the mass

C = system's viscous damping coefficient

R = the system restoring force

P = the forcing function

$\ddot{X}$ = system's acceleration

$\dot{X}$ = system's velocity

X = system's displacement

As shown in the Figure 1.5, the displacement of the system with respect to its fixed base is denoted as X(t). The double dot denotes the second derivative with respect to time, and a single dot denotes the first derivative. In the case of a horizontal ground excitation, the above equation may be written in the form as shown below :

$$M \ddot{X}(t) + C \dot{X}(t) + R(t) = - M \ddot{X}_g(t)$$

where M, C, R(t) are the same as above. In this case, X(t) denotes the displacement of the system relative to the ground and Xg(t) is the displacement of the ground relative to a fixed reference axis. By comparing the above two equations, one can note that the equation of motion for a seismically excited system is the same as that for an externally excited

system if the load is :

$$P(t) = - M \ddot{X}_g(t)$$

However, the precise meaning of X(t) in each case must be remembered. When the first equation is applied to a seismically excited system, X(t) represents the displacement of the system with respect to an accelerating base and the total displacement is:

$$X(t) = x(t) + x_g(t)$$

however, when the equation is applied to an externally loaded system, X(t) also represents the total displacement of the system since the base is fixed. This previous governing equation of motion is normally solved by numerical integration, as closed form solution exists only for a few types of excitation. In this approach, the analysis over the entire duration of excitation is divided into a series of sequential analyses over smaller intervals of time. The response is evaluated at the end of each time increment based on the conditions existing at the beginning of the increment and an assumed response mechanism during the time increment. For multi-degree-freedom system, the governing equation of motion is :

$$[M] \{ \ddot{X} \} + [C] \{ \dot{X} \} + [K] \{ X \} = - [M] \ddot{X}_g$$

where

[M] = is the system mass matrix

[C] = is the system damping matrix

[K] = assembled system stiffness matrix

$\ddot{X}_g$ = ground acceleration

$\{ \dot{X} \}$ = system's velocity

{ X } = vector of lateral displacements of the system relative to the ground

In the program DRAIN2D, the equation is solved at each incremental time step assuming a constant response acceleration within each time step. At the end of each time step, the force level in each member is assessed to see if a member has yielded and if so, the member stiffness is revised for the next time step. The input ground motion is assumed to vary linearly within each time step, i.e., linear interpolation is used to obtain the required acceleration between the input time interval. Several common structural member types are available in the program: trusses, beam, beam-column, panel, and degrading reinforced concrete beam elements.

1.5 Difficulties To Be Resolved

In the design of FDF systems, a major concern is what slip load to use in the dampers. This may be found by trial and error using several realistic ground motions matching that

of the site conditions. This is an expensive and tedious operation to perform and not suitable for practical routine design work.

The concept of optimum slip load was introduced by Pall and was defined as the slip force level of the dampers at which the response of the system (building) is at the minimum. For very high slip load, there will be no slipping, and for very low slip load, large slipping will occur, but the energy dissipation is small. It followed that there is an intermediate level at which the energy dissipation per cycle is a maximum. The concept of an optimum slip load for a frictional type (coulomb) of damping, is not a new concept. In the report by Rubicka (23), it was reported that several investigators were conducting energy dissipation research with dry surface materials, and it was found by the investigators that minimum response would occur for optimum clamping pressure.

1.6 Objectives of Present Study

A simple method is obviously required for preliminary analysis and design purposes. Non-linear response spectra for non-linear MDOF have been proposed to replace the time consuming time-history analysis. It appears that this might be plausible for the FDF systems.But the selection of the optimum

slip load must be resolved first. In chapter 2, a SDOF detailed parametric investigation is carried out to correlate the various variables affecting the dynamic response of the FDF systems. In chapter 3 a detailed study is also carried out to study the behaviours of the MDOF FDF systems under severe earthquake excitations, and from these analyses, a response spectrum is generated for the modal analysis of FDF under seismic loading under optimized condition. In chapter 4 the spectrum generated is tested for its accuracy by comparing the results against those obtained from the time-history analyses. In chapter 5, a new force reduction factor R is introduced for the FDF systems.

1.6.1 Organization of the report

Chapter 1 introduces the friction dampers.

Chapter 2 deals with a parametric study of SDOF systems

Chapter 3 deals with the study of single bay multi-storey steel frame, and a deformation spectrum is generated.

Chapter 4 reports the testing of the deformation response spectrum created in chapter 3.

Chapter 5 introduces the new force modification factor R for the FDF systems

Chapter 6 gives conclusions and recommendations

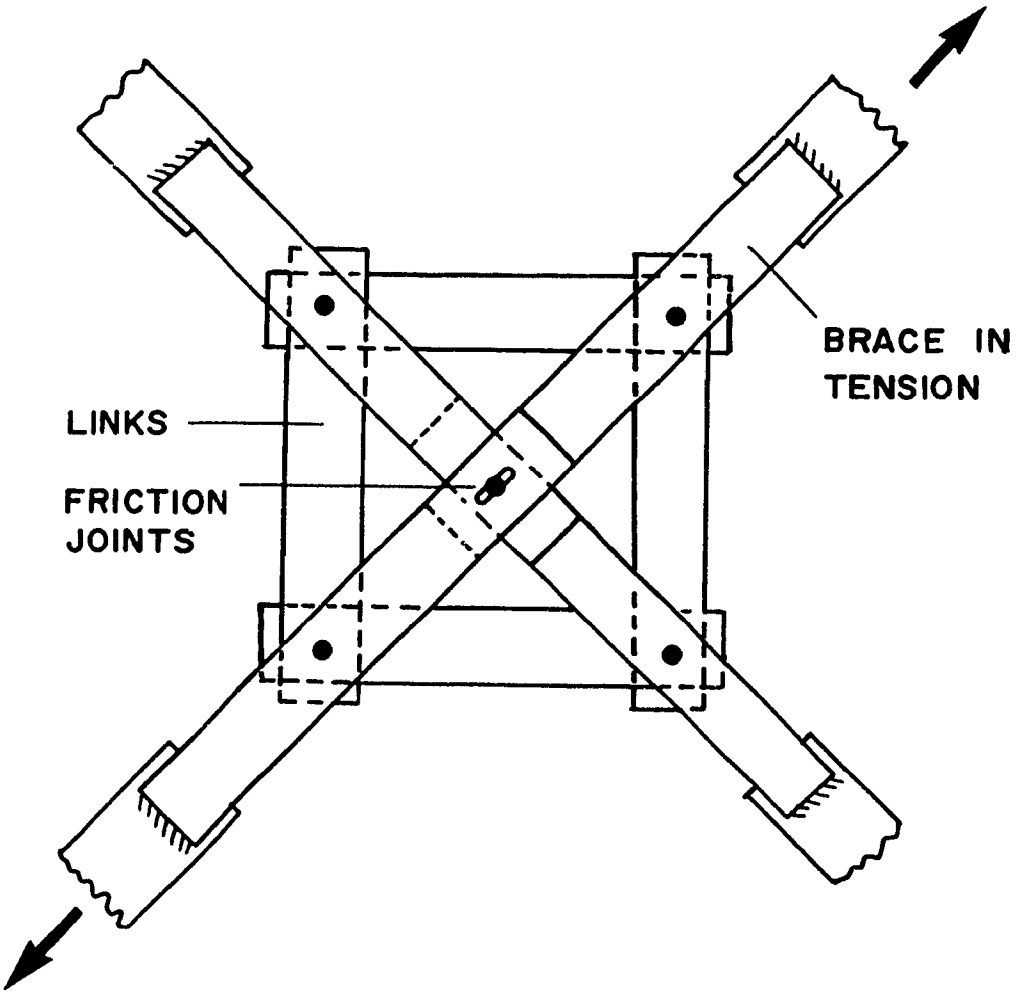

Figure 1.1 Typical tension friction damper (14)

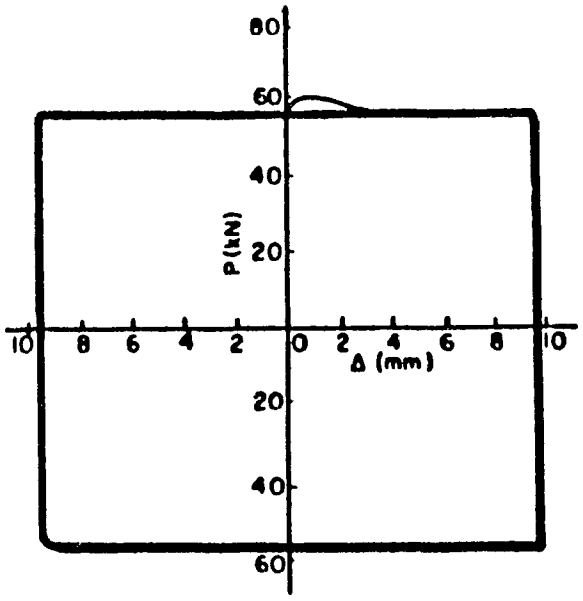

Figure 1.2 Typical hysteresis loop of a damper under cyclic loading (14)

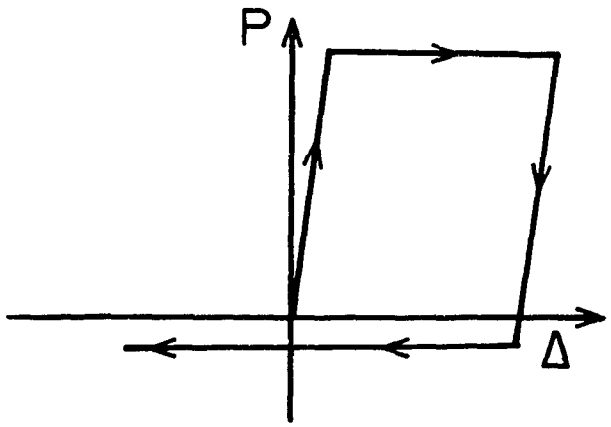

Figure 1.3 Typical hysteretic loop of one diagonal tension friction damper installed with the diagonal brace elements (14)

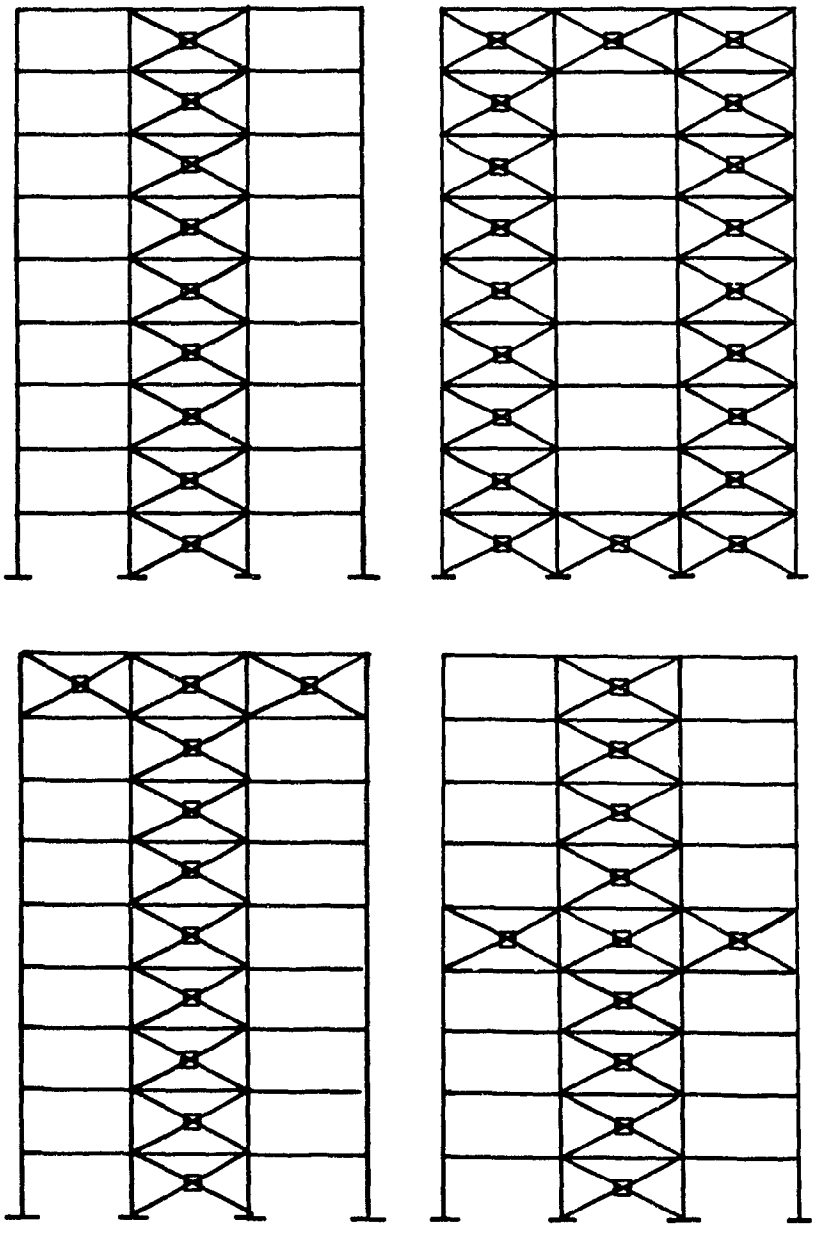

Figure 1.4 Some possible arrangements of friction damped frames (14)

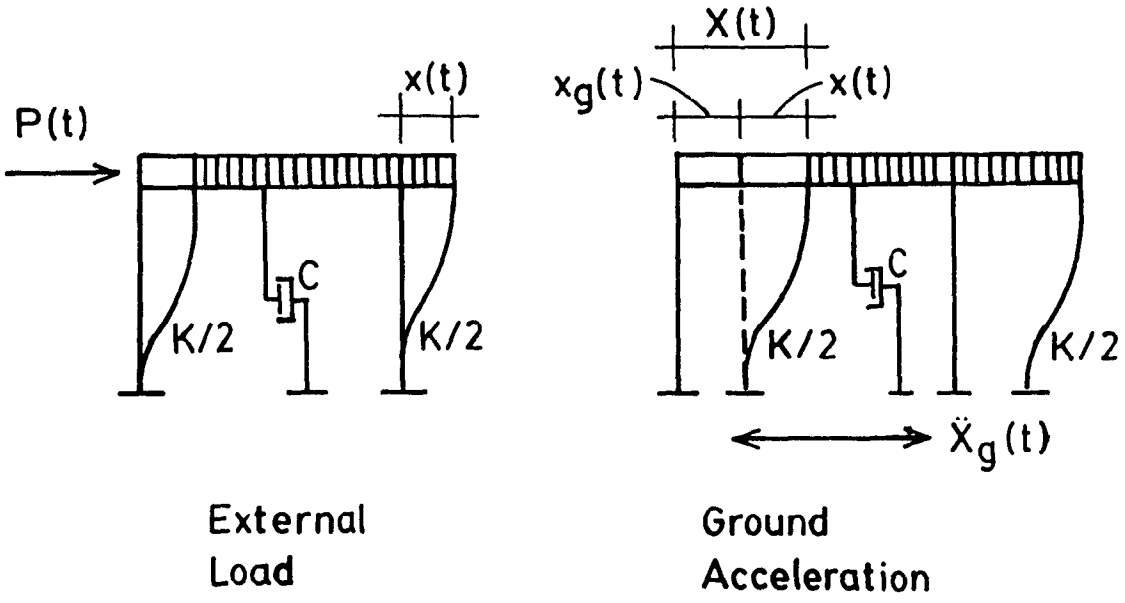

Figure 1.5 SDOF system subjected to external loads

2.0 SINGLE-DEGREE-OF-FREEDOM Friction-Damped Systems

Single-degree-of-freedom systems (SDOF) have been used successfully by many investigators to study the dynamic behaviour of non-linear systems. In this chapter, single degree of freedom systems consisting of a single storey, one bay friction damped frame is studied in details. In this way, the various important parameters can be identified more efficiently. The main parameters of interest are the slip load of the friction devices, the stiffness ratio between the braces and the columns, and the total reactive weight of the building.

2.1 Optimum Slip Load : A Quasi-Static Approach

The value of the optimum slip load for the FDF system is by far the most interesting and important parameter. For this is the variable which can be used to tune the building to reduce the dynamic response and to prevent a resonant response of a building structure in the event of an earthquake. A resonant response is said to occur when the dominant periods of the incoming ground motions matches that of the natural periods of vibration of the building, in which case large deformations and stresses are induced in the building structural members and collapse sometimes is unavoidable. In 1984 Baktash and Marsh (15) proposed a simple expression for

the optimum slip load based on the plastic moment capacity of the floor beam. Since this method serves as a basis for a more refined analysis, it is presented below briefly for the completeness of the section. A refined analysis to include the brace flexibility is considered in the following section. It must be pointed out that the approach method is quasi-static and is accurate for static monotonic loading, but under random like excitations, the solution can only be considered plausible at best.

2.1.1 Method Proposed by Baktash and Marsh

Consider the simple frame shown in Figure 2.1, where the bracing is effective in both tension and compression. The behaviour of this system is very close to that of a cross-braced FDF (incorporating Pall's friction device) where the bracing itself is effective in tension only. Let D be the horizontal deflection due to some lateral force V. It is assumed that this deflection corresponds to the slipping in the friction device. The work done against friction is then:

$$W_1 = V_1 D \qquad (2.1.1)$$

in which V_1 is the horizontal component of the slip force in the diagonal brace. The deflection of the moment resisting frame is related to the portion of the horizontal shear

carried by the frame action. If the stiffness of the frame without the brace is K, then from Figure 2.2, one can write that

$$V - V_1 = K D \qquad (2.1.2)$$

or

$$D = \frac{V - V_1}{K}$$

The energy dissipated by friction becomes

$$W_f = \frac{V_1 (V - V_1)}{K} \qquad (2.1.3)$$

This energy dissipation is maximized with respect to the slipping force by

$$\frac{d W_1}{d V_1} = \frac{V}{K} - \frac{2V_1}{K} = 0 \qquad (2.1.4)$$

which gives

$$V_1 = \frac{V}{2} \qquad (2.1.5)$$

and for the column shear,

$$V_c = \frac{V_1}{2} \qquad (2.1.6)$$

This represents a condition in which the shear force is shared equally between the columns and the diagonal. The maximum moment of the beam due the base shear forces can be found as:

$$M_p = V_c \cdot h = \frac{V_1}{2} h$$

or

$$V_1 = \frac{2 M_p}{h}$$

Since,

$$V_1 = P_s \cos \beta \qquad (2.1.7)$$

where β is the angle of the brace element measures from the horizontal. The optimum slip force for the friction device is then:

$$P_s = \frac{2 M_p}{h \cos \beta} \qquad (2.1.8)$$

In this manner, the optimum slip load for the storey is elegantly determined given the plastic moment capacity of the floor beam.

2.1.2 A More Refined Approach

In the above approach, the lateral deflection D is assumed to correspond with the amount of slipping in the device, thus allowing for no elastic stretching of the brace. This represents the case of infinitely rigid brace. For a practical frame with typical braces for strong winds and moderate earthquakes, the contribution of the stiffness of the braces to the total lateral stiffness is substantial but not infinite. It is clear that for a very flexible brace, the device may not slip at all, and hence there is a need to know the degree of rigidity required for the brace in order that the friction device becomes effective.

Figure 2.3 shows a single bay frction-damped frame system with the brace element effective in tension and compression. For simplification of the mathematical model to be in the derivation, the system is modeled in Fig. 2.4 as a SDOF system composed of two parallel springs in which one, representing the brace, is equipped with a coulomb-friction damper and the other represents the frame itself. The stiffness of the brace is K' and is defined as :

$$K' = \frac{A\ E}{L} \cos^2 \beta \qquad (2.1.9)$$

$$= \alpha\ K$$

where

α = ratio of K'/K

K = the lateral stiffness of the frame without the bracing

A = cross-sectional area of the bracing

E = Young's modulus

L = length of the brace

β = is angle of the brace element measures from the horizontal (see Fig. 2.3)

The horizontal component of the friction force F_f is related to the slipping force P_s by the expression:

$$F_f = P_s \cos \beta \qquad (2.1.10)$$

which is derived on the basis of equivalent energy dissipation. The model is loaded with a monotonically increasing force V which causes a corresponding displacement D. No slipping will occur as long as the force developed in the brace is insufficient to overcome the friction force F_f, i.e.,

$$K' D = \alpha K D < F_f$$

This condition is equivalent to the condition, for no slipping:

$$V < F_f \left(1 + \frac{1}{\alpha} \right)$$

When at the verge of slipping, let

V_0 = the applied force

D_0 = the displacement prior to slipping

We can write

$$F_f = K' D_0 = \alpha K D_0$$

$$V_0 = K (1 + \alpha) D_0 = K D_0 + F_f = F_f \left(1 + \frac{1}{\alpha} \right)$$

Now let the applied force be increased to its final value V, the additional displacement is D_s, which corresponds to slipping in the brace.

$$V = K (D_0 + D_s) + F_f$$

$$V = K \left(\frac{F_f}{\alpha K} + D_s \right) + F_f$$

$$V = F_f \left(1 + \frac{1}{\alpha} \right) + K D_s \qquad (2.1.11)$$

The energy dissipated by friction is :

$$E_f = F_f \, D_s$$

or

$$D_s = \frac{E_f}{F_f}$$

Equation (2.1.11) becomes :

$$V = F_f \left(1 + \frac{1}{\alpha} \right) + K \frac{E_f}{F_f}$$

or

$$E_f = \frac{F_f}{K} \left[V - F_f \left(1 + \frac{1}{\alpha} \right) \right] \qquad (2.1.12)$$

This equation gives the energy loss as function of the independent variables F_f, V, K, and α. To maximize E_f with respect to F_f,

$$\frac{d\,E_f}{d\,F_f} = \frac{1}{K} \left[V - 2\,F_f \left(1 + \frac{1}{\alpha} \right) \right] = 0$$

$$F_f^{opt} = \frac{V}{2(1 + 1/\alpha)} \qquad (2.1.13)$$

$$E_f^{max} = \frac{V^2}{4\,K\,(1 + 1/\alpha)} \qquad (2.1.14)$$

The total shear force in the frame columns is, in terms of the optimum slip load :

$$V - F_f = K (D_o + D_s)$$

$$= \frac{V}{2} \left[\frac{1 + 2/\alpha}{1 + 1/\alpha} \right]$$

$$V - F_f = F_f^{opt} \left(1 + \frac{2}{\alpha} \right) \qquad (2.1.15)$$

The results at optimum condition as shown in the equations (2.1.13), (2.1.14), and (2.1.15) are for a particular imposed force V, which in the case of earthquake excitation varies cyclically depending on the system responses which are functions of the slip load itself. In the previous approach, Baktash and Marsh have chosen V to correspond to the first yielding in beams. F_f^{opt} is found based on beam yielding as done by Baktash and Marsh:

$$M_p = V_c \; h$$

$$M_p = h \; \frac{F_f}{2} \left(1 + 2/\alpha \right)$$

$$F_f^{opt} = \frac{2\ M_p}{h\ (\ 1 + 2/\alpha\ )}$$

Thus the maximum slip load is

$$P_s = \frac{F_f^{opt}}{\cos\ \beta}$$

$$P_s = \frac{2\ M_p}{h\ (1 + 2/\alpha)\ \cos\ \beta} \qquad (2.1.16)$$

The right hand side of the preceding equation is, of course, the same as that of Baktash and Marsh when the parameter α is set to an infinite value. For a well-designed FDF system, the moments in the beams should not reach M_p.

In the present approach, the relative stiffness of the bracing is taken into account, whereby the effect of both member properties and frame geometry can be assessed. In practice, the brace stiffness is normally determined on the basis of service conditions, i.e., for strong wind and moderate seismic forces, and therefore it is likely to be high.

However, in the case of retrofitting existing buildings for upgrading its structural safety against major earthquakes, it may not be necessary to use heavy braces in conjunction with the friction devices. An appropriate brace stiffness can be chosen easily from equation (2.1.14) which is again shown below in a rearranged form:

$$\frac{4\ K\ E_f^{max}}{V^2} = \frac{1}{1 + 1/\alpha} \qquad (2.1.14)$$

This equation is plotted in Figure 2.5 for α up 20. Since the energy dissipated increases at a decreasing rate, as α is increased, it is clear from this figure for α greater than 10, the extra energy dissipated is not significant. For $\alpha = 1$, the term $4\ K\ E_f^{max}/V^2$ equals 0.5, which states that the energy dissipated is 50 % of the maximum possible. For $\alpha = 10$, the rate is 91%. The validity of the argument will be examined in the next section by performing a non-linear dynamic analysis of the SDOF systems.

2.2 OPTIMUM SLIP LOAD : NON-LINEAR ANALYSIS

As stated in the previous sections, the equations derived for the optimum slip load are based on a quasi-static approach, and thus may have little meaning for systems under random excitations. To use the Drain-2D computer program to

model a SDOF system for a parametric study is feasible but the process is tedious and cumbersome. Furthermore, its main output it limited to the maximum deflection. It was decided then to develop a special purpose computer program to carry out the nonlinear analysis of the spring model shown in Figure 2.4. The derivation is shown in details below leading to the development of a simple computer routine.

2.2.1 The Governing Equation of Motion

The equation of motion as obtained in section 1.4 is shown below:

$$M \ddot{X} + C \dot{X} + K X = - M \ddot{X}_g$$

For the system as shown in Figure 2.4, the equation of motion for this system can be written as :

$$M \ddot{X} + C \dot{X} + \dagger K X + Fd = - M \ddot{X}_g \qquad (2.2.1)$$

where

M = the mass of the system

C = the viscous damping coefficient

$\dagger K$ = the stiffness of the system

Fd = the dry friction damping force

X = the relative displacement of the frame

$\dot{X}$ = system's velocity

$\ddot{X}$ = system's acceleration

where dot means the first time derivative of the displacement, and double dots means the second derivative. X_g is the ground displacement. For no slipping, i.e., when

$$K' \,|X| = \alpha K \,|X| < F_f ,$$

then the system stiffness is :

$$|K = K + K'$$

$$Fd = 0$$

During slipping, i.e., when

$$K' \,|X| = \alpha K \,|X| \geq F_f$$

$$|K = K$$

$$Fd = F_f \frac{\dot{X}}{|\dot{X}|}$$

Closed form solutions to the equation of motion such as that of eqn. 2.2.1 exist only for a few loading functions. Since the right side of the governing equation of motion (2.2.1) is likely to be a discontinuous function, a closed form solution may not exist. Therefore step by step numerical

integration is more convenient. The following describes briefly the numerical scheme used for solving the equation.

2.2.2 Numerical Solution to the Equation of Motion

Figure 2.6 shows the bilinear load deformation curve for the simplified model of the system. The equation of motion is solved by assuming a linear response acceleration for the system between each time step, as depicted in Figure 2.7. The numerical scheme for the integration of the equation of motion is developed in a fairly standard fashion as shown in the following reference (24).

At any time t_{i+1} the equation of motion is:

$$M \ddot{X}_{i+1} + C \dot{X}_{i+1} + \mid K X_{i+1} + F_{di+1} = - M \ddot{Xg}_{i+1} \qquad (2.2.2)$$

and at any time t_i:

$$M \ddot{X}_i + C \dot{X}_i + \mid K X_i + Fd_i = - M \ddot{Xg}_i \qquad (2.2.3)$$

Now subtracting equation 2.2.3 from 2.2.2 yields the incremental form of the equation of motion :

$$M(\ddot{X}_{i+1}-\ddot{X}_i) + C(\dot{X}_{i+1}-\dot{X}_i) + \mid K(X_{i+1}-X_i) + (Fd_{i+1}-Fd_i) = - M(\ddot{Xg}_{i+1}-\ddot{Xg}_i) \qquad (2.2.4)$$

The equation of motion in an incremental form is :

$$M\ \ddot{\Delta X} + C\ \dot{\Delta X} + K\ \Delta X + Fd_{i+1} - Fd_i = -M\ \ddot{\Delta X}g \qquad (2.2.5)$$

where ΔX represents the increment between the time t_i and t_{i+1}.

By assuming a linear acceleration response between each time step as shown in Fig. 2.7, the following relations can be derived for the incremental acceleration:

$$\ddot{\Delta X} = \frac{6\ \Delta X}{\Delta t^2} - \frac{6}{\Delta t}\ \dot{X}_i - 3\ \ddot{X}_i \qquad (2.2.6)$$

and for incremental velocity:

$$\dot{\Delta X} = \frac{\ddot{\Delta X}\ \Delta t}{2} + \ddot{X}_i\ \Delta t \qquad (2.2.7)$$

Substituting for $\ddot{\Delta X}$ from eqn. (2.2.6) yields:

$$\dot{\Delta X} = \frac{3\ \Delta X}{\Delta t} - 3\dot{X}_i - \frac{\Delta t}{2}\ \ddot{X}_i \qquad (2.2.8)$$

equations 2.2.6 and 2.2.8 become:

$$\ddot{\Delta X} = \frac{6}{\Delta t^2}\ X - A_n \qquad (2.2.9)$$

$$\dot{\Delta X} = \frac{3}{\Delta t}\ \Delta X - B_n \qquad (2.2.10)$$

where

$$A_n = \frac{6}{\Delta t}\,\Delta\dot{X} + 3\,\ddot{X}_i \qquad (2.2.11)$$

$$B_n = 3\dot{X}_i + \frac{\Delta t}{2}\,\ddot{X}_i \qquad (2.2.12)$$

Substitution of equations 2.2.9 and 2.2.10 into 2.2.5 yield, after rearranging and collecting terms :

$$\left[\frac{6\,M}{\Delta t^2} + \frac{3\,C}{\Delta t} + {}^{\dagger}K\right]\Delta X = M\,A_n + C\,B_n - [Fd_{i+1} - Fd_i] - M\,\Delta\ddot{X}g$$

From the equation shown above, solving for ΔX, one obtains,

$$\Delta X = \frac{\dfrac{6\,M}{\Delta t} + \dfrac{3\,C}{\Delta t} + {}^{\dagger}K}{M\,A_n + C\,B_n - (Fd_{i+1} - Fd_i) - M\,\Delta\ddot{X}g} \qquad (2.2.13)$$

or

$$\Delta X = \frac{P^{*}}{{}^{\dagger}K^{*}} \qquad (2.2.14)$$

where

P^{*} = is the modified effective incremental force of the system

${}^{\dagger}K^{*}$ = is the modified effective incremental stiffness of the system

With the above equations, the response at each time step t_{i+1} can be calculated, knowing the previous response values at time t_i. The incremental change in X is found first. With ΔX known, the change in velocity and acceleration can be found from equations (2.2.9) and (2.2.10) and the solutions at t_{i+1} are updated.

In order to minimize the accumulation of error, the equation of motion, rather than equation 2.2.9, is used to determine the acceleration at the next time step as follows:

$$\ddot{\Delta X} = - \ddot{\Delta X}_g - C\,\dot{\Delta X} - \frac{K}{M}\,\Delta X - \frac{1}{M}\,[\,Fd_{i+1} - Fd_i\,]$$

and

$$\ddot{X}_{i+1} = \ddot{X}_{i+1} + \ddot{\Delta X}$$

Thus an unbalanced force at the end of a time step is converted into the next input ground acceleration. To further reduce the accumulation of errors, the time step is taken as small as possible. Generally a time step of 0.001 sec is used. In some special cases this time step is halved. The choice of time step is done by successive reduction until the responses computed do not seem to change significantly. The program was written using Fortran 77 on the mini-computer VAX 11/785 available at the CBS at the courtesy of SIRICON. Double precision is used throughout for all variables used in the

program. A listing of the source code is shown in the Appendix.

2.2.3 Verification of the Routine

The routine was verified for its reliability before it could be used with confidence. To do this, the Drain-2D program was used to generate the solutions for some test cases. A simple arbitrarily inelastic system is modeled using the Drain-2D frame dynamic analysis. The El Centro data is used as the ground excitations. The same model again is used in the SDOF routine, and the results obtained in both cases are compared. The time-history displacements obtained for both case are plotted as shown by Figure 2.8.1.

For illustration purposes, the initial three seconds of the results obtained are shown only for each case. As can seen from the figure, the two lines are almost identical, except that for the line from the Drain-2D output is seen to zig-zag somewhat. This is due to the rounding off the values to three decimal places internally by the output subroutine OUT1 by DRAIN-2D whereas that of the output for the SDOF routine is plotted with a four decimal place values. Since the output from the Drain-2D does not contain the velocity and acceleration responses, it cannnot be compared with that of the routine. Nevertheless, if the time history solution of

the displacement from the SDOF routine is identical to that of DRAIN-2D, then it can be said that the solutions from the SDOF routine are correctly computed. The only problem of concern is the over-shooting of the loads beyond the yield force level. This is corrected but is not as elegantly done as in the DRAIN-2D routine. This overshooting can be avoided as much as possible by using a time step as small as possible and by using double precision for all computations.

Figure 2.8.2 shows typical hysteretic load-deformation, characteristic of a system under the NBK earthquake excitation, for illustration only. For this particular output a flexible system with K=450 kN/m, mass=10.9 tons, and Ps = 20 kN is used. The plot is obtained from a time-history output and post processing for plotting on the IBM PC. A total of about 3000 points are used for creating the plot. Kinks, observed on the upper levels of the straight line, are due to over shooting of the force level in the brace member. This is due to the large time-step used in the computations for this particular example. Figure 2.8.3 shows the typical plot for the brace element, or the friction element.

2.3 Detailed Investigations

The simple routine described in the previous section is used for the parametric study of nonlinear SDOF FDF

systems. The program can be modified very simply to accommodate changes in the parameters under investigation. Three earthquake records will be used as the ground motion inputs. Two of which, the El Centro and the Olympia earthquakes, were records of actual events, and the third, the Newmark-Blume-Kapur record, was artificially generated. The first seven seconds of the records of the El Centro is scaled to the original peak intensity at 0.33g, and the thirty second 1952 Olympia record scaled to 0.35g. The 15 second artificial Newmark-Blume-Kapur records was generated to match a typical earthquake loading spectrum, having an increasing load with time, then levelling off with a constant load, and then finally unloading. This particular record is scaled to 0.30 g peak intensity.

The NBK record shown in Fig. 2.9.1 is used because of its wide frequency content. This record is more severe than that of El Centro. It was discovered, from analyses of several FDF systems using the NBK records for the same system, to match a maximum response calculated from using a 0.30 g NBK data as ground motion input, about 0.50 g of the El Centro record would be required. The 1940 El Centro record shown in Fig. 2.10.1 was at one time believed to be the strongest to be recorded on firm soils. At 0.33 g it was used extensively for dynamic analysis of structures. Then the 1.25 g was recorded at the San Fernando Dam which proved that higher

acceleration was possible. The Olympia records shown in Fig. 2.11.1 is used also because of its special characteristics on firm soils. Viscous damping ratio frequently used for dynamic analysis of structures ranges from 1 to 5% critical. However with mechanical supplemental damping devices, it is expected that the equivalent damping ratio will exceed the normal 1 to 5 % maximum as usually assumed for the dynamic analysis.

Since the FDF systems will likely provide an equivalent damping ratio in excess of 20 %, it is interesting to examine the dynamic response with higher damping ratios. But most response spectra generated were usually calculated with a critical damping ratio of up to 20 % maximum. By using the solution by Dempsey and Irvine (25), a series of elastic response spectra were developed for critical damping ratios ranges from 0 to 80 %. The integrations were carried out for the NBK, El Centro and the Olympia data. It is noted that for the NBK data, no existing response spectrum can be found for this widely used record. The acceleration, velocity and deformation spectra are created and plotted, but only the acceleration spectra are shown here. Fig. 2.9.2 shows a plot of the response acceleration of a SDOF system subjected to the N.B.K. record with varying critical damping ratios. Fig. 2.10.2 is the same for the EL-Centro record, and Fig.2.11.2 is for the Olympia record. From these acceleration spectral plots, it is evident that the maximum response is reduced

rapidly with increasing damping ratio up to 20 %. Thereafter, the reduction is less significant. This is true for all three earthquake records.

Four SDOF FDF systems were used in the parametric study. Table 2.1 lists the properties of the systems considered. Frame No. 1 represents a single bay with very heavy columns. The mass of about 11 metric tons approximates that of a typical roof load of one bay with some accumulated snow. Frame No. 2 has less stiff columns but with the same mass. Frame No. 3 represents a rather flexible frame with lesser mass of about 7 tons. Frame No.4 is the same as No.3 except the mass is 13 tons. This is done to obtain a higher natural period. Table 2.1 also lists the natural periods of the frames corresponding to α which represents the relative stiffness of the bracing. Since most earthquakes on firm soils have high energy contents in the higher frequency or low period range, the systems chosen seem appropriate enough, since all systems have low first periods of vibration.

The variables of interest in this study are the slip loads and the relative stiffness α of the system. In the analyses, the parameter α is varied from 0 to 12, since beyond which there will be little change in the responses as proposed in the previous section. For each α, the slip load P_s is varied from 0.00 to 60.0 kN. For each P_s value, the response

was computed and the maximum acceleration, velocity and deformation were kept for post-processing. Zero viscous damping was used for all analyses.

A time step of 0.0005 second was used for the 15 second duration NBK earthquake, and this required about 30000 total time steps for the entire record to be computed for each Ps. Therefore for each a value, an internal loop of 120 times were made through the 30000 time step computations yielding 120 data points for plotting the curve of the response. For the 7 second El Centro, a time step of 0.0025 was found to be adequate. And for the 30 second Olympia record, a time-step of 0.001 was used.

The results obtained from the calculations by using the SDOF routine for frame no. 1 are plotted in Figures 2.12.1 to 2.13.3, for frame no. 2 in Figures 2.14.1 to 2.15.3, for frame no. 3 in Figures 2.16.1 to 2.17.3, and for frame No.4 in Figures. 2.18.1 to 2.19.3 for the NBK, El Centro and the Olympia earthquake records respectively. Since only the maximum response of the systems is required for this study, no data from the time history will be presented.

2.3.1 Analysis of Frame # 1

The maximum acceleration response of the frame

subjected to the three different earthquakes all have the similar trend. First, as the slip load increases, the response decreases rapidly to a low point and after which it starts to increase slowly as the slip load increases. This implies that there is a certain slip load at which the spectral acceleration is minimum. This "so called" optimum slip load for all three earthquake records seems to be between 0.12 and 0.20 of the ratio of P_s/Weight for the all the three earthquakes. It is observed that when a reaches 8 say, the further reduction in the response is rather small. The corresponding deformation responses shown in Fig. 2.13.1 to 2.13.3 are seen to decrease rapidly as the slip load is increases. When the low point is reached, it remains rather insensitive after that. With the exception of the Olympia response which seems to increase somewhat after the low point is reached. The low point for the NBK and the El Centro seems to be located in the same neighbourhood of say, 0.15 to 0.20 P_s/Weight. Whereas in the Olympia response, the low point is located at about 0.10 P_s/Weight. Again is observed that when the a reaches 8, reduction in the response is not significant.

2.3.2 Analysis of Frame # 2

The acceleration response for frame no. 2 are plotted in Figure 2.14.1 to Figure 2.14.3. They are almost identical to that of frame no. 1. Again, it is seen that when a exceeds 8,

the reduction in the dynamic response is not that much. The low point for the NBK and El Centro is located at bout 0.18 P_s/Weight. Except that the low point for the Olympia record is shifted to the left to from 0.08 to 0.10 P_s/Weight. For the displacement response, the common low point is again located at about 0.20 P_s/Weight. Again it is observed that little increase in the reduction of the response is obtained.

2.3.3 Analysis of frame # 3

The acceleration response of frame No.3 are plotted in Figures 2.16.1 to 2.16.3. They appear to be almost similar to that of frame 1 and 2. After a low point is reached, the acceleration response starts to increase again. For the this frame the weight used is 7 tons (69 kN). For the N.B.K. record, the low point is located at about 0.20 P_s/Weight. For the EL Centro record the low point is about 0.10 P_s/Weight. The deformation response are plotted in Figures 2.17.1 to 2.17.3. The low point for the N.B.K. and Olympia records is located around 0.20 P_s/Weight. But for the El Centro, the low point is at about 0.10 P_s/Weight.

2.3.4 Analysis of frame # 4

The acceleration response for frame No. 4 are plotted in

Figures 2.18.1 to 2.18.3. The weight used was 128 kN. The low point in this case for the N.B.K. is found to be about 0.10 P_s/Weight. For the El Centro data it is about 0.15 P_s/Weight. But for the Olympia, it appears to be around 0.08 P_s/Weight. The deformation response are plotted in Figure 2.19.1 to 2.19.3. Again the general trend is similar to those shown previously, but in this case the low point for the NBK is around 0.30 P_s/Weight, which that of EL Centro is about 0.10 P_s/Weight. For the Olympia the low point is about 0.20 Ps/Weight.

2.4 Summary

From the observations made on the results shown, the slip load P_s required for a minimum response for a frame is difficult to pin-point. It appears that even for the same frame but analyzed with different ground motions, the P_s for a minimum response is different. But a range of values can be said to be the optimum as the response does not seem to change much. This was observed for all four frames analyzed. It was also found that, from the derivation of the more refined approach to obtain the optimum slip load, the relative stiffness ratio, α does play an important part in the response of the frame. When α exceeds 8 or 10, the incremental energy dissipation is insignificant. The energy balance method will probably give a better picture of the amount of energy

dissipated, but this itself is a major task and will not be dealt here.

The optimum slip load expression (eqn. 2.1.16) is based on a quasi-static approach. This slip load, as limited by beam or column yielding, appears to be the best that one can do in order to strengthen an existing buildings by retrofitting with the friction device. However, the quasi-static "optimum slip load" does not provide any information regarding the design of a new structure against a specific earthquake intensity.

Table 2.1 Systems used for SDOF Analysis

Frame no.	Spring kN/m	Mass metric-tons	α	To (sec)
1	4491	10.9 (107 kN)	0	0.310
			2	0.179
			4	0.139
			6	0.117
			8	0.103
			10	0.093
			12	0.086
2	3000	10.9 (107 kN)	0	0.379
			2	0.219
			4	0.169
			6	0.143
			8	0.126
			10	0.114
			12	0.105
3	2000	7.0 (69 kN)	0	0.372
			2	0.215
			4	0.166
			6	0.140
			8	0.124
			10	0.112
			12	0.103
4	2000	13.0 (128 kN)	0	0.507
			2	0.292
			4	0.227
			6	0.191
			8	0.169
			10	0.153
			12	0.140

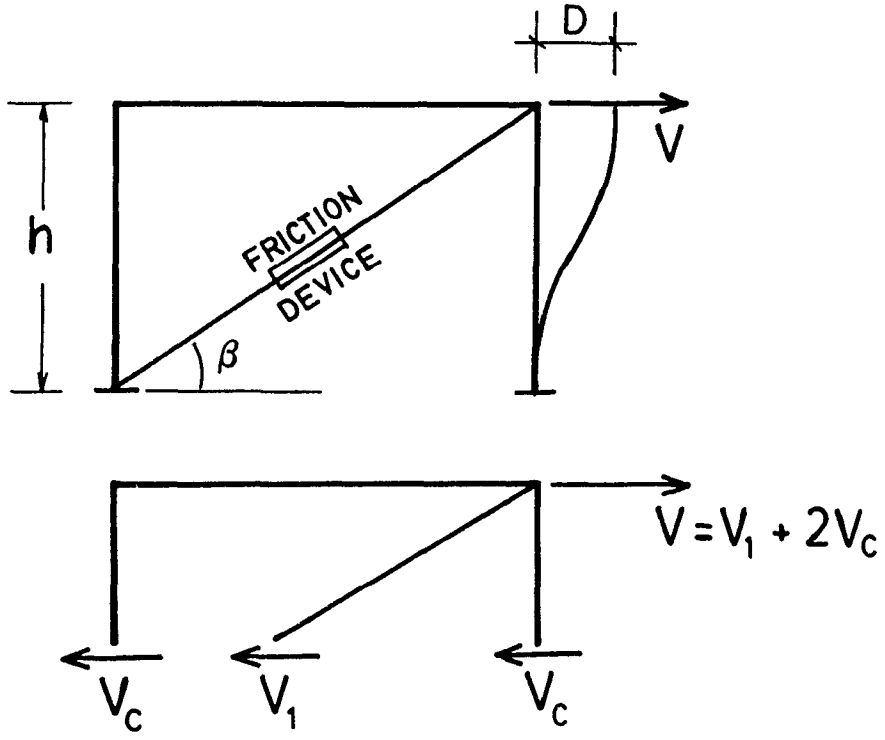

Figure 2.1 Single Storey Braced Frame

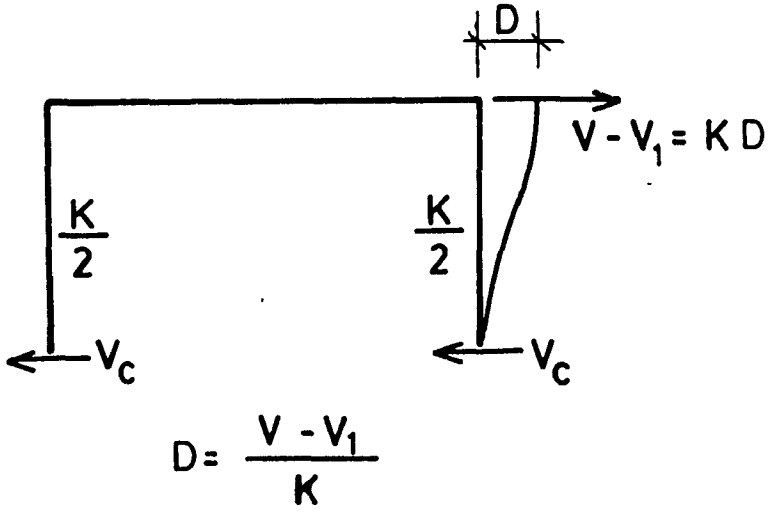

Figure 2.2 Single storey Moment Resisting Frame

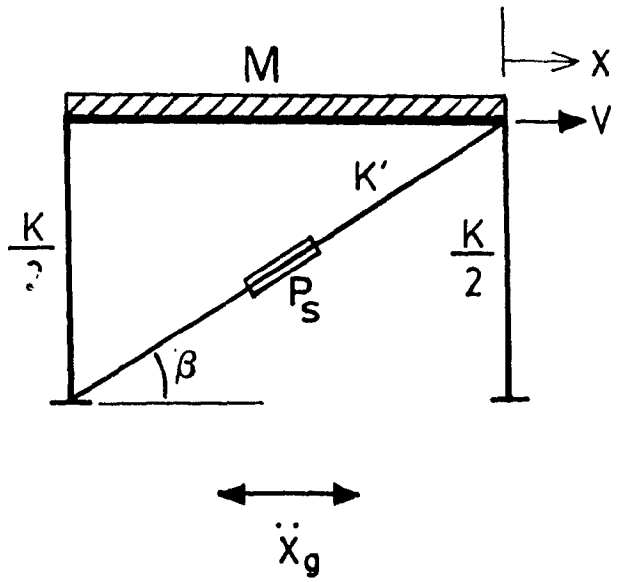

Fig. 2.3 Actual SDOF system for the FDF

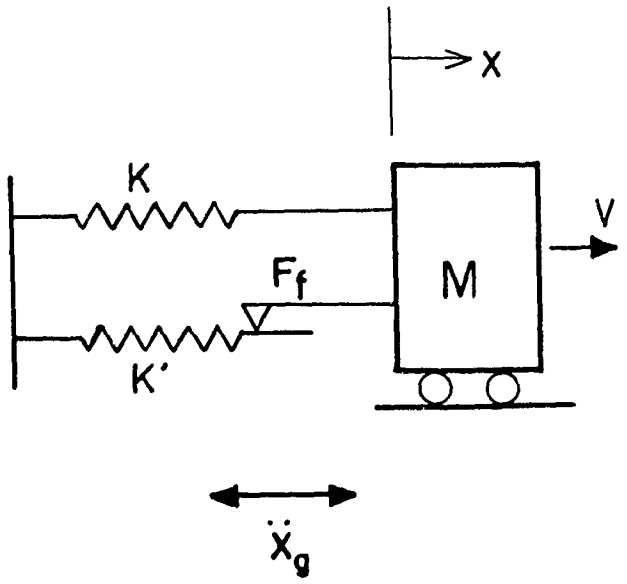

Figure 2.4 Equivalent System

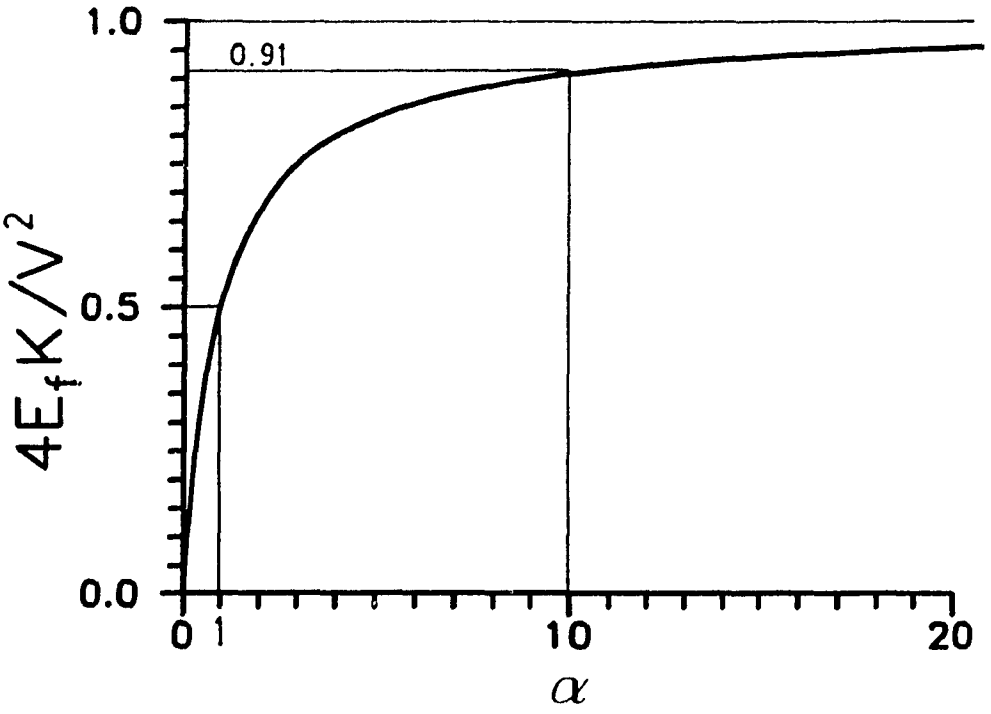

Fig. 2.5 Plot of 4 E_f K / V^2 vs. α

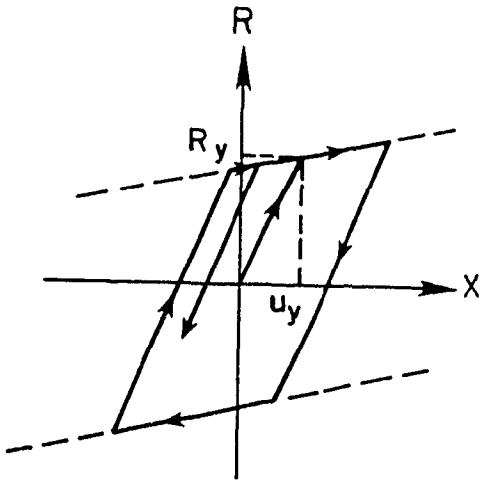

Fig. 2.6 Typical bilinear behaviour

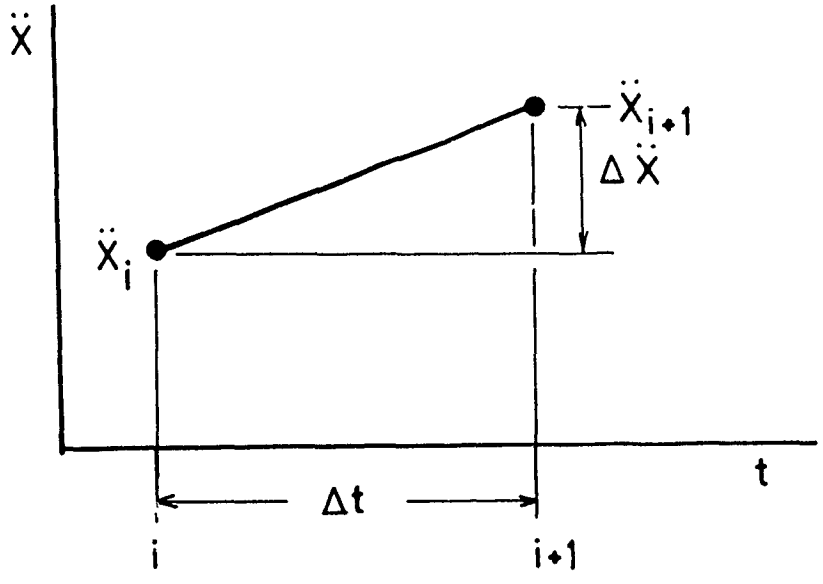

Fig. 2.7 Assumed linear acceleration response

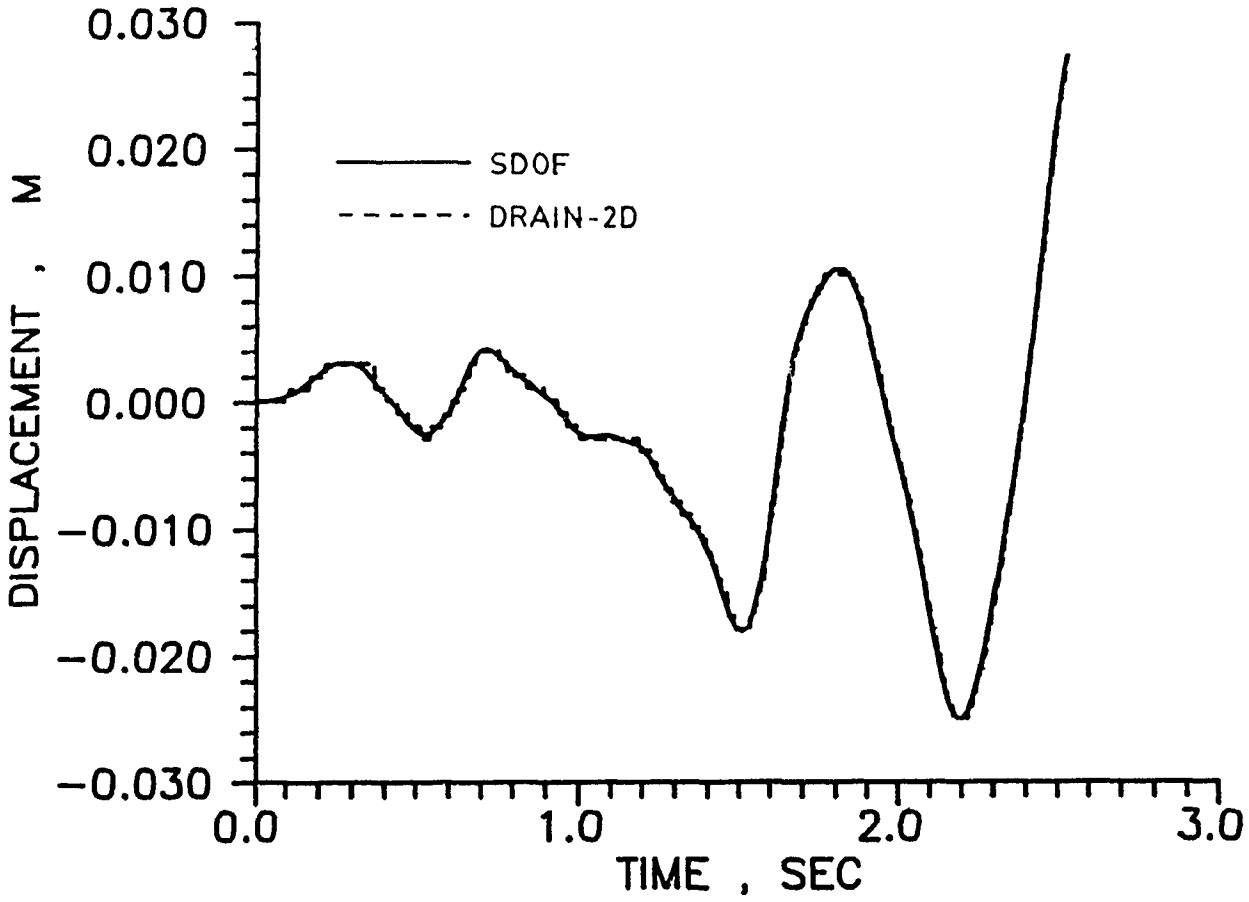

Fig. 2.8.1 Comparison of output for SDOF and DRAIN-2D

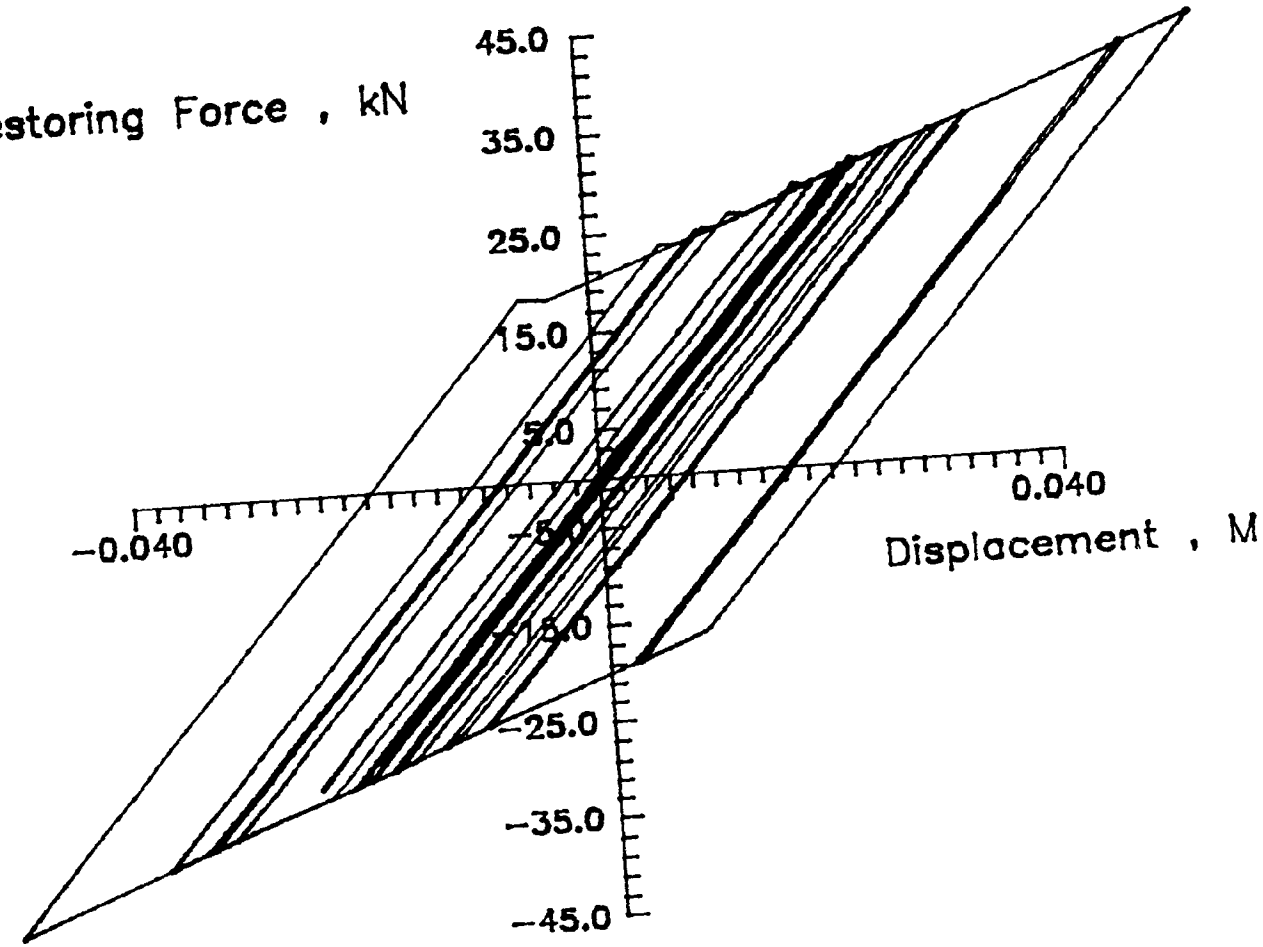

Fig. 2.8.2 Plot of System's force vs deformation

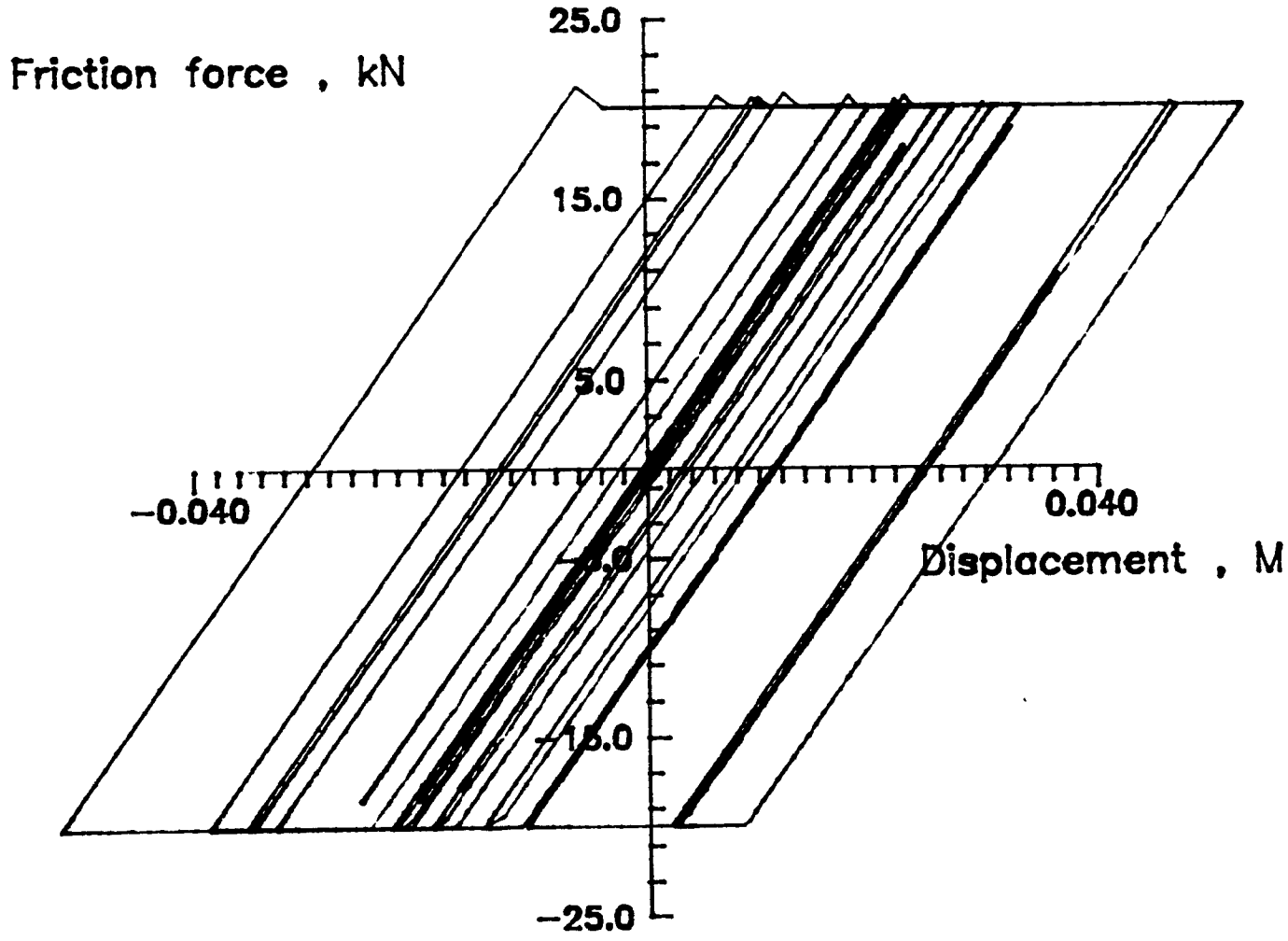

Fig. 2.8.3 Plot of brace's foces vs deformation

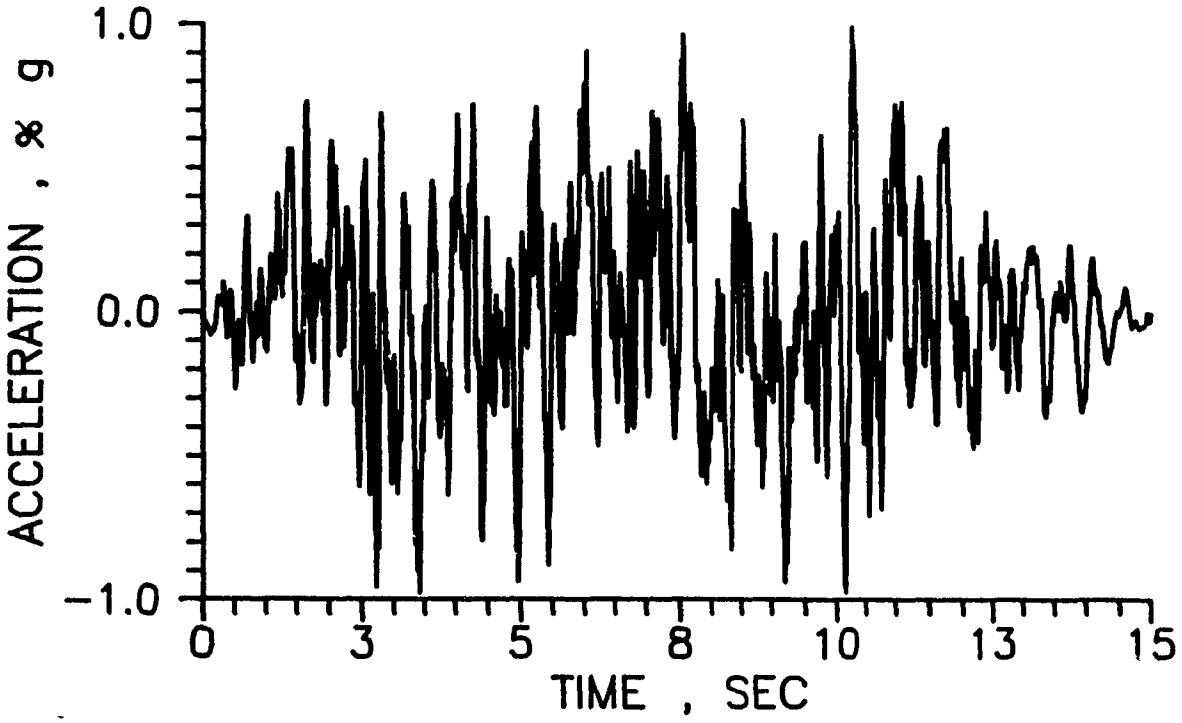

Fig. 2.9.1 Time history record of NBK

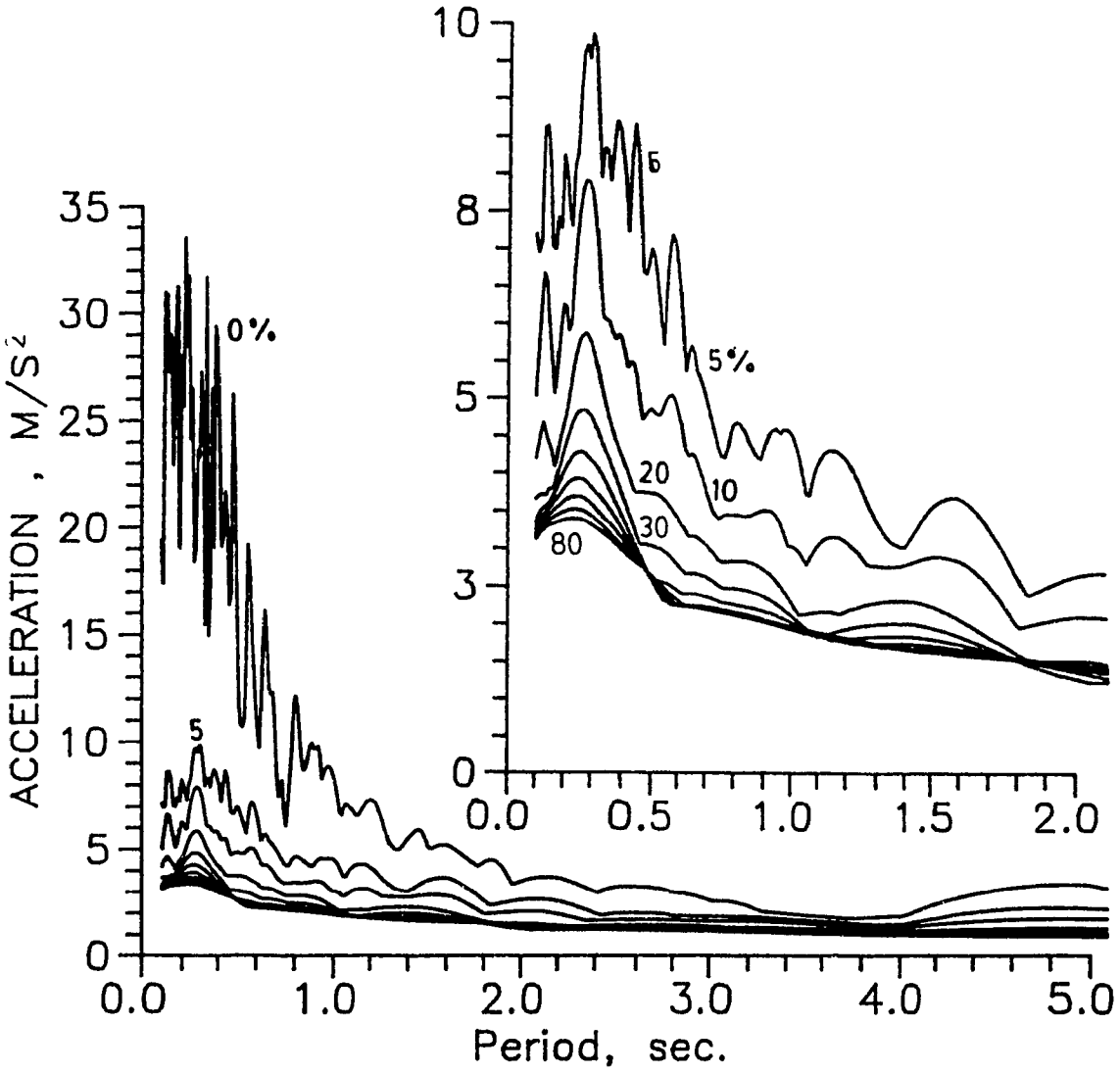

Fig. 2.9.2 Response acceleration of NBK for critical damping 0.0 to 0.8

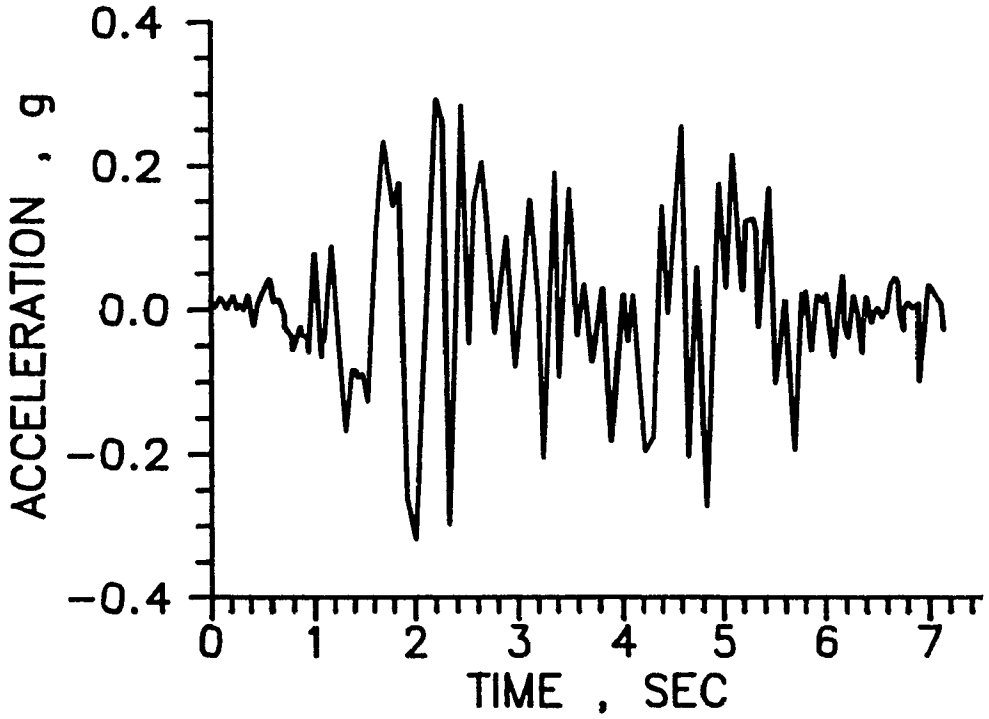

Fig. 2.10.1 Time history record of El Centro

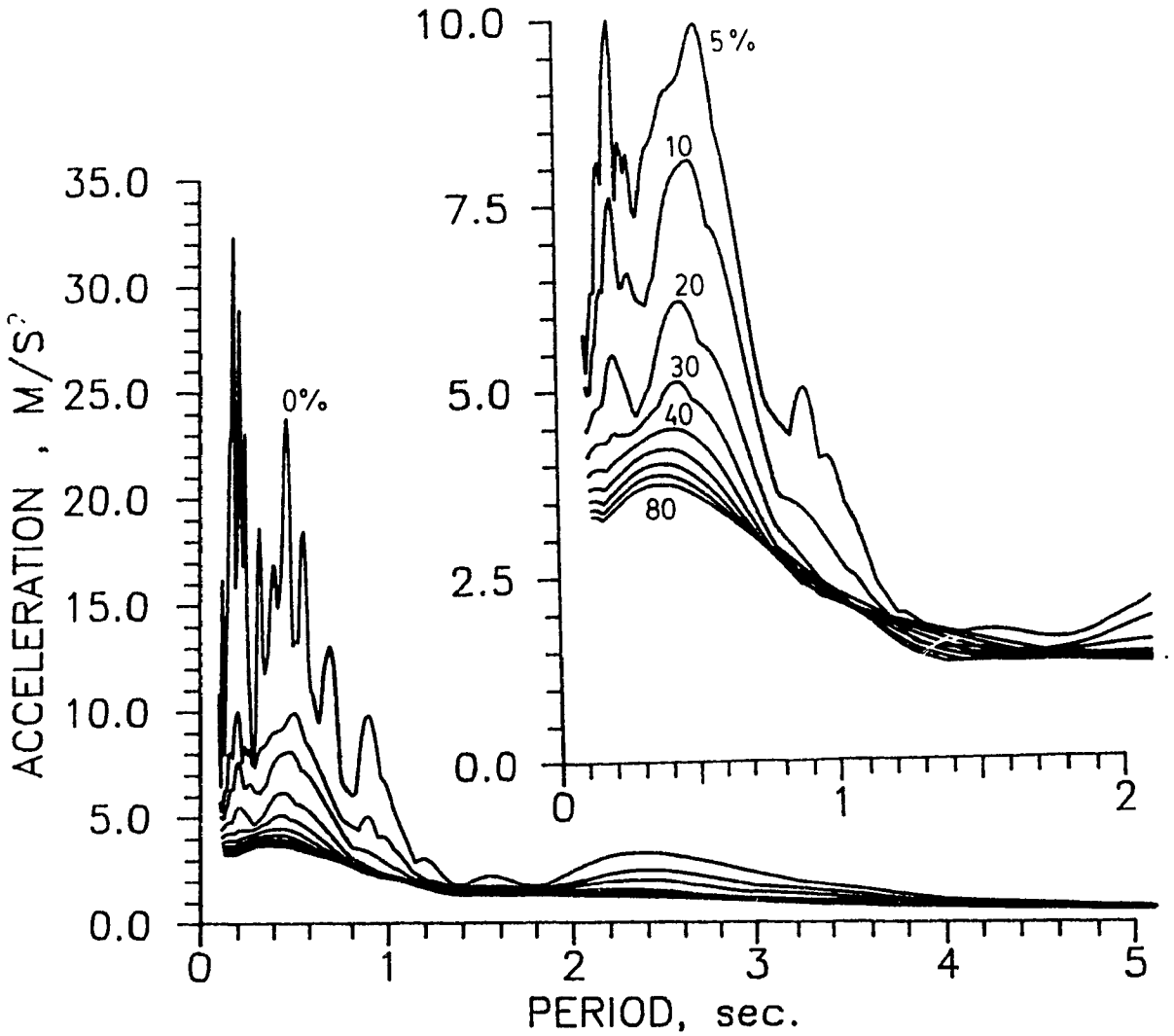

Fig. 2.10.2 Response acceleration of El centro for critical damping 0.0 to 0.8

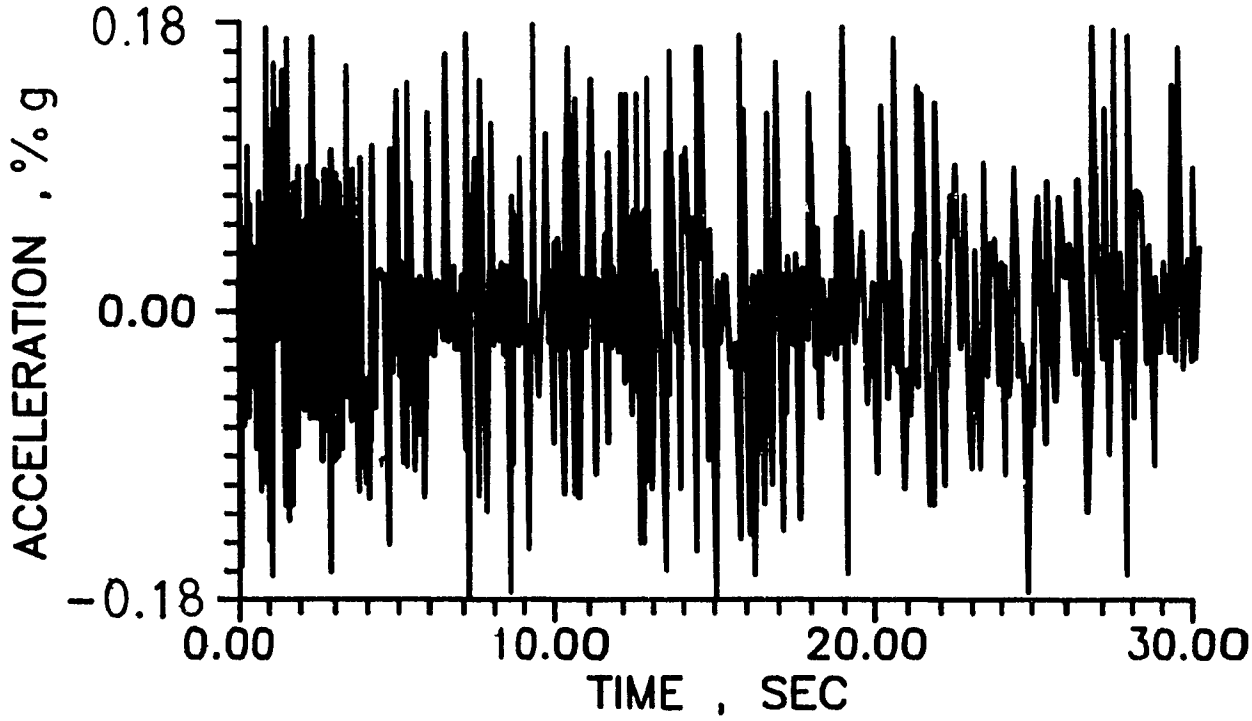

Fig. 2.11.1 Time history record of Olympia

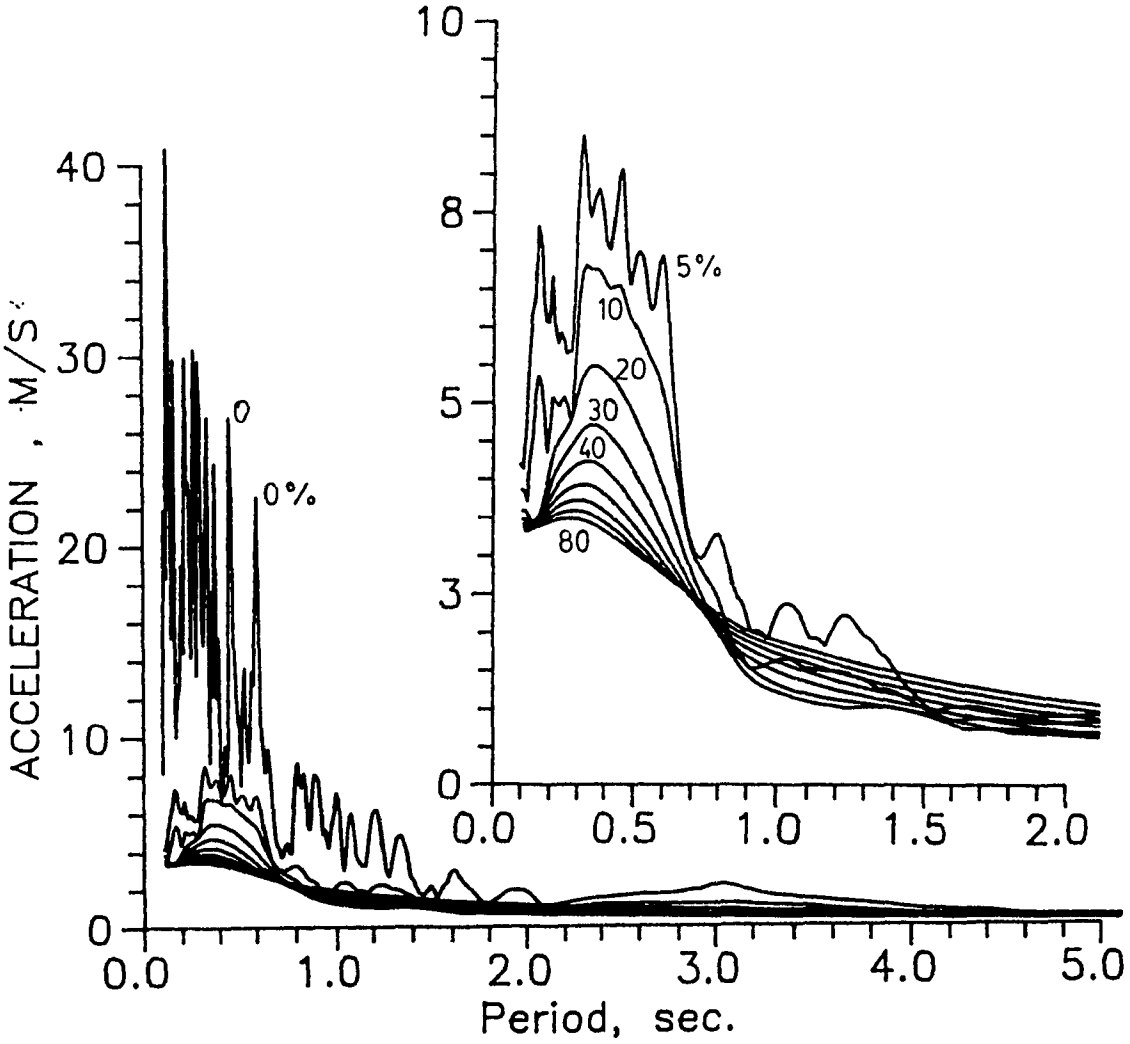

Fig. 2.11.2 Response acceleration of Olympia for critical damping 0.0 to 0.8

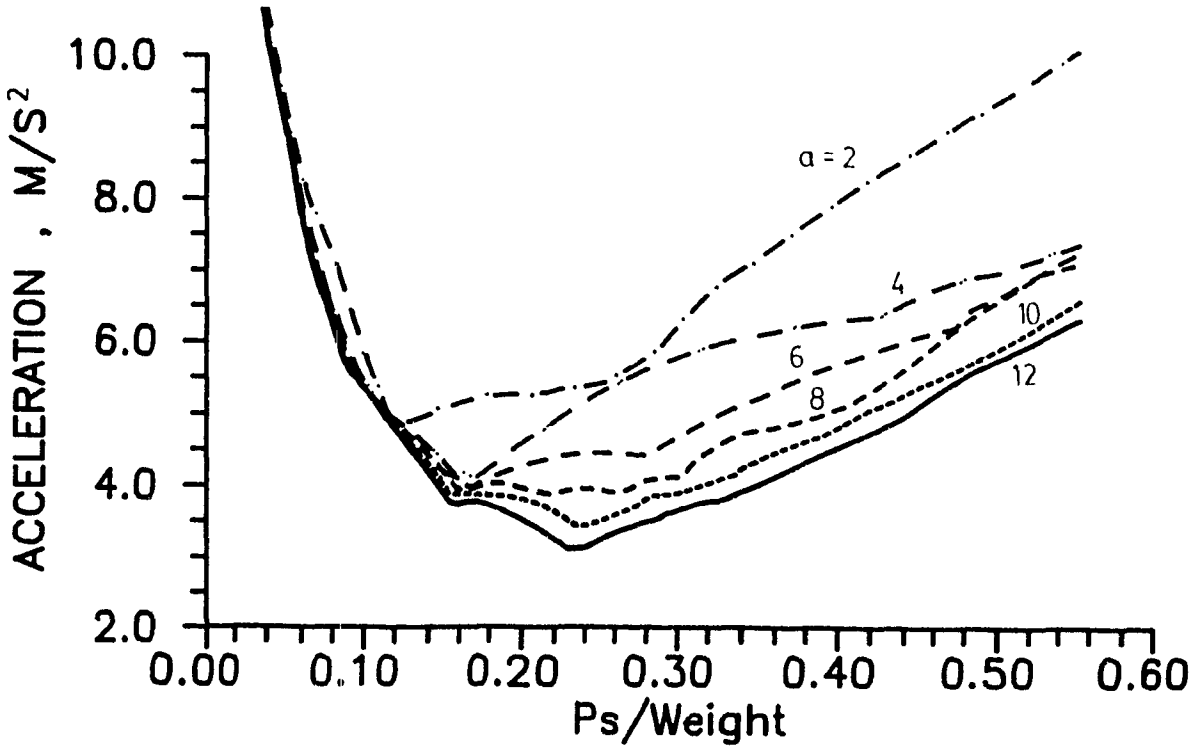

Fig. 2.12.1 Response acceleration for frame no. 1 , NBK

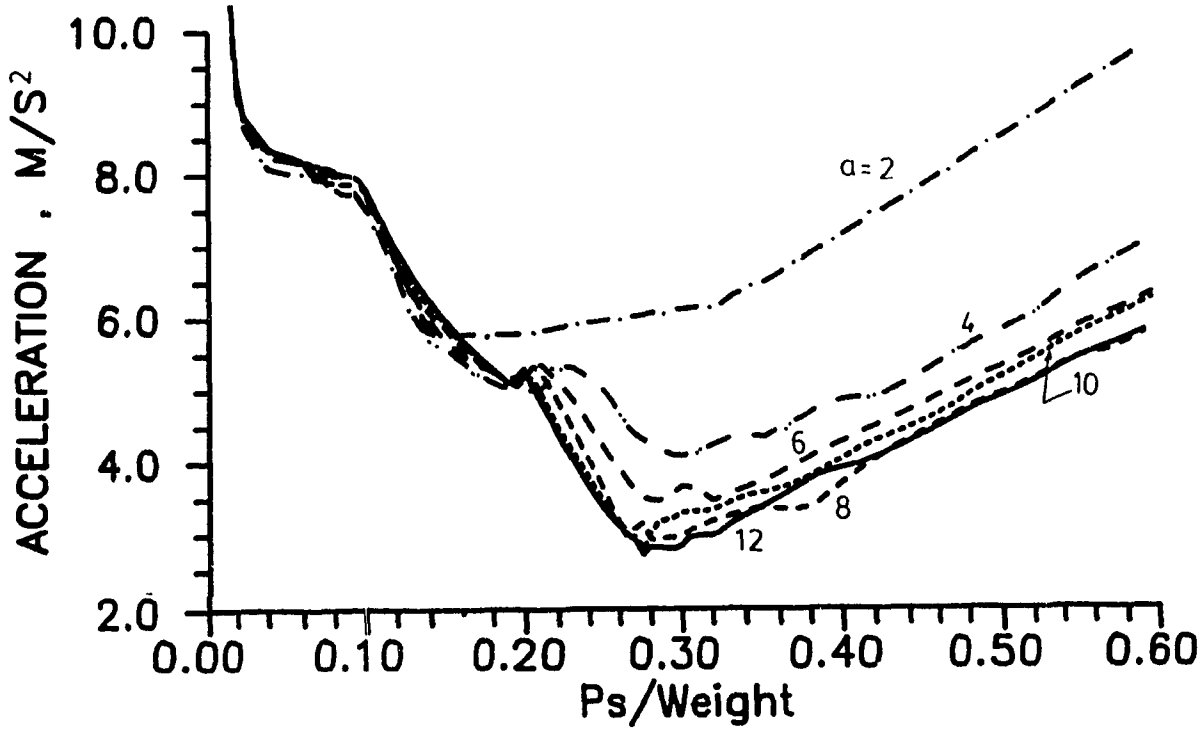

Fig. 2.12.2 Response acceleration for frame no. 1 , El Centro

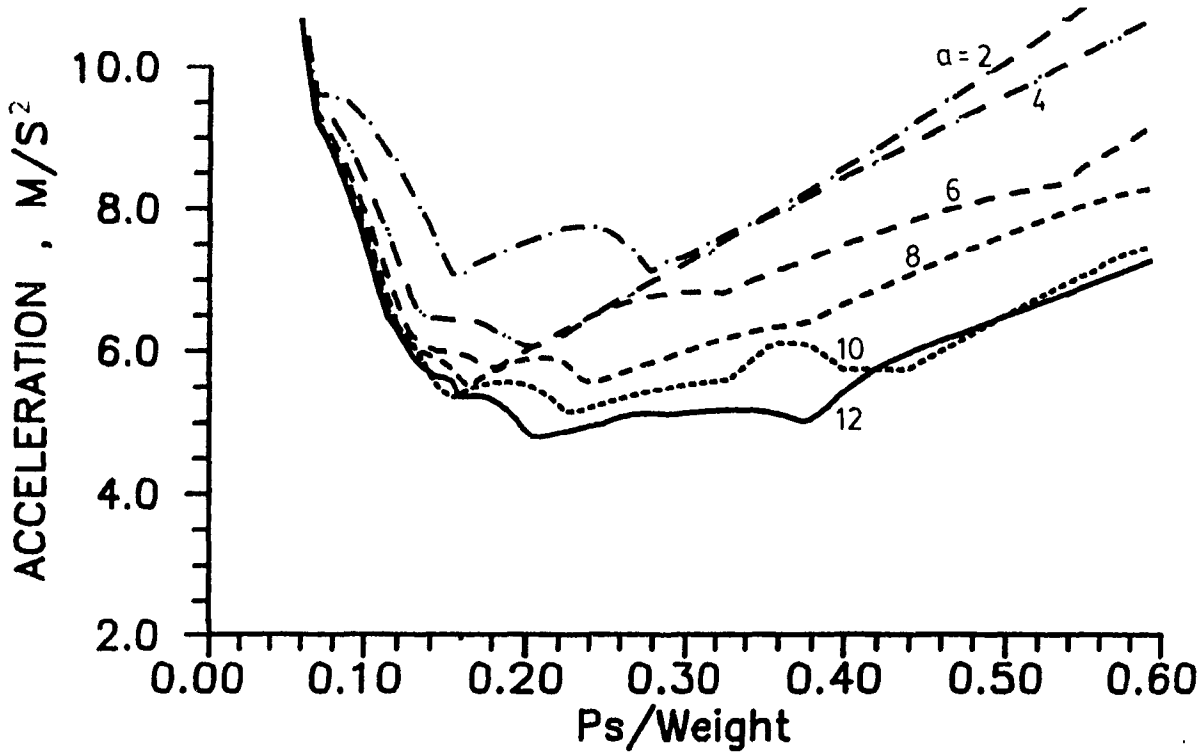

Fig. 2.12.3 Response acceleration for frame no. 1 , Olympia

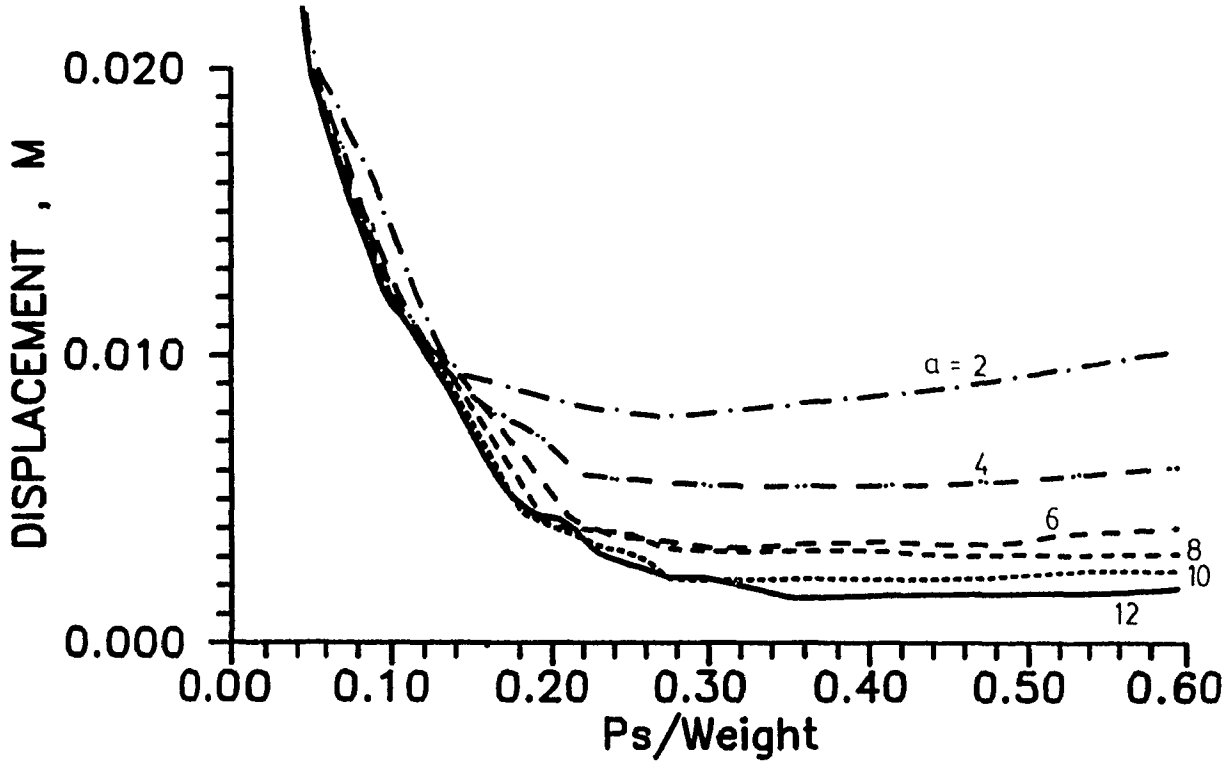

Fig. 2.13.1 Response deformation for frame no. 1 , NBK

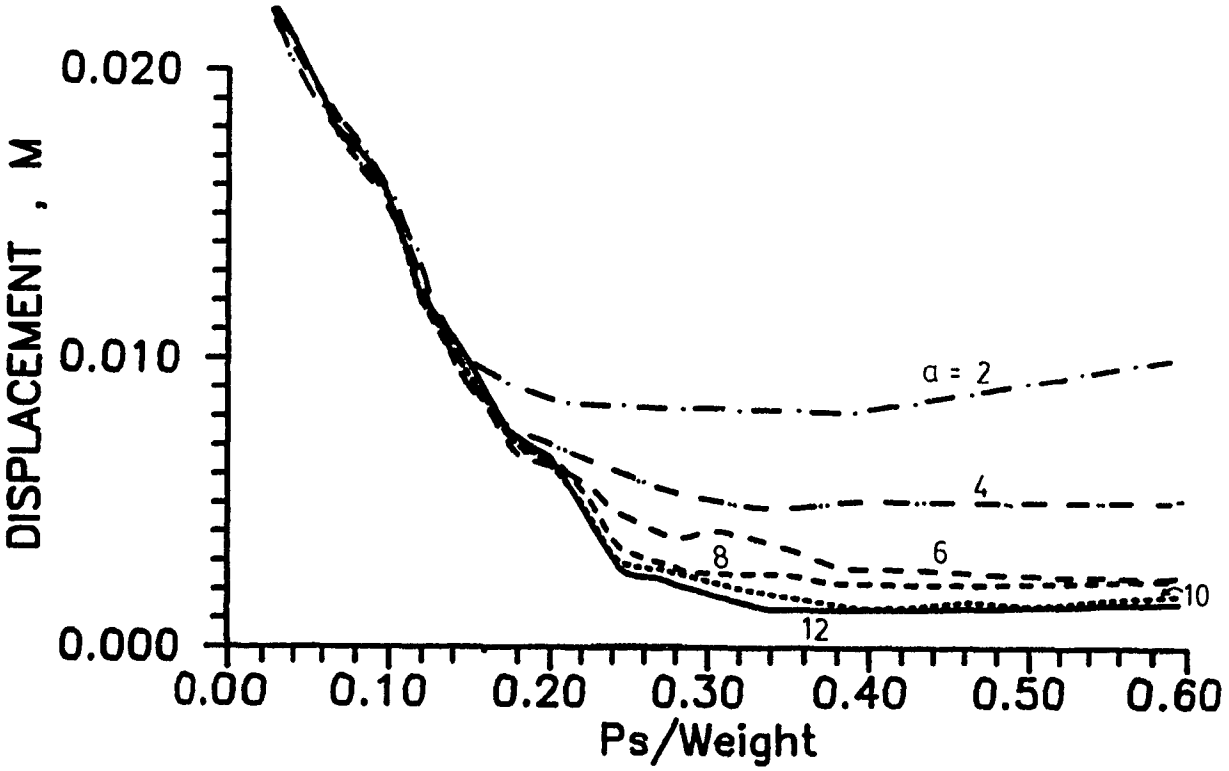

Fig. 2.13.2 Response deformation for frame no. 1 , El Centro

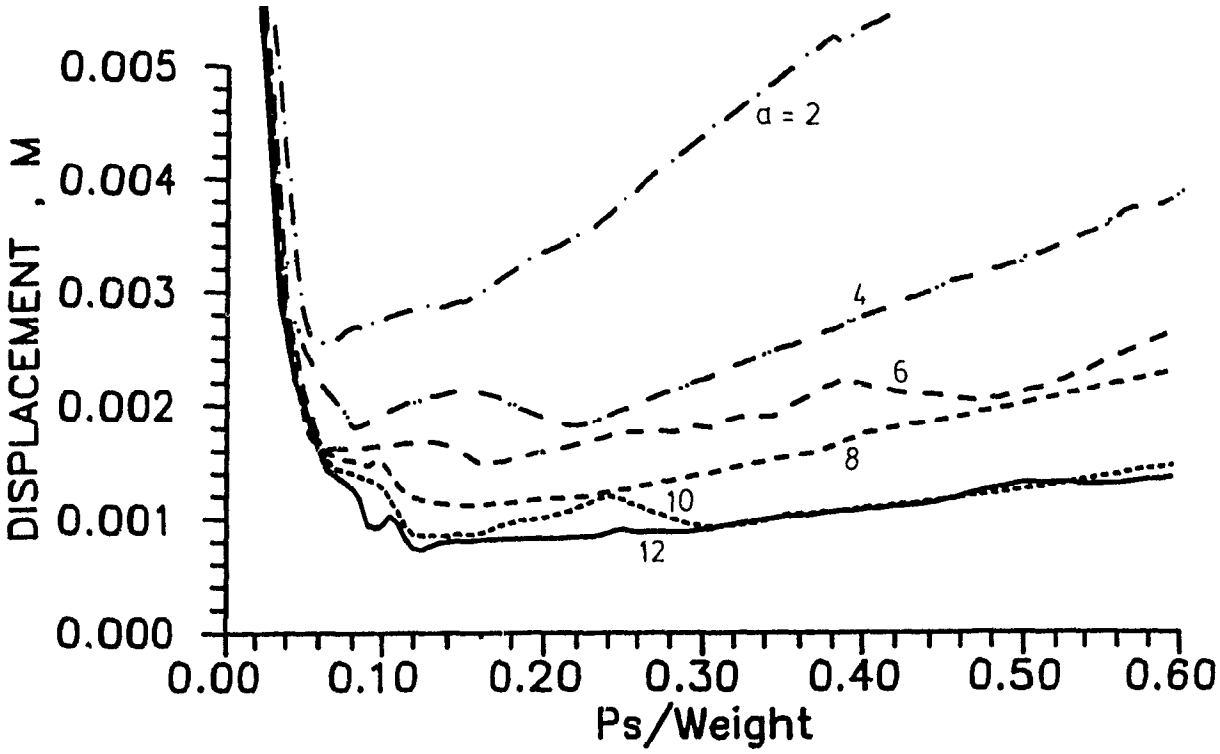

Fig. 2.13.3 Response deformation for frame no. 1 , Olympia

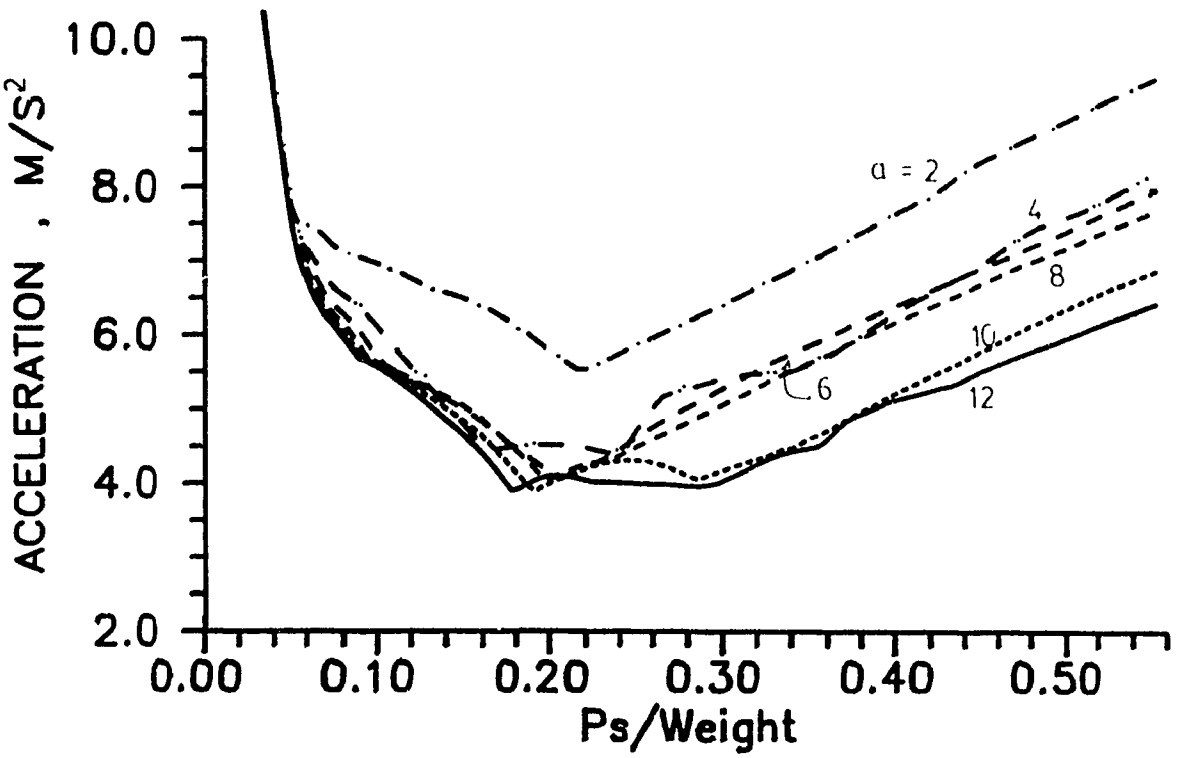

Fig. 2.14.1 Response acceleration for frame no. 2 , NBK

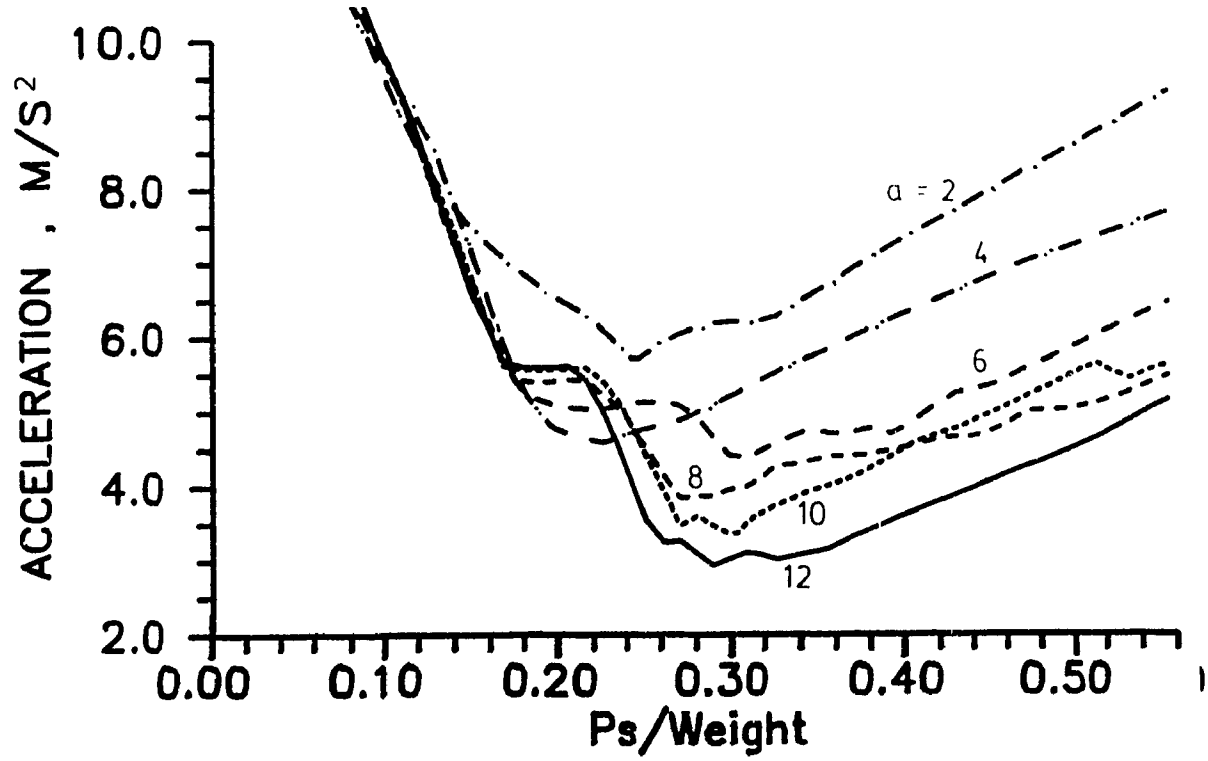

Fig. 2.14.2 Response acceleration for frame no. 2 , El Centro

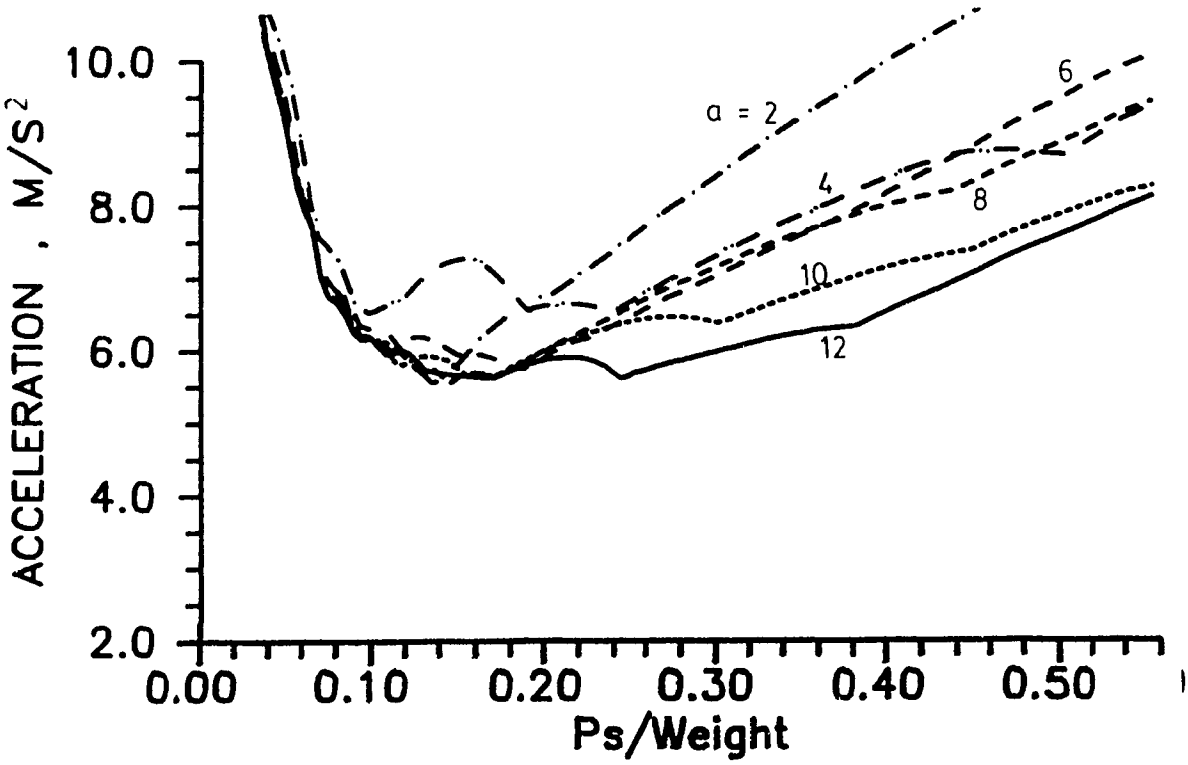

Fig. 2.14.3 Response acceleration for frame no. 2 , Olympia

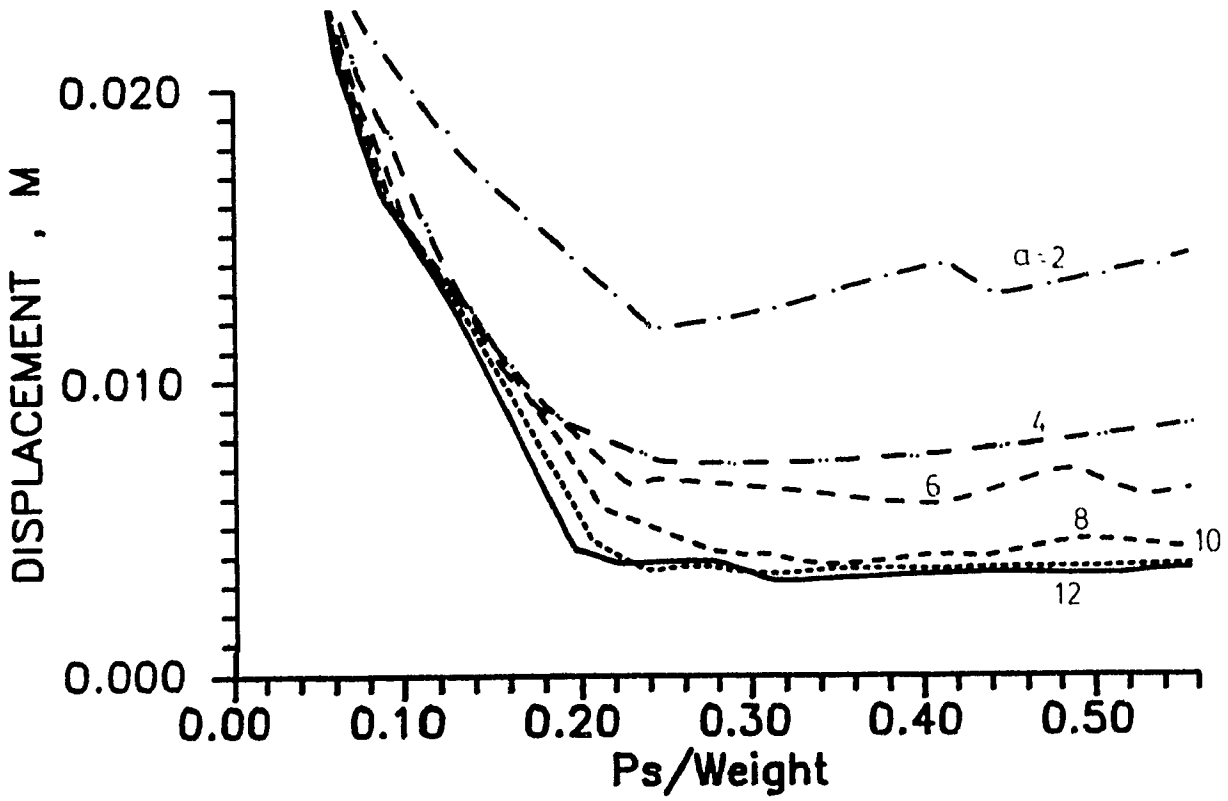

Fig. 2.15.1 Response deformation for frame no. 2 , NBK

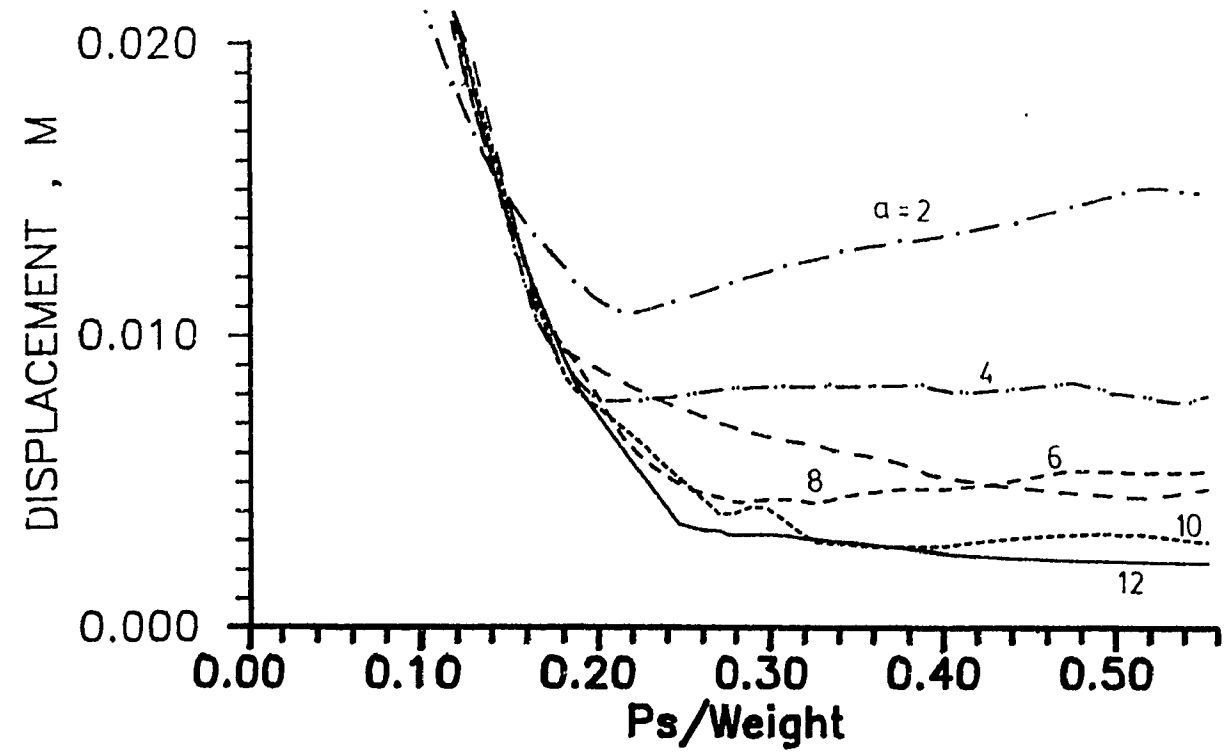

Fig. 2.15.2 Response deformation for frame no. 2 , El Centro

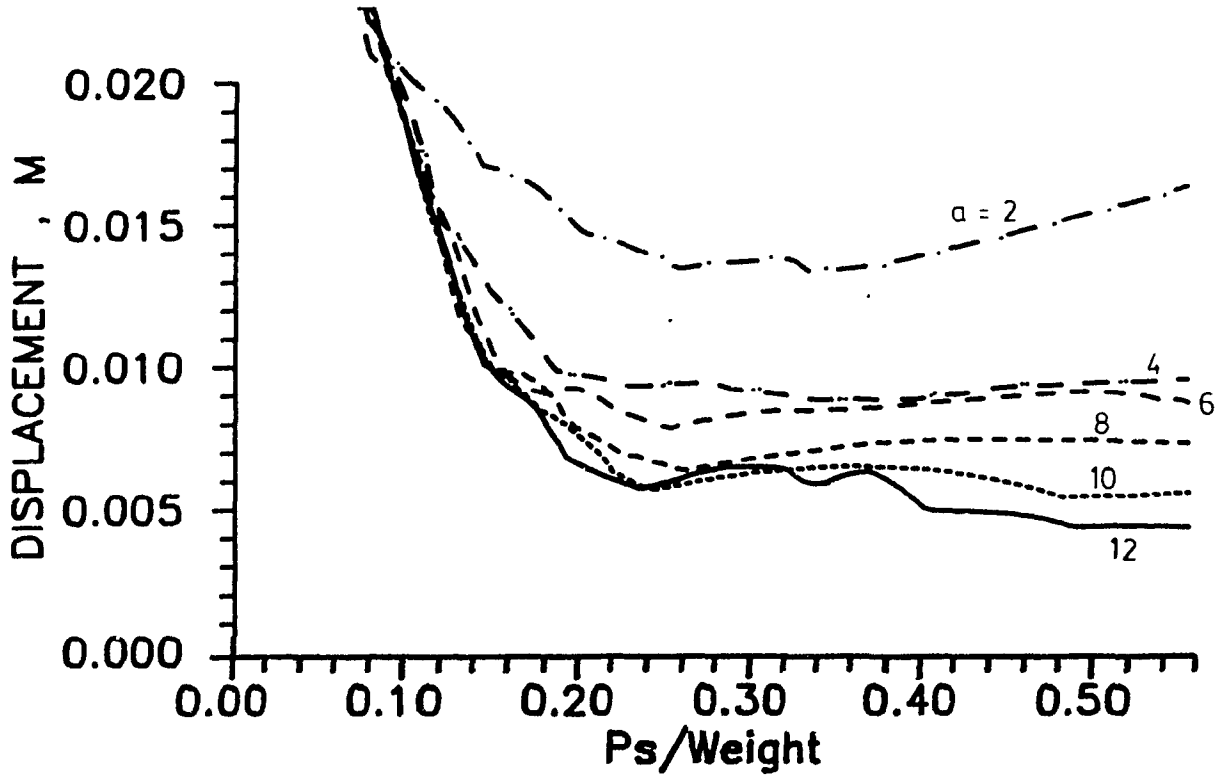

Fig. 2.15.3 Response deformation for frame no. 2 , Olympia

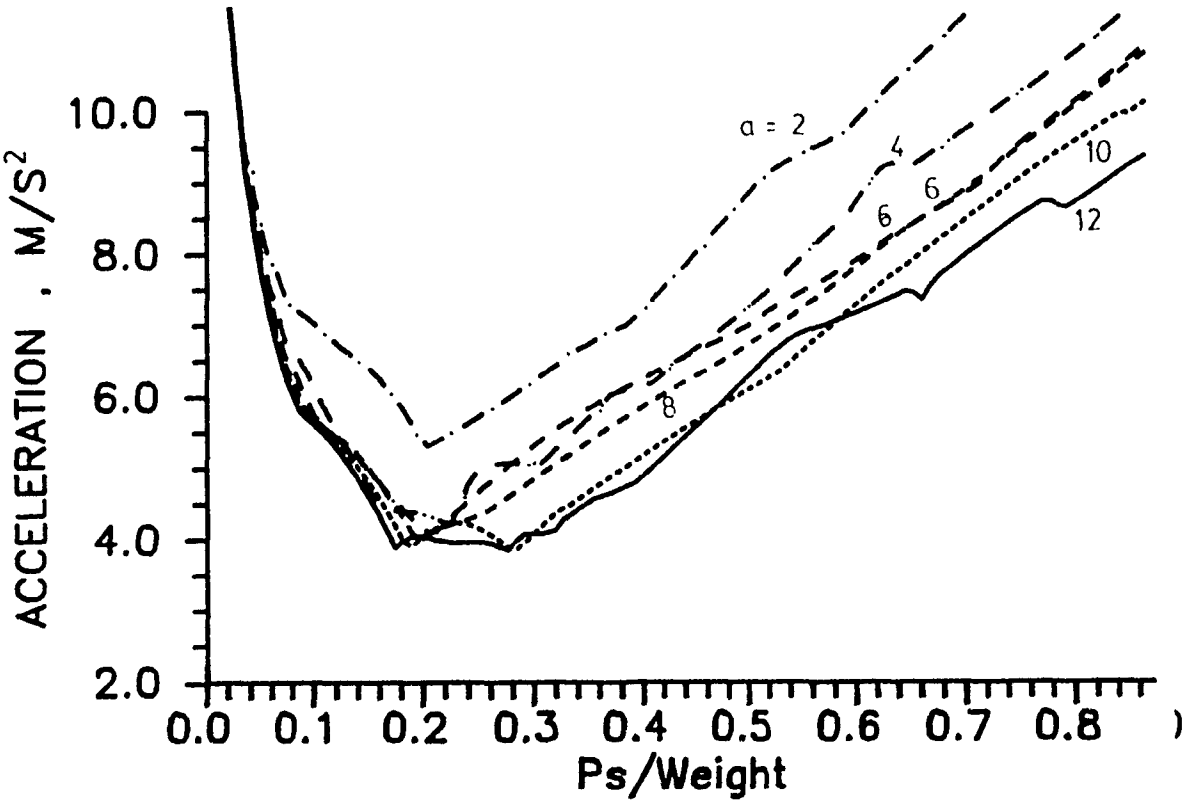

Fig. 2.16.1 Response acceleration for frame no. 3 , NBK

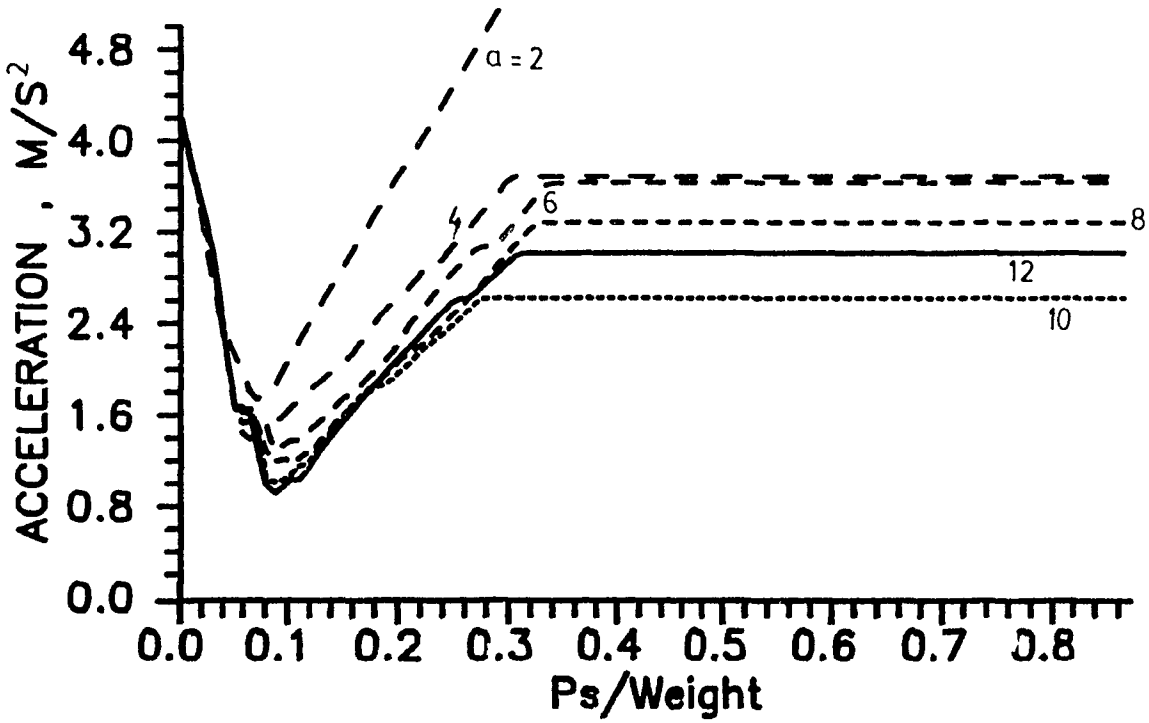

Fig. 2.16.2 Response acceleration for frame no. 3 , El Centro

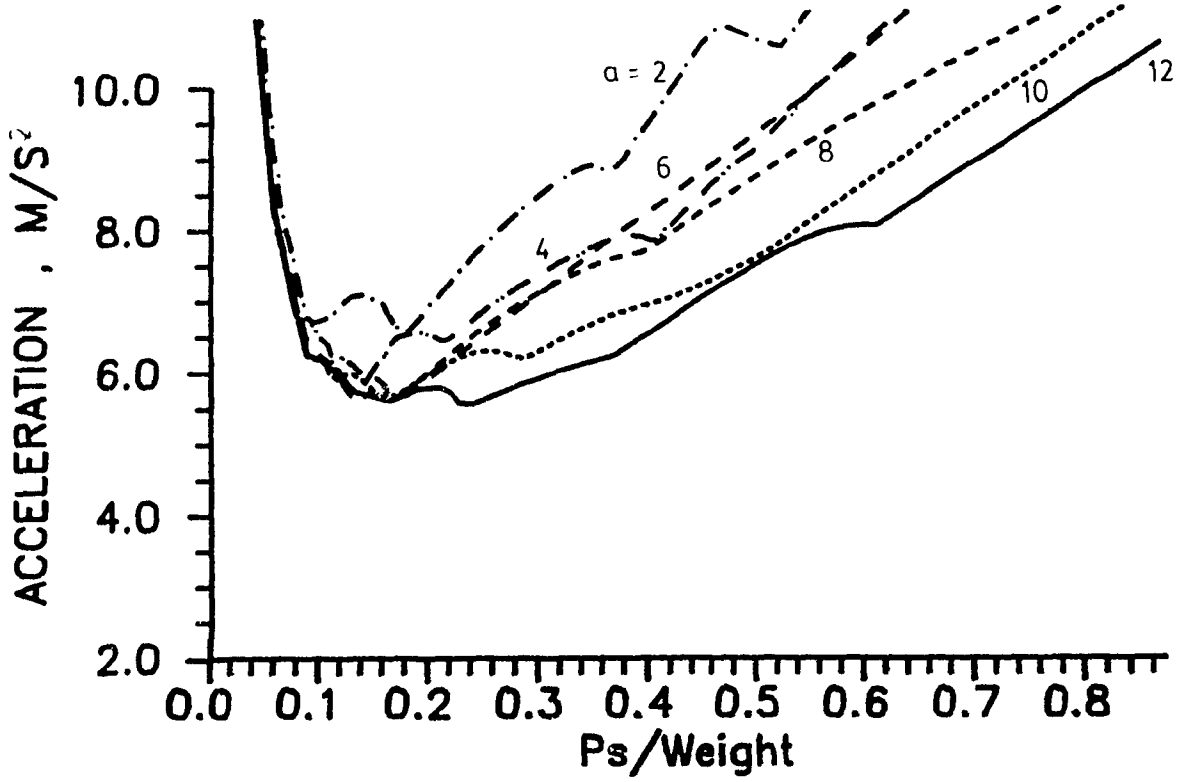

Fig. 2.16.3 Response acceleration for frame no. 3 , Olympia

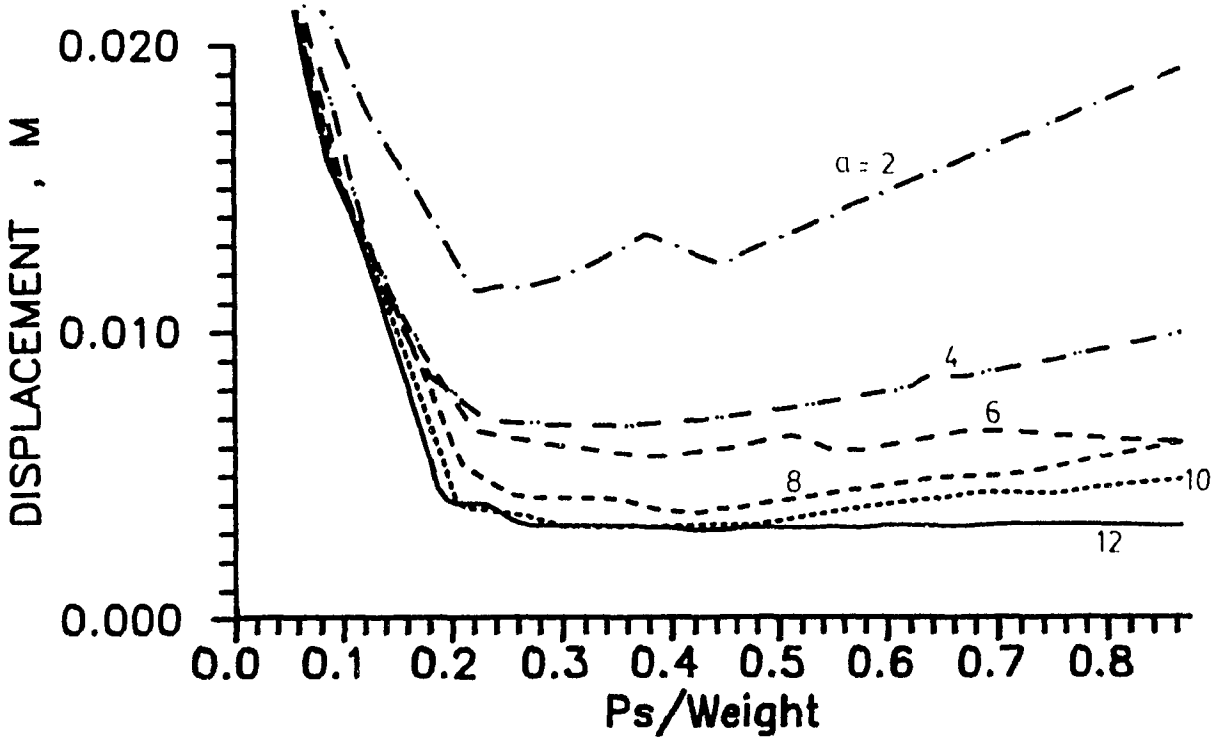

Fig. 2.17.1 Response deformation for frame no. 3 , NBK

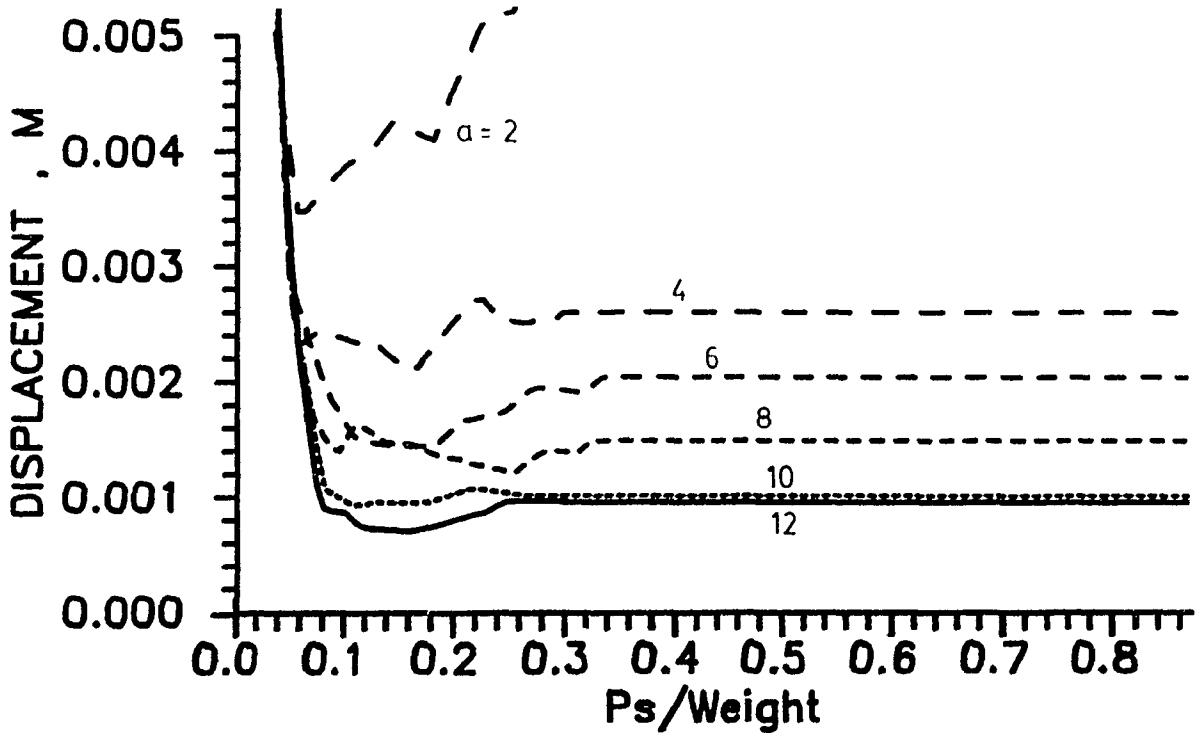

Fig. 2.17.2 Response deformation for frame no. 3 , El Centro

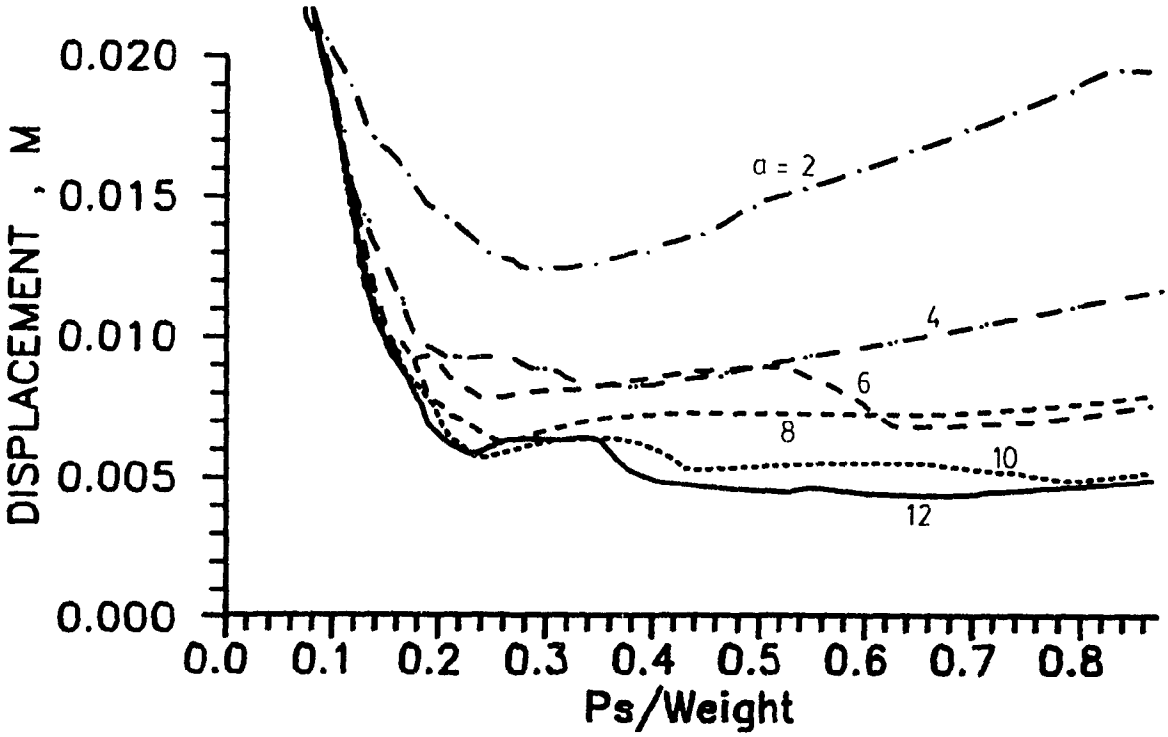

Fig. 2.17.3 Response deformation for frame no. 3 , Olympia

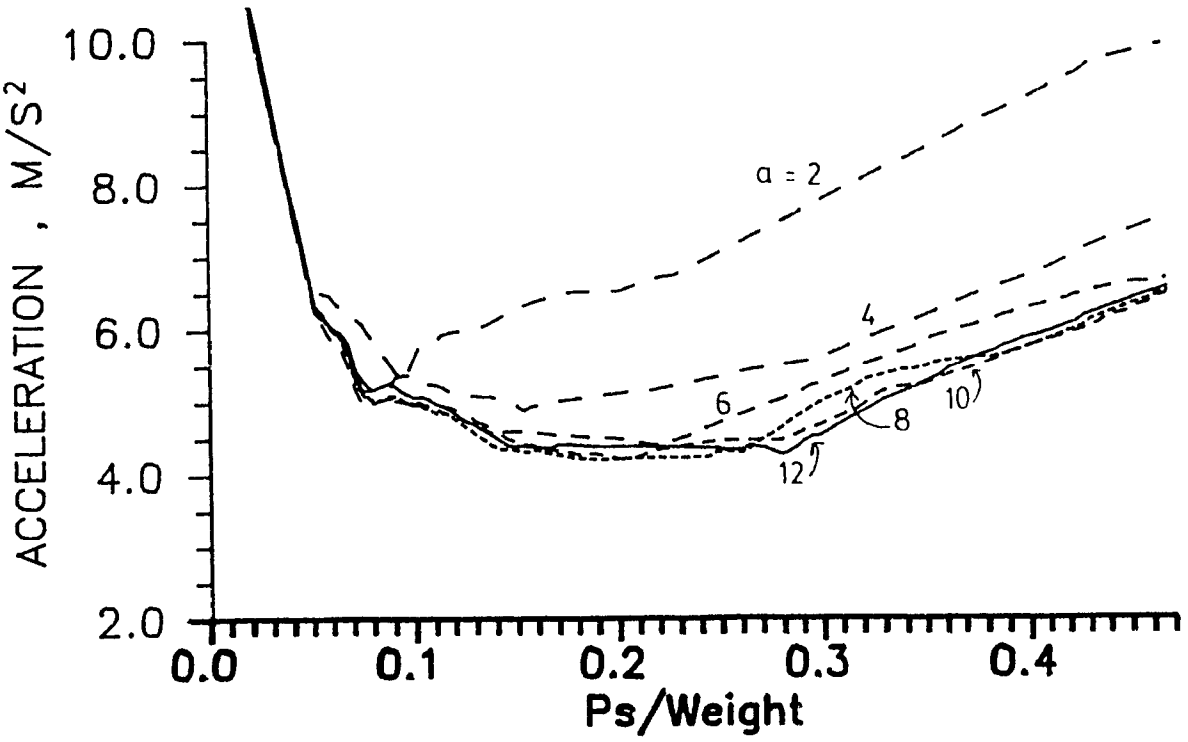

Fig. 2.18.1 Response acceleration for frame no. 4 , NBK

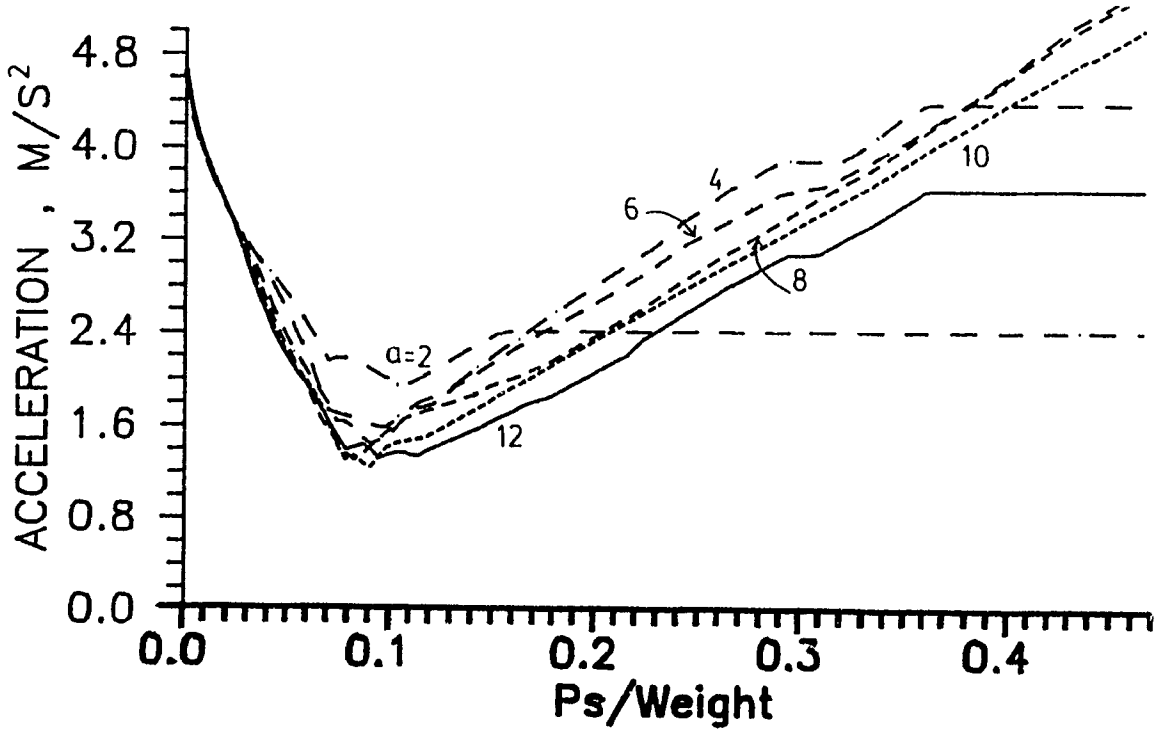

Fig. 2.18.2 Response acceleration for frame no. 4 , El Centro

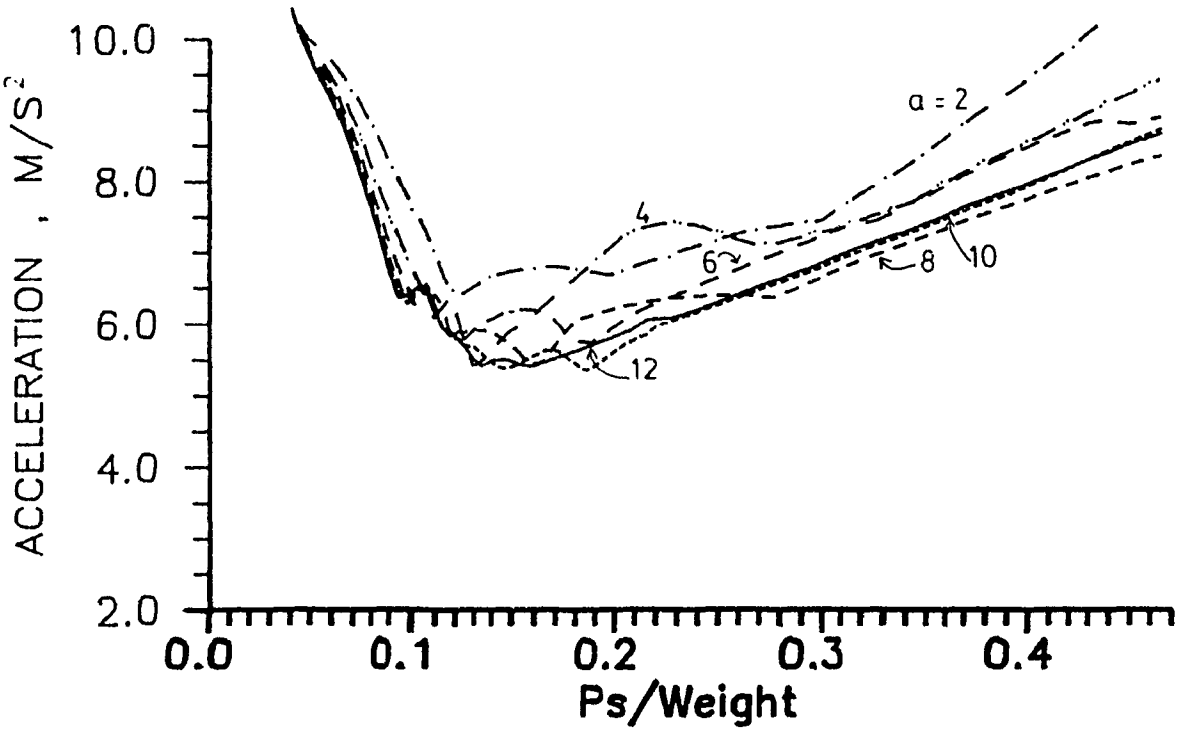

Fig. 2.18.3 Response acceleration for frame no. 4 , Olympia

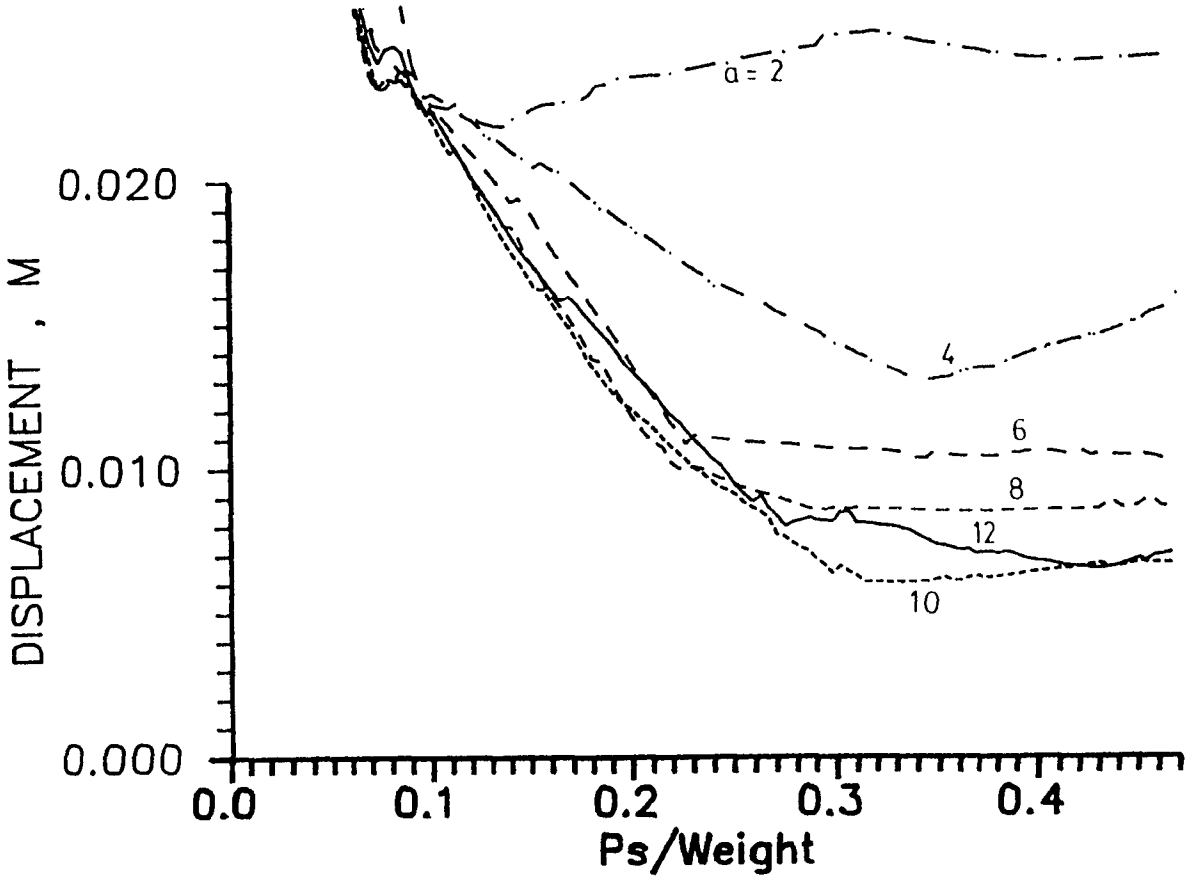

Fig. 2.19.1 Response deformation for frame no. 4 , NBK

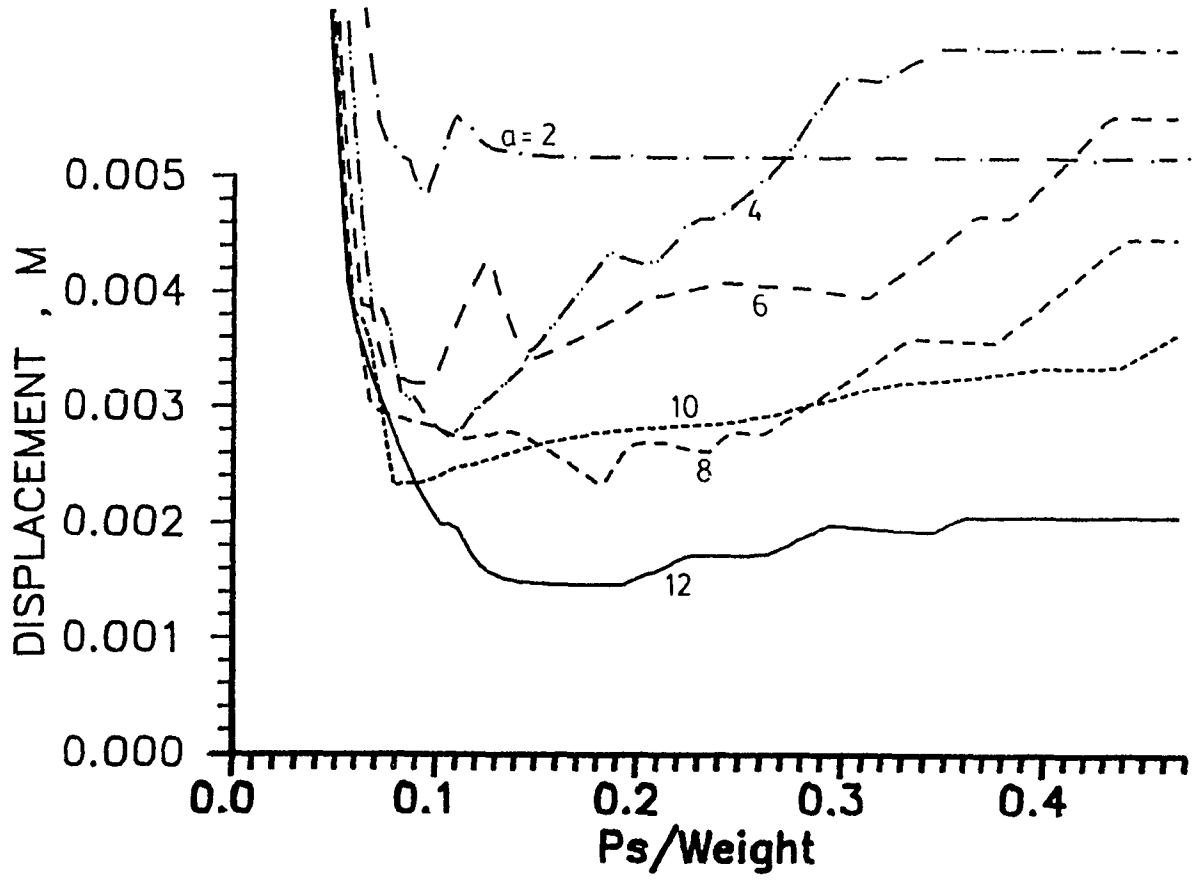

Fig. 2.19.2 Response deformation for frame no. 4 , El Centro

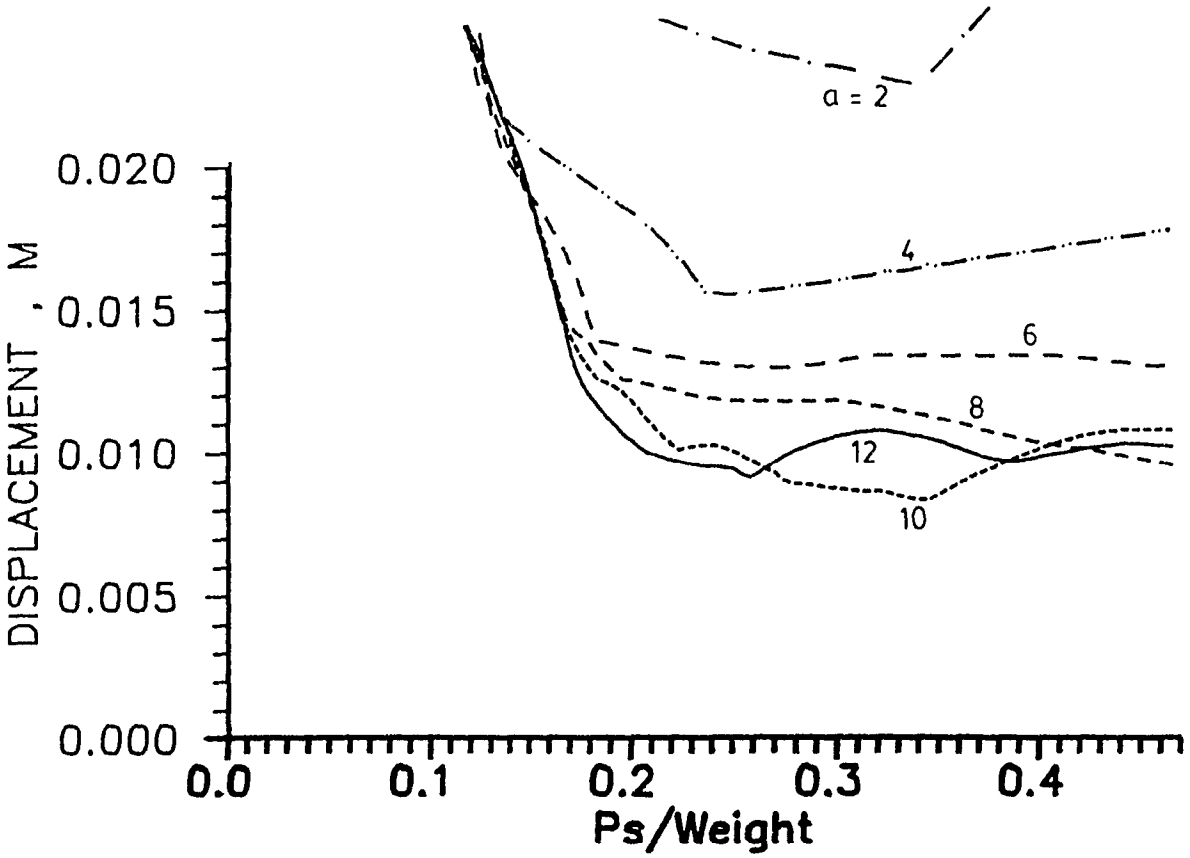

Fig. 2.19.3 Response deformation for frame no. 4 , Olympia

3.0 SINGLE BAY MULTI-STOREY FRICTION DAMPED FRAMES (FDF)

SDOF systems are often used for the generation of linear and non-linear response spectra and in the study of the influences of various parameters of earthquakes record contents, such as the frequency contents and the energy intensity indices. SDOF non-linear systems such as the elasto-plastic, bilinear and the degrading stiffness systems have also been used for such purposes as deliberated by Chopra (27), such non-linear systems serve to model closely the actual behaviour of a building structure. The literature is well documented with material on the behaviour of these systems under the various types of simulated ground motion.

Chopra and Cruz (28) studied the effects of ground motion on single bay, multi-storey shear buildings, and proposed a simplified design guide line based on these studies. Baktash and Marsh also utilized single bay frames to study the performance of friction damped frames against that of eccentrically braced frames. A similar study was carried out by Filiatrault and Cherry (18) who concluded that the FDF system performed better than the base isolated frame. Bagget and Martin (29) used a two DOF system with one artificially generated earthquake time history data to generate non-linear response spectra and to study the accuracy of non-linear response spectrum analysis. Lin and Mahin (30) did a detailed

study of the various non-linear SDOF models and proposed a simplified analysis.

In the previous chapter, SDOF systems were extensively analyzed to identify the main parameters influencing the performance of FDF. A multi-storey building (thus multi-degree-of-freedom-system) equipped with the friction devices does not actually behaviour like a SDOF system, dynamic response from the higher modes might be more important than just the response from first mode. In this chapter, series of steel frames were sized and then subjected to ground motion records. In this way, realistic stiffness and reactive mass of typical buildings will be used to obtain the dynamic response. The deformation results will be used in the next section to develop the deformation spectra for a F.D.F. system under optimum condition.

3.1 Description of Steel Frames Used

To study the behaviour of friction-damped frames under severe earthquake excitations, a series of 150 steel frames were subjected to various ground motion records. The frames are single bay steel frames from one to 25 stories high with different beam-column stiffness ratios. Figure 3.1.1 shows the typical frame used. The ratio of bay width to floor height is kept around two. The steel frames were first sized to meet CSA

A16.1-M84 (31) and the 1985 NBCC standards as unbraced moment resisting frames. The 1985 NBCC quasi- static method was used for sizing the members. The frame should also be checked for wind drift but in this case only seismic effects will be examined.

3.1.1 Typical Design of a Frame

A typical bay for a three storey level frame, as shown in Figure 3.1.2 will be analyzed and sized according to the CAN3 S16.1 Limit State Design for Steel Structures and conforming to the NBCC and its supplements. Assuming that the structure to be that of a building to be located in Montreal, which is in seismic zone 2 according to the NBCC. Figure 3.1.2 also shows the typical calculated loads to be applied. In an actual design process, overall structural stability and configuration must be considered, but in this case since it is only a demonstration design, no actual details of the building will be given.

For the seismic loads according to the NBCC quasi-static approach, the reactive mass in this case will be the sum of the total dead loads and plus 25% of the roof snow loads, or any other live load that might be firmly attached to the floor. The total mass obtained will be used to determine the total base shear arising from the actions for the earthquake.

For this particular frame the total weight is about 368 kN.

Ideally the period of the frame should be found by solving the eigen value problem from the formulated stiffness and the mass matrices of the frame. This is normally done by using a standard dynamic analysis program, as an initial guess, an approximation rule will be used. Using the equation provided in the NBCC supplement, the first period of a three storey building can be estimated as:

$$T_0 = \frac{0.09\ h}{\sqrt{D_s}}$$

$$= 0.09 \times 10.95 / \sqrt{6.0}$$

$$= 0.4 \text{ sec.}$$

or for moment resisting frame (MRF),

$$T_0 = \frac{N}{10}$$

$$= 3/10$$

$$= 0.3 \text{ sec.}$$

The corresponding seismic response factor S for a building located in Montreal where the acceleration and velocity zones are equal, i.e., $Z_a = Z_v$, with a first natural period of To = 0.4 second is about 0.44. Then the total base shear to be applied to the building is computed to be:

$$V = v\ S\ K\ I\ F\ W$$

$$= 0.1 \times 0.44 \times 0.7 \times 1.0 \times 1.0 \times 368$$

$$= 11.3 \quad kN$$

for $S = 0.44$

$K = 0.7$ (for a MRF)

$I = 1.0$

$F = 1.0$

and this base shear is to be distributed according to the mass ratio across the height of the building according to the equation as follows:

$$F_x = V \frac{W_x\ h_x}{\Sigma\ W_x\ h_x}$$

F_1 to F_2 are then the lateral shear forces to be applied to the frame at the floor levels, as shown in Fig. 3.1.2. These forces together with the vertical gravity loads are shown in Figure 3.1.2. In the figure also is shown the structural model to be used for the plane frame analysis. Typical plane frame programs are based on the direct stiffness method of analysis, also known as the matrix displacement method. In this technique, the global structural stiffness is assembled according to some prescribed degree of freedoms, the unknowns are a set of vectors consisting of the displacements under some external forces. Trial section

properties are then used as input data for the modelling of the frame for structural analysis. This initial work was done using a micro-computer based plane frame structural analysis program. Much of the later work was done using the TABS77 program on the VAX 11/785 computer and the SUN microsystem computer.

3.1.2 Analysis and Design of the Steel Frame

For the analysis and the sizing of beams and columns, all possible load combinations should be used to obtain the maximum force envelopes. In theory all possible combinations should be considered and the forces obtained from the structural analyses should be scanned to obtain the maximum force in all members. Most commercial packages for structural analysis have options for load combinations facility. So this itself does not present any problem.

This is done for this particular frame for demonstration only. Not all results for all frames will be shown, but the properties used will be listed for all frames. The maximum design forces can be picked easily for sizing the beams and columns from program output. For a beam column design, one must check for strength and stability under the effects of axial loads and end moments. The S16.1 standard for structural steel design provides interaction equations for

this purpose. For this frame the smallest wide flange, W150X30 will be used as the columns. Because of the relative light loads, this pass the strength and stability checks.

Next the beam sections used will be checked for bending moment requirements. For all the beams, it is assumed that the unsupported lateral length is set at 6 m long. Normally floors beams are assumed to be braced at the top compression flange due to the presence of the concrete deck firmly attached to the beams. In this case a W410X54 wide flange size is chosen to satisfy the strength requirements.

Beam deflections for all three floors due to live loads are minimum. Therefore beam section chosen is deemed to be adequate. Maximum storey drift occurred at the first floor level and is about 10 /3650 and this gives about 1/365. This is above the acceptable norm of about 1/400. But it will be ignored as this is not a real building as such. The overall storey drift is about 26.7/10950 = 1/410.

The MRF designed previously will now be quipped with bracing elements for the attachment of the friction devices on each floor. This will make the MRF into a BMRF and the horizontal stiffness has now increased tremendously, according to the NBCC equation for the first natural period, the first period is still about 0.40 sec. The K factor, however has now

changed to 1.0 since the modified structure is no longer a MRF. The increased in K factor accounts for the fact that a braced frame is less ductile and therefore less capable of undergoing large plastic deformations. Rainer (32) explained that the K factor only assigns relative performance of different structural systems on the basis of observed or expected behaviour in earthquakes. For a BMRF, the quasi-static lateral force requirements are obtained again from the base shear equation.

$$V = 0.1 \times 0.44 \times 1.0 \times 1.0 \times 1.0 \times 368 = 16.2 \text{ kN}$$

Therefore the new set of lateral shears are :

$$F1 = (16.2/11.3)\ 1.9 = 2.7 \text{ kN}$$
$$F2 = (16.2/11.3)\ 3.8 = 5.4 \text{ kN}$$
$$F3 = (16.2/11.3)\ 5.7 = 8.2 \text{ kN}$$

These new forces are then applied to the modified frame as shown in Figure 3.1.3. Only the tension elements are assumed to be effective. Those shown as dashed lines in the figure are the ineffective compression members. Assumed for now a 45x45x6 angle for each brace with total cross sectional area of about 1000 mm^2 will be used as the bracing elements for the three levels. This yields a horizontal stiffness of about 20786 kN/m for the bracing elements and the horizontal

stiffness of the column of the unbraced MRF is about 1698 kN/m. This produces a α ratio of about 12.3.

The new maximum roof deflection computed for the new set of forces is only 2.3 mm. Since these forces do not produce any significant change in the member forces in the structure, there is no need to modify the sections chosen. The final frame with all the sections used is shown in Figure 3.1.4, together with the locations of the friction devices. Also shown in the figure are the three reactive masses due to the dead loads and partial live load on the roof and the floor levels of the structure. These are the masses which will be used in the non-linear analysis of the friction-damped frame.

The actual periods of vibration of the frames are calculated using the TABS77 (33) program, and they are found to be about 1.2 and 0.21 s for the MRF and BMRF respectively. The MRF period is different from that of the code value by a large margin. This is to be expected since the calculated value from the TABS77 program is that of a bare skeletal and does not take the additional stiffness of all other secondary elements such infilled panels, walls, siding, doors and windows. But that of the BMRF appears more reasonable for a three storey frame due to the large lateral stiffness contribution of the brace element.

All subsequent frames used were dealt with in a similar manner before performing the non-linear analysis. All the properties of about 150 frames used are listed in Appendix B together with the masses. All frames were analyzed as MRF first and then as friction-damped frames. The second analysis was carried out to check the adequacy of the members and to make sure that the slip load was not attained under normal service state. Masses were varied for some of the frames to obtain a variation in the period range.

The periods for the structures are calculated by using the TABS77 program. The mass was varied for some of the frames to cover the range of period for typical structures encountered in the construction industry. The fundamental period usually varies from 0.1 to 10 seconds. Shorter frames will naturally have shorter periods, or higher frequency, and higher frames will have longer period and smaller frequency. It is also a well-known fact that most earthquakes have higher energy contents in the higher frequency range. With the exception of special soil characteristics such as the Mexican city old lake bed, which tends to induce a longer period of vibration, most periods are concentrated in the lower period zone. Since it was difficult to design lower frames to produce the required numbers of periods, lower frames were manipulated by changing the mass or the column stiffness.

The selection of design earthquake(s) involves many disciplines and requires the collaborations among many of the professionals. Although continual progress is being made, there is still no consensus about what ground motion characteristics or parameters are significant in exciting a building, and how they can best be quantified for design purposes, especially for structures that behave inelastically. The various aspects of a ground motion affecting structural response include intensity, frequency contents, duration, the number, size, and sequence of acceleration pulses. In addition, it is not certain what structural response parameters should control the design, particularly in the inelastic range. For example, displacement, storey-drift, ductility, acceleration and other factors have been suggested. Moreover, it is not certain how these ground motion and structural parameters are related. Since this is near impossible for the present study, it is necessary to utilize numerous record data to carry out the analysis and there is considerable uncertainty in the selection of the design earthquake(s).

This being said, it is desirable that at least three earthquake records be used. However, as justified below, it was finally decided to used only the N.B.K. record for the rest of the study. The response obtained for a frame is shown in Figure 3.1.5. As can be seen from the figure, if the

parameter of interest is limited only to the upper level deflection, or storey drift, one see that the response for the three different earthquake records have the same tendency. Other frames with different periods were also analyzed and found to behave in a similar fashion.

Next, the intensity of the ground motion is varied to increase the severity of the earthquake. This is done by scaling the record data by the appropriate constant. Figure 3.1.6 shows the effects of scaling the N.B.K. earthquake data for another frame. As the severity of the peak acceleration increases, the response is seen to move upwards. But in general the tendency of the graph is the same for all intensities. Figure 3.1.7 shows the effects when using another earthquake record and again scaling the peak intensities. For the same frame the same resultant effect is obtained if the storey drift is parameter chosen for comparison purposes. The purpose of varying the slip load level for each frame is to determine the level of the so called optimum slip load of the devices for that particular frame manually. As can be seen from these curves, the low point of each curve does not seem to vary much after the initial low plateau has been reached. From these preliminary results obtain, it is decided that in order to save computation time, only the 0.30g N.B.K. artificially generated earthquake data will be used in all subsequent analyses. By this restriction, therefore the

results obtained thereafter can be said to be applicable only to characteristics of the N.B.K. site conditions. For simplicity constant slip force is used for all floor levels even though ideally as the shears are higher at the lower levels, the slip load should also be higher there.

3.2 Modelling of Braces with Friction Device and Analysis Technique

The dampers are modeled in the DRAIN-2D program by using the truss elements with elasto-plastic yielding behaviour. This reduces the total number of elements required and thus reduces the computation costs. This model was originally used by Pall (14) and Filiatrault and Cherry (16) who found that the difference between the actual and more refined damper model and the simplified version varies in the range of about 15% in the final results, and the solution converges when the intensity of the ground motion increase. The yield forces of the truss elements are based on cross sectional area which is normally determined from the service load requirements. The yield stresses for the truss elements for DRAIN-2D are then computed as the slip load divided by the areas. A very small yield stress is assumed for the compression force to avoid the problem of dividing by zero by the program. Filiatrault and Cherry (16) described in details the equivalent energy dissipation mechanism by the truss elements. Figure 3.2 shows

the step-by-step mechanism of the truss element and a friction device under loading at various stages of a cycle.

The computer program DRAIN-2D is used to carry out the non-linear step-by-step analysis in the time domain. It makes use of the constant acceleration scheme for time integration. It has a series of subroutines for the common structural elements for modelling typical building frames. For this work, only the beam-columns, and the truss elements are used. As the full package of the original program is not required, a scaled down version of the original source is used instead. The un-required elements and its corresponding inputs and outputs subroutines area removed. This reduces the program to about one-third of the original size.

For each frame, determination of the optimum slip load was done by increasing the slip load for the frame and an execution carried out. Several more executions were carried out until no further changes in the dynamic response was observed or until the response began to increase. Each individual frame was subjected to the N.B.K. artificial ground motion, which was chosen because of its wide range of frequency contents. The time step used for the integration over the time domain was determined by trial and error. A good rule of thumb will be about To/10 to To/100. A suitable value was obtained when the response with one time step did not

differ significantly from the previous larger value. Generally, the time step chosen was between 0.001 to 0.005 second.

3.3 Analysis of Results

A total of more than 150 frames were analyzed using the DRAIN-2D computer program and each frame is subjected to the 0.30 g N.B.K. earthquake data. For each frame, the slip loads is varied from 0.0 to 50.0 kN. From the results obtained, it was found that for all the frames studied, the displacement responses universally have a similar trend: starting from zero slip load (i.e. unbraced moment resisting frames), the deflection responses decrease rapidly with increasing slip load until a low plateau was reached. Thereafter, further increase in the slip load does not change the response significantly. Typical deflection responses with different levels of slip loads are shown in Figures 3.3.1 to Figure 3.3.33. In Figure 3.3.1, 5 curves were plotted with each curve representing the result of a frame. It's fundamental period of vibration is indicated by the legend shown just below the graph. For example, the square symbol (□) with the numeric number 0.346 next to it implies that the frame represented by the square (□) has a period of 0.346 second. Accordingly, the triangle (△) represents a frame with a period of 0.280 second, the diamond (◇) represents a frame with a period of 0.541

second, the cross (x) has a period of 0.463, and the plus symbol (+) is for a frame with a period of 0.147 second. The same principle is applied for Figures 3.3.1 to 3.3.33.

3.3.1 General Trends

The optimum slip load, i.e.the force in the friction device at which the maximum deflection is smallest, increases slightly as the intensity of the motion is increased. For the frames studied, it was observed that the FDF remained elastic at all time when the slip load was near or at the optimum value. The forces in the members and the floor deflections are observed to decrease as the optimum value is approached. It was also noted that the optimum slip load level was between 10 to 30% of the total weight of the structure. Assuming a slip load at 20% of the structure weight appears to be a reasonable starting point for preliminary design. This is based on two observations of Fig. 3.3.1 to Fig. 3.3.33 :

(i) the frame responses are fairly insensitive to a large change in the slip load near its optimum value, and

(ii) a slip load higher than optimum involves lesser risk than a lower value. It must be mentioned that member forces are greatly reduced for all frames, at optimum slip load or not.

3.3.2 Effects of Earthquake Intensities on optimum slip load

From the comprehensive study of the FDF under simulated earthquake loadings, it appears that the optimum slip load for any given structure is unlikely to be correlated to the total mass of the building. The range varies from 10 to 30 % of the total mass of the building. As shown in Chapter 2, this value is difficult to pinpoint. It seems to vary also with the different earthquake and also for the same earthquake but different intensity, given the same frame and mass. Recalling from Chapter 2, the brace stiffness also plays an important role.

3.4 Approximate Equivalent Damping Study

From all the frames analyzed in the previous section, it is clear that with the increased capability in energy dissipation provided by the dampers, the dynamic response of the building frames are greatly reduced. It would be interesting to determine the equivalent damping that a MRF would have in order to approximate the performance of FDBF. For this purpose, the maximum roof deflection will be used as the parameter for comparison.

DRAIN-2D uses the Rayleigh's damping for the creation of the damping matrix. Rayleigh's damping is assumed to be mass

and stiffness dependent as shown below:

$$[C] = a [M] + b [K] + b_0 [K_0]$$

where

[C] is the system's damping matrix

[M] is the system's mass matrix

[K] is the system's updated current stiffness matrix

$[K_0]$ is the system's original stiffness matrix

a, b, b_0 are damping coefficients

Assuming that the b_0 is equal to zero, that is to say that the damping is not dependent on the original stiffness matrix, the damping equation becomes:

$$[C] = a [M] + b [K]$$

a [M] is known as the inertia damping matrix. The corresponding damping force on each lumped mass is proportional to its momentum. It represents the energy loss associated with change in momentum. The [C] term is known as the stiffness damping matrix. Their corresponding force is proportional to the rate of change of the deformation forces at the joints. It can be shown that :

$$\zeta_n = \frac{a}{2 w_n} + \frac{b w_n}{2}$$

where

ζ_n = damping ratio for the nth mode

w_n = nth mode frequency of vibration

Accordingly the a and b coefficients can be calculated as follows:

$$w_1 = 2\pi f = \frac{2\pi}{T} \qquad (3.4.1)$$

$$\zeta_i = \frac{a}{w_1} + \frac{b\, w_i}{2} \qquad (3.4.2)$$

$$\zeta_j = \frac{a}{2\, w_j} + \frac{b\, w_j}{2} \qquad (3.4.3)$$

Substituting equation (3.4.1) into the last two equations yields:

$$\zeta_i = \frac{a\, T_i}{4\pi} + \frac{b\,\pi}{T_i}$$

$$\zeta_j = \frac{a\, T_j}{4\pi} + \frac{b\,\pi}{T_j}$$

or in matrix form:

$$\begin{bmatrix} \frac{T_i}{4\pi} & \frac{\pi}{T_i} \\ \frac{T_j}{4\pi} & \frac{\pi}{T_j} \end{bmatrix} \begin{bmatrix} a \\ b \end{bmatrix} = \begin{bmatrix} \zeta_i \\ \zeta_j \end{bmatrix}$$

Obtaining a and b by Crammer's rule, they are:

$$a = \frac{4\pi (\zeta_i T_i - \zeta_j T_j)}{(T_i^2 - T_j^2)} \qquad (3.4.4)$$

$$b = \frac{T_i T_j (T_j \zeta_i - T_i \zeta_j)}{\pi (T_j^2 - T_i^2)} \qquad (3.4.5)$$

where

T_i = first period of vibration, sec.

T_j = second period of vibration, sec.

Knowing the first two periods of vibration of the building frames, the two damping coefficients can then be calculated accordingly by using equations (3.4.4) and (3.4.5). For illustration, the seven storey frame no. D7-1 will be used as an example. The response of the frame can be found in Fig. 3.3.23, where the optimum response is found to be about 69 mm for the roof deflection. The periods calculated from TABS77 are:

T_1 = 1.9703 sec.

T_2 = 0.7267 sec.

Their corresponding damping coefficients in terms of the damping ratios are :

$a = 12.5664\ \zeta \qquad b = 0.1690\ \zeta$

With these expressions for the damping coefficients, the damping ratio is increased successively and their a's and b's calculated for the damping matrix. For each analysis on the DRAIN-2D these values are changed until the response matches that of the FDF systems. For this example, the damping ratio required is about 50%. For most of the frames analyzed, damping ratios range from 40 to 100 per cent critical. This ratio is very sensitive to the value of the period used for the determination of the damping coefficient. It is a rule of thumb in the design industry that when determining the period of vibration of a building, N/10 or some other simplified formulae is used. For the seven storey frame, one might expect that the finished building's period of vibration might be in the order of 0.7 to 0.5 sec for most buildings. With these in mind their corresponding damping coefficients will be different from those calculated above, meaning also the equivalent damping found previously will be changed to a lower values instead of the 50% calculated.

3.5 RESPONSE SPECTRUM FOR THE FDF SYSTEMS

Dynamic analysis of buildings or any other built engineering structures as multi-degree-of-freedom systems (MDOF) is a complex procedure. The most accurate solution scheme is to perform a three dimensional time-history analysis of any structures with an unusual geometry, thus incorporating any torsional moment that might been induced due to any eccentricity. This can be done by employing current available commercial finite element programs, or any other frame programs, such as TABS77, or DRAIN-TABS, which are capable of handling complicated behaviours during yielding of structural members. The time-history analysis involves step-by-step integration of the system equations of motions. Although the method is generally applicable, this is a formidable task for even the experienced design engineer, and there are high computing cost involved. More over, the results from such analyses must be carefully evaluated by experienced engineers to obtain the probable forces that might be induced for the actual site conditions.

MDOF systems are normally analyzed elastically by using the response spectrum method, also known as the modal analysis technique. The response-spectra-based modal analysis is considered by many to be the most practical approach. In this method, the MDOF system is viewed as a series of

vibrating SDOF systems responding at their own frequency. The maximum response of the MDOF system can be estimated by superimposing the maximum response from each of the SDOF systems. Several summing procedures are commonly used. The normal summing procedure used is the root sum of square (RSS) method and the sum of the absolute maximum of each of the periods. Due to the use of elastic modes and modal superposition, the method is theoretically limited to linear-systems. However, because of the straight forward nature of the modal analysis method, the inelastic-spectra-based modal analysis is considered a potential method for inelastic structural design.

3.5.1 Equation of Motion

For a vibrating body subjected to an external forcing function, the governing equilibrium equation at any time t as shown in section 1.4 is:

$$M \ddot{X}(t) + C \dot{X}(t) + K X(t) = - M \ddot{X}g(t)$$

As shown in the Figure 1.1, the displacement of the system with respect to its fixed base is denoted as X(t). The governing equation is normally solved by numerical integration. For a SDOF system, the above equation can also be evaluated by using the so called Duhamel integral, as

shown below:

$$Y_n(t) = \frac{T}{M_n w_n} \int_0^t P_n(t) \; e^{-\xi_n w_n (t-\tau)} \sin w_n (t-\tau) \, dt$$

The integration is performed over the entire time history of the earthquake record. The maximum displacements so obtained for each of the frequencies with the corresponding critical damping ratio are known as the pseudo displacements (S_d) for a generalized SDOF system. The pseudo velocity and acceleration are then related in the following manner:

$$S_v = w \; S_d \qquad (3.5.1)$$

$$S_a = w^2 \; S_d \qquad (3.5.2)$$

Because of these simple relationships, the three parameters can be plotted in a special format known as the tripatriate graph. A typical response spectra for the El Centro earthquake is shown in Figure 3.4. From these spectra generated for any given earthquake, one can easily compute the responses of any given system by using the modal analysis method. The method is well known and can be found in most standard texts on structural dynamics, for example Clough and Penzien (34). For low damping values of less than 20%, the displacement, velocity and acceleration responses can be approximately related by the expressions as shown above. The implementation of the response spectrum method

for the analysis of inelastic MDOF systems is not trivial. While modal response of a linear elastic system can be computed independently, modal response becomes coupled once the structure becomes non-linear. It is uncertain how the modes interact with each other. For the simple case of one dominating mode, modal interaction may be ignored. Furthermore, all the members of the structure yield simultaneously, then the response of a MDOF system can be approximated by the response of an elasto-plastic system. Several methods have been used in implementing the response spectrum method for inelastic system. The reliability of these procedures have been investigated. It was found that the approximate design rules for SDOF systems can, for all practical purposes, be extended to two or three degree-of-freedom system shear beam type structures (35).

For damping of more than 20%, the simple equations of 3.5.1 and 3.5.2 are no longer valid. The pseudo responses can no longer be used to obtain the actual response of a complex system. In this case the actual system response will be required. As shown by Hanson et al (12), by using supplemental mechanical dampers, system damping can go as high as 150% of the critical values.

3.5.2 Response Spectrum for the F.D.F. System

The inelastic response spectrum for low damping values is established by finding the response acceleration that would give maximum deflection comparable to that obtained from the non-linear step-by-step analysis. In this preliminary study, the following particular limitations apply:

(i) the N.B.K. earthquake record scaled to 30% g was used to obtain the maximum deflection from the non-linear analysis of the friction damped braced frame operating at its optimum slip load;

(ii) only the first mode was used in the determination of the maximum deflection from the spectrum analysis.

In addition, the spectrum analysis mentioned in (ii) was carried out for the unbraced moment resisting frame since its stiffness represents that of the friction-damped braced frame during the slipping in all the devices. This has the further advantage of facilitating the use of the obtained response spectrum for preliminary sizing of the frame members.

The maximum deflections obtained in the previous section under the optimum slip load conditions were then used to generate the spectral accelerations by using the TABS77 program. This is done by first assuming a certain value for the response acceleration for the frame. A modal analysis is then carried out. The maximum roof deflection obtained from

the modal analysis is noted. Knowing the deflection (from the DRAIN-2D non-linear analysis) for the same frame under optimum slip load conditions, the first values of the response acceleration used is then scaled accordingly to obtain the correct value. The scaled response acceleration is then the response acceleration that would yield the maximum roof deflection for the MRF frame. This is done for each frame analyzed in previous section 3.1. Each individual frame yielded a data point on the response spectrum. Thus, the spectrum was generated for all the frames analyzed in the previous section. Figure 3.5 shows the plot of the final results with the periods of the frames as the horizontal axis and the acceleration as the vertical axis.

Given that the response acceleration spectrum is still a scattered plot, an approximate 90 percentile line is drawn so as to include most of the upper bound values. This is as shown in the graph plotted again in Fig. 3.5. With the given spectrum, an engineer only has to perform a relatively straight forward and simple modal analysis to determine the approximate deformation response of a FDF system at the optimum slip load conditions. A detailed time-history analysis will still have to be carried out at the final design stage as a final check of the structure. Several examples will be used to demonstrate the use of the Figure 3.5 and this is will be carried out in chapter 4.

3.6 Summary

The results obtained from the analyses have shown that, the friction devices have reduced the response of the building frames immensely. For any frame, the response at optimum slip load conditions is the minimum response. Dissipation of the kinetic energy does not have to be optimum to reduce the dynamic response, as shown by the low slip loads of all the frames. The maximum dynamic deformation response of each frame is plotted in terms of graphs for easy visualization. The optimum slip load of a frame appears not to be related to the weight of the building. In actuality, different earthquakes actually induced a different optimum slip load, even for the same frame. Different peak intensities of the same earthquake also tend to yield a different optimum slip load. From the deformations obtained from these frames under optimum slip load conditions for the 0.30g NBK earthquake, a simple deformation response spectrum was developed for the modal response analysis of the FDF systems. The accuracy of the spectra will be discussed in the next chapter.

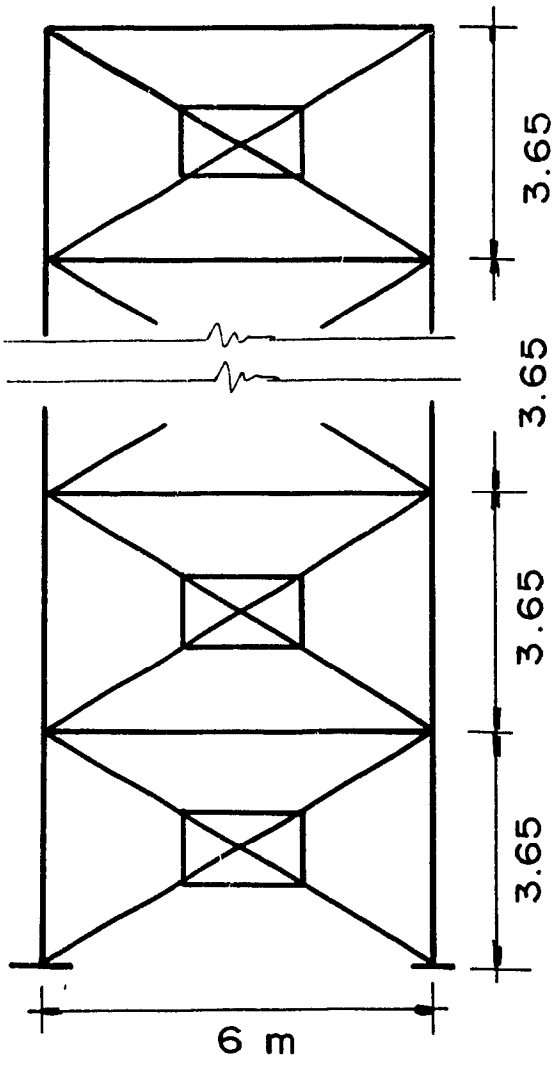

Figure 3.1.1 Typical Steel Frame

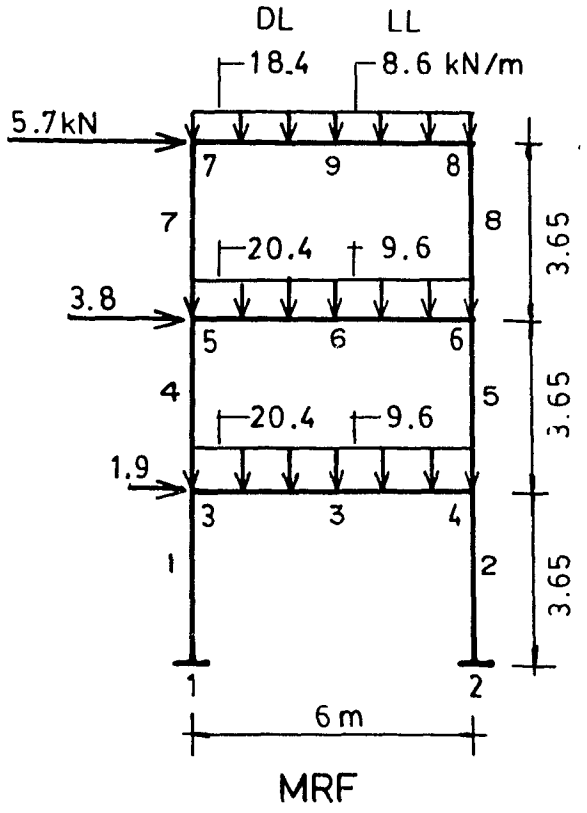

Figure 3.1.2 Three Storey Frame with properties

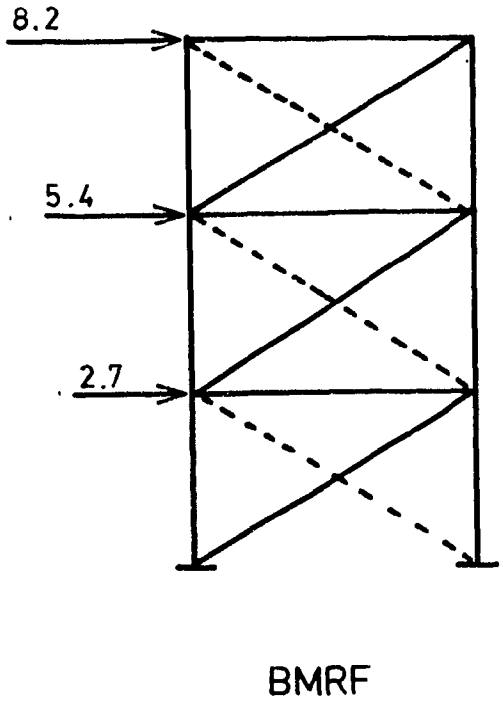

Figure 3.1.3 Modified forces for tne braced frame

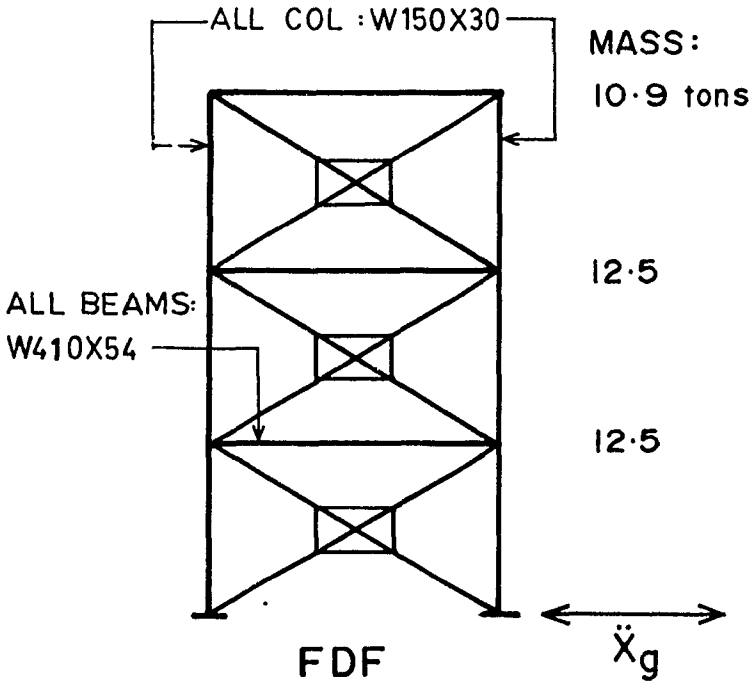

Figure 3.1.4 Final Frame

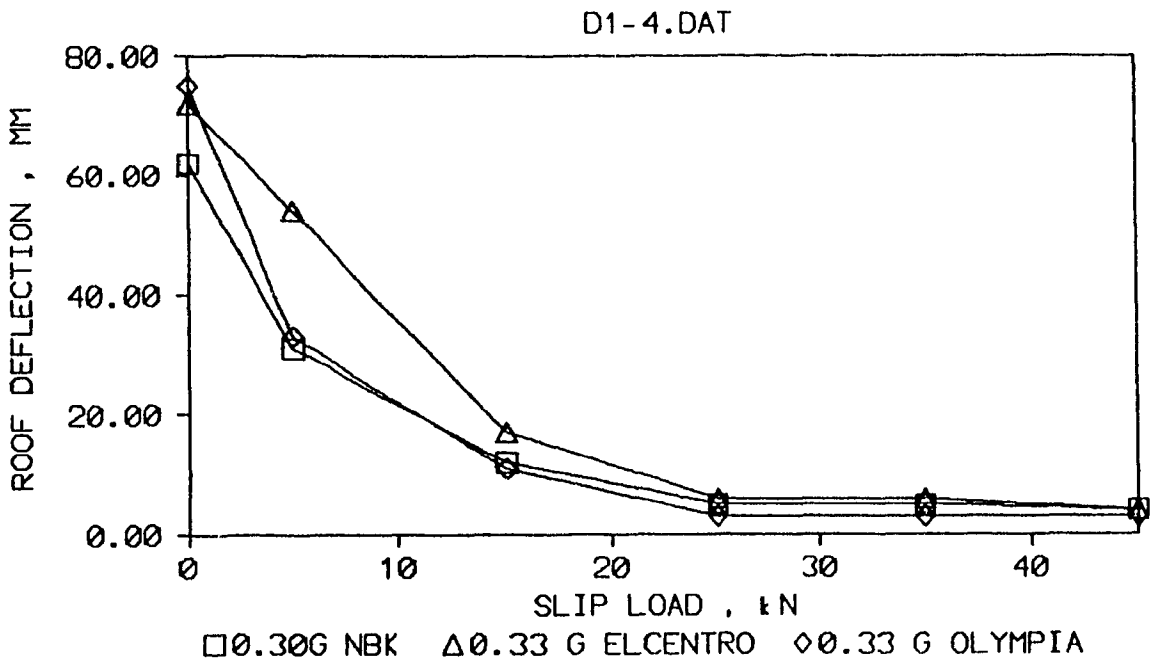

Figure 3.1.5 Typical Roof deflection vs. slip load levels for different earthquake records

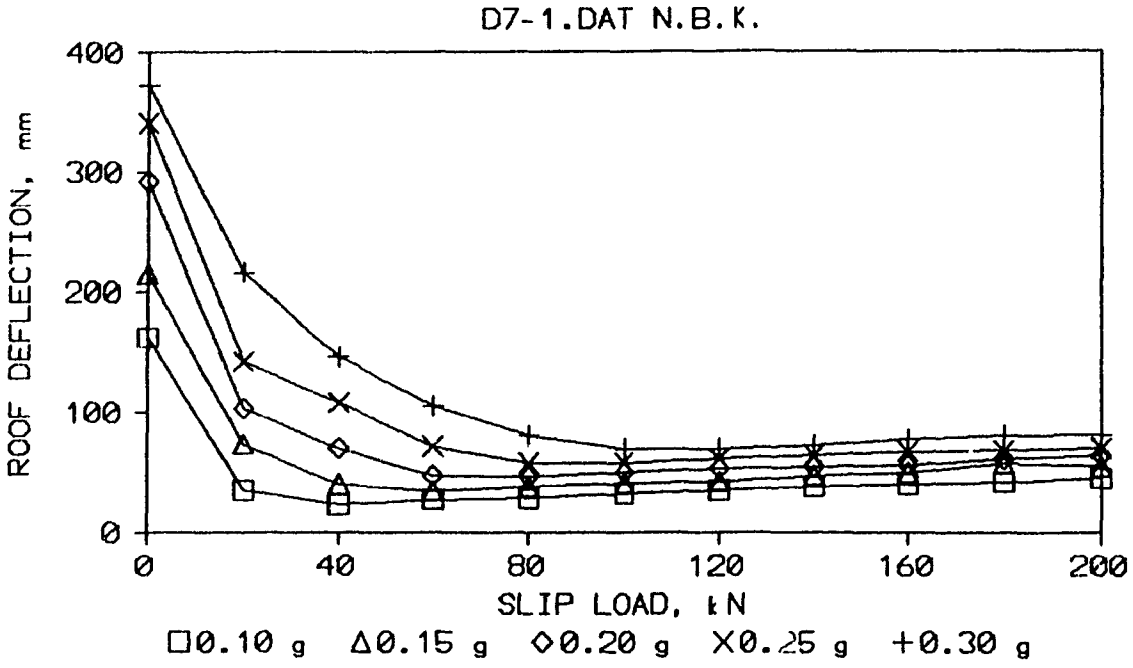

Figure 3.1.6 Typical Roof Deflection response vs. slip load for different peak intensity (NBK)

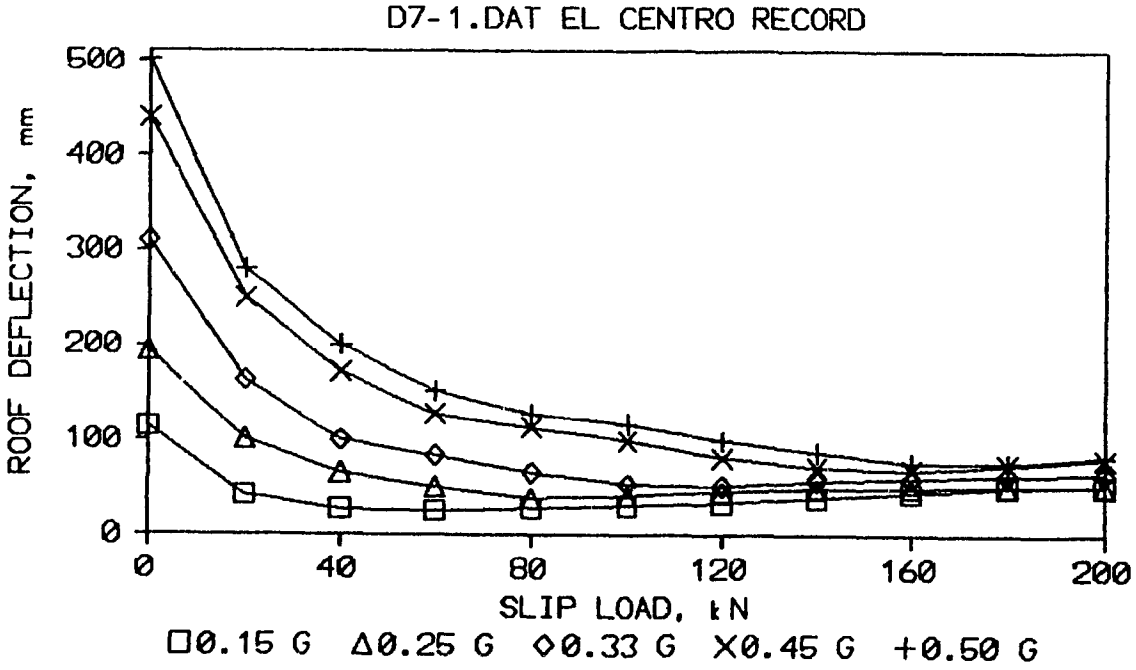

Figure 3.1.7 Typical Deflection response vs. slip load for for different peak intensity (El Centro)

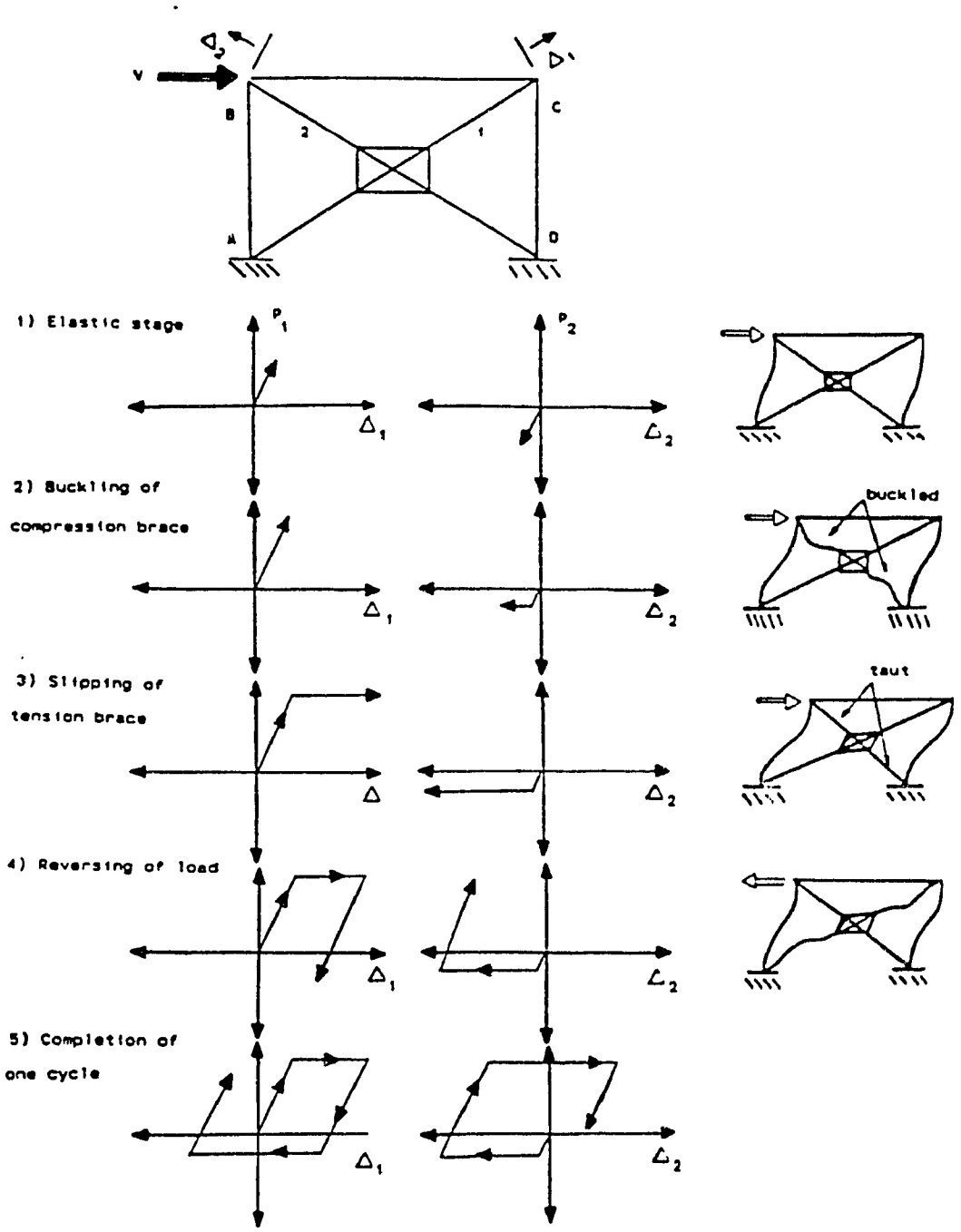

Figure 3.1.8 Typical hysteretic behaviour of a simple friction-damped-braced frame

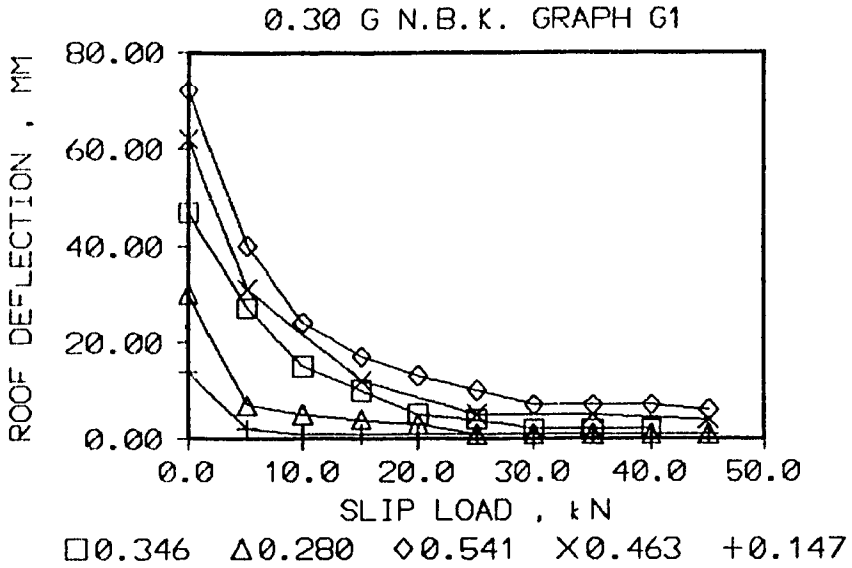

Figure 3.3.1 Deflection response vs. slip load for 0.30 g N. B. K. earthquake record
(MRF To = 0.346, 0.280, 0.541, 0.463, 0.147 sec)

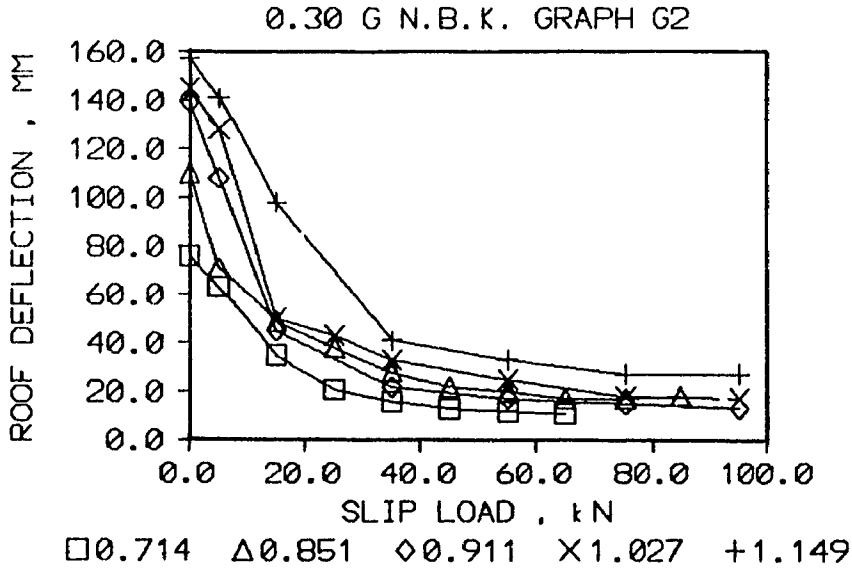

Figure 3.3.2 Deflection response vs. slip load for 0.30 g N. B. K. earthquake record
(MRF To = 0.714, 0.851, 0.911, 1.027, 1.149 sec)

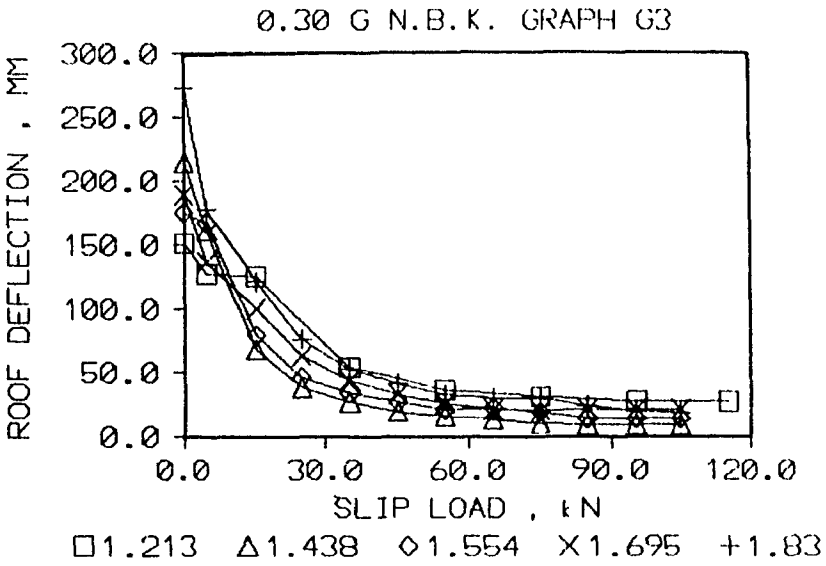

Figure 3.3.3 Deflection response vs. slip load for 0.30 g N. B. K. earthquake record (MRF To = 1.213, 1.438, 1.554, 1.695 1.830 sec)

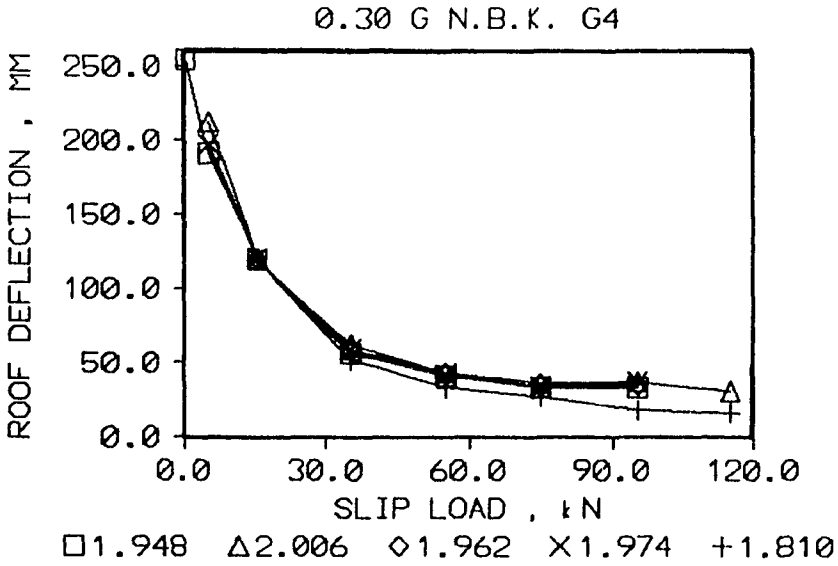

Figure 3.3.4 Deflection response vs. slip load for 0.30 g N. B. K. earthquake record (MRF To = 1.948, 2.006, 1.962, 1.974, 1.810 sec)

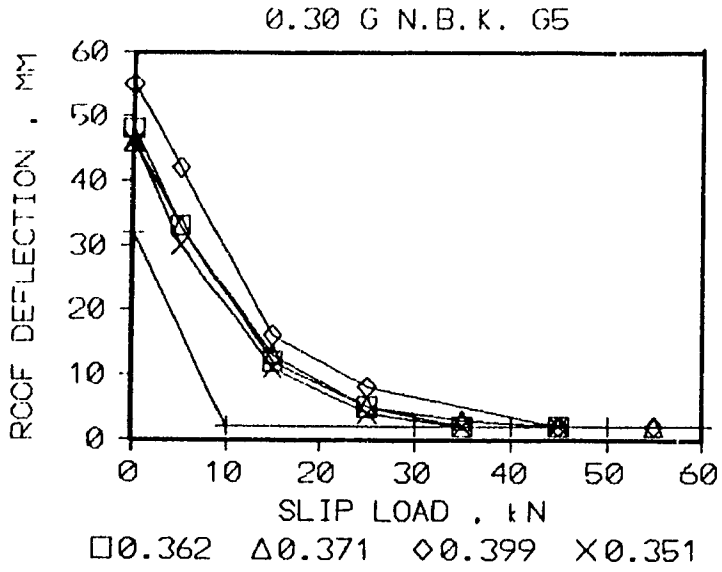

Figure 3.3.5 Deflection response vs. slip load for 0.30 g N. B. K. earthquake record
(MRF To = 0.362, 0.371, 0.399, 0.351, 0.210 sec)

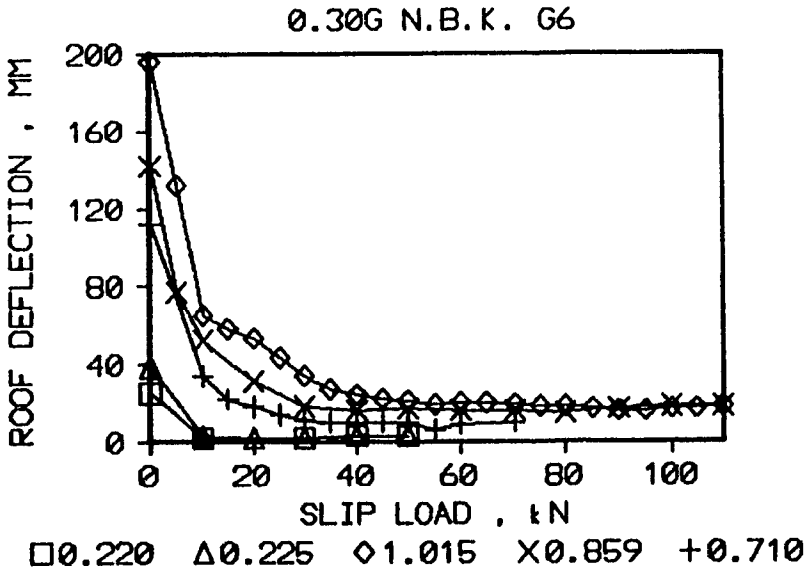

Figure 3.3.6 Deflection response vs. slip load for 0.30 g N. B. K. earthquake record
(MRF To = 0.220, 0.225, 1.015, 0.859, 0.710 sec)

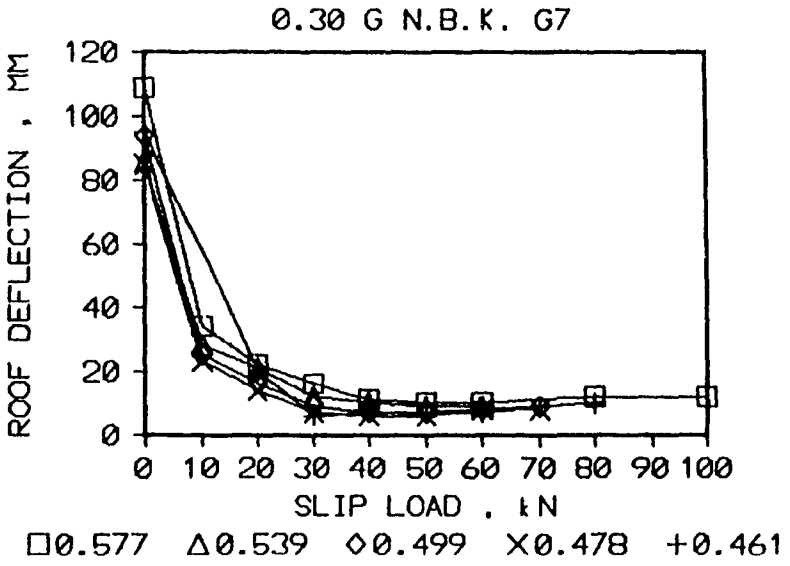

Figure 3.3.7 Deflection response vs. slip load for 0.30 g N. B. K. earthquake record (MRF To = 0.577, 0.539, 0.499, 0.478, 0.461 sec)

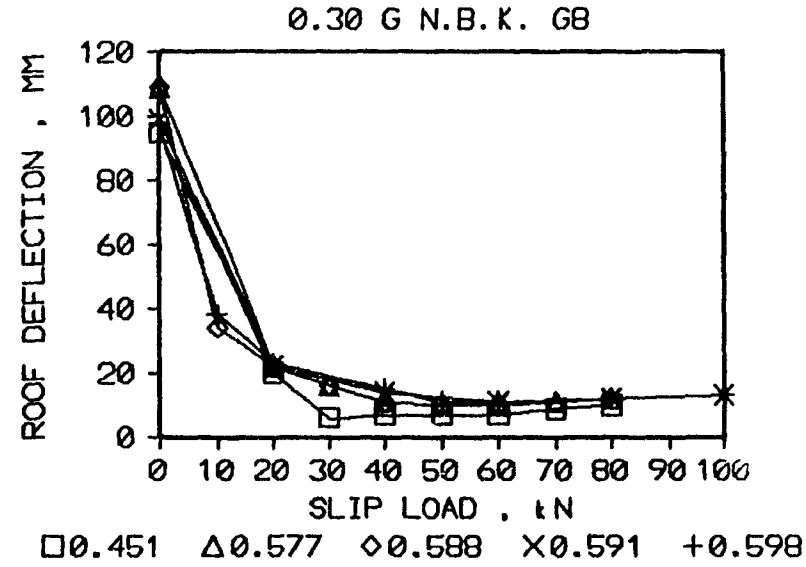

Figure 3.3.8 Deflection response vs. slip load for 0.30 g N. B. K. earthquake record (MRF To = 1.948, 2.006, 1.962, 1.974, 1.810 sec)

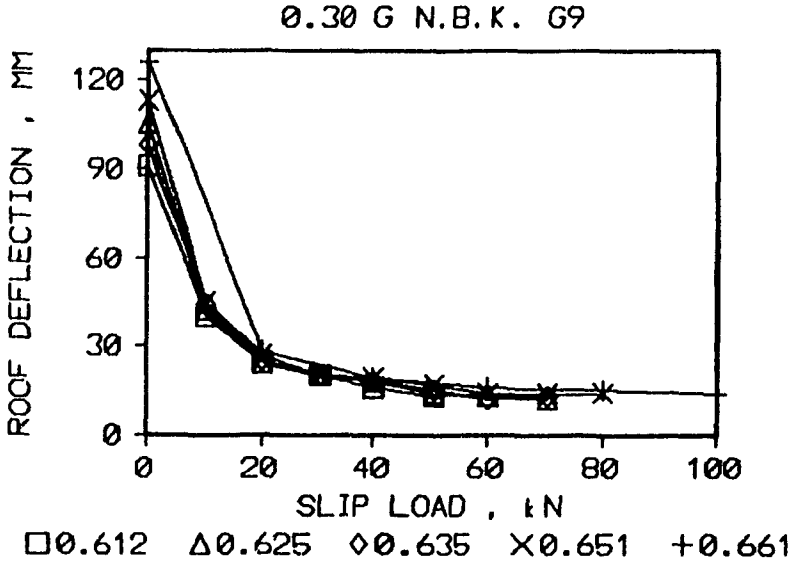

Figure 3.3.9 Deflection response vs. slip load for 0.30 g N. B. K. earthquake record (MRF To = 0.612, 0.625, 0.635, 0.651, 0.661 sec)

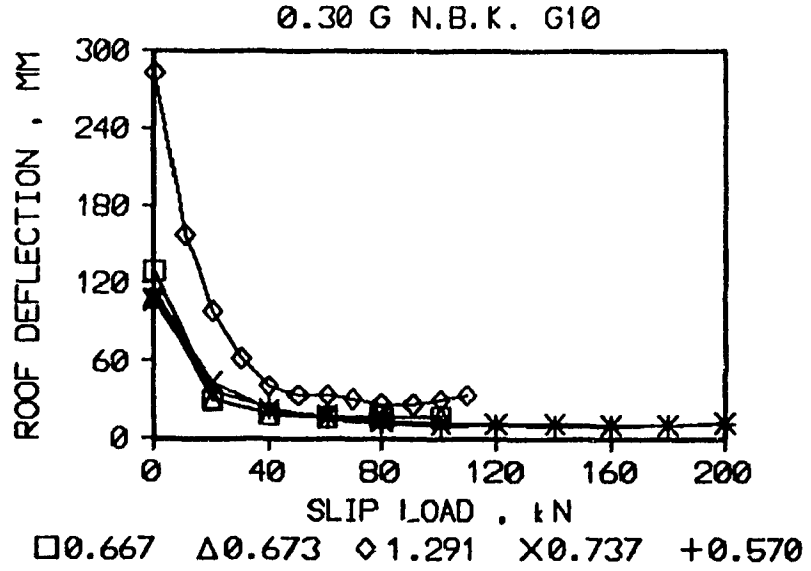

Figure 3.3.10 Deflection response vs. slip load for 0.30 g N. B. K. earthquake record (MRF To = 0.667, 0.673, 1.291, 0.737, 0.570 sec)

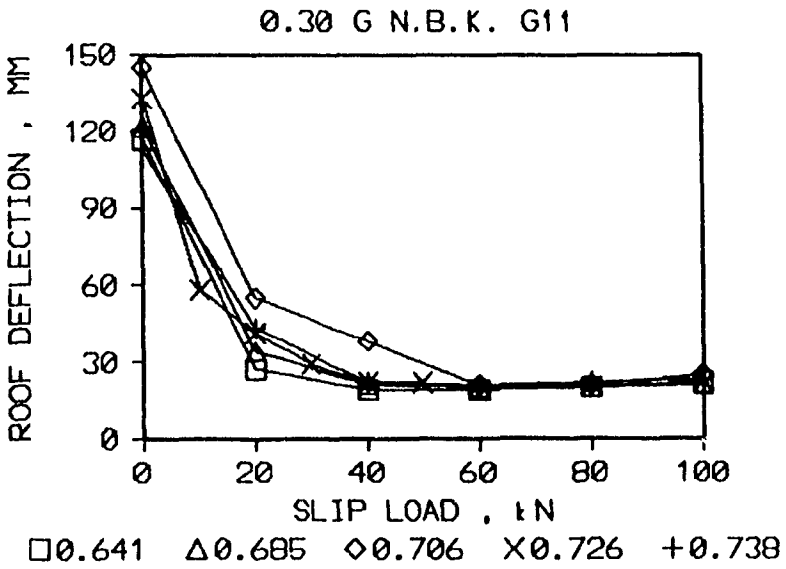

Figure 3.3.11 Deflection response vs. slip load for 0.30 g N. B. K. earthquake record (MRF To = 0.641, 0.685, 0.706, 0.726, 0.738 sec)

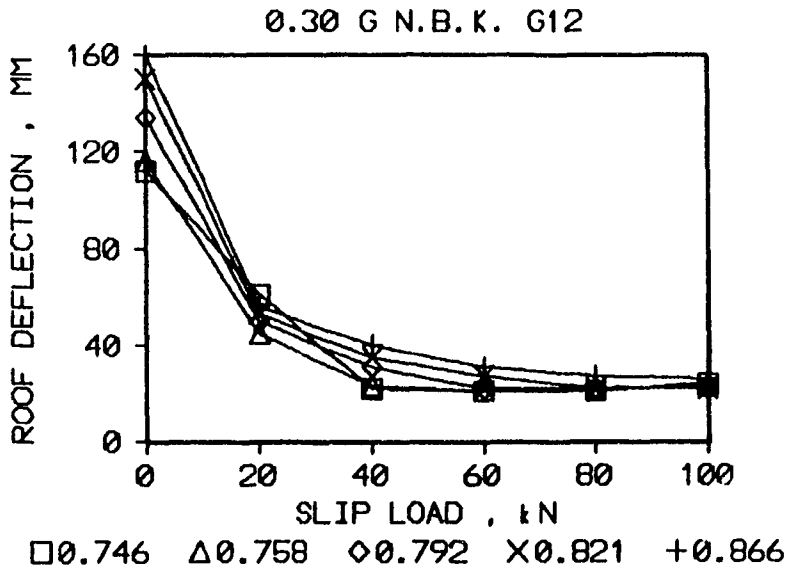

Figure 3.3.12 Deflection response vs. slip load for 0.30 g N. B. K. earthquake record (MRF To = 0.746, 0.758, 0.792, 0.821, 0.866 sec)

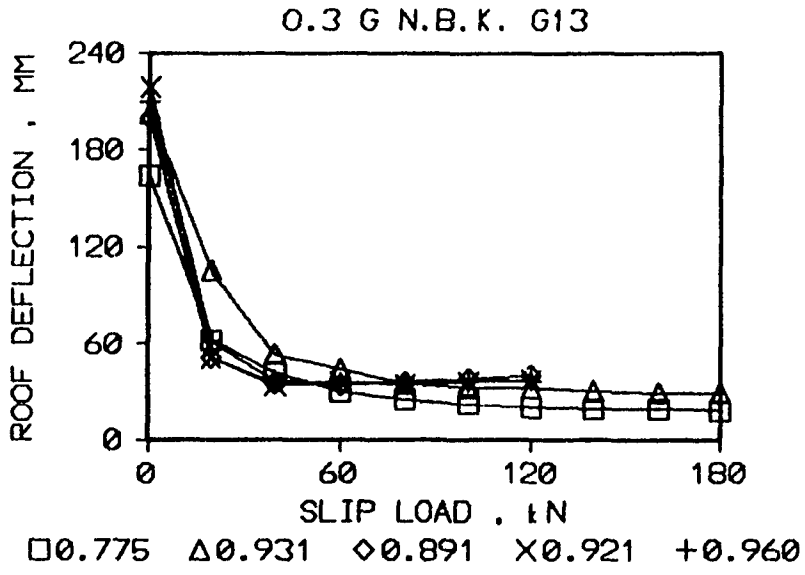

Figure 3.3.13 Deflection response vs. slip load for 0.30 g N. B. K. earthquake record (MRF To = 0.775, 0.931, 0.891, 0.921, 0.960 sec)

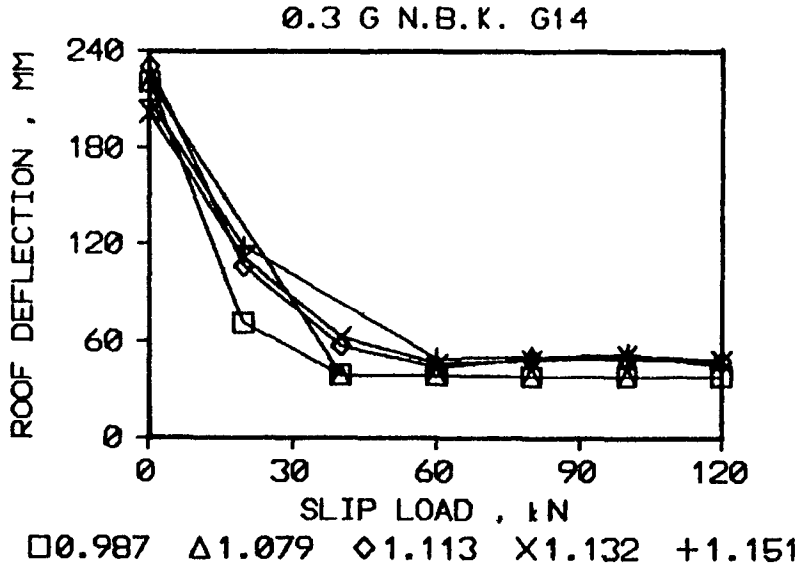

Figure 3.3.14 Deflection response vs. slip load for 0.30 g N. B. K. earthquake record (MRF To = 0.987, 1.079, 1.113, 1.132, 1.151 sec)

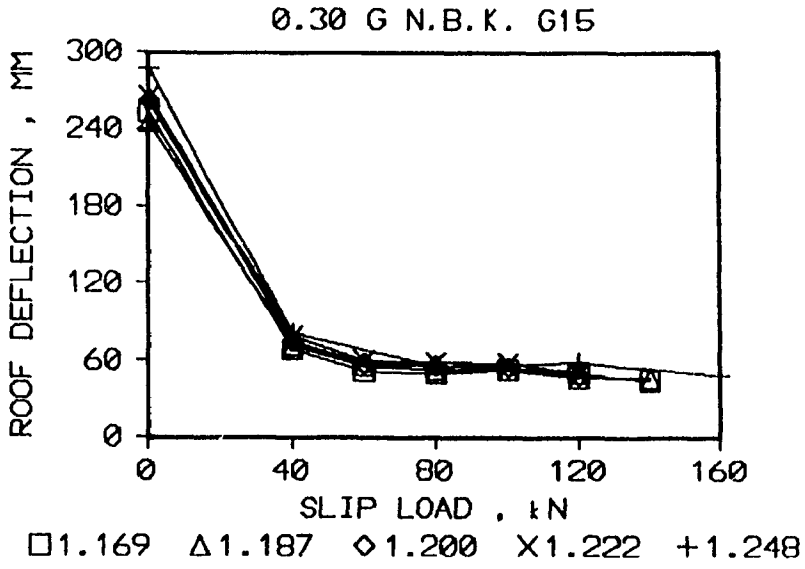

Figure 3.3.15 Deflection response vs. slip load for 0.30 g N. B. K. earthquake record (MRF To = 1.169, 1.187, 1.200, 1.222, 1.248 sec)

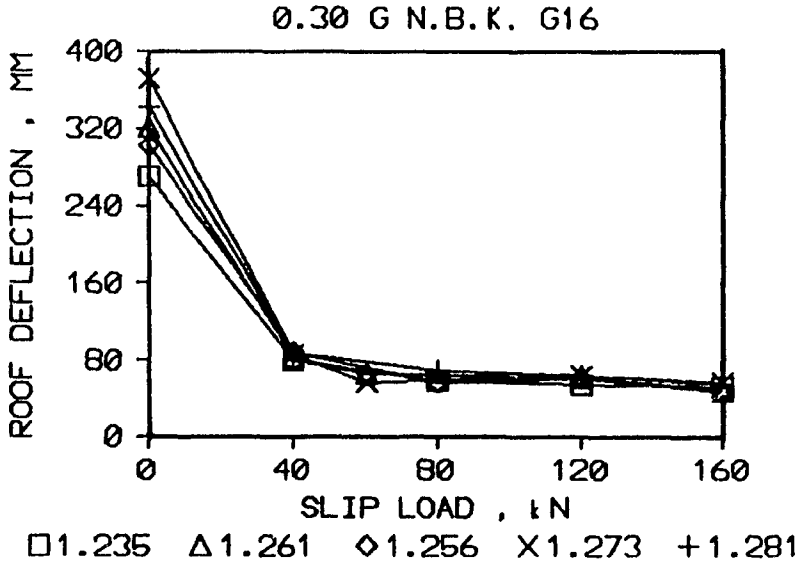

Figure 3.3.16 Deflection response vs. slip load for 0.30 g N. B. K. earthquake record (MRF To = 1.235, 1.261, 1.256, 1.273, 1.281 sec)

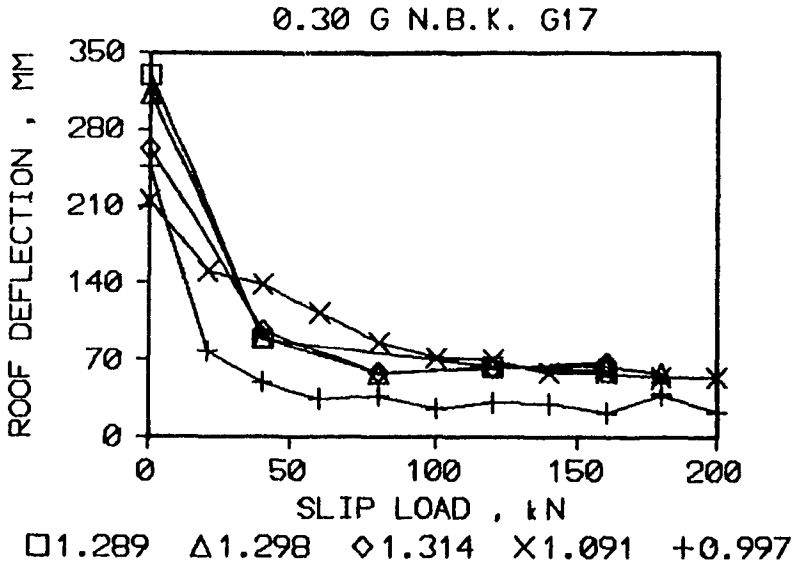

Figure 3.3.17 Deflection response vs. slip load for 0.30 g N. B. K. earthquake record
(MRF To = 1.289, 1.298, 1.314, 1.091, 0.997 sec)

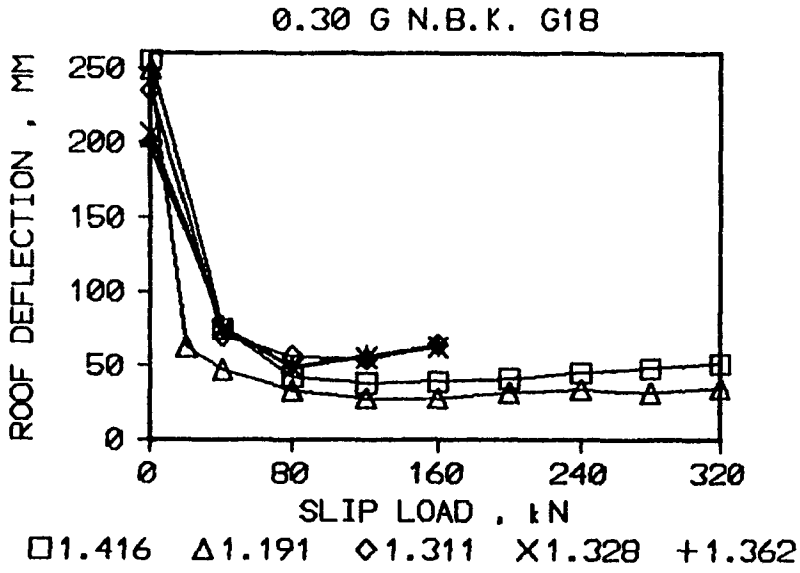

Figure 3.3.18 Deflection response vs. slip load for 0.30 g N. B. K. earthquake record
(MRF To = 1.416, 1.191, 1.311, 1.320, 1.362 sec)

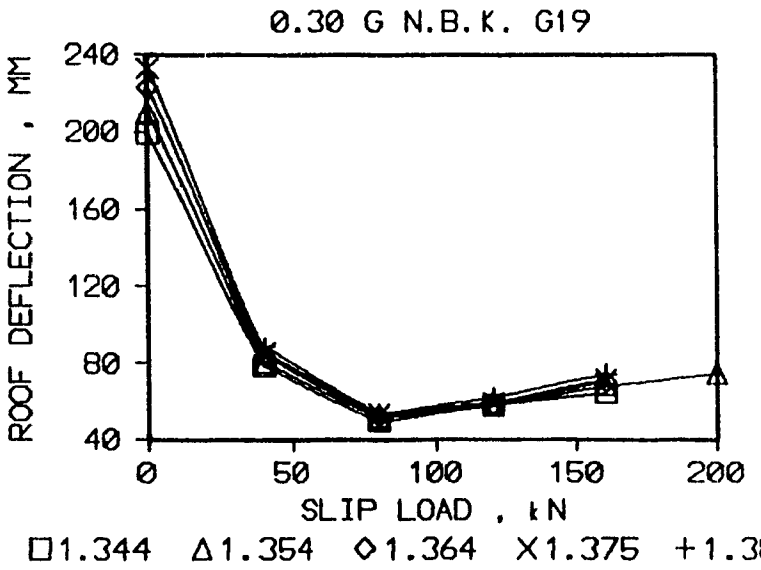

Figure 3.3.19 Deflection response vs. slip load for 0.30 g N. B. K. earthquake record (MRF To = 1.344, 1.354, 1.364, 1.375, 1.386 sec)

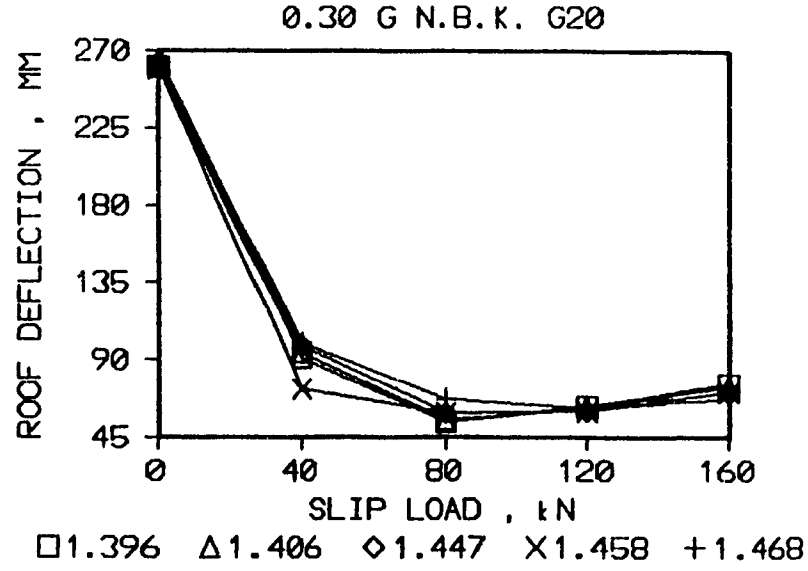

Figure 3.3.20 Deflection response vs. slip load for 0.30 g N. B. K. earthquake record (MRF To = 1.396, 1.406, 1.447, 1.458, 1.468 sec)

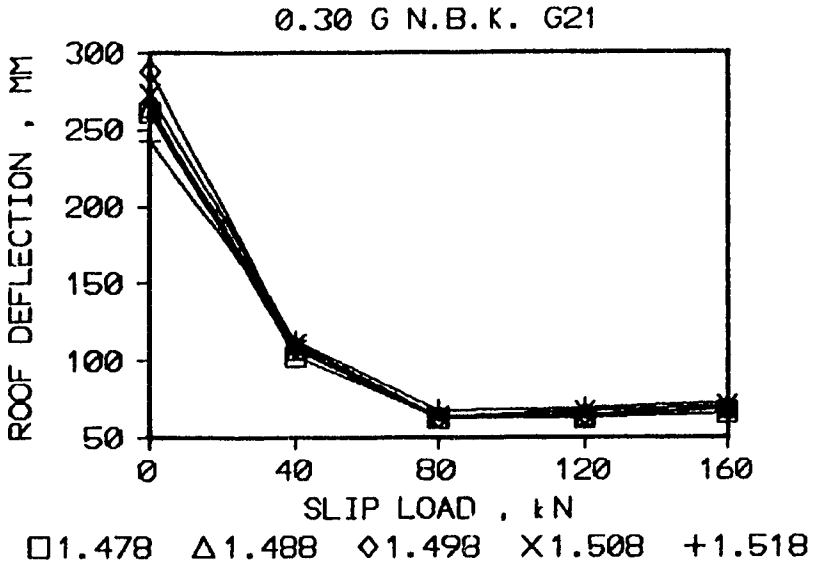

Figure 3.3.21 Deflection response vs. slip load for 0.30 g N. B. K. earthquake record (MRF To = 1.478, 1.488, 1.498, 1.508, 1.510 sec)

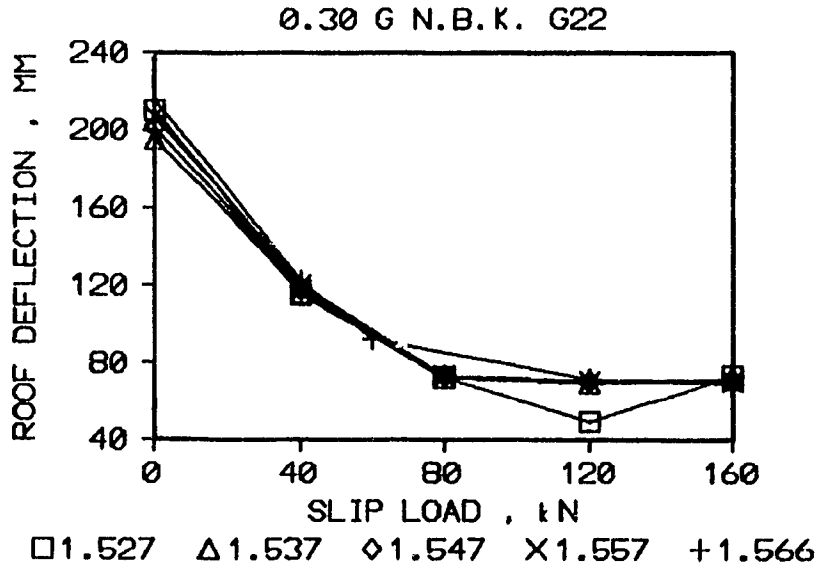

Figure 3.3.22 Deflection response vs. slip load for 0.30 g N. B. K. earthquake record (MRF To = 1.527, 1.537, 1.547, 1.557, 1.566 sec)

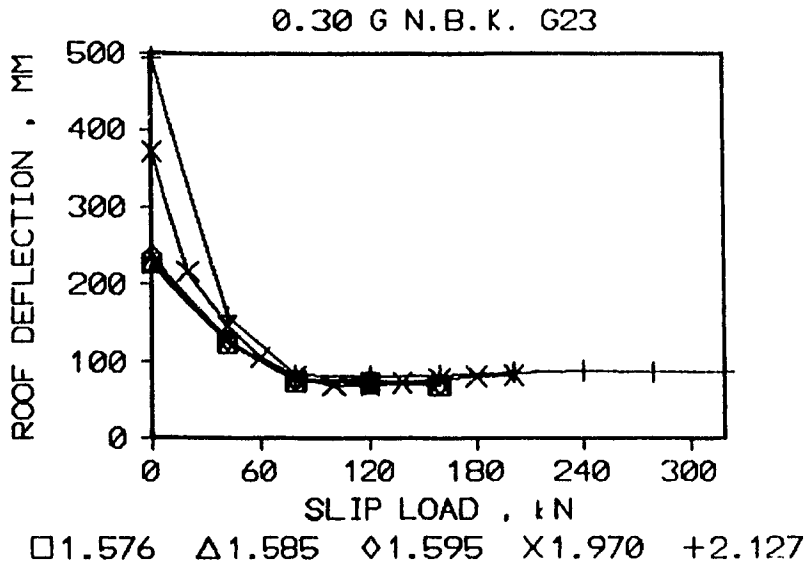

Figure 3.3.23 Deflection response vs. slip load for 0.30 g N. B. K. earthquake record
(MRF To = 1.576, 1.585, 1.595, 1.970, 2.127 sec)

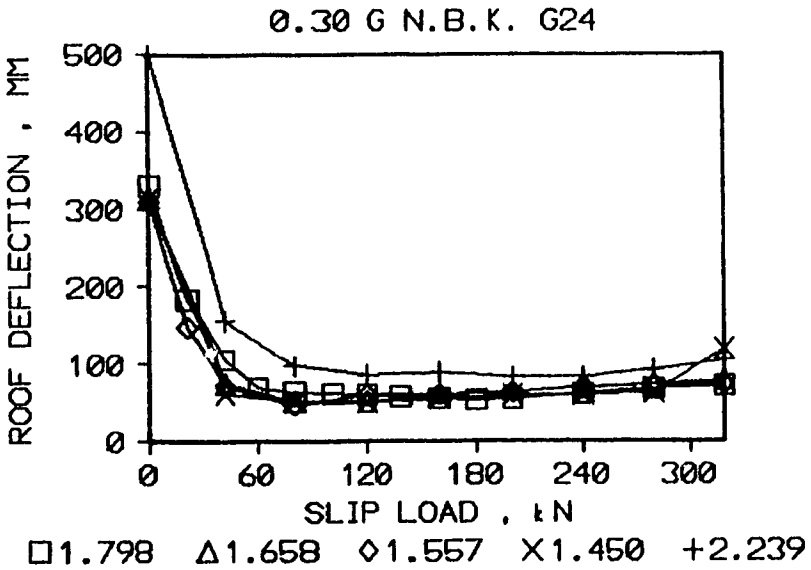

Figure 3.3.24 Deflection response vs. slip load for 0.30 g N. B. K. earthquake record
(MRF To = 1.798, 16581, 1.557, 1.453, 2.239 sec)

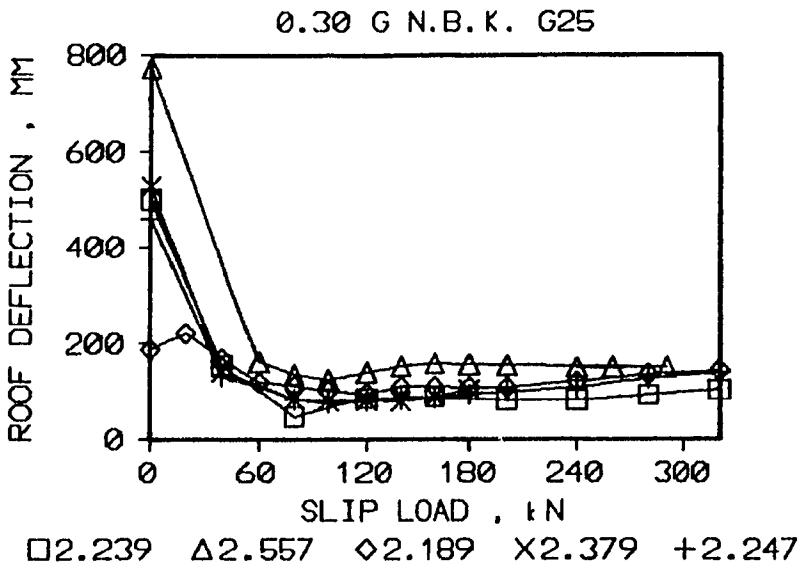

Figure 3.3.25 Deflection response vs. slip load for 0.30 g N. B. K. earthquake record (MRF To = 2.239, 2.557, 2.189, 2.379, 2.247 sec)

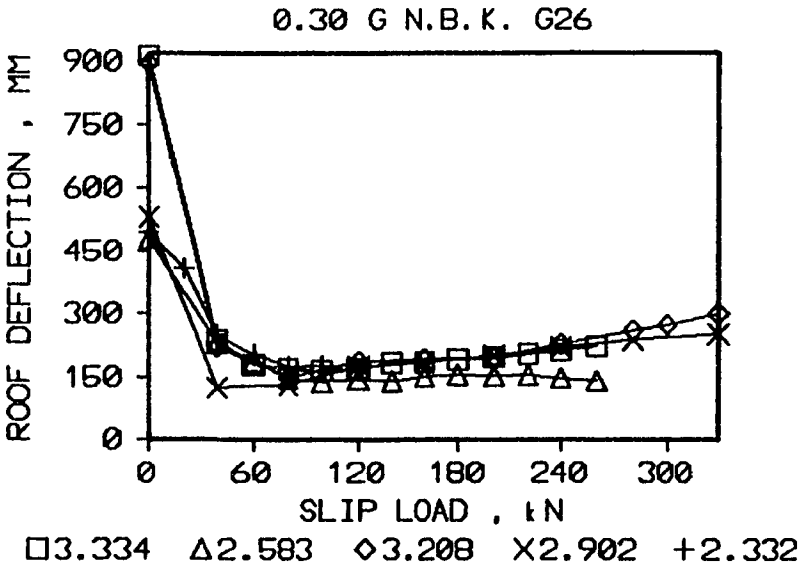

Figure 3.3.26 Deflection response vs. slip load for 0.30 g N. B. K. earthquake record (MRF To = 3.334, 2.583, 3.200, 2.902, 2.332)

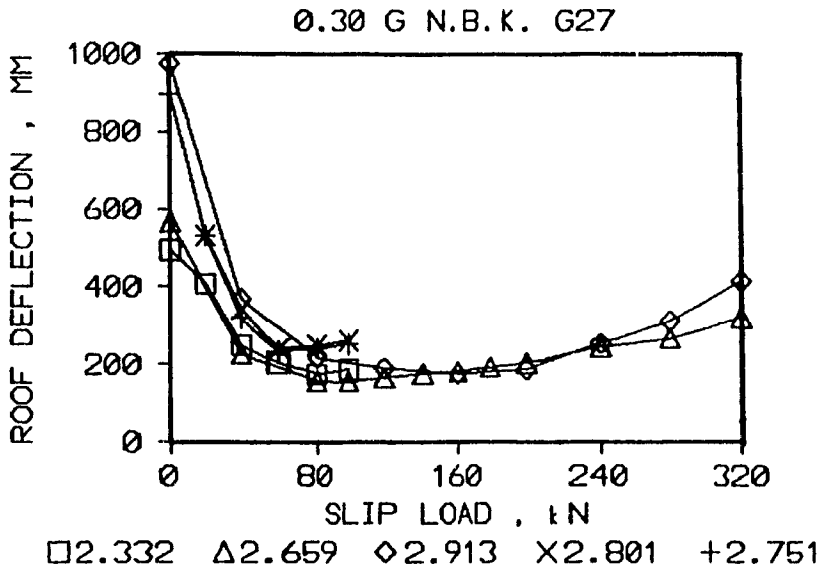

Figure 3.3.27 Deflection response vs. slip load for 0.30 g N. B. K. earthquake record
(MRF To = 2.332, 2.659, 2.913, 2.801, 2.751 sec)

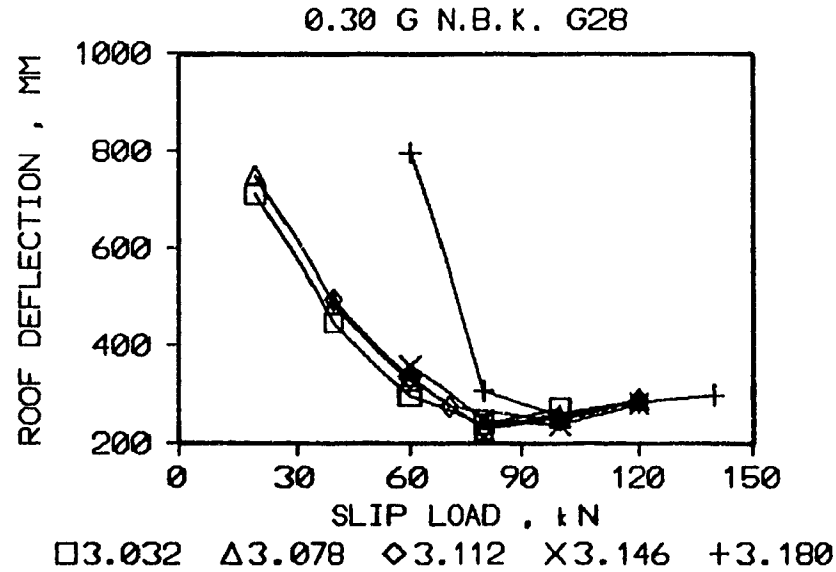

Figure 3.3.28 Deflection response vs. slip load for 0.30 g N. B. K. earthquake record
(MRF To = 3.032, 3.078, 3.112, 3.146, 3.180 sec)

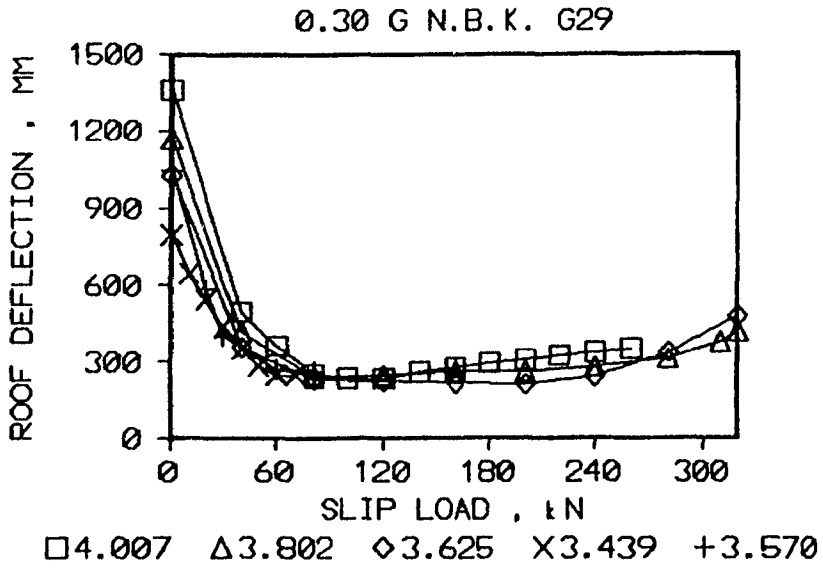

Figure 3.3.29 Deflection response vs. slip load for 0.30 g N. B. K. earthquake record (MRF To = 4.007, 3.802, 3.625, 3.439, 3.570 sec)

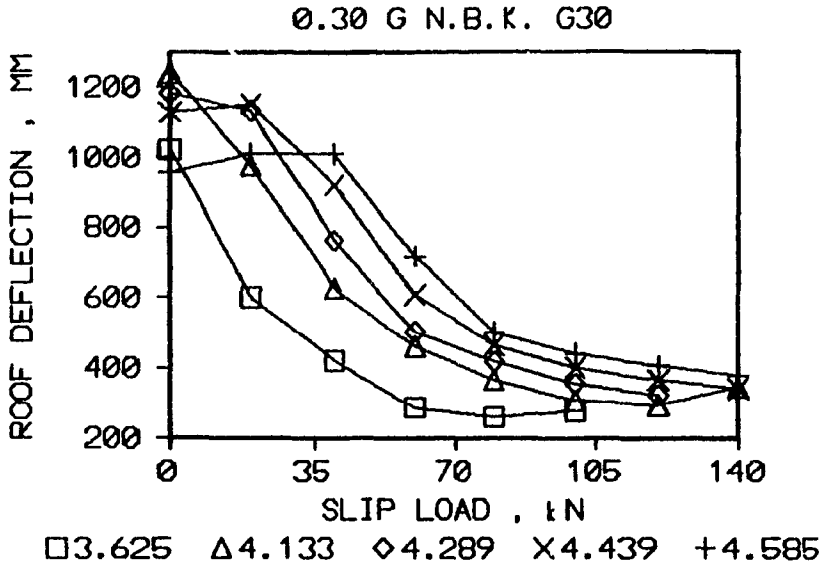

Figure 3.3.30 Deflection response vs. slip load for 0.30 g N. B. K. earthquake record (MRF To = 3.625, 4.133, 4.289, 4.439, 4.585 sec)

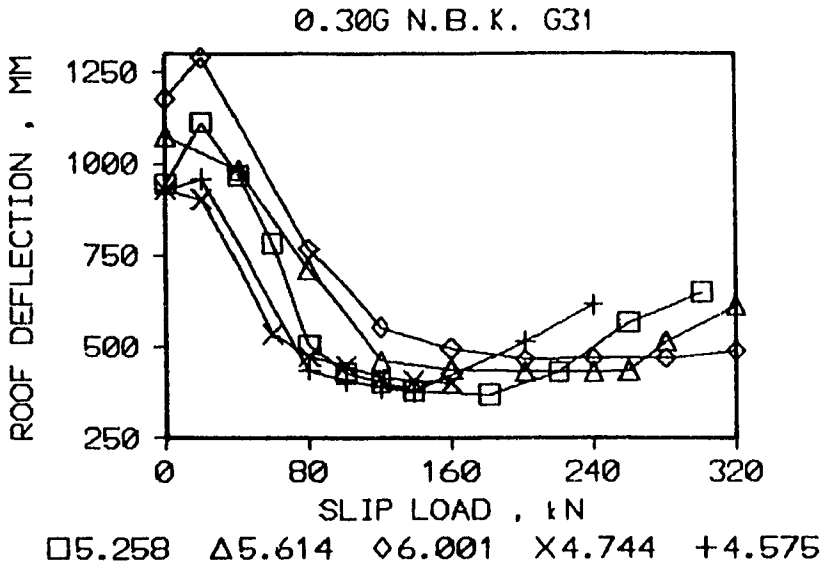

Figure 3.3.31 Deflection response vs. slip load for 0.30 g N. B. K. earthquake record (MRF To = 5.258, 5.614, 6.001, 4.744, 4.575 sec)

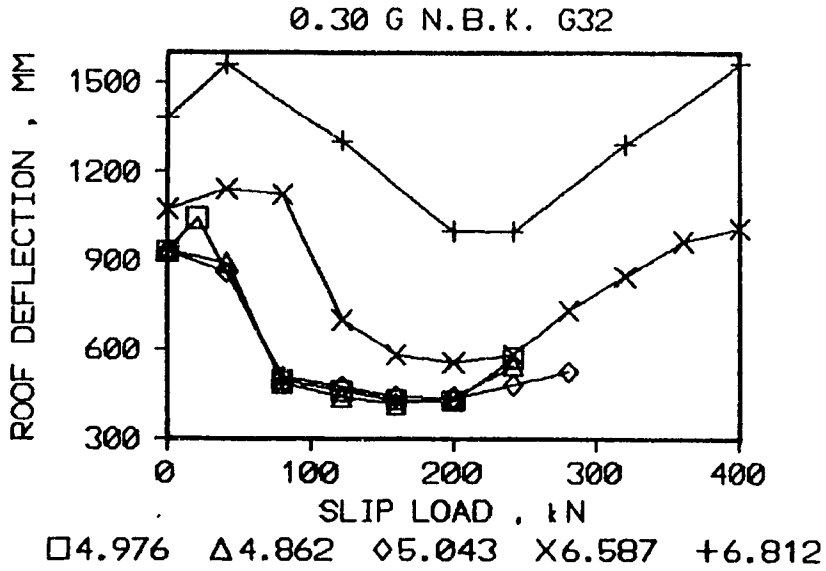

Figure 3.3.32 Deflection response vs. slip load for 0.30 g N. B. K. earthquake record (MRF To = 4.976, 4.862, 5.043, 6.587, 6.812 sec)

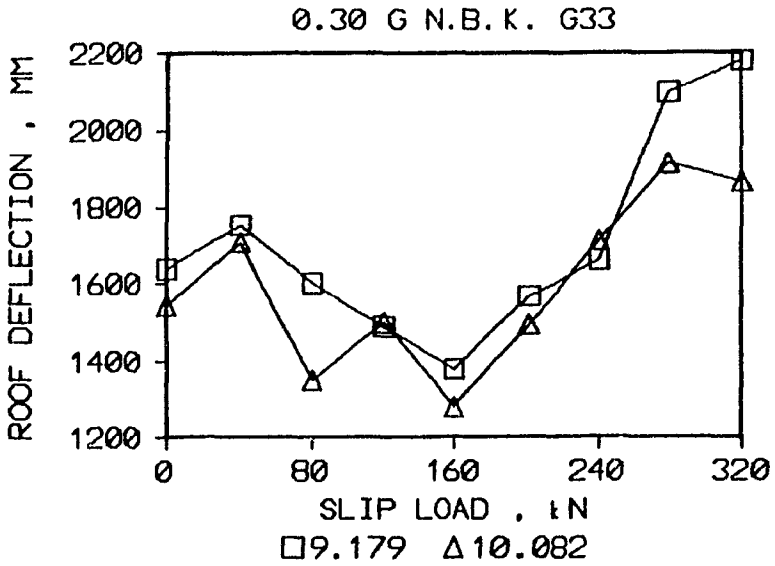

Figure 3.3.33 Deflection response vs. slip load for 0.30 g N. B. K. earthquake record
(MRF To = 9.179, 10.082 sec)

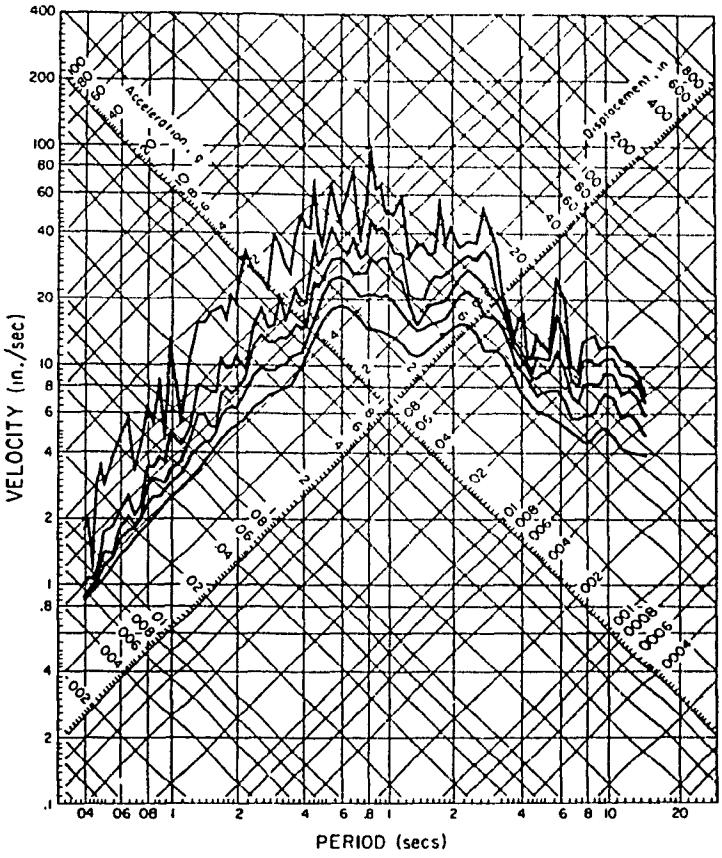

Fig. 3.4 Response Spectrum for the 1940 El Centro Earthquake

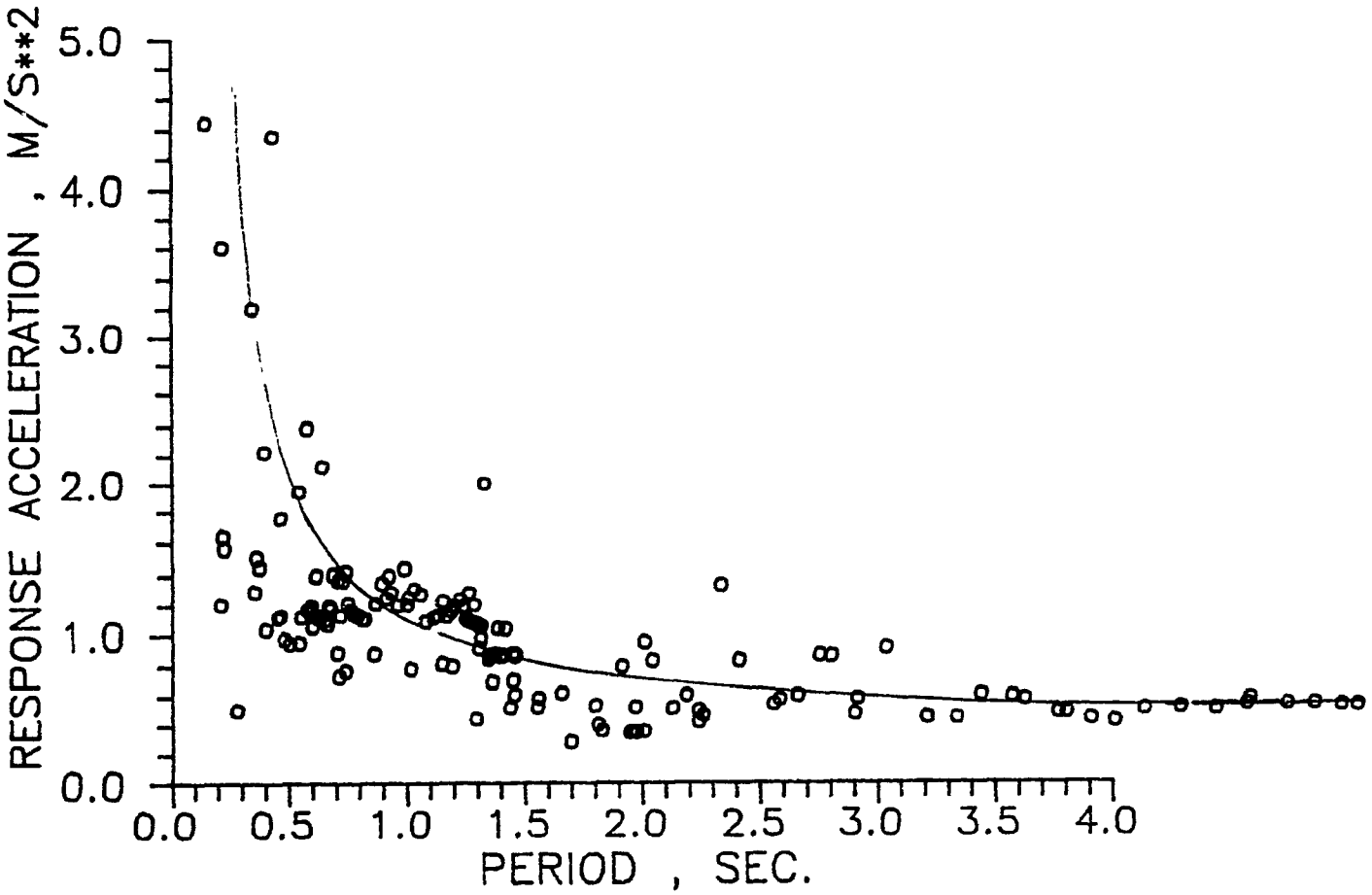

Figure 3.5 Resposne Spectrum for the Friction-damped-Frames

4.0 Simplified Analysis of Friction Damped Frames

In this chapter the response deformation spectrum created for the FDF systems in the earlier chapter will be utilized for the approximate analysis of the FDF systems at the optimum conditions as illustrative examples. Several example frames will be used to illustrate the modal response analysis techniques and to test the accuracy and effectiveness of the generated response spectrum. Published data found in the literature will be used as input for these examples. Forces induced on the building structures and the deformations developed by the seismic forces will be matched against those from the time-history analyses. Comparison of the results obtained from these analyses will be highlighted.

The detailed formations and applications of the theory of modal response analysis can be found in most standard texts for structural dynamics (34). The modal response analysis is also incorporated as one of the analysis options in the TABS77 computer program, it will be used as the tool to verify the response spectrum generated in the previous chapter.

For the spectrum-based modal analysis, one of the main variables used in the theory of modal analysis is the frequency of vibration for the elastic system. These can be found by setting up the proper mass and stiffness matrices of the system and solving them for their proper eigen values. A brief outline of the theory is given in appendix B.

4.1 Frame No. 1 (Workman's frame)

As the first illustration, consider the ten story braced steel frame shown in Fig. 4.1.1. This is the Workman's frame reported in the DRAIN-2D manual. The properties and dimensions used are those obtained from the manual's example. Imperial units are used here mainly because of convenience of reference as this frame was widely studied by many researchers.

The optimum slip load of the frame was obtained by a series of analyses using the DRAIN-2D program based on minimum roof level deflection response. N.B.K. earthquake was used as the ground motion input. Again, the 0.30 g was used as the scaling factor. Other pertinent data include : zero critical damping; a reactive mass of 0.3419 kips-sec^2/inch per floor; no static loads; and constant slip load for all floors. A brace area of 3.38 in^2 (2200 mm^2)is used and this corresponds to the α values range from 6.5 to 1.0 for the frame. The outcomes from the time-history are plotted in Fig. 4.1.2. The optimum slip load for this frame for minimum roof deflection response appears to be about 70 kips with a minimum roof deflection of about 8 inches at the roof level. All devices are observed to have slipped throughout the floors. It is interesting to note that the estimated optimum slip load based on equation 2.1.8 as suggested by Baktash is about 85 kips. An average M_p was used and was based on the average value of the

floor beams. The approximate equivalent critical damping ratio at the optimum slip load condition for the MRF is about 14%. The results obtained at the optimum slip load condition were retained for comparison against the modal response analysis.

To perform the modal response analysis, the frequencies must be obtained first. These were obtained by using the same properties and dimensions from the same frame used in the time-history analysis. Knowing the periods of the MRF frame, the corresponding approximate response accelerations are then obtained from the response spectrum of Fig. 3.5. These are shown below together with the periods. They are then used as input (as the modal response accelerations) to the modal analysis effected with the TABS77 program.

i	T_i (s)	a (in/s^2)
1	3.769	19.7
2	1.270	39.4
3	0.702	51.2
4	0.469	86.6
5	0.339	121.1

The root sum of square summation method is used to obtain the probable maximum response envelopes. Figures 4.1.3 and 4.1.4 show the envelopes for the floor deflections and the maximum storey shear of the building respectively. As can be seen from the figure, the maximum floor deflection envelopes compare favourably except at the roof level. The maximum deflection by modal analysis is about 20% less than that of

time history analysis. The storey shears plotted are the total column shear which excluded the forces in the braces. The shear distribution envelopes shown in Fig. 4.1.4 are relatively good from the tenth floor to the fourth floor. From there onwards the time-history results depart from that of the modal analysis. This is to be expected since the spectrum was generated by matching maximum deflection only. As the spectrum is generated with a reduced stiffness of a MRF, whereas that of the FDF is much stiffer in the lateral direction before yielding, therefore for the same deflection, the reduced stiffness of the MRF obviously will produce smaller stresses in its members. In the FDF case at 0.30g N.B.K., two floor beams were seen to have developed plastic hinges. This is seen in Fig. 5.1 and all the columns remained elastic.

4.2 Frame No. 2

Frame No. 2 is the one-third scale nine storey frame recently tested at Berkeley for the FDF system (18). The properties of the frame were obtained from the report by Huckelbridge (34). Figure 4.2.1 shows the dimensions and properties of the frame. Again, imperial units are used only for convenience since the original data are in the same units. No static loads are applied and constant slip loads are used throughout. A mass of 0.01294 kips-sec^2/in is assigned to each floor. A brace area of 0.5 in^2 (330 mm^2) is used and this corresponds to the α of 1.3 to 1.0 for the frame. Figure 4.2.2

shows the plot of floor deflection envelopes versus the slip loads. It appears that the optimum slip load is about 15 kips. From equation 2.1.8, the estimated optimum slip load is about 13.1 kips. This values is close to the value obtained from the time-history analyses. The equivalent critical damping ratio for the MRF is about 16 %. The periods of vibrations for the frame are calculated and their corresponding response accelerations are:

i	T_i (s)	a (in/s^2)
1	0.43314	102.3
2	0.14118	157.4
3	0.08064	161.4
4	0.05479	165.3
5	0.04039	169.2

These values are then used as inputs for the modal dynamic analysis. Figures 4.2.3 and 4.2.4 show the deflection envelopes and maximum base storey shear envelopes from the results of the results of the test frame. In this example, the displacement envelopes do not seem to match very well. The time history result appears to be about 45 % more than that of the modal analysis. It could be explained by the fact that only the first mode of 0.5 second happens to be in the strong energy contents of the ground motion data and the frame was severely shaken by it. The response spectrum does not adequately cover this period range of response. Again the time history storey shear is about twice the magnitude of that from the modal analysis. One can easily visualize this by

plotting the higher damping ratio response spectrum from Figure 2.9.2. A peak is observed in the 0.4 to 0.5 sec. range with a response acceleration of about 5 m/s^2. This seems to be the right number required to match the response for the DRAIN-2D output. All members of the FDF remained elastic as shown in Fig. 5.2.

4.3 Frame No. 3 (UBC Frame)

The third example is the three storey steel frame tested at UBC by Cherry and Filiatrault. The actual prototype of the model is the first three floors of the Workman's frame, which is used as the frame No. 1. The model is shown in Figure 4.3.1 together with the dimensions and properties used. A brace area of 36 mm^2 is used and this gives the α values of about 1.0 for the frame. The optimum slip load obtained by Cherry and Filiatrault from the time history analysis is about 7 kN for the 0.30g NBK ground motion record. In this case, the estimated optimum slip load value is about 18.8 kN. The equivalent critical damping ratio for the MRF is about 40 %. The following lists the periods of vibration and the their corresponding response accelerations. A floor mass of 0.850 tons are assigned to the third and second floors, and 0.575 ton to the first floor, no static
loads are applied.

i	T_i (s)	a (m/s^2)
1	0.39434	2.7
2	0.10902	4.3
3	0.05506	4.4

Figure 4.3.2 shows the maximum displacement versus the slip load plot for this particular frame. From the plot it appears that the optimum slip load is about 7 kN as found by Cherry and Filiatrault for a peak acceleration of 0.30 g. From the modal analysis, the floor displacement envelope seems to agree well with that of the time-history. The maximum roof level displacements is off by about 20 %. The difference can be best explained by the response acceleration so obtained from the graph is that from the upper bound values. The storey shears is still off by about 50%. From Fig. 5.3, no plastic hinge was seen to have developed for FDF example no.3.

4.4 Frame No. 4 (Example 1 of DRAIN-2D)

The fourth example is the first example in the original DRAIN-2D manual. It is a ten storey frame with typical stiffness and masses and the properties and dimensions are as shown in Figs. 4.4.1. A brace area of 8.0 in^2 (5120 mm) is used and this gives the α values of 2.3 to 1.0 for the frame. This corresponds to a yield force of about 352 kips. A quick analysis with the TABS program for the BMRF showed that the maximum load on the ground floor brace element is about 250 kips. So this indicates that the brace element will function

properly during service conditions.

The frame is then subjected to the NBK ground motion and the floor deflection versus slip load curve is as shown in Fig. 4.4.2. The curve decreases to a small plateau at about 70 kips and then moves upward again, and then decreases again. So it appears that the optimum slip load for this frame, given the particular ground motion is about 70 kips. The equivalent critical damping ratio for the MRF is about 20%. The periods of vibrations of the frame and the response acceleration are as follow:

i	T_i (s)	a (in/s^2)
1	2.6423	19.7
2	0.9314	47.2
3	0.5324	70.8
4	0.3663	161.4
5	0.2652	188.9

The corresponding floor deformation is plotted together with that of the DRAIN-2D in Fig. 4.4.3. This time the maximum displacement at the roof level is off by about 25% and the storey shear is off by only about 22%. All the floor beams of the first seven floors of the FDF were found to have developed plastic hinges, and so have all the ground floor columns. The locations of the yield hinges are shown in Fig. 5.4.

4.5 Frame No. 5

Example no. 5 is the six storey high, two bay test

frame used by A. K. Jain for the study of reinforced concrete frame with steel bracing elements (35). In this example, the original material property was retained, also the stiffness degrading model was used for the reinforced concrete beam elements. A dead load of 27 kN/m is used for the frame. Properties and dimensions used are shown in Figure 4.5.1. A brace area of 3000 mm^2 is used and this corresponds to the α values of 2.3 to 1.3 for the frame. The first fundamental period of the frame calculated by using TABS is about 1.30 sec for the MRF. A concrete compressive strength of 15 MPa and for the steel a yield strength of 415 MPa are used for computing the yield stresses for the members. Reinforcements of rebars are as per the descriptions given in the test review by the author.

The same frame is modeled on the DRAIN-2D program and the optimum slip load condition is obtained in the usual way. This is shown in Fig. 4.5.2. The deflection at optimum slip load is about 48 mm. The equivalent critical damping ratio for the MRF at optimum slip load condition is about 15 %. The first five modes of vibrations and their response accelerations are:

i	T_i (s)	a (m/s^2)
1	1.3026	1.0
2	0.4177	2.3
3	0.2276	3.6
4	0.1488	4.4
5	0.1081	4.8

These are used as the input acceleration spectrum for the modal analysis on the TABS. Figure 4.5.3 shows the envelopes of the maximum storey drifts from the DRAIN-2D and the TABS outputs. The displacements envelopes for the two analyses appear reasonable. This time the roof displacements are off by about 9% only. As for the storey shear, the same phenomenon is observed. A factor of about two is required for the TABS77 output to produce the same effects. For the FDF, only one ground floor column reached yield condition as shown in Fig. 5.5.

4.6 Summary

From the results obtained for the test frames from the this chapter, it is observed that the spectrum generated is sufficiently accurate for the preliminary design of a FDF system under optimum slip load conditions. The response spectrum method was used for the analysis of several example frames at their optimum slip load conditions. The results obtained manifested that the maximum deflection response can be evaluated quite reasonably. The column shear forces on the other hand were not as good as the deflection results. The modal response spectrum method of analysis is an approximate method.

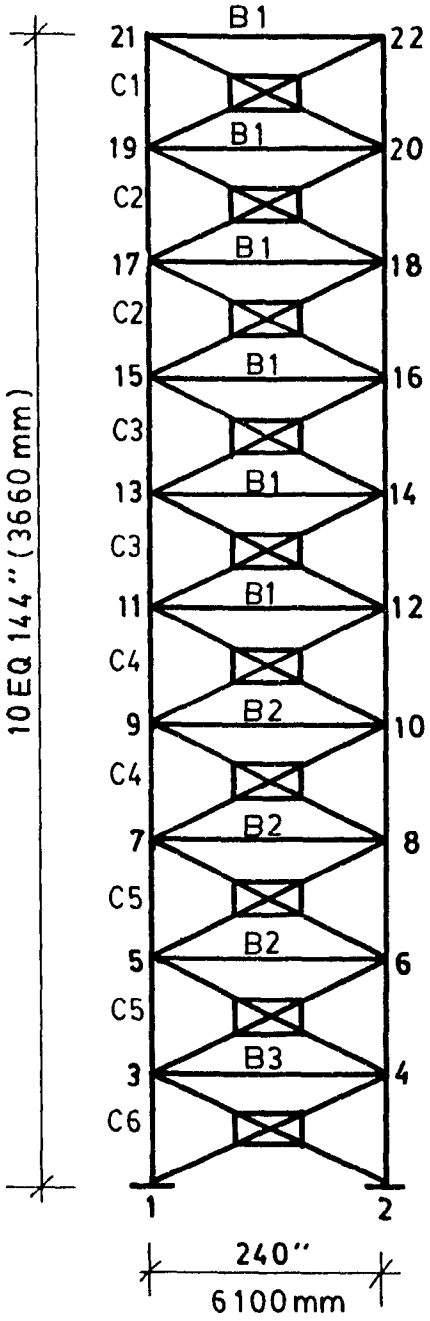

MASS = 0.3419 $\frac{\text{Kip-s}^2}{\text{in}}$ PER FLOOR

B1	W18 X 50
B2	W18 X 60
B3	W18 X 77
C1	W14 X 34
C2	W14 X 53
C3	W14 X 78
C4	W14 X 103
C5	W14 X 119
C6	W14 X 184

1 Kip = 4.448 kN

1" = 25.4 mm

Figure 4.1.1 Frame No. 1

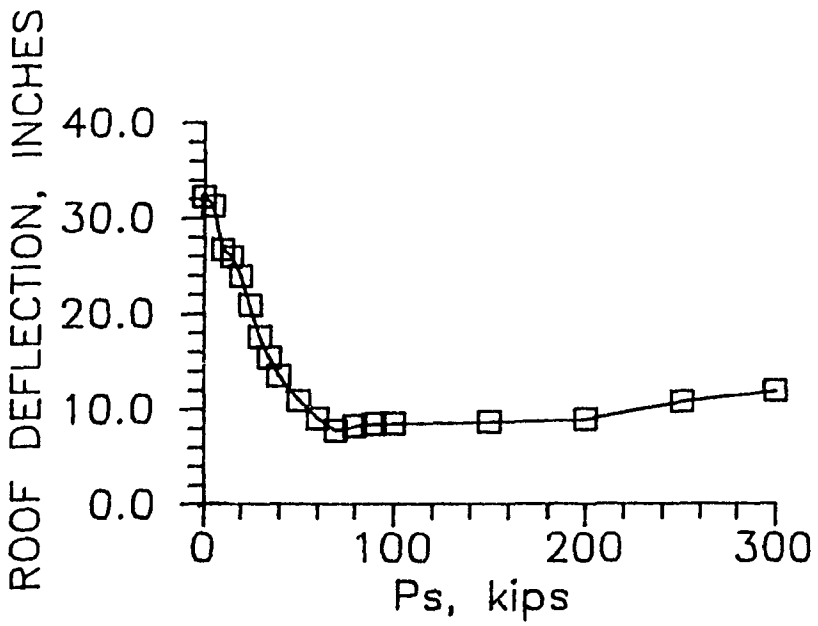

Figure 4.1.2 Deformation vs. slip load for frame no. 1

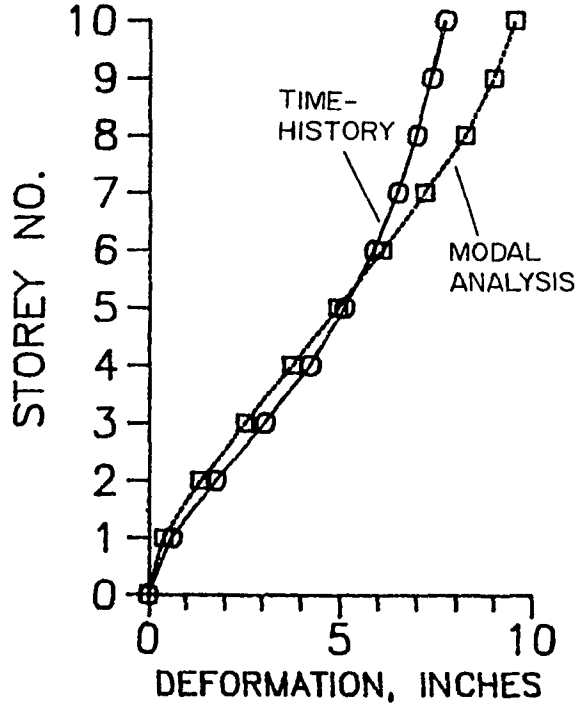

Figure 4.1.3 Maximum storey deformation for frame no. 1

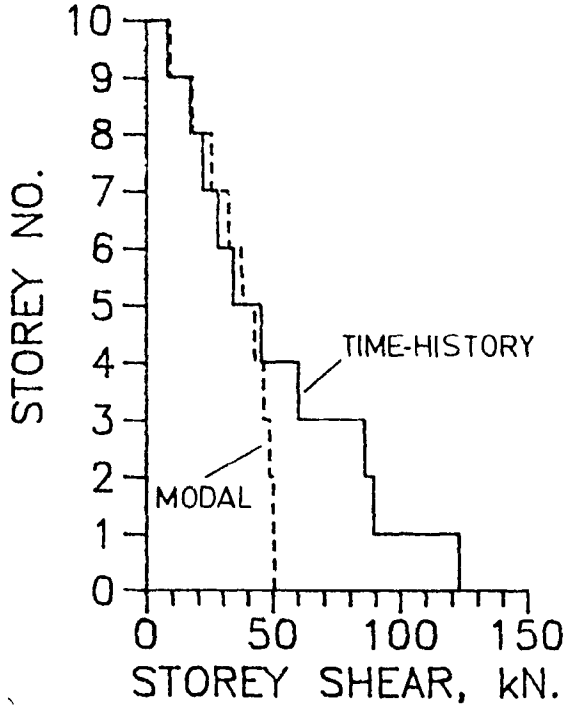

Figure 4.1.4 Maximum storey shear for frame no. 1

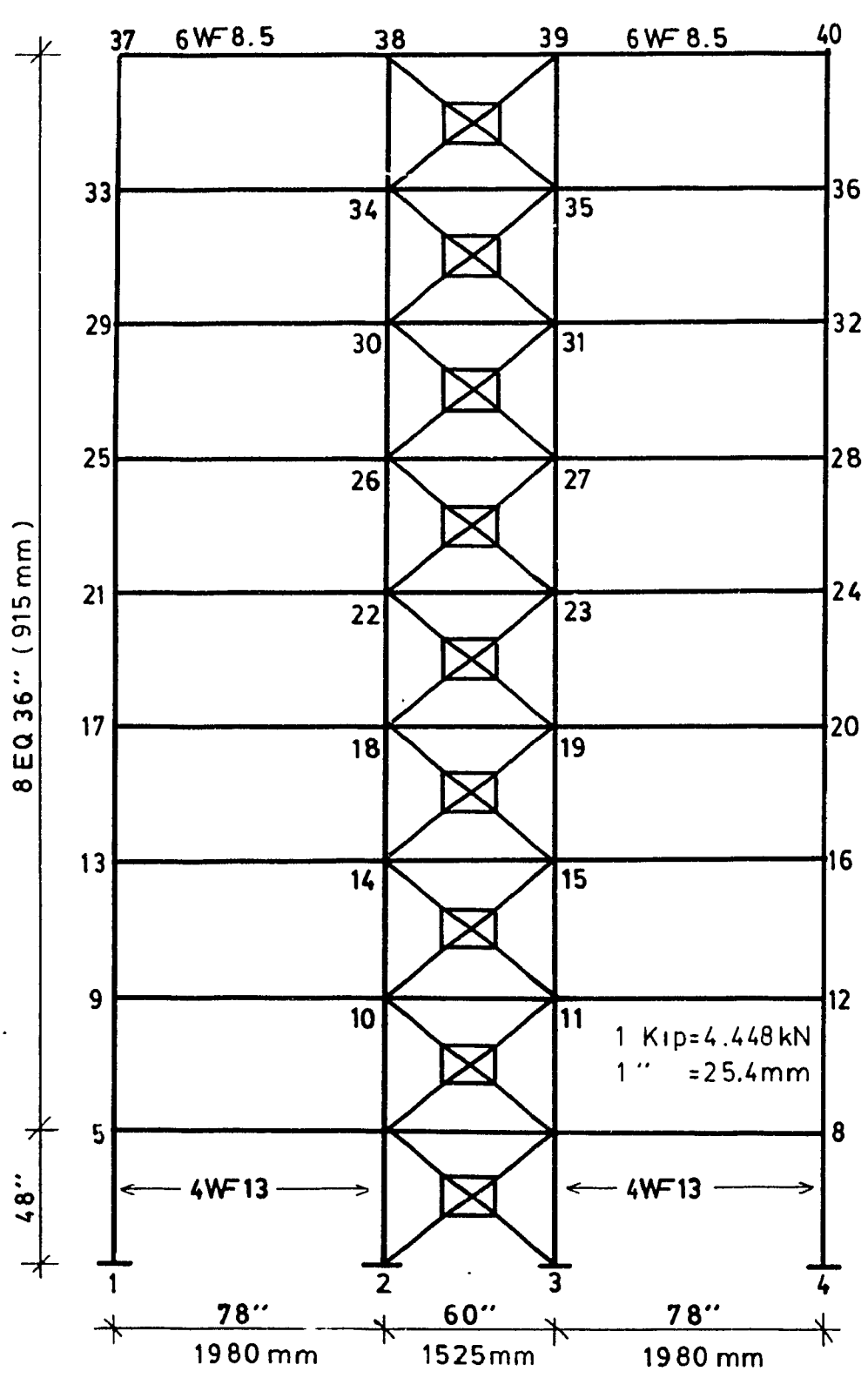

Figure 4.2.1 Frame No. 2

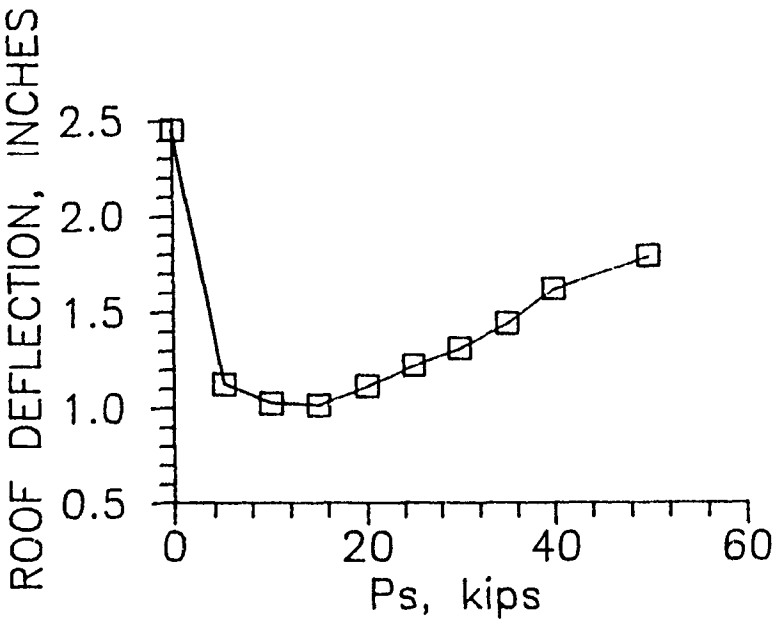

Figure 4.2.2 Deformation vs. slip load for frame no. 2

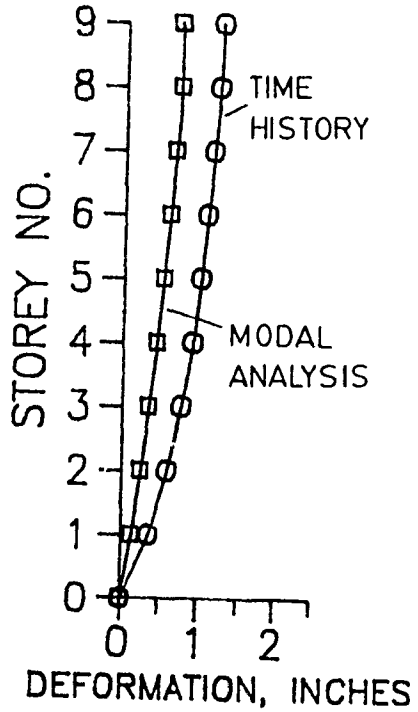

Figure 4.2.3 Maximum storey deformation for frame no. 2

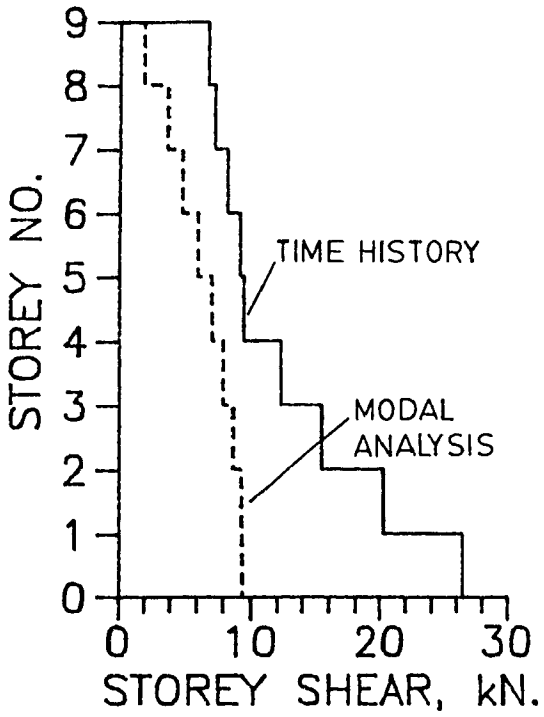

Figure 4.2.4 Maximum storey shear for frame no. 2

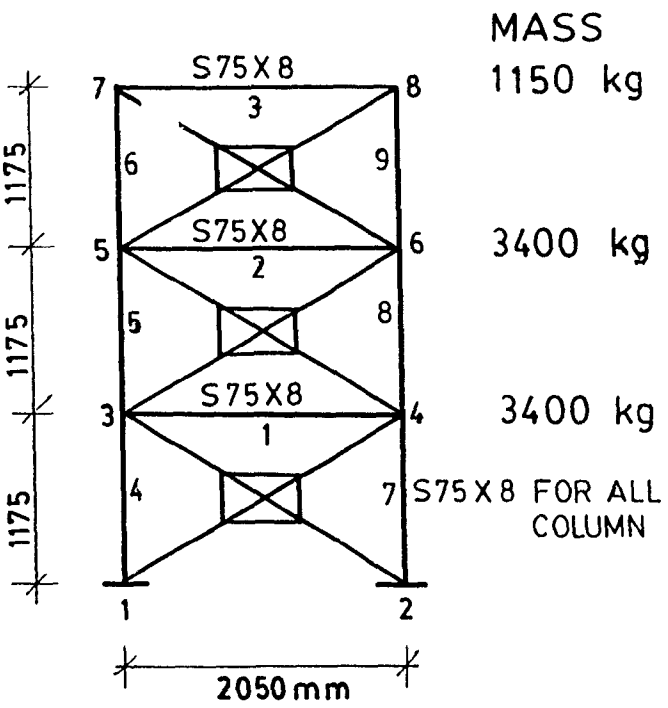

Figure 4.3.1 Frame No. 3

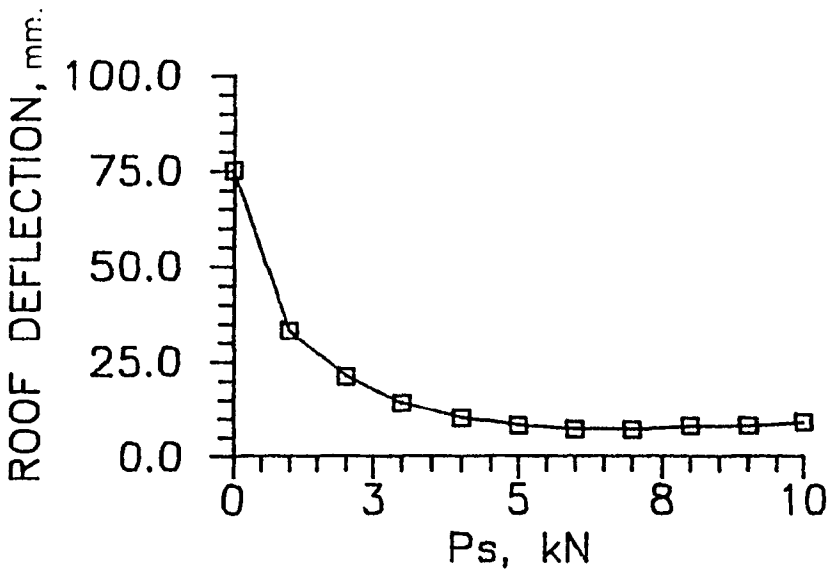

Figure 4.3.2 Deformation vs. slip load for frame no. 3

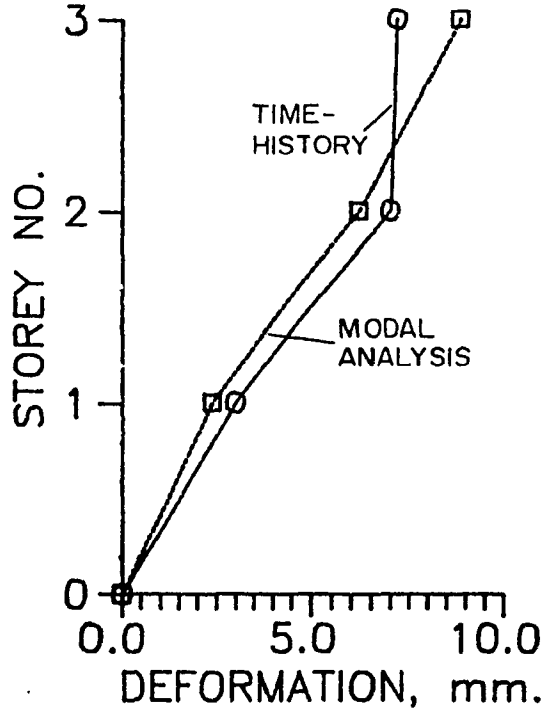

Figure 4.3.3 Maximum storey deformation for frame no. 3

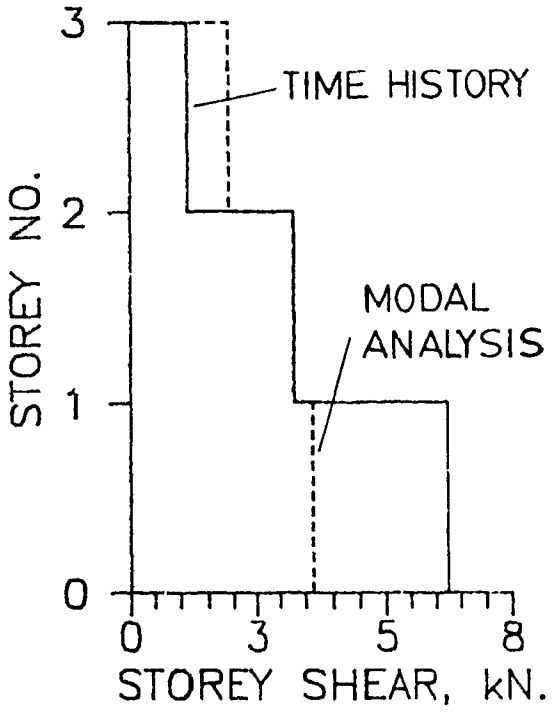

Figure 4.3.4 Maximum storey shear for frame no. 3

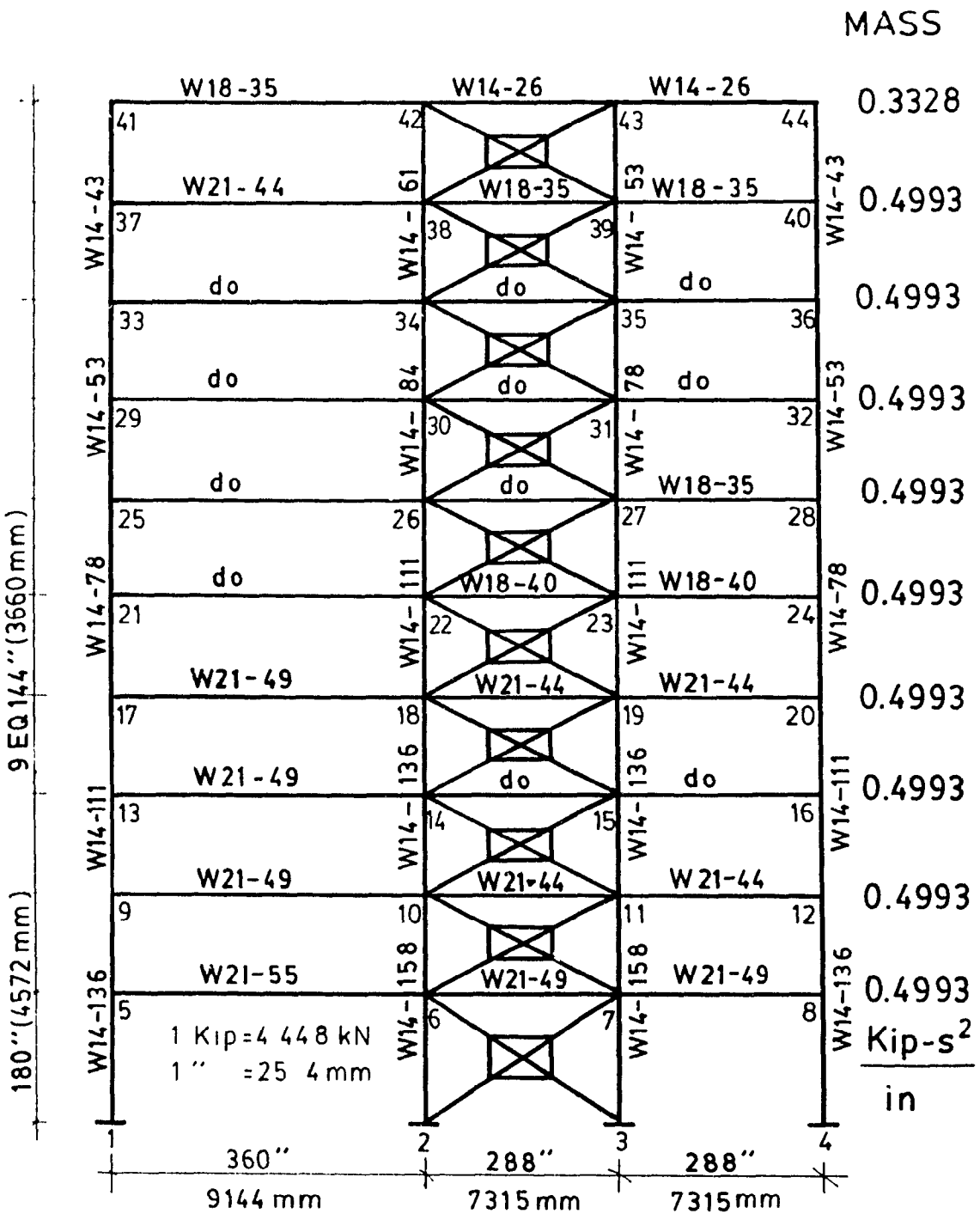

Figure 4.4.1 Frame No. 4

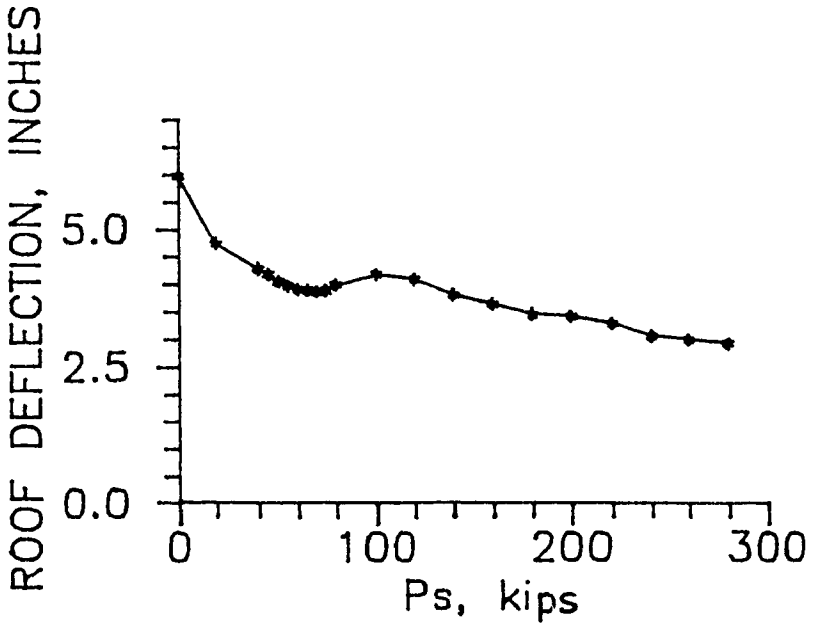

Figure 4.4.2 Deformation vs. slip load for frame no. 4

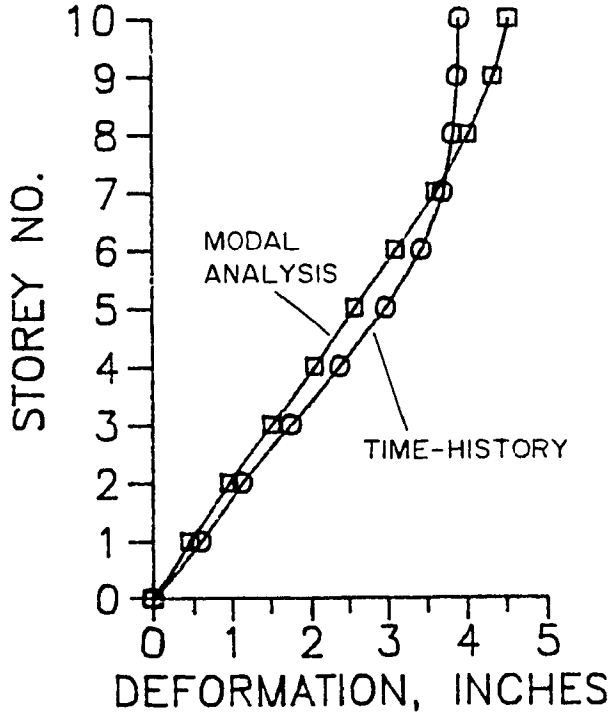

Figure 4.4.3 Maximum storey deformation for frame no. 4

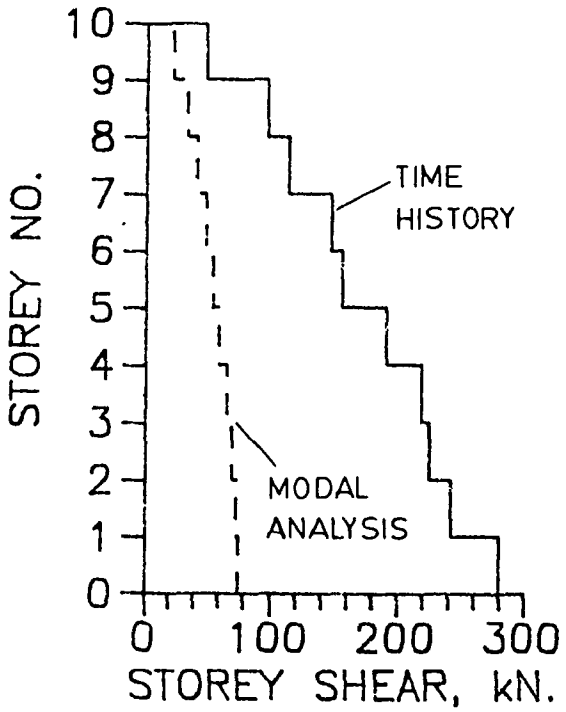

Figure 4.4.4 Maximum storey shear for frame no. 4

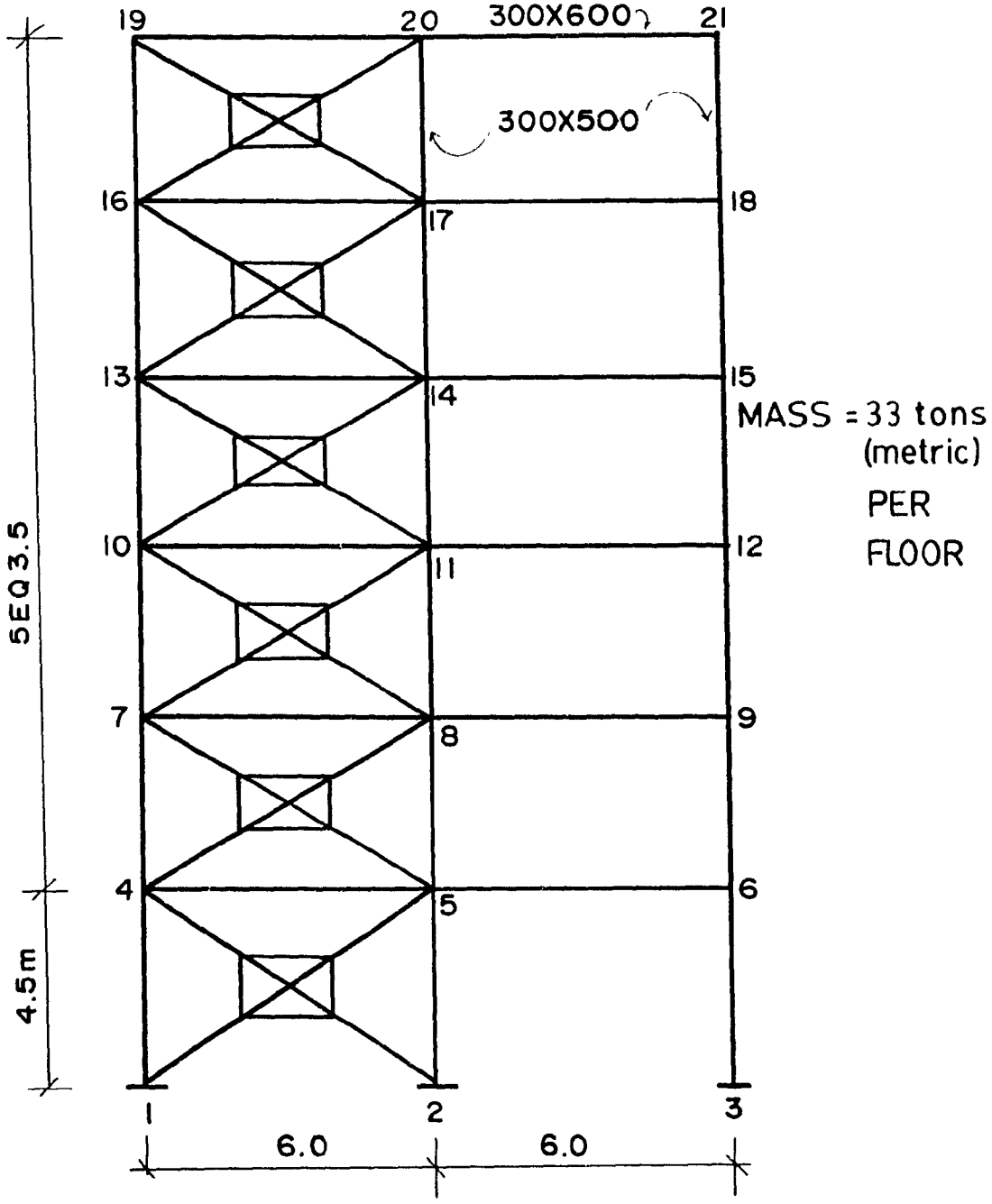

Figure 4.5.1 Frame No. 5

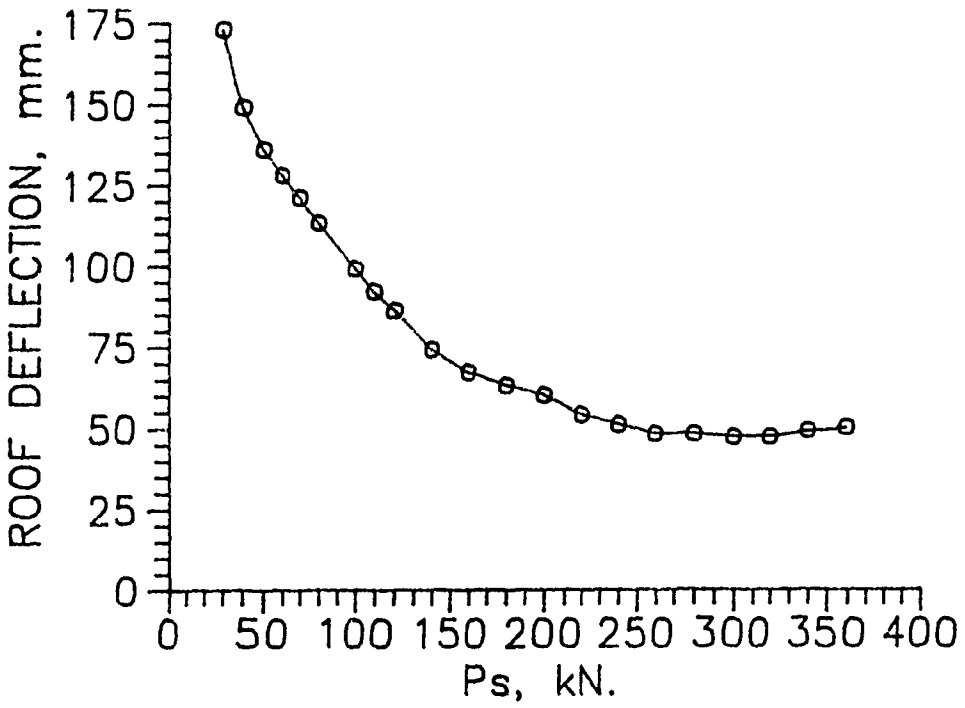

Figure 4.5.2 Deformation vs. slip load for frame no. 5

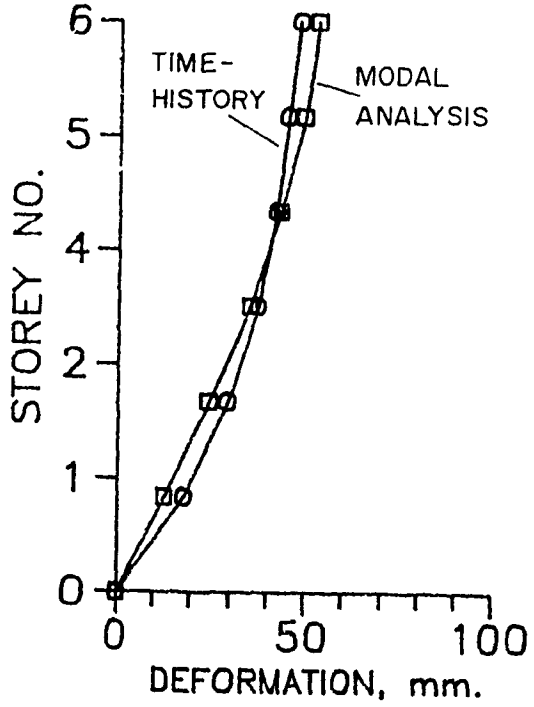

Figure 4.5.3 Maximum storey deformation for frame no. 5

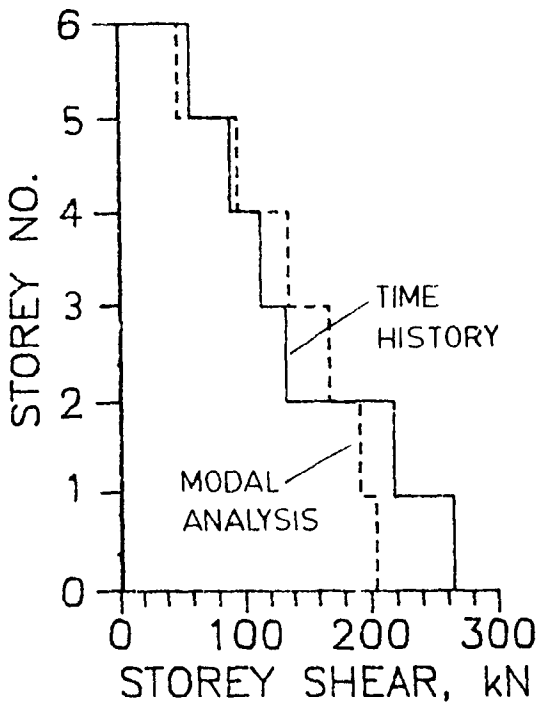

Figure 4.5.4 Maximum storey shear for frame no. 5

5.0 FORCE REDUCTION FACTOR FOR THE FDF

The objective of the seismic provisions of the National Building Code of Canada is to protect the occupants of buildings from the destructive effects of earthquakes. This is done by specifying suitable design forces and special details in structural requirements so that the probability of building collapse or injuring people is low. Recalling from section 1.3, the total base shear for a building is calculated according to the equation provided by the NBCC as:

$$V = v\ S\ I\ F\ K\ W$$

The total base shear is then distributed over the building height as static lateral loads and member forces are then obtain from the structural analysis. The design forces specified in buildings codes are considerably smaller than the levels corresponding to elastic structural response that results from the given seismic actions. This is reflected in a structural system coefficient, the K factor. Rainer (1987) explained that the K factors used in the base shear equation only reflect the performance of the type of structural system used under seismic forces. They are merely a means for assigning relative merit to different aseismic structural systems on the basis of observed or expected behaviour during earthquakes, their numerical values have no absolute rational interpretation. The structural behaviour coefficient, K is intended to account for the energy dissipation capacities of

different types or structural system due to inelastic deformation and damping. These factors can be related to the inelastic behaviour of a building structure and the corresponding lower forces produced during the dynamic response. A factor of 0.7 is suggested for ductile moment-resisting frames (MRF) systems. The MRF systems are deemed to be more ductile and therefore able to undergo large plastic deflections, i.e. higher damping. Other structural systems are given a K value higher than 0.7 as they are not as ductile as the MRF. Since the FDF system is more capable of energy dissipation than MRF a K coefficient of less than 0.7 can be expected.

The K factors can be related to the system ductility of the structure, since it is a reduction in the forces in the inelastic stage. System ductility is difficult to define for multi-degree-of-freedom systems, but it can be defined easily for a single-degree-of-freedom vibrating system.

The base shear equation V computed from the semi-empirical base shear equation from the NBCC assumes plastic behaviour in the structure during a major earthquake. The seismic force on the structure is reduced when compared to the elastic response of the same building. It is unrealistic to design structures to behave elastically during a major earthquake. Only special structures such as nuclear reactors

are normally designed to behave in the elastic range. By observing the base shear equation, assuming other things being equal, (i.e. zonal velocity ratio v is fixed for particular site conditions, S is the seismic response factor depending on the frequency of the building, which can be governed by either the acceleration or the velocity contents of the earthquake, F is the foundation factor which is fixed for particular foundation soil conditions, W is the total reactive weight which is unchanged), we can see that only the K factor remains to be manipulated for other systems, such as the FDF, the eccentrically braced frames, and base-isolator systems. Difficulties may arise when assigning the traditional K factors for these innovative systems, as it was developed in an empirical manner.

The seismic response factor S, which is depend on the fundamental period of the building, is a function of the stiffness of the structure. If the global structural stiffness of the building is expected to remain unchanged during an earthquake, then the response factor will remain unchanged. But for a new system, such as the FDF and the base isolator systems, the lateral stiffness of the building is expected to change due to the yielding of certain pre-selected members for energy dissipation. As a result, it is more convenient to use the newly introduced force reduction factor R, for the study of the effectiveness of the FDF systems in energy

dissipation.

Rainer (1987) proposed this new force reduction factor, R, for the modification of the seismic design requirements of the 1985 NBCC. Comparing the new equation to the old equation:

$$V = v\ S\ K\ I\ F\ W \qquad \text{(old)}$$

$$V = \frac{v\ \bar{S}\ I\ F\ W}{R}\ U \qquad \text{(new)}$$

it is seen that the S factor has now become $\bar{S}$ the new elastic response spectrum factor. In the new equation the numerator represents the base shear of the elastic response, and R is a factor which accounts for the force reduction due to the ductile behaviour of non-linear systems, or due to increased damping. A new factor U, called the calibration factor, is introduced to maintain the design base shears at the same level of protection for buildings with good to excellent capability of resisting seismic loads consistent with the R factor used. The new S for the case where the zonal acceleration and the velocity ratios are equal, i.e. $Z_a = Z_v$, is suggested to be:

$$\bar{S} = \frac{1.5}{\sqrt{T}} \quad < 3.0$$

instead of the old $S = 0.22/\sqrt{T}$. The factor of 3.0 is the

upper bound value due to the elastic amplification with a 5% damping in the high frequency range. Equating the new and the old base shear equations we get :

$$v\ S\ I\ F\ K\ W = \frac{v\ \bar{S}\ I\ F\ W}{R}$$

$$S\ K = \frac{\bar{S}}{R}$$

$$\frac{0.22}{\sqrt{T}}\ K = \frac{1.5}{\sqrt{T}\ R}\ K$$

giving:

$$R = 6.8/K$$

This results in the following table translating the K factor into R's :

K-factor (1985 NBCC)	Derived R (a=1.5)	Derived R (a=1.0)
0.7	9.71	6.47
0.8	8.50	5.66
1.0	6.80	4.53
1.3	5.23	3.49
2.0	3.40	2.27
3.0	2.26	1.51

Where the first column is the original K factor for the various common structural systems (a live load factor of 1.5 is used). Column 2 is the R factor for the load factor of 1.5 as applied to the existing live load due to earthquake. Thus it can be seen that for the MRF with a K factor of 0.7, the corresponding elastic forces is about six times higher.

5.1 Examples for MRF

These newly derived R factors are of course based on the assumed K factors previously assigned in the 1985 edition of the NBCC. To compute the R factor from actual dynamic analysis is possible but tedious, as numerous buildings must be analyzed before an average R factor can be said to be representative of the type of construction used. Nevertheless it is still possible to carry out a limited experimentation to examine the R factor for the MRF systems. For this analysis the five examples studied previously in chapter 4 will be utilized. Initially the total base shear of a non-linear MRF is determined (from the time-history dynamic analysis), then a second analysis is executed for the same MRF but this time the yield forces are increased to some arbitrarily high magnitudes to prevent yielding, thus making the MRF an elastic system through out the time-history analysis.

The R factor for the MRF system is then equal to the total elastic base shear divided by the non-linear total base shear, as shown by the simple equation:

$$R_{MRF} = \frac{V_{elastic}}{V_{inelastic}}$$

By this way one can compare the reduced forces induced

in the non-linear MRF to the elastic one. To do this, a sufficiently large number of time history earthquake records must be utilized on many frames with different frequency range in order to arrive at a credible figure. For this elementary case study, however, only three earthquakes will be used. The 0.30g NBK artificial earthquake, the 0.33g El Centro earthquake, and the Olympia earthquake scaled to 0.33g will be used. The previous five examples used in chapter four are analyzed again through DRAIN-2D and the results are tabulated in Table 5.1.

From the table, it can be noticed that the R factor computed from the three earthquakes for frame 1 is about 2.5. This is lower than the expeted value of 4 for the MRF according the 1990 NBCC. For frame 2 the calculated R factor is about 2.4, this is again lower than 4 for a MRF, but since this is an experimental frame and did not represent genuinely a realistic building. For example no. 3 the R factor is 1.6. Again, this frame is an experimental frame and therefore did not truly duplicate an actual building frame. For example no. 4 the computed R factor is 5.8. For example no. 5 the estimated R factor is about 2.5. An overall average R factor of 3.0 is obtained for the five examples. It must bear in mind that the derived R factor is based on the traditional K factor which assumed a certain level of ductility factor. This ductility is easily defined for that of a SDOF system with

clear yield level, but for a building frame and therefore a MDOF system, it is not as clear. From the results obtained for these test frames, it can be said that the R factors derived by using the K factors are higher than the R values actually computed by using the test frames.

5.2 Examples for FDF

With the new set of force reduction factors as defined in the previous section, the subsequent section will seek to specify a new R factor for the FDF systems instead of the traditional K factor. The new R factor is simple to quantify for new structural systems or new materials when compared to the rather empirical nature of the current K factors. Since the elastic base shears are promptly calculated by either the modal response spectrum method, or by utilizing the step-by-step integration of the equations of motions, the force reduction factor can be established by comparing the results with non-linear dynamic analyses.

For the FDF system, the base shears would be computed under the optimum slip load conditions. The elastic base shears would be those computed by assuming that the FDF systems remain elastic without yielding anywhere in the building, in other words, the elastic base shear is that of the elastic braced-moment-resisting-frame, or BMRF. In

equation form:

$$R_{FDF} = \frac{V_{BMRF}}{V_{FDF}}$$

For the following simple development of the force reduction factor R for the FDF systems, a total of three earthquake records are to be used to estimate the base shear for the BMRF and its corresponding FDF. The average of the three base shears computed will be used to determine the R factor. The earthquakes records are the 0.30g NBK, the 0.33g El Centro, and the 0.30g Olympia records. It is a well known fact that the structures in the intermediate and long period range, will induce higher forces by earthquake with high velocity contents. In this study it is assumed for now that the acceleration is the dominant case for the following exercises.

The same data of example frames 1 to 5 are used except that for the BMRF cases, in which all the yield stresses are increased in order to avoid yielding in the members. Six analyses are carried out for each frame, three elastic ones and three non-linear ones for three different earthquakes. The main results obtained are tabulated in Table 5.2.

Frame no. 1 is subjected to the three different earthquakes as FDF's with the optimum slip load as established

earlier in the previous chapter. At the optimum slip load conditions, the total base shears computed for the three earthquakes are 182.7, 154.0 and 115.9 kN. for the 0.30g NBK, 0.33g El Cento and the 0.33g Olympia respectively. It may be mentioned that the 0.30g NBK induced the highest base shear of the three. The same frame is then revised with high yield forces for all the structural members for the elastic analysis. Of the three records used, again the NBK data is seen to have induced the highest base shears in the elastic BMRF cases. For the BMRF, the base shears are 1089.4, 656.0 and 462.0. For the R factors, the 0.30g NBK produced a R of 6.0, the 0.33g El Centro produced an R of 4.3, and the 0.33g Olympia produced an R of 4.0. This is summarized as shown in Table 5.2. For example in no. 1 an average R factor of 4.8 is obtained. This 4.8 factor is higher than the 3.5 factor in the MRF for 0.30g NBK.

For the example no. 2, the 0.30g NBK produced an R factor of 2.7, the 0.33g El Centro an R of 3.9, and the 0.33g Olympia an R of 3.8. This is probably due to the fact that frame no. 2 is a 1/3 scale experimental model of a prototype building, and itself is a very light frame as it was designed initially to study the behaviour of uplift under the columns. The dominant periods of vibrations of the frame are probably outside the frequencies of the three earthquakes, as a results the frame is not severely shaken by the ground

effects. Nevertheless a average R of about 3.5 is obtained for this frame.

For frame no. 3 the 0.30g NBK case gives a R factor of 6.7, the El Centro gives 4.1, and the Olympia record yields a factor 2.7. The 2.7 factor is probably due to the low base shear induced by the BMRF. The period of the frame is probably outside the range of effective shaking of the Olympia record. In this case, the average R is about 4.5.

Example no. 4 is a more realistic building frame since the dimensions used are representative of the typical buildings. In this case the NBK case gives a factor of 6.3, the El Centro gives 7.2, and the Olympia gives 13.4. The overall average R factor is about 8.9.

Example no. 5 gives the factor of 6.2, 5.4, and 5.0 for the 0.30g NBK, 0.33g El Centro and the .33g Olympia records respectively. An average of 5.2 is obtained for this case. From the above five examples, it is obvious that the R factor obtained for the FDF systems is at least 4.0. If the results of examples 2 and 3 can be disregarded, since they are experimental models of prototypes, the R factor then is least 4.8. Comparing that with the R factor for the MRF systems, which has a average factor of about 3.7. Thus the FDF systems should have a higher R value than the MRF systems.

By comparing the total base shears induced in the nonlinear MRF systems against that of the FDF systems, for the case of the 0.30g NBK, it is noted that the FDF systems have a slightly higher base shear than the MRF systems. This is to be expected since the FDF systems have a higher initial lateral resistance prior to the slipping of the dampers, thus inducing higher forces. But it is observed that the maximum lateral deflection induced by the MRF is at least twice that of the FDF. Which means the FDF has a better storey drift control than the MRF.

Fig. 5.1 shows the locations of plastic hinges for both the MRF and FDF for example no. 1. From the figure it is observed that the MRF has more yielding than the FDF. Nine floor beams have yielded in the MRF, whereas only two have yielded in the FDF. Similarly, the MRF has eight plastic hinges in the columns and none of the columns has yielded in the FDF. Fig. 5.2 shows the same formations of plastic hinges in the MRF and no yielding in the FDF for example no. 2. Fig. 5.3 also shows the yield locations for the MRF and no yielding for the FDF. Fig. 5.4 shows extensive formation of plastic hinges in the MRF and FDF. But the FDF is seen to be less critical than the MRF. In Fig. 5.5 the MRF is seen to have suffered great damage with yielding in beams and columns. In the FDF only one hinge is found. In all, although the base shear is slightly higher in the FDF than the MRF, the

deflection in the FDF is lower, and with less yielding in the structural members.

5.3 Effects of Peak Intensity

It is a well known fact that the same earthquake time-history data but with a different peak accelerations will induce a different dynamic response in the same system. To see the effects of different peak acceleration on the R factors, the NBK data was scaled to 0.50g peak acceleration for the frames and further analyses were performed. The results are tabulated in Table 5.3.

For frame no. 1, the R factor has increased from 6.0 to 8.5. The elastic BMRF shear has increased by a factor 0.5/0.3=1.67. Because of the nonlinearity of the FDF system, the total base shear has gone up only by 17%. The R factor for the example no. 2 in this case has decreased slightly from 2.7 to 2.6. Because of the light weight of the frame, increasing the peak acceleration has no effects on this frame. For example no. 3 the R factor is also seen to have decreased from 6.7 to 5.5. For example no. 4 the R factor has increased from 6.3 to 9.4 , this is due to the large increase in the elastic base shear. For frame no. 5 the R factor has increased from 5.6 to 6.5.

5.4 Summary

The force reduction factor R for the FDF frames for the five frames calculated ranges from 3.5 to 8.9, with an average of about 5.4. The R factor obtained for the MRF system in this case study is about 3.0. This is lower than those expected for the moment-resisting-frames, which is for now being pegged at 4.0 under the latest revision to the NBCC (37). From these examples, it can be concluded that the R factor for the FDF system is higher than that of the MRF system. By increasing the peak ground acceleration, the elastic base shear has increased by a substantial amount, but the FDF base shear is seen to increased only marginally, as reflected by the R factor computed.

Table 5.1 Typical R factors for the MRF systems

	0.30g NBK	0.33g El Centro	0.33g Olympia	R Average
Frame no. 1	kips	kips	kips	
V(el)	552.9	248.8	324.6	
V(inel)	157.1	140.8	157.6	
R	3.5	1.8	2.1	2.5
Frame no. 2	kips	kips	kips	
V(el)	80.7	61.7	93.1	
V(inel)	36.0	31.3	32.2	
R	2.2	2.0	2.9	2.4
Frame no. 3	kN	kN	kN	
V(el)	58.1	32.9	41.8	
V(inel)	28.4	27.1	28.7	
R	2.1	1.2	1.5	1.6
Frame no. 4	kips	kips	kips	
V(el)	1841.0	1258.1	1755.1	
V(inel)	290.0	287.6	258.7	
R	6.3	4.4	6.8	5.8
Fr me no. 5	kN	kN	kN	
V(el)	2175.0	722.7	827.3	
V(inel)	503.0	440.2	481.0	
R	6.2	1.6	1.7	2.5
Average R	3.7	2.2	3.0	3.0

1 kip = 4.448 kN

Table 5.2 Typical R factors for the FDF systems

	0.30g NBK	0.33g El Centro	0.33g Olympia	R Average
Frame no. 1	kips	kips	kips	
BMRF	1089.4	656.0	462.5	
FDF	182.7	154.0	115.9	
R	6.0	4.3	4.0	4.8
Frame no. 2	kips	kips	kips	
BMRF	107.2	39.0	112.3	
FDF	39.62	10.1	29.4	
R	2.7	3.9	3.8	3.5
Frame no. 3	kN	kN	kN	
BMRF	60.7	48.8	25.2	
FDF	9.0	11.3	9.3	
R	6.7	4.1	2.7	4.5
Frame no. 4	kips	kips	kips	
BMRF	2096.0	2169.0	3782.0	
FDF	331.0	301.0	280.0	
R	6.3	7.2	13.4	8.9
Frame no. 5	kN	kN	kN	
BMRF	2901.0	2506.0	2215.0	
FDF	469.0	474.0	445.0	
R	6.2	5.4	5.0	5.2
Average R	5.6	4.9	5.8	5.4

1 kip = 4.448 kN

Table 5.3 R factors for different intensity

	0.30g NBK	0.50g NBK
Frame no. 1	kips	kips
BMRF	1089.7	1821.0
FDF	182.7	214.9
R	6.0	8.5
Frame no. 2	kips	kips
BMRF	107.2	100.5
FDF	39.6	38.5
R	2.7	2.6
Frame no. 3	kN	kN
BMRF	60.7	80.4
FDF	9.0	14.5
R	6.7	5.5
Frame no. 4	kips	kips
BMRF	2096.0	3487.0
FDF	331.0	372.0
R	6.3	9.4
Frame no. 5	kN	kN
BMRF	2901.0	4227.0
FDF	469.0	645.3
R	6.2	6.6
Average R	5.6	6.5

1 kip = 4.448 kN

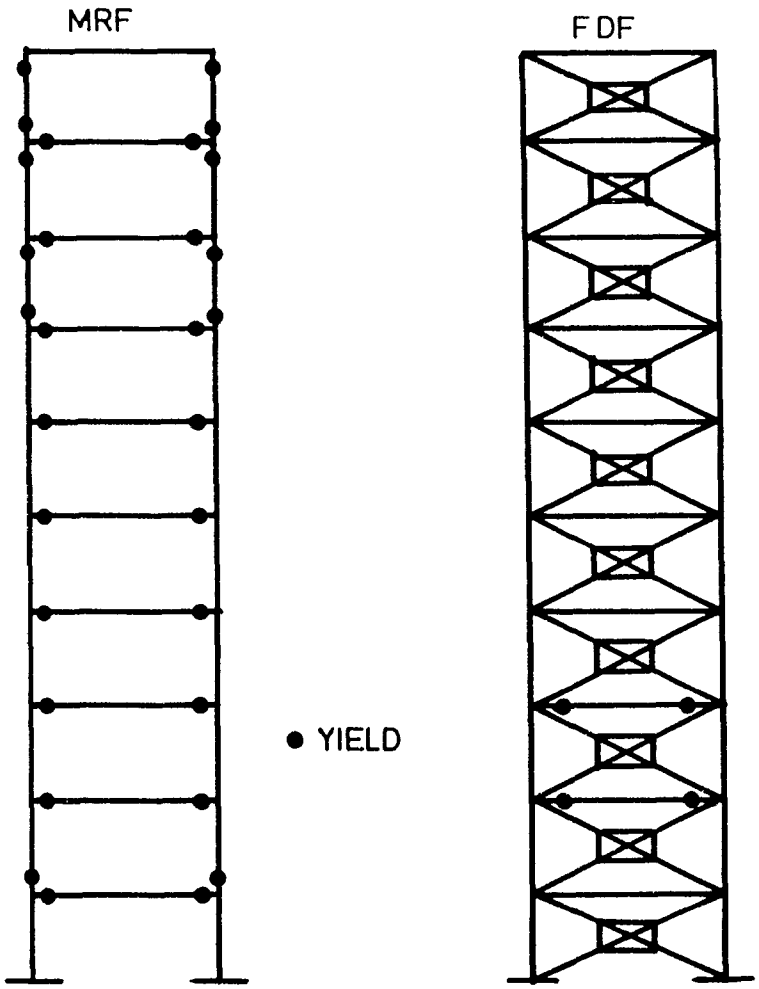

Fig. 5.1 Locations of hinges for example 1

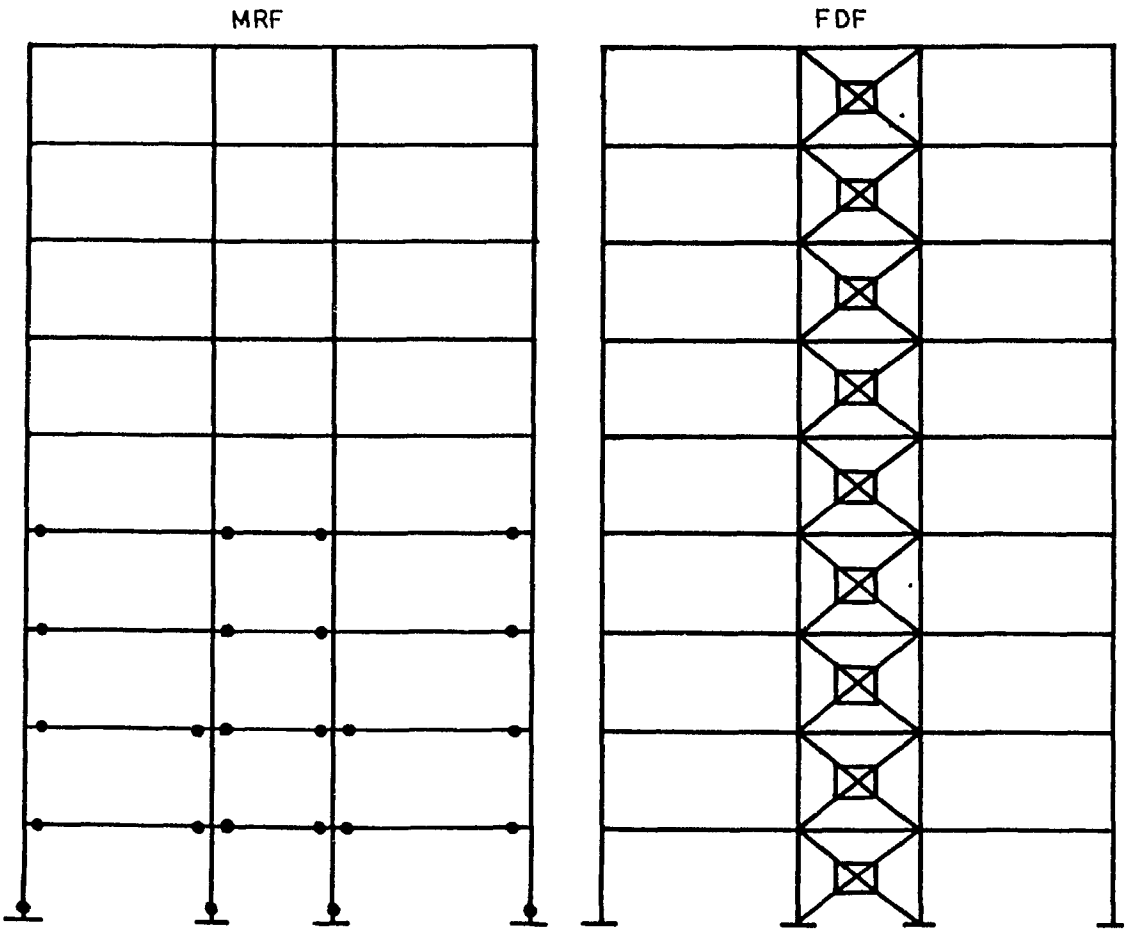

Fig. 5.2 Locations of hinges for example 2

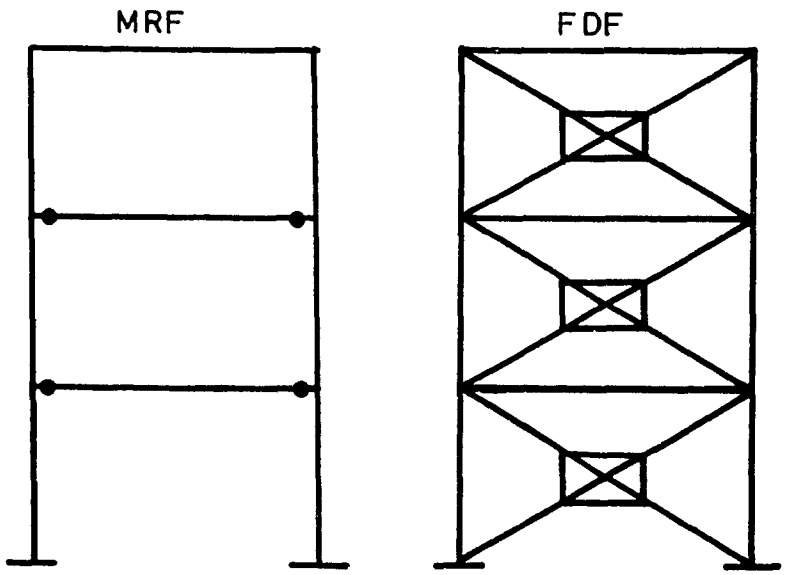

Fig. 5.3 Locations of hinges for example 3

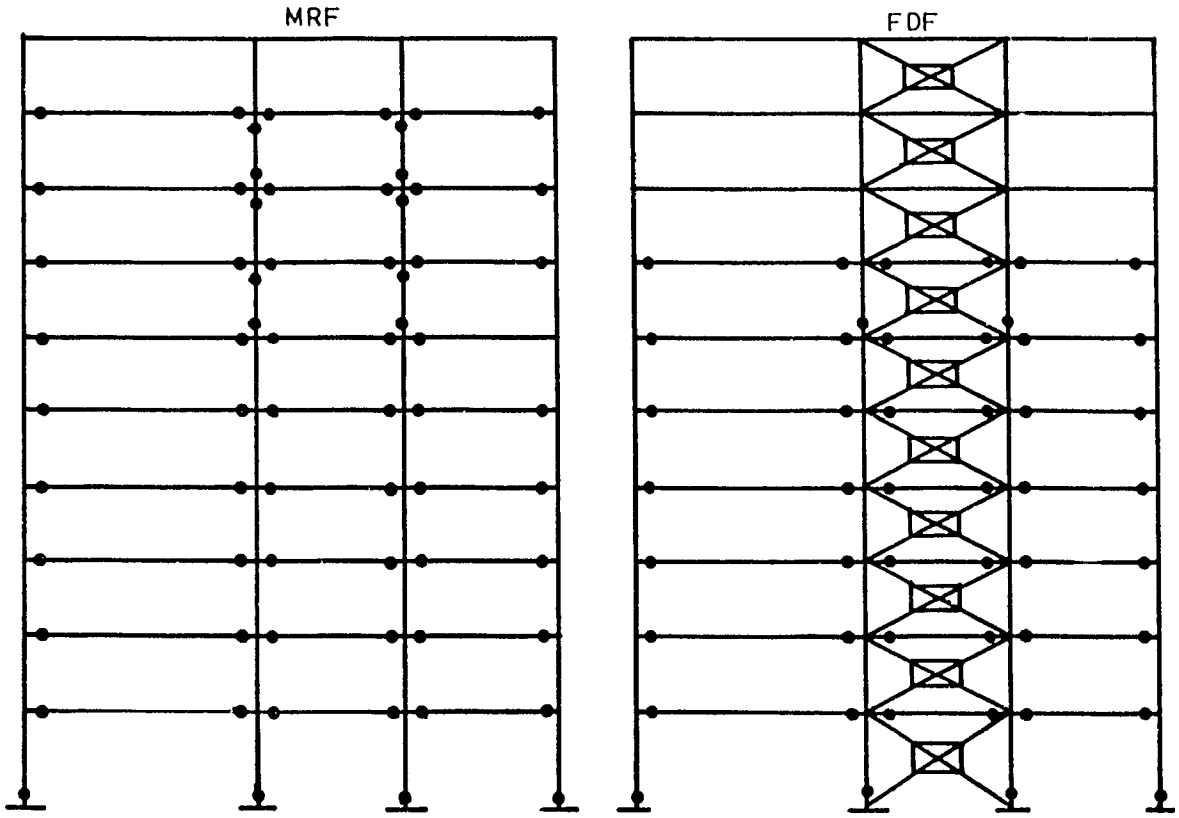

Fig. 5.4 Locations of hinges for example 4

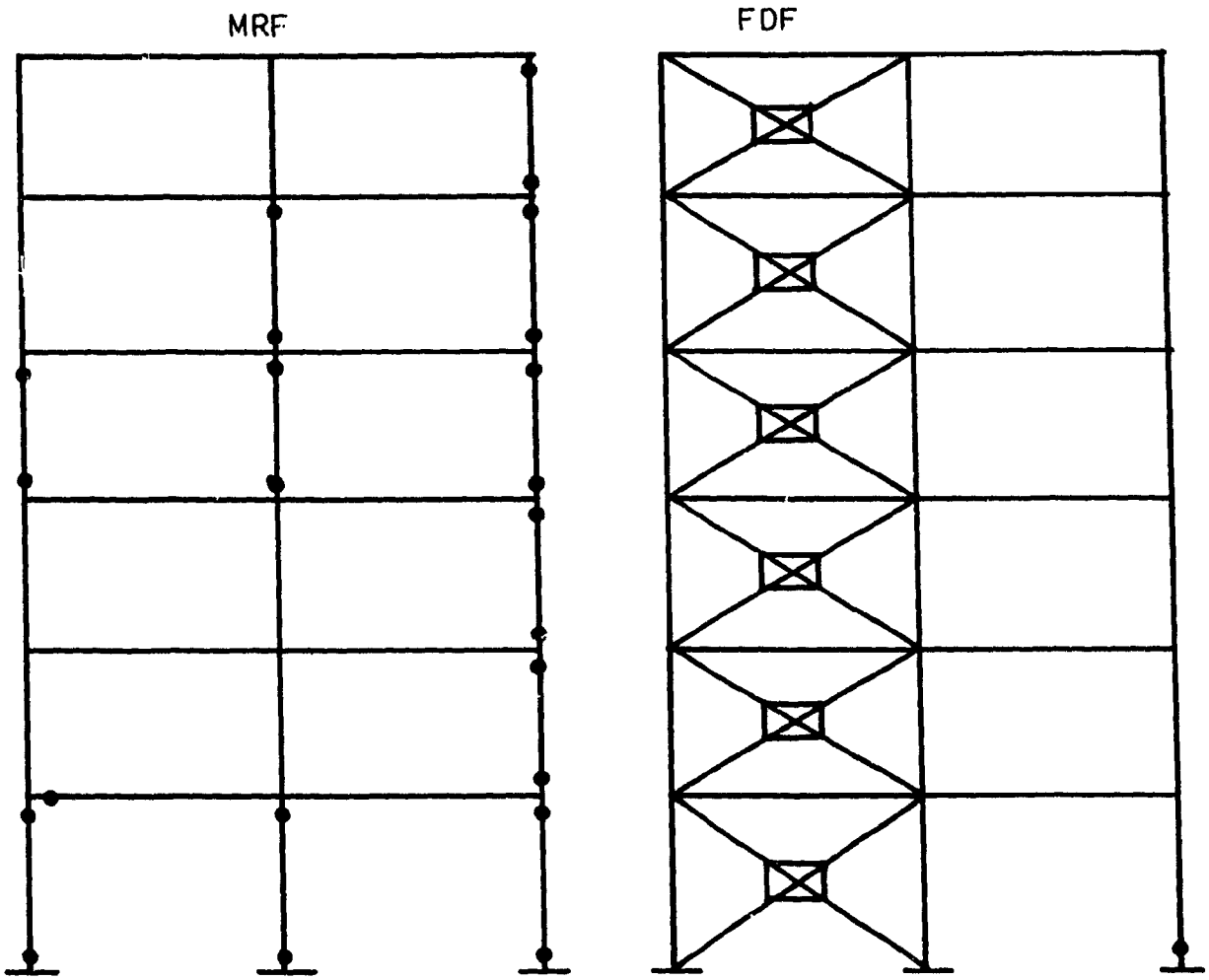

Fig. 5.5 Locations of hinges for example 5

6.0 CONCLUSIONS

From the studies carried out in the previous chapters, several conclusions can be drawn:

i. The relative stiffness of the brace element to the column lateral stiffness (α) does play an important role in the amount of energy being dissipated. From chapter 2 it was deduced and proved that α greater than 10 is not necessary, so long as the service requirements are met.

ii. The so called optimum slip load appears to have little to do with reactive weight of the building, at least not directly. This is based on the observations made in chapter 3. The optimum slip load also seems to vary with the type of earthquakes and the peak intensity of the earthquake. It may be said that each earthquake appeared to require a different optimum slip load.

iii. A deformation spectrum is generated for the simplified analysis of the FDF system by the modal method. This spectrum is sufficiently accurate for predicting the deformation of the FDF systems under the optimum slip load conditions only. The maximum deflection computed from the modal response analysis using the response spectrum is sufficiently accurate.

iv. An average R factor of about 5.4 was obtained for the FDF systems based on five building frames. For the MRF system, an average R factor about 3.0 was obtained. This is lower than the value anticipated. This proved that the K factor for the FDF systems is indeed lower than 0.7. In other words the R factor for the FDF systems should be higher than those assigned to the MRF structural systems

6.1 RECOMMENDATIONS FOR FURTHER STUDIES

i. More realistic structural frames should be used for the derivation of the force reduction factor (R) for the FDF structural systems.

ii. Analytical solutions for the optimum slip loads for SDOF systems could be derived for simple loading functions. The results from these analyses should produce very valuable information.

REFERENCES

1. "Learning lessons from the rubble of Mexico City", ENR, September 4, 1986, p. 20 - 28.

2. Notes about The December 1988 Armenian earthquake, Earthquakes and Volcanoes, VOL. 21, #2, 1989, U.S. Geological Survey, p. 68-78

3. Kelly, J.M., Tsai, H. C., "Seismic Response of Light Internal Equipment in Base Isolated Structures", Report No. UCB/EERC-84/17. Earthquake Engineering Research Centre, University of California, Berkeley, 1984.

4. ATC-17, Seminar on Base Isolation and Passive Energy Dissipation, San Francisco, California, 1986.

5. Kelly, J. M., "Aseismic base Isolation : review and bibliography", Soil Dynamics and Earthquake Engineering", 1986, VOL. 5, No.3, p. 202-216

6. Chopra, A. K., Clough, R. W., Clough, D. P., "Earthquake resistance of Buildings with a Soft first Storey", Earthquake Engineering and Structural Dynamics, VOL. 1, 1973, p.347-355

7. Robinson, W. H., "Lead-rubber Hysteretic Bearing Suitable for protection Structures during Earthquakes", Earthquake Engineering and Structural Dynamics, VOL. 10, 1982, 593-604

8. Kelly, J. M., Skinner, M. S.,Beucke, K. E., "Experimental Testing of an Energy-absorbing Base Isolation System", Report No. UCB/EERC-80/35. Earthquake Engineering Research Centre, University of California, Berkeley, 1980.

9. Mayes, R. L., Buckle., I. G., "Seismic Isolation : A Solution to the Earthquake Problems of the Precast Concrete Industry", PCI Journal May-June, 1988, p. 34-54

10. Steimer, S . F., Barwig, B. B., "Seismic base Isolation for Steel Structures", Canadian Journal of Civil Engineering, VOL. 12, 1985, p.73-81

11. Povov, E. P., Bertero, V. V., "Seismic Analysis of some Steel Building Frames", Journal of the Engineering Mechanics Division, VOL. 106, NO. EM1, February, 1980, p. 75-92

12. Hanson, R. D., D. M. Bergman, S. A. Ashour, " Supplemental Mechanical Dampers for Improved Seismic Response of Building", 3rd U. S. Conference on Earthquake Engineering, 1986, 1129-1140

13. Zayas, V. A., Low, S. S., Mahin, S. A., " The FPS : Earthquake Resisting System : Experimental Report", Report NO. UCB/EERC-87/01. Earthquake Engineering Research Centre, University of California, Berkeley, June 1987.

14. Pall A. S., Marsh, C., "Response of Friction Damped Braced Frames", Journal of the Structural Division, ASCE, VOL. 108, NO. STP6, June, 1982, p. 1313-1323

15. Baktash, P., Marsh, C., Damped Moment Resistant Braced Frames: A comparative study", Canadian Journal of Civil Engineering, June, 1987, 342-346

16. Filiatrault, A., Cherry, S., "Performance evaluation of friction damped braced frames under simulated earthquake loads", Earthquake Engineering Laboratory Report, Department of Civil Engineering, University of British Columbia, Vancouver, B. C. Nov., 1985.

17. Pall, A. S., Verganelakis, V., Marsh, C., "Friction dampers for seismic control of Control of Concordia University library building", The 5th Canadian Conference on Earthquake Engineering, 1986, Ottawa, Ontario, p. 191-200

18. Aiken, I. D., Kelly, J. M., Pall, A. S., "Seismic response of a nine-story steel frame with friction damped cross-bracing",Report NO. UCB/EERC-88/17, Earthquake Engineering Research Centre, University of California, Berkeley, 1988

19. Filiatrault, A., Cherry, S., "Comparative Performance of Friction Damped Systems and Base Isolation Systems for Earthquake Retrofit and Aseismic Design", Earthquake Engineering and Structural Dynamics, VOL. 16, 1988, p. 389-416

20. NBCC Supplement, 1985, Commentary J

21. Kannan, A. E., Powell, G. M., "DRAIN-2D: A general purpose computer program for dynamic analysis of inelastic plane structures", Report NO. UCB/EERC-73/6, Earthquake Engineering Research Centre, University of California, Berkeley, 1973

22. Guendelman-Israel, R., Powell,G. M., "DRAIN-TABS : A computer program for inelastic earthquake response of 3D building", Report NO. UCB/EERC-77/8, Earthquake Engineering Research Centre, University of California, Berkeley, 1977

23. Rubicka, J. E., "Forced Vibration in Systems with Elastically supported dampers", M.I.T., June, 1957

24. Class notes on Earthquake Engineering, Concordia University.

25 Dempsey, K. M., Irvine, H. M., "A Note on the Numerical Evaluation of Duhamel Integral", Earthquake Engineering and Structural Dynamics, VOL. 16, 1978, p. 511-515

26. Housner, G. W., Martel, R. R., Alford, J. L.,"Spectrum Analysis of Strong-Motion earthquakes",Bulletin of the Seismological Society of America, VOL. 43, no. 2, April 1953, p.97-119

27. Chopra, A. K., "Dynamics of Structures - A Primer", Earthquake Engineering Research Centre, Berkeley, California, 1981.

28. Chopra, A. K., Cruz, E. F., "Simplified Procedures for earthquake Analysis of Buildings", ASCE, J. of Structural Engineering, VOL. 112, # No. 3, March, 1986, p. 461-480

29. Bagget, J. F., Martin, J. B., "Evaluation of the Inelastic Spectrums design method for two DOF Structures under earthquake loadings", Engineering Structures, VOL. 5, 1983, October, p.247-254

30. Mahin, S. A., Lin, J., "Construction of Inelastic Response Spectra for SDOF systems", Report No. UCB/EERC-83/17, Earthquake Engineering Research Centre, University of California, Berkeley, 1983.

31. CSA S16.1-M84, "Steel Structures in Buildings - Limits States Design"

32. Rainer, J. H., "Force reduction factors for the Seismic provisions of the National Building Code of Canada", Canadian Journal of Civil Engineering, Vol. 14, 1987, p. 447-454

33. Wilson, E. L., Dovey, H. H., Habibullah, A., "Three Dimensional Analysis of Building Systems", Report No. UCB/EERC-72/8, Earthquake Engineering Research Centre, University of California, Berkeley, 1972.

34. Clough, R. W., Penzien J., "Dynamics of Structures", McGraw-Hill Inc., 1975

35. Lin, J., Mahin, S. A., "Effect of Inelastic Behaviour on the Analysis and design of Earthquake Resistant Structures", Report No. UCB/EERC-85/08, Earthquake Engineering Research Centre, University of California, Berkeley, June, 1985.

36. Jain, A. K., "Seismic Response of Reinforced Concrete Frames with Steel Bracings", Journal of Structural Engineering, VOL. 11, no. 10, October, 1985, 2138-2148

37. Proposed revision to the 1985 NBCC, Associate Standing Committee

APPENDIX A

PROGRAM LISTING OF SDOF ROUTINE

```
      PROGRAM FRICTON
      DOUBLE PRECISION X(30000),V(30000),Z(30000),ZA(30000),
     +     TIME(30000),G(30000),T(30000),T1(30000),ACC(30000),
     +     T15(30000),TIME5(30000),C1(30000),C2(30000),
     +     R(30000),CHECK(20),G5(30000),Z5(30000),DELP0(30000),
     +     C10(20),C20(20),XMAXK(300),VMAXK(300),ACCMAXK(300),
     +     ALPHAK(300),PERIOD(300),PSK(300)
      INTEGER COUNT,ICOM(30000),JCOM(40)
      CHARACTER*70  TITLE
      REAL*8 PP,TIM,DELT,DELP,SCALE,
     +     PI,XMAX,VMAX,ACCMAX,KG,MASS,PS,K1,K2,ALPHA
     +     KNEW,PNEW,AN,BN,DELA,DELV,THETA,FF,DAMP
      OPEN(3,FILE='XMAXALP.DAT',STATUS='NEW')
      OPEN(4,FILE='VMAXALP.DAT',STATUS='NEW')
      OPEN(5,FILE='AMAXALP.DAT',STATUS='NEW')
      OPEN(6,FILE='VMAXPER.DAT',STATUS='NEW')
      OPEN(7,FILE='AMAXPER.DAT',STATUS='NEW')
      OPEN(8,FILE='XMAXPER.DAT',STATUS='NEW')
      OPEN(9,FILE='XMAXPS.DAT',STATUS='NEW')
      OPEN(10,FILE='VMAXPS.DAT',STATUS='NEW')
      OPEN(11,FILE='AMAXPS.DAT',STATUS='NEW')
      READ(1,90) TTITLE
90    FORMAT(A70)
      WRITE(*,101) TITLE
      WRITE(2,101) TITLE
101   FORMAT(' ',A70)
      READ(1,*) NOPAIRS
      READ(1,*) NSTEPS
      READ(1,*) DELT
      READ(1,*) DELP
      READ(1,*) SCALE
      READ(1,*) MASS
      READ(1,*) DAMP
      READ(1,*) PS
      READ(1,*) K1
      READ(1,*) ALPHA
      READ(1,*) JCOM(20)
      READ(1,*) JCOM(19)
      READ(1,*) JCOM(18)
      READ(1,*) JCOM(14)
      WRITE(*,109)
      NOPAIRS,NSTEPS,DELT,DELP,SCALE,MASS,DAMP,PS,K1,
     +ALPHA,JCOM(20),JCOM(19),JCOM(18)
      WRITE(2,109)
      NOPAIRS,NSTEPS,DELT,DELP,SCALE,MASS,DAMP,PS,K1,
     +ALPHA,JCOM(20),JCOM(19),JCOM(18)
 109    FORMAT(
     + ' NOPAIRS    = ', I5,/,
```

```
     + ' NSTEPS     = ', I5,/,
     + ' DELT       = ', F10.4,/,
     + ' DELP       = ', F10.4,/,
     + ' SCALE      = ', F10.4,/,
     + ' MASS       = ', F10.4,/,
     + ' DAMPING    = ', F10.4,/,
     + ' PS         = ', F10.4,/,
     + ' K1         = ', F10.4,/,
     + ' ALPHAK(1) = ', F10.4,/,
     + ' TIME-HIST  OUTPOUT INT.  E.Q.INPUT ',/,5X,I2,10X,I2,
     +   12X,I2,/)
        PI=3.141592654D-00
        NPS = 120
        NMASS = 200
        NK1   = 200
        NALPHA = 200

C       READ E.Q. DATA

        COUNT = NOPAIRS
        DO 9001 K=1, NOPAIRS ,1
            READ(1,*) (T(K),ZA(K))
 9001   CONTINUE

C     PRINT INPUT EARTHQUAKE DATA

        IF(JCOM(18).EQ.1) THEN
           WRITE (2,206)
 206       FORMAT(' ', ' INPUT E.Q. DATA ')
           DO 300 I=1,NOPAIRS,1
       WRITE(2,200) T(I), ZA(I)
 200         FORMAT(2F17.6)
 300       CONTINUE
       ENDIF

C     MULTIPLY E.Q. DATA BY SCALE FACTOR

        DO 140 JJJ=1,NOPAIRS,1
         Z(JJJ)=ZA(JJJ)*SCALE
  140   CONTINUE

C      TO PRINT SCALED E.Q. DATA

          IF(JCOM(17).EQ.1)THEN
              DO 150 J=1,NOPAIRS ,1
                 WRITE(2,149)  (T(J), Z(J) )
         WRITE(*,149)  (T(J), Z(J) )
  150         CONTINUE
          ENDIF
  149   FORMAT(2F17.6)

C       INTERPOLATE E.Q. DATA
```

```
      DO 160  I=1,COUNT,1
      TIME(I) = T(I)
         TIME5(I)= T(I)
  160 CONTINUE

         CALL INTER (NSTEPS,TIME,Z,DELT,T1,G)

C        INITIALIZE VARIABLES

       DO 9950 KK=1,NPS,1
            X(1)       = 0.0
            V(1)       = 0.0
            ACC(1)     = 0.0
            XMAX       = 0.0
            VMAX       = 0.0
            ACCMAX     = 0.0
            ALPHAK(KK) = ALPHA
            K2 = ALPHA * K1
            KG = K1 + K2
            PERIOD( KK ) = SQRT(MASS/KG)*2.0*PI
            JCOM( 1 ) = 0
            PSK(KK) = PS
            FF = PSK(KK)
            JCOM(16) = 0

         DO 3000 I=2, NSTEPS,1

     CALL RESP1I,X,V,ACC,DELT,MASS,DAMP,KG,DELV,DELX,G)

       IF(  ABS(C2(I-1)) .LT.FF.AND.JCOM(16).EQ.0 ) THEN
            C1(I)=C1(I-1)+K1*DELX
            C2(I)=C2(I-1)+K2*DELX
            R(I)= C1(I)+C2(I)
            KG=K1+K2
            ICOM(I)=0
            N1=0
            N2=0
            N5=0
            IF(ABS(C2(I)).GE.FF) THEN
               CALL CORRECT (I,FF,DELP0,C2,C1)
               GOTO 4001
            ENDIF
            GOTO 4090
       ENDIF
C-------------------------------------------------

 4001  IF(JCOM(10).EQ.0) THEN
            JCOM(10)=1
            IF(C2(I).GT.0.0)THEN
              JCOM(8)=1
              GOTO 4010
            ELSE
```

```
                JCOM(9)=1
                GOTO 4020
              ENDIF
          ENDIF
          IF(JCOM(8).EQ.1) GOTO 4010
          IF(JCOM(9).EQ.1) GOTO 4020
C-----------YIELD IN +VE DIRECTION FIRST-----------
 4010     IF( ABS( C2(I) ).GE.FF.OR.JCOM(16).NE.0 )THEN
               JCOM(16) = 1
               IF( V(I).GT.0.0 .AND. JCOM(15).EQ.0 ) THEN
                             KG=K1
                             ICOM(I)=1
                             N10=0
                             N1=0
                             C2(I) = FF
                             C1(I) = C1(I-1) + K1*DELX
                             R(I)  = C1(I) + C2(I)
                             GOTO 4090
               ELSEIF ( V(I).LT.0.0 .OR. JCOM(40).EQ.0) THEN
                     KG=K1+K2
                     N2 = 0
                     N5 = 0
                     JCOM(15)=1
                     ICOM(I) = 2
                         IF(N1.EQ.0) THEN
                               N1=1
                               CHECK(2)=X(I-1)
                               CHECK(3)=C2(I-1)
                               CHECK(5)=ABS(2.0*FF)
                         ENDIF
                     C1(I) = C1(I-1) + K1*DELX
                     C2(I) = C2(I-1) + K2*DELX
                     R(I)  = C1(I) + C2(I)
                     CHECK(4) = ABS( CHECK(3) - C2(I) )
                           IF( ABS(C2(I) ).LT.FF) THEN
                               N10= 0

                               N5 = 0
                           ENDIF
                           IF(C2(I).GE.FF) THEN
                              KG = K1
                              ICOM(I)=1
                              N10=0
                                  IF(N5.EQ.0) THEN
                                    CALL CORRECT (I,FF,DELP0,C1,C2)
                                     N5=1
                                  ENDIF
                              JCOM(15)=0
                           ELSEIF(C2(I).LT.-FF) THEN
                                 IF(N10.EQ.0) THEN
                                   CALL CORRECT (I,FF,DELP0,C1,C2)
                                   N10=1
```

```
                                    ENDIF
                                  KG=K1
                                  C2(I) = -FF
                                  C1(I) = C1(I-1) + K1*DELX
                                  R(I)  = C1(I) + C2(I)
                                  ICOM(I) = 3
                                  GOTO 4090
                                ENDIF
                    ENDIF
            ENDIF
               GOTO 4090
C-----------IF YIELD IN THE -VE DIRECTION ----------

 4020    IF( ABS( C2(I) ).GE.FF.OR.JCOM(16).NE.0 )THEN
               JCOM(16) = 1
               IF( V(I).LT.0.0 .AND. JCOM(15).EQ.0 ) THEN
                             KG=K1
                             ICOM(I)=-1
                             N10=0
                             N1=0
                             C2(I) = -FF
                             C1(I) = C1(I-1) + K1*DELX
                             R(I)  = C1(I) + C2(I)
                             GOTO 4090
               ELSEIF ( V(I).GT.0.0 .OR. JCOM(40).EQ.0) THEN
                     KG=K1+K2
                     N2 = 0
                     N5 = 0
                     JCOM(15)=1
                     ICOM(I) = -2
                         IF(N1.EQ.0) THEN
                               N1=1
                               CHECK(2)=X(I-1)
                               CHECK(3)=C2(I-1)
                               CHECK(5)=ABS(2.0*FF)
                         ENDIF
                     C1(I) = C1(I-1) + K1*DELX
                     C2(I) = C2(I-1) + K2*DELX
                     R(I)  = C1(I) + C2(I)
                     CHECK(4) = ABS( CHECK(3) - C2(I) )
                           IF( ABS(C2(I) ).LT.FF) THEN
                               N10= 0

                               N5 = 0
                           ENDIF
                           IF(C2(I).LT.-FF) THEN
                              KG = K1
                              ICOM(I)=-1
                              N10=0
                                   IF(N5.EQ.0) THEN
                                     CALL CORRECT (I,FF,DELP0,C1,C2)
                                      N5=1
```

```
                                    ENDIF
                                  JCOM(15)=0
                                ELSEIF(C2(I).GT.FF) THEN
                                    IF(N10.EQ.0) THEN
                                      CALL CORRECT (I,FF,DELP0,C1,C2)
                                      N10=1
                                    ENDIF
                                  KG=K1
                                  C2(I) = FF
                                  C1(I) = C1(I-1) + K1*DELX
                                  R(I)  = C1(I) + C2(I)
                                  ICOM(I) = -3
                                  GOTO 4090
                                ENDIF
                    ENDIF
          ENDIF
C-------------- ACCELERATION COMPUTED FROM THE E.O.M. --------

 4090    IF(ABS(C2(I)).LT.FF)     DELP0(I) = 0.0
         ACC(I)= ( -MASS*G(I)-R(I)-DAMP*V(I)+DELP0(I) )/MASS
C--------------------- CHECK FOR MAX VALUES-------
 3501          IF( ABS(X(I)).GE.ABS(XMAX) ) THEN
 XMAX = X(I)
                          TXMAX = T1(I)
ENDIF
                  IF( ABS(V(I)).GE.ABS(VMAX) ) THEN
                          VMAX = V(I)
                          TVMAX = T1(I)
                  ENDIF
                  IF( ABS(ACC(I)).GE.ABS(ACCMAX) ) THEN
                          ACCMAX = ACC(I)
                          TACCMAX = T1(I)
                  ENDIF
 3000   CONTINUE
                XMAXK(KK)    = ABS(XMAX)
                VMAXK(KK)    = ABS(VMAX)
                ACCMAXK(KK) = ABS(ACCMAX)
                PS           = PS + 0.50
C               ALPHA        = ALPHA  + 0.01
 9950   CONTINUE
C-----------------TIME HISTORY OUTPUT--------------------
                  IF(JCOM(20).EQ.1) THEN
     WRITE(2,3999)
                          IF(JCOM(14).EQ.1) WRITE(*,3999)
                  ENDIF
 3999FORMAT(' ',/,
     +   ' TIME(I)     X(I)      V(I)    ACC(I)  DELP0
     +    C2(I)      C1(I)      R(I)  YIELD ')
IF(JCOM(20).EQ.1) THEN
           DO 3500 I=1,NSTEPS,JCOM(19)
           WRITE(2,4000) T1(I),X(I),V(I),ACC(I),DELP0(I),
     +     C2(I),C1(I),R(I),ICOM(I)
```

```
                IF(JCOM(14).EQ.1)
                          WRITE(*,4000)T1(I),X(I),V(I),ACC(I),
     +                    DELPO(I),C2(I),C1(I),R(I),ICOM(I)
                IF(NNN.EQ.23) THEN
                    IF(JCOM(14).EQ.1) WRITE(*,3999)
                    WRITE(2,3999)
                    NNN=1
                ENDIF
               NNN=NNN+1
3500        CONTINUE
         ENDIF
4000FORMAT(F9.5,F9.4,F8.3,1X,2(F8.3,1X),3(F9.2,1X),I2)
WRITE(2,4089)
4089    FORMAT('    ALPHAK(KK)    PERIOD(KK)    XMAXK(KK)    VMAXK(KK)

     +      ACCMAXK(KK)')
       DO 9980 KK=1,NALPHA,1
            WRITE(2,4070)ALPHAK(KK),PERIOD(KK),XMAXK(KK),VMAXK(KK),
     +                                                  ACCMAXK(KK)
              IF(N20.GT.25) THEN
                WRITE(2,4089)
                N20=1
              ENDIF
              N20=N20+1
9980     CONTINUE
4070     FORMAT(5(F12.5,1X))
         WRITE(3,101) TITLE
         WRITE (3,4029)
4029     FORMAT('       ALPHA           XMAX   '     )
         DO 5062 KK=1,NALPHA,1
5062        WRITE(3,5070) ALPHAK(KK),XMAXK(KK)
         WRITE(4,101) TITLE
         WRITE (4,4039)
4039     FORMAT('       ALPHA            VMAX   '     )
         DO 5065 KK=1,NALPHA,1
5065        WRITE(4,5070) ALPHAK(KK),VMAXK(KK)
         WRITE(5,101) TITLE
         WRITE (5,4049)
4049     FORMAT('        ALPHAK           ACCMAX   '     )
         DO 5075 KK=1,NALPHA,1
5075        WRITE(4,5070) ALPHAK(KK),ACCMAXK(KK)
         WRITE(6,101) TITLE
         WRITE(6,4045)
4045     FORMAT('    PERIOD            VMAX   ')
         DO 5080 KK=1,NALPHA, 1
5080        WRITE(6,5070) PERIOD(KK),VMAXK(KK)
         WRITE(7,101) TITLE
         WRITE(6,4059)
4059     FORMAT('   PERIOD            ACCMAX   ')
         DO 5090  KK=1,NALPHA,1
5090        WRITE(7,5070) PERIOD(KK),ACCMAXK(KK)
         WRITE(8,101) TITLE
```

```
      WRITE(8,4069)
4069  FORMAT('  PERIOD            XMAX   ')
      DO 5095  KK=1,NALPHA,1
5095      WRITE(8,5070) PERIOD(KK),XMAXK(KK)
      WRITE(9,101) TITLE
      WRITE(9,4079)
4079  FORMAT('       PS(KK)        XMAX      ' )
      DO 5100  KK=1,NPS,1
5100    WRITE(9,5070) PSK(KK),XMAXK(KK)
      WRITE(10,101) TITLE
      WRITE(10,4088)
4088  FORMAT('     PS(KK)             VMAXK(KK)    ')
      DO 5115  KK = 1,NPS,1
5115       WRITE(10,5070) PSK(KK), VMAXK(KK)
      WRITE(11,101)  TITLE
      WRITE(11,4099)
4099  FORMAT('     PS(KK)             ACCMAX(KK)     ')
      DO 5120 KK=1,NPS,1
5120      WRITE(11,5070)  PSK(KK), ACCMAXK(KK)
5070  FORMAT(F13.5,4X,F13.5)
      END
      SUBROUTINE INTER (NSTEPS5,TIME5,Z5,DELT5,T15,G5)
DOUBLE PRECISION Z(30000),TIME(30000),G(30000),T(30000),
     +  T1(30000),T15(30000),TIME5(30000),G5(30000),Z5(30000)
      REAL*8 PP,TIM,DELT,DELP,SCALE,
     +  PI,XMAX,VMAX,ACCMAX,KG,MASS,K1,K2,
     +  KNEW,PNEW,AN,BN,DELA,DELV,DAMP
      N = 1
  TIM = 0.0
      T15(1)= 0.0
      G5(1)= 0.0
              DO 30  MSTEP = 2, NSTEPS5
       TIM = TIM + DELT5
10            IF(TIM.LE.TIME5(N+1))  GO TO 20
N = N + 1
GO TO 10
 20   PP = (TIM -TIME5(N)) / (TIME5(N+1) - TIME5(N))
G5(MSTEP) = PP * Z5(N+1) + (1.0 - PP)*Z5(N)
              T15(MSTEP)= TIM
 30   CONTINUE
      RETURN
      END
      SUBROUTINE RESP1(I,X,V,ACC,DELT,MASS,DAMP,KG,DELV,DELX,G)

      DOUBLE PRECISION X(30000),V(30000),G(30000),ACC(30000)
      REAL*8 PP,TIM,DELT,DELP,SCALE,
     +  pi,XMAX,VMAX,ACCMAX,KG,MASS,K1,K2,
     +  KNEW,PNEW,AN,BN,DELA,DELV,FF,DAMP
      AN = 6.0*V(I-1)/DELT + 3.0*ACC(I-1)
      BN = 3.0*V(I-1) + DELT*ACC(I-1)/2.0
      PNEW = -MASS*( G(I) - G(I-1) ) + AN*MASS + DAMP*BN
      KNEW = (6.00)*MASS/( DELT**2 )+3.000*DAMP/DELT + KG
```

```
DELX = PNEW/KNEW
DELV = (3.00000)*DELX/DELT - BN
X(I) = X(I-1) + DELX
V(I) = V(I-1) + DELV
RETURN
END
SUBROUTINE CORRECT (I,FF,DELPO,C1,C2)
DOUBLE PRECISION C1(30000),C2(30000),DELPO(30000)
REAL*8 FF,FF1
IF(C2(I).GT.0.0) FF1=FF
IF(C2(I).LT.0.0) FF1=-FF
DELPO(I) = C2(I) - FF1
RETURN
END
```

APPENDIX B

Properties of frames used

Frame #	storey	columns	beams	mass (tons)
1	1	W200X46	W410X54	10.9
2	1	W250X80	W460X97	10.9
3	1	W150X30	W310X39	10.9
4	1	W200X27	W310X39	8.0
5	1	W250X80	W460X97	5.0
6	1	W150X30	W310X39	19.0
7	1	W150X30	W310X39	27.0
8	1	W150X22	W310X39	22.0
9	1	W150X22	W310X39	28.0
10	1	M100X19	W310X33	35.0
11	1	M100X19	W310X33	39.0
12	1	M100X19	W310X33	18.0
13	1	M100X19	W310X33	21.0
14	1	M100X19	W310X33	25.0
15	1	M100X19	W310X33	29.0
16	1	M100X19	W310X33	33.0
17	1	M100X19	W310X33	35.0
18	1	M100X19	W310X33	33.5
19	1	M100X19	W310X33	33.9
20	1	M100X19	W310X33	28.5
21	1	W200X46	W410X54	11.9
22	1	W200X46	W410X54	12.5
23	1	W200X46	W410X54	14.5
24	1	W200X46	W410X54	11.2
25	1	W200X46	W410X54	4.0
26	1	W200X46	W410X54	4.2
27	1	W200X46	W410X54	4.4
28	1	W200X46	W410X54	4.6
29	2	W200X27	W410X54	10.9
	1	W200X27	W410X54	12.5
30	2	W200X27	W410X54	9.0
	1	W200X27	W410X54	9.0
31	2	W200X27	W410X54	6.0
	1	W200X27	W410X54	6.0
32	2	W200X36	W410X54	8.0
	1	W200X36	W410X54	8.0
33	2	W200X36	W410X54	7.0
	1	W200X36	W410X54	7.0
34	2	W200X36	W410X54	6.0
	1	W200X36	W410X54	6.0
35	2	W200X36	W410X54	5.5
	1	W200X36	W410X54	5.5
36	2	W200X36	W410X54	5.1
	1	W200X36	W410X54	5.1
37	2	W200X36	W410X54	4.9

	1	W200X36	W410X54	4.9
38	2	W200X36	W410X54	8.0
	1	W200X36	W410X54	8.0
39	2	W200X36	W410X54	8.3
	1	W200X36	W410X54	8.3
40	2	W200X36	W410X54	8.4
	1	W200X36	W410X54	8.4
41	2	W200X36	W410X54	8.6
	1	W200X36	W410X54	8.6
42	2	W200X36	W410X54	9.0
	1	W200X36	W410X54	9.0
43	2	W200X36	W410X54	9.4
	1	W200X36	W410X54	9.4
44	2	W200X36	W410X54	9.7
	1	W200X36	W410X54	9.7
45	2	W200X36	W410X54	10.2
	1	W200X36	W410X54	10.2
46	2	W200X36	W410X54	10.5
	1	W200X36	W410X54	10.5
47	2	W200X36	W410X54	10.7
	1	W200X36	W410X54	10.7
48	2	W310X202	W410X54	10.9
	1	W310X202	W410X54	10.9
49	3	W150X30	W410X54	12.5
	2	W150X30	W410X54	12.5
	1	W150X30	W410X54	10.9
50	3	W250X67	W410X54	12.5
	2	W250X67	W410X54	12.5
	1	W250X67	W410X54	10.9
51	3	W200X36	W460X61	12.5
	2	W200X36	W460X61	12.5
	1	W200X36	W460X61	10.9
52	3	W200X59	W410X54	7.0
	2	W200X59	W410X54	7.0
	1	W200X59	W410X54	7.0
53	3	W200X59	W410X54	8.0
	2	W200X59	W410X54	8.0
	1	W200X59	W410X54	8.0
54	3	W200X59	W410X54	8.5
	2	W200X59	W410X54	8.5
	1	W200X59	W410X54	8.5
55	3	W200X39	W410X54	9.0
	1	W200X39	W410X54	9.0
	1	W200X39	W410X54	9.0
56	3	W200X36	W410X54	9.3
	2	W200X36	W410X54	9.3
	1	W200X36	W410X54	9.3
57	3	W200X36	W410X54	9.5
	2	W200X36	W410X54	9.5
	1	W200X36	W410X54	9.5
58	3	W200X36	W410X54	9.8

	2	W200X36	W410X54	9.8
	1	W200X36	W410X54	9.8
59	3	W200X36	W410X54	10.7
	2	W200X36	W410X54	10.7
	1	W200X36	W410X54	10.7
60	3	W200X36	W410X54	11.5
	2	W200X36	W410X54	11.5
	1	W200X36	W410X54	11.5
61	3	W200X36	W410X54	12.8
	2	W200X36	W410X54	12.8
	1	W200X36	W410X54	12.8
62	4	W200X31	W460X61	10.9
	3	W250X101	W460X61	12.5
	2	W250X101	W460X61	12.5
	1	W250X101	W460X61	12.5
63	4	W200X31	W460X62	17.0
	3	W250X101	W460X61	17.0
	2	W250X101	W460X61	17.0
	1	W250X101	W460X61	17.0
64	4	W200X31	W410X54	7.5
	3	W200X59	W410X54	7.5
	2	W200X59	W410X54	7.5
	1	W200X59	W410X54	7.5
65	4	W200X31	W410X54	8.0
	3	W200X59	W410X54	8.0
	2	W200X59	W410X54	8.0
	1	W200X59	W410X54	8.0
66	4	W200X31	W410X54	8.7
	3	W200X59	W410X54	8.7
	2	W200X59	W410X54	8.7
	1	W200X59	W410X54	8.7
67	4	W200X31	W410X54	9.2
	3	W200X59	W410X54	9.2
	2	W200X59	W410X54	9.2
	1	W200X59	W410X54	9.2
68	4	W200X31	W410X54	11.0
	3	W200X59	W410X54	11.0
	2	W200X59	W410X54	11.0
	1	W200X59	W410X54	11.0
69	4	W200X31	W410X54	11.7
	3	W200X54	W410X54	11.7
	2	W200X59	W410X54	11.7
	1	W200X59	W410X54	11.7
70	4	W200X31	W410X54	12.1
	3	W200X59	W410X54	12.1
	2	W200X59	W410X54	12.1
	1	W200X59	W410X54	12.1
71	4	W200X31	W410X54	12.5
	3	W200X59	W410X54	12.5
	2	W200X59	W410X54	12.5

	1	W200X59	W410X54	12.5
72	4	W200X31	W410X54	12.9
	3	W200X59	W410X54	12.9
	2	W200X59	W410X54	12.9
	1	W200X59	W410X54	12.9
73	4	W200X31	W510X54	13.3
	3	W200X59	W410X54	13.3
	2	W200X59	W410X54	13.3
	1	W200X59	W410X54	13.3
74	4	W200X31	W410X54	13.6
	3	W200X59	W410X54	13.6
	2	W200X59	W410X54	13.6
	1	W200X59	W410X54	13.6
75	4	W200X31	W410X54	14.1
	3	W200X59	W410X54	14.1
	2	W200X59	W410X54	14.1
	1	W200X59	W410X54	14.1
76	4	W200X31	W410X54	14.4
	3	W200X59	W410X54	14.4
	2	W200X59	W410X54	14.4
	1	W200X59	W410X54	14.4
77	4	W200X31	W410X54	14.7
	3	W200X59	W410X54	14.7
	2	W200X59	W410X54	14.7
	1	W200X59	W410X54	14.7
78	4	W200X31	W410X54	14.7
	3	W200X59	W410X54	15.0
	2	W200X59	W410X54	15.0
	1	W200X59	W410X54	15.0
79	4	W200X31	W410X54	14.9
	3	W200X59	W410X54	14.9
	2	W200X59	W410X59	14.9
	1	W200X59	W410X54	14.9
80	4	W200X31	W410X54	15.3
	3	W200X59	W410X54	15.3
	2	W200X59	W410X54	15.3
	1	W200X59	W410X54	15.3
81	4	W200X31	W410X54	15.5
	3	W200X59	W410X54	15.5
	2	W200X59	W410X54	15.5
	1	W200X59	W410X54	15.5
82	4	W200X31	W410X54	15.7
	3	W200X59	W410X54	15.7
	2	W200X59	W410X54	15.7
	1	W200X59	W410X54	15.7
83	4	W200X31	W410X54	15.9
	3	W200X59	W410X54	15.9
	2	W200X59	W410X54	15.9
	1	W200X59	W410X54	15.9
84	4	W200X31	W410X54	16.3
	3	W200X59	W410X54	16.3

	2	W200X59	W410X54	16.3
	1	W200X59	W410X54	16.3
85	5	W200X31	W410X54	10.9
	4	W200X49	W410X54	12.5
	3	W200X49	W410X54	12.5
	2	W200X49	W410X54	12.5
	1	W200X49	W410X54	12.5
86	5	W200X31	W460X74	10.9
	4	W250X89	W460X74	12.5
	3	W250X89	W460X74	12.5
	2	W250X89	W460X74	12.5
	1	W250X89	W460X74	12.5
87	5	W200X31	W410X54	14.0
	4	W200X49	W410X54	14.0
	3	W200X49	W410X54	14.0
	2	W200X49	W410X54	14.0
	1	W200X49	W410X54	14.0
88	5	W200X31	W410X54	9.9
	4	W200X49	W410X54	9.9
	3	W200X49	W410X54	9.9
	2	W200X49	W410X54	9.9
	1	W200X49	W410X54	9.9
89	5	W200X31	W410X54	12.0
	4	W200X49	W410X54	12.0
	3	W200X49	W410X54	12.0
	2	W200X49	W410X54	12.0
	1	W200X49	W410X54	12.0
90	5	W200X31	W410X54	12.3
	4	W200X49	W410X54	12.3
	3	W200X49	W410X54	12.3
	2	W200X49	W410X54	12.3
	1	W200X49	W410X54	12.3
91	5	W200X31	W410X54	12.4
	4	W200X49	W410X54	12.4
	3	W200X49	W410X54	12.4
	2	W200X49	W410X54	12.4
	1	W200X49	W410X54	12.4
92	5	W200X31	W410X54	12.4
	4	W200X49	W410X54	12.6
	3	W200X49	W410X54	12.6
	2	W200X49	W410X54	12.6
	1	W200X49	W410X54	12.6
93	5	W200X31	W410X54	12.8
	4	W200X31	W410X54	12.8
	3	W200X49	W410X54	12.8
	2	W200X49	W410X54	12.8
	1	W200X49	W410X54	12.8
94	5	W200X31	W410X54	13.0
	4	W200X49	W410X54	13.0
	3	W200X49	W410X54	13.0
	2	W200X49	W410X54	13.0

	1	W200X49	W410X54	13.0
95	5	W200X31	W410X54	13.2
	4	W200X49	W410X54	13.2
	3	W200X49	W410X54	13.2
	2	W200X49	W410X54	13.2
	1	W200X49	W410X54	13.2
96	5	W200X31	W410X54	13.4
	4	W200X49	W410X54	13.4
	3	W200X49	W410X54	13.4
	2	W200X49	W410X54	13.4
	1	W200X49	W410X54	13.4
97	5	W200X31	W410X54	13.6
	4	W200X49	W410X54	13.6
	3	W200X49	W410X54	13.6
	2	W200X49	W410X54	13.6
	1	W200X49	W410X54	13.6
98	5	W200X31	W410X54	13.8
	4	W200X49	W410X54	13.8
	3	W200X49	W410X54	13.8
	2	W200X49	W410X54	13.8
	1	W200X49	W410X54	13.8
99	5	W200X31	W410X54	14.0
	4	W200X31	W410X54	14.0
	3	W200X49	W410X54	14.0
	2	W200X49	W410X54	14.0
	1	W200X49	W410X54	14.0
100	5	W200X31	W410X54	14.2
	4	W200X49	W410X54	14.2
	3	W200X49	W410X54	14.2
	2	W200X49	W410X54	14.2
	1	W200X49	W410X54	14.2
101	5	W200X31	W410X54	14.4
	4	W200X49	W410X54	14.4
	3	W200X49	W410X54	14.4
	2	W200X49	W410X54	14.4
	1	W200X49	W410X54	14.4
102	5	W200X31	W410X54	14.6
	4	W200X49	W410X54	14.6
	3	W200X49	W410X54	14.6
	2	W200X49	W410X54	14.6
	1	W200X49	W410X54	14.6
103	5	W200X31	W410X54	14.8
	4	W200X49	W410X54	14.8
	3	W200X49	W410X54	14.8
	2	W200X49	W410X54	14.8
	1	W200X49	W410X54	14.8
104	5	W200X31	W410X54	15.0
	4	W200X49	W410X54	15.0
	3	W200X49	W410X54	15.0
	2	W200X49	W410X54	15.0
	1	W200X49	W410X54	15.0

105	5	W200X31	W410X54	15.2
	4	W200X49	W410X54	15.2
	3	W200X49	W410X54	15.2
	2	W200X49	W410X54	15.2
	1	W200X49	W410X54	15.2
106	5	W200X31	W410X54	15.4
	4	W200X49	W410X54	15.4
	3	W200X49	W410X54	15.4
	2	W200X49	W410X54	15.4
	1	W200X49	W410X54	15.4
107	5	W200X31	W410X54	15.6
	4	W200X49	W410X54	15.6
	3	W200X49	W410X54	15.6
	2	W200X49	W410X54	15.6
	1	W200X49	W410X54	15.6
108	5	W200X31	W410X54	15.8
	4	W200X49	W410X54	15.8
	3	W200X49	W410X54	15.8
	2	W200X49	W410X54	15.8
	1	W200X49	W410X54	15.8
109	5	W200X31	W410X54	16.0
	4	W200X49	W410X54	16.0
	3	W200X49	W410X54	16.0
	2	W200X49	W410X54	16.0
	1	W200X49	W410X54	16.0
110	5	W200X31	W410X54	16.2
	4	W200X49	W410X54	16.2
	3	W200X49	W410X54	16.2
	2	W200X49	W410X54	16.2
	1	W200X49	W410X54	16.2
111	5	W200X31	W410X54	16.4
	4	W200X49	W410X54	16.4
	3	W200X49	W410X54	16.4
	2	W200X49	W410X54	16.4
	1	W200X49	W410X54	16.4
112	5	W200X31	W410X54	16.6
	4	W200X49	W410X54	16.6
	3	W200X49	W410X54	16.6
	2	W200X49	W410X54	16.6
	1	W200X49	W410X54	16.6
113	5	W200X31	W410X54	16.8
	4	W200X49	W410X54	16.8
	3	W200X49	W410X54	16.8
	2	W200X49	W410X54	16.8
	1	W200X49	W410X54	16.8
114	5	W200X31	W410X54	17.0
	4	W200X49	W410X54	17.0
	3	W200X49	W410X54	17.0
	2	W200X49	W410X54	17.0
	1	W200X49	W410X54	17.0
115	7	W200X27	W410X54	10.9

	6	W200X27	W410X54	12.5
	5	W200X27	W410X54	12.5
	4	W200X27	W410X54	12.5
	3	W250X49	W410X54	12.5
	2	W250X49	W410X54	12.5
	1	W250X49	W410X54	12.5
116	7	W200X27	W410X54	14.0
	6	W200X27	W410X54	14.0
	5	W200X27	W410X54	14.0
	4	W200X27	W410X54	14.0
	3	W250X49	W410X54	14.0
	2	W250X49	W410X54	14.0
	1	W250X49	W410X54	14.0
117	7	W200X27	W410X54	10.0
	6	W200X27	W410X54	10.0
	5	W200X27	W410X54	10.0
	4	W200X27	W410X54	10.0
	3	W250X49	W410X54	10.0
	2	W250X49	W410X54	10.0
	1	W250X49	W410X54	10.0
118	7	W200X27	W410X54	8.5
	6	W200X27	W410X54	8.5
	5	W200X27	W410X54	8.5
	4	W200X27	W410X54	8.5
	3	W250X49	W410X54	8.5
	2	W250X49	W410X54	8.5
	1	W250X49	W410X54	8.5
119	7	W200X27	W410X54	7.5
	6	W200X27	W410X54	7.5
	5	W200X27	W410X54	7.5
	4	W200X27	W410X54	7.5
	3	W250X49	W410X54	7.5
	2	W250X49	W410X54	7.5
	1	W250X49	W410X54	7.5
120	7	W200X27	W410X54	6.5
	6	W200X27	W410X54	6.5
	5	W200X27	W410X54	6.5
	4	W200X27	W410X54	6.5
	3	W250X49	W410X54	6.5
	2	W250X49	W410X54	6.5
	1	W250X49	W410X54	6.5
121	7	W200X27	W410X54	15.5
	6	W200X27	W410X54	15.5
	5	W200X27	W410X54	15.5
	4	W200X27	W410X54	15.5
	3	W250X49	W410X54	15.5
	2	W250X49	W410X54	15.5
	1	W250X49	W410X54	15.5
122	8	W200X27	W410X54	10.9
	7	W200X27	W410X54	12.5
	6	W200X27	W410X54	12.5

	5	W200X36	W410X54	12.5
	4	W200X36	W410X54	12.5
	3	W200X36	W410X54	12.5
	2	W200X59	W410X54	12.5
	1	W200X59	W410X54	12.5
123	8	W200X27	W410X54	10.0
	7	W200X27	W410X54	10.0
	6	W200X27	W410X54	10.0
	5	W200X36	W410X54	10.0
	4	W200X36	W410X54	10.0
	3	W200X36	W410X54	10.0
	2	W200X59	W410X54	10.0
	1	W200X59	W410X54	10.0
124	9	W200X27	W410X54	10.0
	8	W200X36	W410X54	10.0
	7	W200X36	W410X54	10.0
	6	W200X36	W410X54	10.0
	5	W200X36	W410X54	10.0
	4	W200X59	W410X54	10.0
	3	W200X59	W410X54	10.0
	2	W200X59	W410X54	10.0
	1	W250X67	W410X54	10.0
125	9	W200X27	W410X54	9.0
	8	W200X36	W410X54	9.0
	7	W200X36	W410X54	9.0
	6	W200X36	W410X54	9.0
	5	W200X36	W410X54	9.0
	4	W200X59	W410X54	9.0
	3	W200X59	W410X54	9.0
	2	W200X59	W410X54	9.0
	1	W250X67	W410X54	9.0
126	10	W200X27	W410X54	10.9
	9	W200X27	W420X54	12.5
	8	W200X27	W410X54	12.5
	7	W200X27	W410X54	12.5
	6	W200X36	W410X54	12.5
	5	W200X36	W410X54	12.5
	4	W200X36	W410X54	12.5
	3	W200X36	W410X54	12.5
	2	W200X59	W410X54	12.5
	1	W200X59	W410X54	12.5
127	10	W200X27	W410X54	10.9
	9	W200X27	W420X54	12.5
	8	W200X36	W410X54	12.5
	7	W200X59	W410X54	12.5
	6	W200X59	W410X54	12.5
	5	W250X67	W410X54	12.5
	4	W250X67	W410X54	12.5
	3	W250X67	W410X54	12.5
	2	W250X80	W410X54	12.5
	1	W250X80	W410X54	12.5

128	10	W200X27	W410X54	11.0	
	9	W200X27	W420X54	11.0	
	8	W200X36	W410X54	11.0	
	7	W200X59	W410X54	11.0	
	6	W200X59	W410X54	11.0	
	5	W250X67	W410X54	11.0	
	4	W250X67	W410X54	11.0	
	3	W250X67	W410X54	11.0	
	2	W250X80	W410X54	11.0	
	1	W250X80	W410X54	11.0	
129	10	W200X27	W410X54	9.0	
	9	W200X27	W420X54	9.0	
	8	W200X36	W410X54	9.0	
	7	W200X59	W410X54	9.0	
	6	W200X59	W410X54	9.0	
	5	W250X67	W410X54	9.0	
	4	W250X67	W410X54	9.0	
	3	W250X67	W410X54	9.0	
	2	W250X80	W410X54	9.0	
	1	W250X80	W410X54	9.0	
130	10	W200X27	W410X54	10.0	
	9	W200X36	W420X54	10.0	
	8	W200X36	W410X54	10.0	
	7	W200X59	W460X61	10.0	
	6	W200X59	W460X61	10.0	
	5	W250X67	W460X61	10.0	
	4	W250X67	W460X61	10.0	
	3	W250X67	W410X74	10.0	
	2	W250X80	W410X74	10.0	
	1	W250X80	W410X74	10.0	
131	10	W200X27	W410X54	13.5	
	9	W200X36	W420X54	13.5	
	8	W200X36	W410X54	13.5	
	7	W200X59	W460X61	13.5	
	6	W200X59	W460X61	13.5	
	5	W250X67	W460X61	13.5	
	4	W250X67	W460X61	13.5	
	3	W250X67	W410X74	13.5	
	2	W250X80	W410X74	13.5	
	1	W250X80	W410X74	13.5	
132	11	W200X27	W410X54	10.0	D11-1.DAT
	10	W200X27	W410X54	10.0	
	9	W200X27	W420X54	10.0	
	8	W200X36	W410X54	10.0	
	7	W200X36	W460X61	10.0	
	6	W200X59	W460X61	10.0	
	5	W250X59	W460X61	10.0	
	4	W250X59	W460X61	10.0	
	3	W250X59	W410X74	10.0	
	2	W250X59	W410X74	10.0	
	1	W250X67	W410X74	10.0	

133	11	W200X27	W410X54	12.0	D11-2.DAT
	10	W200X27	W410X54	12.0	
	9	W200X27	W420X54	12.0	
	8	W200X36	W410X54	12.0	
	7	W200X36	W460X61	12.0	
	6	W200X59	W460X61	12.0	
	5	W250X59	W460X61	12.0	
	4	W250X59	W460X61	12.0	
	3	W250X59	W410X74	12.0	
	2	W250X59	W410X74	12.0	
	1	W250X67	W410X74	12.0	
134	11	W200X27	W410X54	11.1	D11-3.DAT
	10	W200X27	W410X54	11.1	
	9	W200X27	W420X54	11.1	
	8	W200X36	W410X54	11.1	
	7	W200X36	W460X61	11.1	
	6	W200X59	W460X61	11.1	
	5	W250X59	W460X61	11.1	
	4	W250X59	W460X61	11.1	
	3	W250X59	W410X74	11.1	
	2	W250X59	W410X74	11.1	
	1	W250X67	W410X74	11.1	
135	11	W200X27	W410X54	11.4	D11-4.DAT
	10	W200X27	W410X54	11.4	
	9	W200X27	W420X54	11.4	
	8	W200X36	W410X54	11.4	
	7	W200X36	W460X61	11.4	
	6	W200X59	W460X61	11.4	
	5	W250X59	W460X61	11.4	
	4	W250X59	W460X61	11.4	
	3	W250X59	W410X74	11.4	
	2	W250X59	W410X74	11.4	
	1	W250X67	W410X74	11.4	
136	11	W200X27	W410X54	13.0	D11-5.DAT
	10	W200X27	W410X54	13.0	
	9	W200X27	W420X54	13.0	
	8	W200X36	W410X54	13.0	
	7	W200X36	W460X61	13.0	
	6	W200X59	W460X61	13.0	
	5	W250X59	W460X61	13.0	
	4	W250X59	W460X61	13.0	
	3	W250X59	W410X74	13.0	
	2	W250X59	W410X74	13.0	
	1	W250X67	W410X74	13.0	
137	11	W200X27	W410X54	13.4	D11-6.DAT
	10	W200X27	W410X54	13.4	
	9	W200X27	W420X54	13.4	
	8	W200X36	W410X54	13.4	
	7	W200X36	W460X61	13.4	
	6	W200X59	W460X61	13.4	
	5	W250X59	W460X61	13.4	

	4	W250X59	W460X61	13.4	
	3	W250X59	W410X74	13.4	
	2	W250X59	W410X74	13.4	
	1	W250X67	W410X74	13.4	
138	11	W200X27	W410X54	13.7	D11-7.DAT
	10	W200X27	W410X54	13.7	
	9	W200X27	W420X54	13.7	
	8	W200X36	W410X54	13.7	
	7	W200X36	W460X61	13.7	
	6	W200X59	W460X61	13.7	
	5	W250X59	W460X61	13.7	
	4	W250X59	W460X61	13.7	
	3	W250X59	W410X74	13.7	
	2	W250X59	W410X74	13.7	
	1	W250X67	W410X74	13.7	
139	11	W200X27	W410X54	14.0	D11-8.DAT
	10	W200X27	W410X54	14.0	
	9	W200X27	W420X54	14.0	
	8	W200X36	W410X54	14.0	
	7	W200X36	W460X61	14.0	
	6	W200X59	W460X61	14.0	
	5	W250X59	W460X61	14.0	
	4	W250X59	W460X61	14.0	
	3	W250X59	W410X74	14.0	
	2	W250X59	W410X74	14.0	
	1	W250X67	W410X74	14.0	
140	11	W200X27	W410X54	13.7	D11-9.DAT
	10	W200X27	W410X54	13.7	
	9	W200X27	W420X54	13.7	
	8	W200X36	W410X54	13.7	
	7	W200X36	W460X61	13.7	
	6	W200X59	W460X61	13.7	
	5	W250X59	W460X61	13.7	
	4	W250X59	W460X61	13.7	
	3	W250X59	W410X74	13.7	
	2	W250X59	W410X74	13.7	
	1	W250X67	W410X74	13.7	
141	13	W200X27	W410X54	10.9	D13-1.DAT
	12	W200X27	W410X54		
	11	W200X27	W410X54	14.3	
	10	W200X36	W410X54	14.3	
	9	W200X36	W420X54	14.3	
	8	W200X36	W410X54	14.3	
	7	W200X36	W460X61	14.3	
	6	W200X36	W460X61	14.3	
	5	W250X59	W460X61	14.3	
	4	W250X59	W460X61	14.3	
	3	W250X59	W410X74	14.3	
	2	W250X59	W410X74	14.3	
	1	W250X67	W410X74	14.3	

142	13	W200X27	W410X54	10.9	D13-2.DAT
	12	W200X27	W410X54	11.0	
	11	W200X27	W410X54	11.0	
	10	W200X36	W410X54	11.0	
	9	W200X36	W420X54	11.0	
	8	W200X36	W410X54	11.0	
	7	W200X36	W460X61	11.0	
	6	W200X36	W460X61	11.0	
	5	W250X59	W460X61	11.0	
	4	W250X59	W460X61	11.0	
	3	W250X59	W410X74	11.0	
	2	W250X59	W410X74	11.0	
	1	W250X67	W410X74	11.0	
143	13	W200X27	W410X54	10.0	D13-3.DAT
	12	W200X27	W410X54	10.0	
	11	W200X27	W410X54	10.0	
	10	W200X36	W410X54	10.0	
	9	W200X36	W420X54	10.0	
	8	W200X36	W410X54	10.0	
	7	W200X36	W460X61	10.0	
	6	W200X36	W460X61	10.0	
	5	W250X59	W460X61	10.0	
	4	W250X59	W460X61	10.0	
	3	W250X59	W410X74	10.0	
	2	W250X59	W410X74	10.0	
	1	W250X67	W410X74	10.0	
144	13	W200X27	W410X54	9.0	D13-3A.DAT
	12	W200X27	W410X54	9.0	
	11	W200X27	W410X54	9.0	
	10	W200X36	W410X54	9.0	
	9	W200X36	W420X54	9.0	
	8	W200X36	W410X54	9.0	
	7	W200X36	W460X61	9.0	
	6	W200X36	W460X61	9.0	
	5	W250X59	W460X61	9.0	
	4	W250X59	W460X61	9.0	
	3	W250X59	W410X74	9.0	
	2	W250X59	W410X74	9.0	
	1	W250X67	W410X74	9.0	
145	13	W200X27	W410X54	9.7	D13-5.DAT
	12	W200X27	W410X54	9.7	
	11	W200X27	W410X54	9.7	
	10	W200X36	W410X54	9.7	
	9	W200X36	W420X54	9.7	
	8	W200X36	W410X54	9.7	
	7	W200X36	W460X61	9.7	
	6	W200X36	W460X61	9.7	
	5	W250X59	W460X61	9.7	
	4	W250X59	W460X61	9.7	
	3	W250X59	W410X74	9.7	
	2	W250X59	W410X74	9.7	

	1	W250X67	W410X74	9.7	
146	13	W200X27	W410X54	10.0	D13-6.DAT
	12	W200X27	W410X54	10.0	
	11	W200X27	W410X54	10.0	
	10	W200X36	W410X54	10.0	
	9	W200X36	W420X54	10.0	
	8	W200X36	W410X54	10.0	
	7	W200X36	W460X61	10.0	
	6	W200X36	W460X61	10.0	
	5	W250X59	W460X61	10.0	
	4	W250X59	W460X61	10.0	
	3	W250X59	W410X74	10.0	
	2	W250X59	W410X74	10.0	
	1	W250X67	W410X74	10.0	
147	13	W200X27	W410X54	13.0	D13-7.DAT
	12	W200X27	W410X54	13.0	
	11	W200X27	W410X54	13.0	
	10	W200X36	W410X54	13.0	
	9	W200X36	W420X54	13.0	
	8	W200X36	W410X54	13.0	
	7	W200X36	W460X61	13.0	
	6	W200X36	W460X61	13.0	
	5	W250X59	W460X61	13.0	
	4	W250X59	W460X61	13.0	
	3	W250X59	W410X74	13.0	
	2	W250X59	W410X74	13.0	
	1	W250X67	W410X74	13.0	
148	13	W200X27	W410X54	14.0	D13-8.DAT
	12	W200X27	W410X54	14.0	
	11	W200X27	W410X54	14.0	
	10	W200X36	W410X54	14.0	
	9	W200X36	W420X54	14.0	
	8	W200X36	W410X54	14.0	
	7	W200X36	W460X61	14.0	
	6	W200X36	W460X61	14.0	
	5	W250X59	W460X61	14.0	
	4	W250X59	W460X61	14.0	
	3	W250X59	W410X74	14.0	
	2	W250X59	W410X74	14.0	
	1	W250X67	W410X74	14.0	
149	13	W200X27	W410X54	15.0	D13-9.DAT
	12	W200X27	W410X54	15.0	
	11	W200X27	W410X54	15.0	
	10	W200X36	W410X54	15.0	
	9	W200X36	W420X54	15.0	
	8	W200X36	W410X54	15.0	
	7	W200X36	W460X61	15.0	
	6	W200X36	W460X61	15.0	
	5	W250X59	W460X61	15.0	
	4	W250X59	W460X61	15.0	
	3	W250X59	W410X74	15.0	

	2	W250X59	W410X74	15.0	
	1	W250X67	W410X74	15.0	
150	13	W200X27	W410X54	16.0	D13-10.DAT
	12	W200X27	W410X54	16.0	
	11	W200X27	W410X54	16.0	
	10	W200X36	W410X54	16.0	
	9	W200X36	W420X54	16.0	
	8	W200X36	W410X54	16.0	
	7	W200X36	W460X61	16.0	
	6	W200X36	W460X61	16.0	
	5	W250X59	W460X61	16.0	
	4	W250X59	W460X61	16.0	
	3	W250X59	W410X74	16.0	
	2	W250X59	W410X74	16.0	
	1	W250X67	W410X74	16.0	
151	15	W200X27	W460X61	10.9	D15-1.DAT
	14	W200X27	W460X61	12.5	
	13	W200X27	W460X61	10.0	
	12	W200X27	W460X61	10.0	
	11	W200X27	W460X61	10.0	
	10	W200X36	W460X61	10.0	
	9	W200X36	W460X61	10.0	
	8	W200X36	W460X61	10.0	
	7	W200X36	W460X61	10.0	
	6	W200X36	W460X61	10.0	
	5	W250X36	W460X61	10.0	
	4	W250X36	W460X61	10.0	
	3	W250X36	W460X64	10.0	
	2	W250X59	W460X64	10.0	
	1	W250X59	W460X61	10.0	
152	15	W200X27	W460X61	14.0	D15-2.DAT
	14	W200X27	W460X61	14.0	
	13	W200X27	W460X61	14.0	
	12	W200X27	W460X61	14.0	
	11	W200X27	W460X61	14.0	
	10	W200X36	W460X61	14.0	
	9	W200X36	W460X61	14.0	
	8	W200X36	W460X61	14.0	
	7	W200X36	W460X61	14.0	
	6	W200X36	W460X61	14.0	
	5	W250X36	W460X61	14.0	
	4	W250X36	W460X61	14.0	
	3	W250X36	W460X64	14.0	
	2	W250X59	W460X64	14.0	
	1	W250X59	W460X61	14.0	
153	15	W200X27	W460X61	16.0	D15-3.DAT
	14	W200X27	W460X61	16.0	
	13	W200X27	W460X61	16.0	
	12	W200X27	W460X61	16.0	
	11	W200X27	W460X61	16.0	
	10	W200X36	W460X61	16.0	

	9	W200X36	W460X61	16.0	
	8	W200X36	W460X61	16.0	
	7	W200X36	W460X61	16.0	
	6	W200X36	W460X61	16.0	
	5	W250X36	W460X61	16.0	
	4	W250X36	W460X61	16.0	
	3	W250X36	W460X64	16.0	
	2	W250X59	W460X64	16.0	
	1	W250X59	W460X61	16.0	
154	15	W200X27	W460X61	10.0	D15-4.DAT
	14	W200X27	W460X61	10.0	
	13	W200X27	W460X61	10.0	
	12	W200X27	W460X61	10.0	
	11	W200X27	W460X61	10.0	
	10	W200X36	W460X61	10.0	
	9	W200X36	W460X61	10.0	
	8	W200X36	W460X61	10.0	
	7	W200X36	W460X61	10.0	
	6	W200X36	W460X61	10.0	
	5	W250X36	W460X61	10.0	
	4	W250X36	W460X61	10.0	
	3	W250X36	W460X64	10.0	
	2	W250X59	W460X64	10.0	
	1	W250X59	W460X61	10.0	
155	15	W200X27	W460X61	9.3	D15-5.DAT
	14	W200X27	W460X61	9.3	
	13	W200X27	W460X61	9.3	
	12	W200X27	W460X61	9.3	
	11	W200X27	W460X61	9.3	
	10	W200X36	W460X61	9.3	
	9	W200X36	W460X61	9.3	
	8	W200X36	W460X61	9.3	
	7	W200X36	W460X61	9.3	
	6	W200X36	W460X61	9.3	
	5	W250X36	W460X61	9.3	
	4	W250X36	W460X61	9.3	
	3	W250X36	W460X64	9.3	
	2	W250X59	W460X64	9.3	
	1	W250X59	W460X61	9.3	
156	15	W200X27	W460X61	11.0	D15-6.DAT
	14	W200X27	W460X61	11.0	
	13	W200X27	W460X61	11.0	
	12	W200X27	W460X61	11.0	
	11	W200X27	W460X61	11.0	
	10	W200X36	W460X61	11.0	
	9	W200X36	W460X61	11.0	
	8	W200X36	W460X61	11.0	
	7	W200X36	W460X61	11.0	
	6	W200X36	W460X61	11.0	
	5	W250X36	W460X61	11.0	

	4	W250X36	W460X61	11.0	
	3	W250X36	W460X64	11.0	
	2	W250X59	W460X64	11.0	
	1	W250X59	W460X61	11.0	
157	15	W200X27	W460X61	10.5	D15-7.DAT
	14	W200X27	W460X61	10.5	
	13	W200X27	W460X61	10.5	
	12	W200X27	W460X61	10.5	
	11	W200X27	W460X61	10.5	
	10	W200X36	W460X61	10.5	
	9	W200X36	W460X61	10.5	
	8	W200X36	W460X61	10.5	
	7	W200X36	W460X61	10.5	
	6	W200X36	W460X61	10.5	
	5	W250X36	W460X61	10.5	
	4	W250X36	W460X61	10.5	
	3	W250X36	W460X64	10.5	
	2	W250X59	W460X64	10.5	
	1	W250X59	W460X61	10.5	
158	15	W200X27	W460X61	11.3	D15-8.DAT
	14	W200X27	W460X61	11.3	
	13	W200X27	W460X61	11.3	
	12	W200X27	W460X61	11.3	
	11	W200X27	W460X61	11.3	
	10	W200X36	W460X61	11.3	
	9	W200X36	W460X61	11.3	
	8	W200X36	W460X61	11.3	
	7	W200X36	W460X61	11.3	
	6	W200X36	W460X61	11.3	
	5	W250X36	W460X61	11.3	
	4	W250X36	W460X61	11.3	
	3	W250X36	W460X64	11.3	
	2	W250X59	W460X64	11.3	
	1	W250X59	W460X61	11.3	
159	17	W200X27	W410X46	16.0	D17-1.DAT
	16	W200X27	W410X46	16.0	
	15	W200X27	W410X46	16.0	
	14	W200X27	W410X46	16.0	
	13	W200X27	W410X46	16.0	
	12	W200X27	W410X46	16.0	
	11	W200X36	W410X46	16.0	
	10	W200X36	W410X46	16.0	
	9	W200X36	W410X46	16.0	
	8	W200X36	W410X46	16.0	
	7	W200X36	W410X46	16.0	
	6	W200X36	W410X46	16.0	
	5	W250X36	W410X46	16.0	
	4	W250X59	W410X46	16.0	
	3	W250X59	W410X46	16.0	
	2	W250X67	W410X46	16.0	
	1	W250X67	W410X46	16.0	

160	17	W200X27	W410X46	22.0	D17-2.DAT
	16	W200X27	W410X46	22.0	
	15	W200X27	W410X46	22.0	
	14	W200X27	W410X46	22.0	
	13	W200X27	W410X46	22.0	
	12	W200X27	W410X46	22.0	
	11	W200X36	W410X46	22.0	
	10	W200X36	W410X46	22.0	
	9	W200X36	W410X46	22.0	
	8	W200X36	W410X46	22.0	
	7	W200X36	W410X46	22.0	
	6	W200X36	W410X46	22.0	
	5	W250X36	W410X46	22.0	
	4	W250X59	W410X46	22.0	
	3	W250X59	W410X46	22.0	
	2	W250X67	W410X46	22.0	
	1	W250X67	W410X46	22.0	
161	19	W200X27	W410X54	16.0	D19-1.DAT
	18	W200X27	W410X54	18.0	
	17	W200X36	W410X54	18.0	
	16	W200X36	W410X54	18.0	
	15	W200X36	W410X54	18.0	
	14	W200X36	W410X54	18.0	
	13	W200X36	W410X54	18.0	
	12	W200X36	W410X54	18.0	
	11	W200X36	W410X54	18.0	
	10	W200X36	W410X54	18.0	
	9	W200X59	W410X54	18.0	
	8	W200X59	W410X54	18.0	
	7	W200X59	W410X54	18.0	
	6	W200X59	W410X54	18.0	
	5	W250X59	W410X54	18.0	
	4	W250X67	W410X54	18.0	
	3	W250X67	W410X54	18.0	
	2	W250X80	W410X54	18.0	
	1	W250X80	W410X54	18.0	
162	19	W200X27	W410X54	21.0	D19-2.DAT
	18	W200X27	W410X54	21.0	
	17	W200X36	W410X54	21.0	
	16	W200X36	W410X54	21.0	
	15	W200X36	W410X54	21.0	
	14	W200X36	W410X54	21.0	
	13	W200X36	W410X54	21.0	
	12	W200X36	W410X54	21.0	
	11	W200X36	W410X54	21.0	
	10	W200X36	W410X54	21.0	
	9	W200X59	W410X54	21.0	
	8	W200X59	W410X54	21.0	
	7	W200X59	W410X54	21.0	
	6	W200X59	W410X54	21.0	
	5	W250X59	W410X54	21.0	

	4	W250X67	W410X54	21.0	
	3	W250X67	W410X54	21.0	
	2	W250X80	W410X54	21.0	
	1	W250X80	W410X54	21.0	
163	21	W200X27	W410X54	21.0	D21-1.DAT
	20	W200X27	W410X54	21.0	
	19	W200X36	W410X54	21.0	
	18	W200X36	W410X54	21.0	
	17	W200X36	W410X54	21.0	
	16	W200X36	W410X54	21.0	
	15	W200X36	W410X54	21.0	
	14	W200X36	W410X54	21.0	
	13	W200X36	W410X54	21.0	
	12	W200X36	W410X54	21.0	
	11	W200X59	W410X54	21.0	
	10	W200X59	W410X54	21.0	
	9	W200X59	W410X54	21.0	
	8	W200X59	W410X54	21.0	
	7	W200X59	W410X54	21.0	
	6	W250X67	W410X54	21.0	
	5	W250X67	W410X54	21.0	
	4	W250X80	W410X54	21.0	
	3	W250X80	W410X54	21.0	
	2	W250X80	W410X54	21.0	
	1	W250X80	W410X54	21.0	
164	21	W200X27	W410X54	19.0	D21-2.DAT
	20	W200X27	W410X54	21.0	
	19	W200X36	W410X54	21.0	
	18	W200X36	W410X54	21.0	
	17	W200X36	W410X54	21.0	
	16	W200X36	W410X54	21.0	
	15	W200X36	W410X54	21.0	
	14	W200X36	W410X54	21.0	
	13	W200X36	W410X54	21.0	
	12	W200X36	W410X54	21.0	
	11	W200X59	W410X54	21.0	
	10	W200X59	W410X54	21.0	
	9	W200X59	W410X54	21.0	
	8	W200X59	W410X54	21.0	
	7	W200X59	W410X54	21.0	
	6	W250X67	W410X54	21.0	
	5	W250X67	W410X54	21.0	
	4	W250X80	W410X54	21.0	
	3	W250X80	W410X54	21.0	
	2	W250X80	W410X54	21.0	
	1	W250X80	W410X54	21.0	
165	23	W200X27	W410X54	21.0	D23-1.DAT
	22	W200X27	W410X54	21.0	
	21	W200X36	W410X54	21.0	

	20	W200X36	W410X54	21.0	
	19	W200X36	W410X54	21.0	
	18	W200X36	W410X54	21.0	
	17	W200X36	W410X54	21.0	
	16	W200X36	W410X54	21.0	
	15	W200X36	W410X54	21.0	
	14	W200X36	W410X54	21.0	
	13	W200X59	W410X54	21.0	
	12	W200X59	W410X54	21.0	
	11	W200X59	W410X54	21.0	
	10	W200X59	W410X54	21.0	
	9	W200X59	W410X54	21.0	
	8	W200X67	W410X54	21.0	
	7	W200X67	W410X54	21.0	
	6	W250X80	W410X54	21.0	
	5	W250X80	W410X54	21.0	
	4	W250X80	W410X54	21.0	
	3	W250X80	W410X54	21.0	
	2	W250X80	W410X54	21.0	
	1	W250X80	W410X54	21.0	
166	25	W200X27	W410X54	23.0	D25-1.DAT
	24	W200X27	W410X54	23.0	
	23	W200X36	W410X54	23.0	
	22	W200X36	W410X54	23.0	
	21	W200X36	W410X54	23.0	
	20	W200X36	W410X54	23.0	
	19	W200X36	W410X54	23.0	
	18	W200X36	W410X54	23.0	
	17	W200X36	W410X54	23.0	
	16	W200X36	W410X54	23.0	
	15	W200X59	W410X54	23.0	
	14	W200X59	W410X54	23.0	
	13	W200X59	W410X54	23.0	
	12	W200X59	W410X54	23.0	
	11	W200X59	W410X54	23.0	
	10	W250X67	W410X54	23.0	
	9	W250X67	W410X54	23.0	
	8	W250X80	W410X54	23.0	
	7	W250X80	W410X54	23.0	
	6	W250X80	W410X54	23.0	
	5	W250X80	W410X54	23.0	
	4	W250X131	W410X54	23.0	
	3	W250X131	W410X54	23.0	
	2	W250X131	W410X54	23.0	
	1	W250X131	W410X54	23.0	

APPENDIX C

To perform a dynamic response of a structure, it is normally required to determine the frequency of vibration of the system. For this the basic equations of motion are required. The basic equation of motion of an undamped, free vibrating system is:

$$[M] \{ \ddot{X} \} + [K] \{ X \} = \{ 0 \} \qquad (B.1)$$

The terms are the same as those defined in the previous chapters. For the steady state condition, the simple harmonic solution is found to be :

$$\{ X \} = \{ A \} \sin (wt + O) \qquad (B.2)$$

Substituting into the equation of motion (B.1) above yields:

$$-w^2 [M] \{ A \} \sin(wt + O) + [K] \{ A \} \sin(wt + O) = \{ 0 \}$$

rearranging:

$$\{ [K] - w^2 [M] \} \{ A \} \sin (wt + O) = \{ 0 \}$$

or:

$$[K] - w^2 [M] \{ A \} = \{ 0 \} \qquad (B.3)$$

The above equation can be solved easily by using the well-known Crammer's rule as shown below:

$$\{A\} = \frac{\{0\}}{|[K] - w^2[M]|}$$

where $|\ \ |$ denotes the determinant for a matrix. For a non-trivial solution, the denominator determinant vanishes, or:

$$|[K] - w^2[M]| = 0 \qquad (B.4)$$

Equation 4.4 is the classical eigenvalue problem in the form of:

$$[K]\{\phi\} = [M]\{\phi\}U^2$$

where

U^2 = is the diagonal matriz of eigenvalues

$\{\phi\}$ = is the matrix of corresponding eigenvectors

or in a more tradional form, the above equation is :

$$[B][Y] = [X]\{Y\}$$

which leads to a set of n eigenvalues (natural frequencies) and n eigenvectors (mode shapes). The frequency vector is defined as:

$$\{ w \} = \begin{bmatrix} w_1 \\ w_2 \\ \cdot \\ \cdot \\ \cdot \\ w_n \end{bmatrix} \qquad (B.5)$$

Knowing the frequency vector, substitute back into equation (4.2) yields:

$$[K] - w^2 [M] \{ A \} = \{ 0 \}$$

With w^2 known it is now possible to solve for $\{ A \}$, since the $[K]$ and the $[M]$ matrices are asssumed to be known beforehand. A closer examination of the form of the equation reveals that no exact solution can be obtained for $\{ A \}$ but a relative magnitude can be found in terms of any of the coordinate. The solutions so obtained are known as the mode shapes of the elastic system. These are the free vibrating shapes for each mode if the each individual mode were to behave independently from its anothers. These mode shapes possess a special property known as the orthogonality of the mode shapes. The orthogonality of the mode shapes can be shown for any MDOF systems such that:

$$[\phi_m^T] [M] [\phi_n] = 0 \qquad m = n$$

$$[\phi_m^T] [K] [\phi_n] = 0 \qquad m = n$$

Accordingly, one can form a matrix $[\phi]$ in which each

column is a mode shape, this is if:

$$[\,\Phi\,] = [\;\{\phi_1\}\;\{\phi_2\}\;\{\phi_3\}\;\{\phi_4\}\;..\;\{\phi_n\}\;] \qquad (B.6)$$

$$[\,\phi\,] = \begin{bmatrix} \phi_{11} & \cdot & \cdot & \cdot & \cdot & \phi_{1n} \\ \phi_{12} & & & & & \phi_{2n} \\ \cdot & & & & & \cdot \\ & & & & & \\ \phi_{1n} & & & & & \phi_{nn} \end{bmatrix}$$

Then, for n DOF systems, the orthogonality conditions can be written as:

$$[\,\phi\,]^T\,[\,M\,]\,[\,\phi\,] = [\,\backslash\,]$$

$$[\,\phi\,]^T\,[\,K\,]\,[\,\phi\,] = [\,\backslash\,]$$

where [\ ] denotes a diagonal matrix. To normalize the [Φ] one must scale the mode shapes such that :

$$[\,\Phi\,]^T\,[\,M\,]\,[\,\Phi\,] = [\,I\,] \qquad (B.7)$$

For dynamic analysis, the displaced position of a system can be represented by the free vibration mode shapes. These shapes constitute the number of DOF independent displacements patterns, the amplitudes of which may serve as generalized coordinates to express any form of displacements. For any given elastic system, the displacements are given by the mode shape vector (ϕ) multiplied by the modal amplitude [Y_n].

Thus:

$$x_r = \Phi_r \, Y_r \qquad (B.8)$$

The total displacement is then obtained as:

$$X = \phi_1 Y_1 + \phi_2 Y_2 + \phi_3 Y_3 + \ldots\ldots \quad \phi_n Y_n$$

or in matrix notation:

$$x = [\,\Phi\,]\,[\,Y\,] \qquad (B.9)$$

To obtain [Y], it is easier to post multiply $[\,\Phi\,]_n^T$ by [M] [X] :

$$[\,\phi\,]_n^T\,[\,M\,]\,[\,x\,] = [\,\phi\,]_n^T\,[\,M\,]\,[\,\Phi\,]\,[\,Y\,]$$

The right hand side then is:

$$[\,\phi\,]_n^T\,[\,M\,]\,[\,\Phi\,]\,[\,Y\,] = \phi_1^T\,[\,M\,\phi_1\,Y_1$$

$$+ \phi_n^T\,[\,M\,]\,\phi_2\,Y_2 \quad + \phi_r^T\,[\,M\,]\,\phi_n\,Y_n$$

All terms will vanish except the n^{th} term because of the orthogonality with respect to mass :

$$[\,\phi\,]_n^T\,[\,M\,] \quad [\,x\,] = [\,\phi\,]_r^T \quad [\,M\,]\,[\,\phi\,]_r \quad Y_r$$

$$Y_n = \frac{[\phi]_n^T [M] [x]}{[\phi]_n^T [M] [\phi]_n} \qquad (B.10)$$

For an undamped system, the equations of motion becomes:

$$[M][\ddot{X}] + [K][X] = [P(t)] \qquad (B.11)$$

but

$$[X] = [\Phi][Y]$$

$$[\dot{X}] = [\Phi][\dot{Y}]$$

$$[\ddot{X}] = [\Phi][\ddot{Y}]$$

Since the mode shapes do not change with time, the last equations of motion become:

$$[M][\Phi][\ddot{Y}] + [K][\Phi][Y] = [P(t)]$$

Premultiply by $[\phi]_n^T$ one gets :

$$\phi_n^T [M][\Phi][\ddot{Y}_n] + [\phi]_n^T [K][\Phi][Y] = [\phi]_n^T P(t)$$

expanding the left hand side gives :

$$\phi_n^T [M][\Phi]_n \ddot{Y}_n + \phi_n^T [K] Y_n = \phi_n^T P(t)$$

introducing:

$M_n = \phi_n^T [M] \phi_n$ the generalized mass

$K_n = \phi_n^T [K] \phi_n$ the generalized stiffness

$P_n(t) = \phi_n^T P(t)$ the generalized load

and rewriting, gives :

$$M_n \ddot{Y}_n + K_n Y_n = P_n(t) \qquad (B.12)$$

which is the generalized equation of motion for a SDOF system for mode n. Equation (4.12) is a set of N independent equations of motion, one for each mode. It also can be shown that:

$$K_n = w_n^2 M_n$$

The above procedure allows a MDOF system be converted into a series of independent SDOF systems. For a damped system, the similar procedure is applied with the inclusion of a damping matrix. The procedure uncouples the equations of motion due to the orthogonality of the mode shapes. Knowing the period of free vibration for each of the mode of the system, the dynamic response can be found by integrating the Duhamel's integral:

$$Y_n(t) = \frac{T}{M_n w_n} \int_0^t P_n(t) \; e^{-\xi_n w_n (t-\tau)} \sin w_n (t-\tau) \, dt$$

The response for each mode can be found successively and the overall response for the whole system is found by

superposition, thus the name "mode superposition method". For a typical modal analysis, one only has to determine the free vibrating frequencies of a system and then pick up the response parameters of interest from a computed response spectrum. Then the superposition method is used to determine the overall response. This gives fairly accurate assessment of the dynamic behaviors of a system. For MDOF systems under earthquake like loadings, the equations of motion are:

$$M_n \ddot{Y}_n + C_n \dot{Y}_n + K Y_n = \phi_n M \ddot{v}_g(t)$$

$$= \phi n \, M \{ 1 \} \ddot{v}_g (t)$$

$$= \Gamma_n \ddot{v}_g(t)$$

where

$\Gamma_n = \phi_n M \{ 1 \}$

= is the modal participation factor

$\ddot{x}_g$ = is the ground acceleration

The modal response from the earthquake again can be computed from the Duhamel's integral:

$$Y_n(t) = \frac{\Gamma}{M_n w_n} \int_0^t v_g(t) \, e^{- \xi_n w_n (t-\tau)} \sin w_n (t-\tau) \, dt$$

Once again the relative geometric displacements are:

$$x_n = \phi_n \frac{\Gamma_n}{M_n w_n}$$

and the total displacements are summed by:

$$\{ x \} = \Phi \quad Y_r$$

The vector { x } will yield the elastic displacement of the system under the earthquake ground motions.